LEADING PIPELINE RESEARCH

Catalog No. PR-244-18702-R01

Evaluation of Casing Integrity for Underground Storage Wells

US-3J

PRCI Contract No. PR-244-18702

PHMSA Contract 693JK31810014 - Project #747

C-FER Project No. C430

Prepared for the

Underground Storage Technical Committee

of

Pipeline Research Council International, Inc.

and

Pipeline and Hazardous Materials Safety Administration

Prepared by:

C-FER Technologies (1999) Inc.

Authors: Gang Tao, PhD, PEng; Mark Stephens, MSc, PEng

Reviewers: Brian Wagg, MSc, PEng

Release Date: May 26, 2021

Version	Date of Last Revision	Date of Uploading	Comments
Draft 01	March 10, 2021	March 11, 2021	Initial draft
Final	May 26, 2021	May 26, 2021	Final

C-FER Technologies
A SUBSIDIARY OF ALBERTA INNOVATES

Final Report

Evaluation of Casing Integrity for Underground Storage Wells

Confidential to
Pipeline Research Council International, Inc. and Pipeline and Hazardous Materials Safety Administration

Prepared by
Gang Tao, PhD, PEng
Mark Stephens, MSc, PEng

Reviewed by
Brian Wagg, MSc, PEng

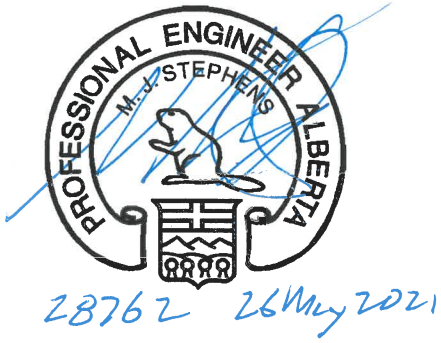

Approved By B Wagg

APEGA ID 51856

Date May 26 2021

May 2021
C430

APEGA Permit: P04487

PROJECT TEAM

Evaluation of Casing Integrity for Underground Storage Wells		**C-FER Project: C430**
Task/Deliverable	**Contributors**	**Responsible Professional**
Literature Review of Logging Technologies and Remaining Burst Strength Prediction Models; Logging Tool Test Evaluation; Physical Coupon and Burst Tests; Finite Element Analysis; Remaining Burst Strength Prediction Model Evaluation	Gang Tao, PhD, PEng	Gang Tao, PhD, PEng
Framework for Reliability-based Casing Corrosion Management	Mark Stephens, MSc, PEng Diana Abdulhameed, PhD	Mark Stephens, MSc, PEng

REVISION HISTORY

Evaluation of Casing Integrity for Underground Storage Wells			**C-FER Project: C430**		
Revision	**Date**	**Description**	**Prepared**	**Reviewed**	**Approved**
1	March 10, 2021	Draft	GT/MJS	BTW	BTW
2	May 26, 2021	Final	GT/MJS	BTW	BTW

Disclaimer

This report is furnished to Pipeline Research Council International, Inc. (PRCI) under the terms of PRCI contract PR-244-18702, between PRCI and C-FER Technologies (1999) Inc. (C-FER). The contents of this report are published as received from C-FER. The opinions, findings, and conclusions expressed in the report are those of the authors and not necessarily those of PRCI, its member companies, or their representatives. Publication and dissemination of this report by PRCI should not be considered an endorsement by PRCI of C-FER, or the accuracy or validity of any opinions, findings, or conclusions expressed herein.

In publishing this report, PRCI and C-FER make no warranty or representation, expressed or implied, with respect to the accuracy, completeness, usefulness, or fitness for purpose of the information contained herein, or that the use of any information, method, process, or apparatus disclosed in this report may not infringe on privately owned rights. PRCI and C-FER assume no liability with respect to the use of, or for damages resulting from the use of, any information, method, process, or apparatus disclosed in this report. By accepting the report and utilizing it, you agree to waive any and all claims you may have, resulting from your voluntary use of the report, against PRCI and C-FER.

This work was funded in part, under the Department of Transportation, Pipeline and Hazardous Materials Safety Administration. The views and conclusions contained in this document are those of the authors and should not be interpreted as representing the official policies, either expressed or implied, of the Pipeline and Hazardous Materials Safety Administration, the Department of Transportation, or the U.S. Government.

Abstract

C-FER Technologies (1999) Inc., ("C-FER") conducted a multi-phase study to further advance the ability to predict the remaining casing burst capacity for underground natural gas storage wells. This project is co-funded by the Pipeline Research Council International, Inc. (PRCI) and the US Department of Transportation (DOT), Pipeline and Hazardous Materials Safety Administration (PHMSA).

This project included a literature review of casing corrosion logging technologies and remaining burst capacity prediction models. Three casing corrosion logging tools, selected based on the outcome of a preceding PRCI casing logging tool test program, were tested to further evaluate their performance in detecting and sizing various metal loss features on casing specimens. Physical burst tests with capped ends were conducted on 20 specimens selected from the logged casing joints to benchmark the burst prediction models. Advanced finite element analysis (FEA) was also performed to evaluate the effect of in-situ downhole load conditions on the remaining burst capacity of corroded casing. A reliability-based framework was outlined to quantitatively address various uncertainties associated with the casing corrosion integrity management. This report summarizes the work completed, the key results and conclusions, as well as recommendations for future initiatives.

Project Team

Andrew Lloyd*	Enterprise Products
Mark Thompson	Enterprise Products
Luke Dewig	TC Energy
Tara Fuchs	TransGas Ltd.
Rocky Halbgewachs	TransGas Ltd.
Ray Harris	National Fuel Gas Supply Corporation
Robert Heine	Williams Companies, Inc.
Larry Kennedy	Pacific Gas and Electric Company
David Xu	Pacific Gas and Electric Company
Robert Kurima	Chevron Pipe Line Company
F. Leeson	Dominion Energy Transmission, Inc.
Mike Olesko	Plains All American Pipeline, LP
Jim Tomlinson	Marathon Pipe Line LLC
Jeff Sutherland	Baker Hughes, a GE company
Zoe Shall	Pipeline Research Council International, Inc.
Gang Tao	C-FER Technologies (1999) Inc.

*Project Team Leader

Table of Contents

List of Figures and Tables

List of Figures

List of Tables

List of Nomenclature

σ_1	axial stress in the uncorroded pipe body
σ_2	hoop stress in the uncorroded pipe body
σ_{cm}	circumferential stress in the metal loss area
σ_{eq}	von Mises equivalent stress
σ_{lm}	longitudinal stress in the metal loss area
σ_L	axial compressive stress in the pipe body in BS 7910 method
σ_{ref1}	axial stress in the metal loss in BS 7910 method
σ_{ref2}	hoop stress in the metal loss in BS 7910 method
σ_{ref}	reference stress
σ_{SMYS}	specified minimum yield strength
σ_{SMTS}	specified minimum tensile strength
$\dot{\sigma_a}$	axial stress increment
$\dot{\sigma_h}$	hoop stress increment
$\dot{\sigma_r}$	radial stress increment
σ_u	ultimate tensile strength
ε_a	axial strain
$\dot{\varepsilon_a}$	axial strain increment
ρ_c	cement slurry hydrostatic pressure gradient
ρ_d	drilling fluid hydrostatic pressure gradient
ρ_w	displacement fluid hydrostatic pressure gradient
θ	circumferential angle of the metal loss area
λ	longitudinal flaw length parameter
λ_c	circumferential flaw length parameter
ν	Poisson's ratio
κ	casing curvature
τ	time
τ_1, τ_2	time interval
A	cross-section area of the metal loss
A_0	nominal cross-section area of the pipe wall
A^i	cross-section area of the metal loss for subsection *i*
A_0^i	nominal cross-section area of the pipe wall for subsection *i*
A_f	cross-section area of the region of local metal loss
A_m	cross section area of the cylindrical structure
A_w	effective area on which pressure acts
c	circumferential width of the metal loss area
C	failure consequence
d	maximum depth of the metal loss
d_{ave}	average depth of the metal loss
d_{max}	maximum feature depth
D	nominal outer diameter of the pipe
D_i	nominal inner diameter of the pipe
E	Young's modulus
F	axial load

F_{bu}	buoyancy force
F_h	total casing hanging weight in air
F_T	maximum tensile load in a casing string at the top of the well
f_u	tensile strength in DNVGL-RP-F101 method
$g(x)$	limit state function
h	true vertical depth of the well
h_c	final vertical depth interval of the cement
h_d	final vertical depth interval of the drilling fluid
H_1	axial compressive load factor in BS 7910 method
L	longitudinal dimension of the metal loss
M	Folias factor
$MAWP_r$	maximum allowable working pressure
M^i	Folias factor for subsection *i* in RSTRENG method
M_t	Folias factor in API 597-1 Level 1 method
M_t^i	Folias factor for subsection *i* in API 579-1 Level 2 method
M_s^C	Folias factor based on the circumferential extent of the local thinned area
M_t^C	Folias factor based on the circumferential extent of the local thinned area
p_f	probability of failure
p_{fi}	annual probability of failure
p_{max}	maximum allowable probability of failure
p_t	total annual probability of casing failure
P	internal pressure
P_F	predicted burst pressure
r_a	pressure resistance of part through-wall corrosion feature
R	casing reliability
R_T	casing reliability target
$\bar{R}$	casing risk level
$\bar{R}_{max}$	maximum tolerable level of casing risk
R_i	inside radius of the pipe
R_t	remaining thickness ratio
R_T	reliability target
RSF	remaining strength factor
RSF^i	remaining strength factor for subsection *i*
s	shear stress
S	allowable stress
S_{flow}	flow stress
S_F	nominal pipe body hoop stress limit at failure
t	pipe nominal wall thickness
W_c	casing weight per unit length

List of Acronyms

API	American Petroleum Institute
ASME	American Society of Mechanical Engineers

ASTM	American Society for Testing and Materials
C-FER	C-FER Technologies (1999) Inc.
CAD	computer-aided design
CSA	Canadian Standards Association
COV	coefficient of variation
CTP	critical thickness profile
DAS	data acquisition system
DLS	dogleg severity
DOT	Department of Transportation
DWS	Deep Well Simulator
EC	eddy current
EM	electromagnetic
FEA	finite element analysis
FORM	first order reliability method
LS	laser scan
LPC	Line Pipe Corrosion
LTA	local thinned area
MEC	magnetic eddy current
MFC	multi-finger caliper
MFL	magnetic flux leakage
MOP	maximum operating pressure
ILI	inline inspection
OD	outer diameter
PDO	Petroleum Development of Oman
PHMSA	Pipelines and Hazardous Materials Safety Administration
POD	probability of detection
POF	probability of failure
PRCI	Pipeline Research Council International, Inc.
RBDA	reliability-based design and assessment
SF	safety factor
SMYS	specified minimum yield strength
SMTS	specified minimum tensile strength
SORM	second order reliability method
TVD	true vertical depth
UGS	underground gas storage
UT	ultrasonic testing
UTS	ultimate tensile strength
VME	von Mises equivalent stress
WT	wall thickness
YS	yield strength

1 - Executive Summary

C-FER Technologies (1999) Inc. ("C-FER") conducted a multi-phase study to further advance the knowledge to predict the remaining casing burst capacity for underground natural gas storage wells. This project is co-funded by the Pipeline Research Council International, Inc. (PRCI) and the US Department of Transportation (DOT), Pipeline and Hazardous Materials Safety Administration (PHMSA). The objective of this research project is to improve the understanding of several key aspects of well casing corrosion assessment, contributing to increased confidence in evaluation of storage well casing integrity. This project included the following tasks:

- A literature review was conducted on casing corrosion logging technologies and remaining burst capacity prediction models commonly used by industry;
- Three casing corrosion logging tools, selected based on the outcome of a preceding PRCI casing logging tool test program, were tested to further evaluate their performance in detecting and sizing various metal loss features on casing specimens. Three casing configurations that are most commonly used in depleted reservoir gas storage wells were selected in the test:
  - 4.5 inch, 11.6 ppf J55
  - 5.5 inch, 15.5 ppf J55
  - 7.0 inch, 23 ppf J55
- Physical burst tests with capped-end condition were conducted on 20 specimens selected from the logged casing joints to benchmark the burst prediction models;
- Advanced finite element analysis (FEA) was performed to evaluate the effect of in-situ downhole load conditions on the remaining burst capacity of corroded casing; and
- A reliability-based framework was outlined to demonstrate the process to quantitatively address various uncertainties associated with the inputs required in remaining burst strength calculations for downhole casing integrity management.

Based on the work completed, the key findings and outcomes are as follows:

<u>Casing Corrosion Logging Technologies</u>

- Commercial tools based on ultrasonic testing (UT) and magnetic flux leakage (MFL) generally have the capability to conduct high-resolution inspection of isolated casing corrosion features. However, note that significant variations can exist among vendor deliverables and tool performance even for tools using the same technology. Therefore, communication between operators and logging service providers is critical to ensure that the final deliverable meets the operational and regulatory requirements. In the pipeline industry, American Petroleum Institute (API) Standard 1163 [1] suggests that pipeline operators co-operate with service providers to choose the proper inspection technology that meets the operator's goals and objectives. The operator shall provide information on the physical characteristics and constraints of the pipeline to service providers, and the service provider shall state whether the chosen inline inspection (ILI) system can meet the written performance specification. The same information exchange should also apply to downhole casing inspections;
- The prototype tools based on the magnetic eddy current (MEC) technology tested in this project also demonstrated good performance that is comparable to commercial logging tools.

Further commercialization of this technology to supplement existing casing corrosion logging technologies is recommended;

- The multi-finger caliper (MFC) tool can physically measure the casing inner-wall profile, which may be used to diagnose the casing deformation and metal loss due to internal corrosion. The MFC tool cannot inspect metal loss on the outer surface of the casing. The sizing accuracy of MFC tools is directly related to the casing diameter and the measurement resolution (i.e. the number of caliper fingers and axial sampling rate). In addition, it appears that nominal casing dimensions are often assumed in interpretating MFC logs for metal loss estimation, which can introduce significant error. Therefore, the MFC tools may be used as an initial screening tool to obtain estimates of internal corrosion and deformation of casing strings. Due to several limitations, MFC tools are not recommended for comprehensive casing corrosion assessments for gas storage wells;
- Tools based on electromagnetic (EM) technologies can conduct through-tubing corrosion logging. The literature review indicated that significant variations exist among vendor tools, including tool configurations, operating modes and measurement capabilities. An important factor in the performance of these EM tools in through-tubing applications is that they can only estimate the average wall loss around the circumference of the casing strings. Therefore, they are not suitable for characterizing discrete corrosion features. In addition, it appears that metal loss must be severe to be confidently detected and quantified by these tools. Nevertheless, additional investigation involving quantitative lab test evaluation is warranted to better understand the capability of these tools;
- Comparing results from multiple tools with different technologies can help minimize measurement uncertainties; and
- Compared to the practice in the pipeline industry of validating ILI tool performance with direct measurements on excavated pipe, it is extremely difficult to validate casing corrosion logging tool response in real wells. This project and the preceding PRCI casing logging tool test projects demonstrated that lab tests can be an efficient approach to collect high quality data for quantitative validation of corrosion logging tool performance.

<u>Remaining Burst Strength Prediction of Corroded Casing</u>

- All burst test specimens in this project showed a plastic collapse failure mode in the blunt metal loss regions, resulting in either a small leak or ductile rupture;
- All analytical models used to predict remaining burst strength under-estimate the remaining burst strength by approximately 10% to 36% based on the current physical test results;
- Among the analytical prediction models reviewed that are practical for downhole applications, American Society of Mechanical Engineers (ASME) B31G and modified B31G remaining burst strength prediction models were found to have the lowest random error levels when compared to the 20 burst test results obtained in this project;
- The RSTRENG model for remaining burst strength may be difficult to use in downhole applications as it requires a detailed river bottom characterization of features which is difficult to obtain from current log data;
- The LPC-1, BS 7910, DNVGL-RP-F101 and the API 579-1 models appeared to show a dependency of the prediction accuracy on the casing diameter-to-thickness (D/t) ratio;

- FEA prediction using the actual material stress-strain relationship and the metal loss profile was found to achieve fairly good agreement with the physical burst test results. Particularly, the failure criterion based on plastic collapse was found to significantly improve the prediction accuracy compared to the von Mises equivalent stress ("VME") based failure criterion;
- The downhole in-situ locked-in axial load conditions were found to have a marginal impact on the remaining burst strength of casing. Such effect may be accounted for with an empirical factor applied to the remaining burst strength predictions. Additional study is required to further validate the findings of the locked-in axial load effect; and
- The casing material showed time-dependent stress-strain response in the post-yield region in the coupon tests. Therefore, the casing burst strength obtained from lab tests (under a relatively high strain rate) would tend to over-estimate the actual burst strength in the underground storage well, where the casing is under sustained pressure (i.e. extremely low strain rate). Further investigation of the strain-rate effect on the remaining burst strength of corroded casing is warranted to ensure appropriate safety margins are considered in predicting the remaining burst strength.

Reliability-based Casing Corrosion Management Framework

- A reliability-based assessment framework is described that addresses issues of key importance with respect to casing corrosion integrity management based on high-resolution integrity logs, including: feature-specific probability estimation; the treatment of inspection-related uncertainties; appropriate measures of casing reliability; the development of reliability assessment criteria; and the relationship between measured casing damage severity, the extent of repair and the required time to next inspection.
- The use of the proposed framework is illustrated with an analysis of a hypothetical casing string for which high-resolution metal loss corrosion data is assumed to be available. The demonstration analysis shows how casing log data can be used to estimate casing reliability as a function of time, how selected corrosion feature remediation affects the reliability projections and how this information can be used to support the determination of the required time to next inspection.

Based on the findings and outcomes of this research program, the following recommendations for future work are made:

Casing Corrosion Logging Tool Evaluation and Improvement

- Further lab test evaluation of high-resolution casing logging tools is recommended to improve the understanding of the tool response to a broader range of casing corrosion features. Additional metal loss features with complex profiles should be included in the tests. The expanded test data sets are expected to form the basis for determining uncertainty parameters for each logging tool, which can be implemented into the quantitative reliability-based casing corrosion management system;
- Industry should consider developing a more rigorous downhole corrosion logging system qualification guideline. The guideline could be based on guidelines used in the pipeline industry, such as API Standard 1163 [1], but will be adapted to meet the unique conditions for downhole applications. This guideline would facilitate a standardized workflow and consistent

output from service providers, and would minimize the gaps between the stated logging tool performance and the well operators' expectations; and

- Industry should consider a comprehensive lab test evaluation of through-tubing logging tools. It is expected that this test program would invite multiple through-tubing logging tool vendors with various logging technologies. The through-tubing tool test program should include specially designed severe metal loss features that fall within the detection range of the tools that was identified in this project. The outcome of the test program is expected to provide an understanding of the tools' performance on a comparative basis. Most importantly, the test program would help operators to establish an appropriate expectation about these tools' capabilities, and to make informed decisions to use through-tubing tools for monitoring or screening purposes.

Improvement of Remaining Burst Strength Prediction Models for Corroded Casing

The results of this and previous projects suggest that the remaining burst strength prediction models developed for pipelines have the tendency to under-estimate the burst strength of casing. Further improvement of remaining burst strength prediction models for downhole casing is warranted. The following considerations are recommended in future study:

- Additional full-scale burst testing should be conducted for casing specimens with a broader range of metal loss features and additional casing grades that are used in underground gas storage (UGS) wells. The burst test program should consider both capped-end and axially constrained conditions (i.e. representative of downhole conditions). Burst tests under axially constrained conditions are expected to validate the findings in this project, and to help establish a methodology to account for the impact on the remaining burst strength calculation, if deemed necessary;
- Advanced FEA should be conducted, along with the full-scale burst tests, to further validate the plastic collapse failure criterion identified in this project. The highly accurate predication capability of the advanced FEA would allow modeling of a broader range of scenarios (e.g. a variety of metal loss features, casing configurations and in-situ load conditions), while minimizing the number of physical burst tests required to validate the model. The validated FEA approach would offer the advantage of improved efficiency and reduced cost in generating a large quantity of cases for calibrating the remaining burst strength prediction model;
- Based on a combination of expanded physical burst tests and FEA cases, further study can be performed to improve the accuracy of remaining burst strength prediction models for the downhole casing application. In addition, development of new models may be considered with incorporation of the post-yield stress-strain relationship and a plastic collapse failure mechanism;
- Additional study is required to understand the mechanical properties and the burst failure of vintage casings in existing UGS wells. Special attention should be paid to the ductility of vintage casing materials and their burst failure mode (i.e. ductile versus brittle), which could have a significant impact on the prediction capability of existing remaining burst strength prediction models; and
- Industry should also consider further investigation of the strain-rate effect on the remaining burst strength of corroded casing. The strain rate effect should be properly accounted for in

calibrating remaining burst strength prediction models based on physical slow strain-rate burst tests.

Identification and Mitigation of Other Downhole Threats

- Further research is recommended to identify and better understand additional downhole threats that may compromise casing integrity in UGS wells. For critical threats identified, the research effort should focus on selection of proper inspection tools and mitigation strategies. The additional downhole threats include, but are not limited to:
  - potential environmental-assisted cracking in casing pipe body and threaded connections that can significantly reduce the casing strength;
  - casing deformation (e.g. parting, collapse, formation movement, buckling) that could occur in weak formation, tectonically active areas and salt cavern storage wells; and
  - long-term casing connection sealability and structural integrity, especially for wells using standard API connections and/or wells subjected to high frequency temperature and pressure cycles; and
- Additional studies should investigate issues related to cement integrity and remediation methods to help improve the overall UGS well integrity.

Further Development of Reliability-based Casing Corrosion Management Methodology

The framework developed and described in this work provides a means to utilize casing inspection data obtained from high-resolution downhole integrity logs to estimate casing reliability (i.e. annual probability of failure) and to predict how the reliability will change (i.e. probability of failure will increase) with time due to corrosion feature growth. It also provides a means to relate feature characteristics (i.e. depth, length and growth rates) and candidate remediation strategies to the required time to next inspection, provided a reliability threshold (i.e. limit on allowable probability of failure) can be defined.

However, there is as yet no consensus on the maximum allowable probability of casing failure. To facilitate broader use of the proposed reliability-based framework, additional work is required to develop consensus-based casing reliability thresholds, with due consideration of casing failure mode (i.e. leak versus burst). And to the extent that the reliability thresholds should also reflect the consequences of casing failure, a risk-consistent approach to the development of reliability thresholds is recommended that would require higher reliability thresholds (i.e. lower allowable failure probabilities) for casings where the consequences of failure are higher.

Lastly, note that the optimal casing corrosion management strategy will balance the risk reduction achieved by casing feature remediation against the risk increase associated with additional well entry for casing feature remediation and/or re-inspection. While a framework for managing the overall well risk with due consideration of the additional well risk posed by well entry is provided in a companion research project, further work is required to directly incorporate these considerations into the casing corrosion management framework.

2 - Introduction

The integrity of UGS wells relies on the ability of the wellbore casing to resist operating pressures and act as a primary wellbore barrier, while the casings are often subjected to corrosive environments and other loading conditions (e.g. geomechanical and temperature). To assess casing strength subjected to corrosion, current best practices involve periodic measurement of the casing condition using a range of logging tool technologies to characterize metal loss features and then using this information to calculate the remaining burst capacity using various methods. To compensate for the uncertainties in the casing material properties, logging measurement accuracy, loading conditions and calculation methods, various safety factors are typically applied throughout the process, which can lead to significant uncertainties in the safety level associated with the current condition of the well casing. To increase the confidence in the estimated safety level, improvements could be made to reduce the amount of uncertainty associated with each of the components involved in the remaining burst strength calculation. These could include:

1. Identification of suitable logging technologies that can minimize the measurement uncertainty;
2. Identification of suitable burst strength prediction models and quantification of the model uncertainty; and
3. Quantification of effects of additional in-situ loads on remaining burst strength predictions.

In addition, a reliability-based assessment methodology can be used instead of traditional deterministic methods to account for the various uncertainties in remaining burst strength calculations for casing integrity management. By combining the estimated remaining burst capacity with the expected operating conditions in the well, the operator can estimate the likelihood that the burst capacity of the casing will be exceeded, leading to improved decisions regarding well interventions and operating parameters.

This project investigated several key components for the well casing corrosion assessment with the following objectives:

- Obtain an improved understanding of the accuracy and repeatability of commercial logging tool technologies used to measure wall loss in well casing;
- Expand the data set of corroded casing burst test results;
- Benchmark burst prediction models using the expanded set of burst test data and FEA;
- Outline a reliability-based burst capacity assessment framework to account for material property, measurement, load and model uncertainties to improve confidence in the evaluation of storage well casing integrity, leading to improved decisions regarding well interventions and operating parameters.

This project includes several key tasks. This report is organized with each of the tasks documented in a separate chapter as follows:

- A literature review was conducted on various downhole casing corrosion logging technologies. The focus of the review was to identify existing validation programs and case studies that could provide insights into a quantitative understanding of the performance of each technology and specific vendor tools. Special attention was paid to the through-tubing logging

tools based on EM technologies. An additional literature review was conducted on remaining burst strength prediction models that have been widely used in the pipeline and other industries. The models reviewed were benchmarked with full-scale burst tests to assess their prediction capability for casing specimens with metal loss. A summary of the literature review is documented in Section 4;

- Three casing corrosion logging tools, selected based on a preceding PRCI casing logging tool test project, were further tested in this project. Three casing sizes (listed in Table 1) that are commonly used in depleted reservoir storage wells were included in a test well setup. Details of the metal loss features were not disclosed to the vendors, making it a true "blind" test. Upon completion of the logging tests, a performance analysis of each logging tool was conducted based on the logging report provided by each vendor. A description of the logging tool test setup, test execution and tool performance results are summarized in Section 5;
- Upon completion of the logging tool test, 20 full-scale burst test specimens were made from the casing joints that were logged. Physical burst tests were conducted with the capped-end condition. The full-scale burst test data were used to benchmark the remaining burst prediction models reviewed in this project. In addition, coupon tensile tests were conducted to obtain the mechanical properties of the casing specimens. The mechanical properties were used as the inputs for assessing the prediction capability of the remaining burst strength prediction models. In addition, the stress-strain curves from the coupon tests were used in a subsequent task of FEA modeling of the burst test specimens. Section 6 describes the setup, execution and key results of the physical tests, including the coupon and burst tests;
- Advanced FEA was performed to predict the burst strength of the 20 burst test specimens based on the actual metal loss profiles. The analyses were conducted under both capped-end condition and the in-situ downhole load condition. Analysis under the capped-end condition established the basis for identifying an appropriate failure criterion in predicting the burst strength. Upon establishing the appropriate failure criterion, additional analysis was performed under the in-situ load condition to investigate the impact of the axial constraint (by the cement) on casing burst strength. Section 7 describes the details of the FEA study;
- Based on the physical burst test results and the FEA study, evaluation of the remaining burst strength prediction models was conducted to quantitatively assess the prediction capabilities. A summary of the prediction model evaluation is documented in Section 8;
- A reliability-based casing remaining strength assessment framework was outlined to quantitatively account for uncertainties in various input parameters used to evaluate well casing integrity, including material properties, loading conditions, measurement and model accuracy. A demonstration analysis was conducted to illustrate the workflow of the reliability-based assessment framework. This reliability-based assessment framework is described in Section 9;
- A summary of key conclusions of this project is provided in Section 10; and
- Recommendations for future work to address the gaps identified in this research and to further improve the knowledge for UGS casing integrity management are provided in Section 11.

Table 1 – Casing Samples

Outside Diameter (inch)	Weight (pounds per foot)	Grade	Wall Thickness (inch)	D/t
4.5	11.6	J55	0.250	18.0
5.5	15.5	J55	0.275	20.0
7.0	23.0	J55	0.317	22.1

3 - Impact from the Research Results

This project is expected to have the following key impacts:

- The logging tool test results will provide an improved understanding of the accuracy and repeatability of commercial logging tool technologies used to measure well casing wall loss, which in turn will help UGS operators to make more informed decisions regarding well intervention and operation. The data set collected in the logging tool lab tests can be expanded with future tests and can be used to better quantify uncertainties related to logging tool performance;
- The 20 physical burst tests executed in this project will make a significant contribution to the corroded casing burst test data set available to industry. The expanded burst test data set of corroded casing will also enable further improvement and development of remaining burst strength prediction models for downhole casing. In addition, the burst test data set can be used to quantify uncertainties of remaining burst strength prediction models to be implemented in a quantitative reliability-based casing corrosion management system;
- The quantitative evaluation of various remaining burst strength prediction models against physical burst test results will provide insights into the predication capability of these models for downhole casing applications. The identification of limitations associated with existing remaining burst strength prediction models, developed for the pipeline and petrochemical industries, when applied to downhole casing, will provide directional guidance for future model development;
- Validation of the plastic collapse failure criterion using advanced FEA will establish a robust approach to obtaining more accurate estimation of the remaining burst strength of corroded pipe (i.e. for ductile failure mode) in an advanced fitness-for-service assessment for downhole casing, pipeline and other industries;
- The findings on the effect of axial constraint on the remaining burst capacity of corroded casing could have a significant impact on the direction of future research in this area. Subject to further validation, these findings could potentially lead to reconsideration of technical approaches required to address these issues in current industry standards or practices; and
- The reliability-based framework outlined in this project will demonstrate a process to quantitatively address various uncertainties associated with the input parameters used in well casing corrosion management. As previously demonstrated in the pipeline industry, further development of this workflow can lead to improved efficiency in casing integrity management for UGS operators. Further research and development could lead to broad acceptance of this methodology within the UGS industry and potential incorporation into industry best practices or standards.

4 - Literature Review

4.1 - Casing Corrosion Logging Technologies

Periodic casing corrosion inspection by running downhole logging tools is one of the key components in well integrity management. Various casing logging technologies have been used in the industry over the last few decades. The literature review in this project indicated that majority of public literature is based on field case studies of a limited number of logging tools by a single vendor. Studies focusing on quantitative evaluation of logging tool performance, such as detection capabilities (e.g. probability of detection, false calls) and metal loss feature sizing accuracy, were found to be extremely rare. The limitation of the existing literature and lack of independent review of various logging technologies, tool variations and vendor deliverables created a significant barrier for operators in making informed choices of the most appropriate logging technology and services from vendors.

This section presents an overview of a variety of logging technologies that are commonly used for casing corrosion inspection. Information about different technologies and vendor tool variations was collected from public literatures. Particular interest was paid to the EM technology that is capable of measuring wall thickness of multiple concentric casing strings. In addition, key findings and conclusions from the preceding PRCI casing logging tool test program [2] are presented as additional references.

4.1.1 - Multi-finger Caliper (MFC) Tool

Figure 1 shows a schematic of a typical MFC tool. MFC tools use up to 80 spring-loaded "fingers" to provide a direct, physical measurement of the casing internal wall profile as the tool is pulled towards the surface. The measured casing inner wall profile can be used to interpret a variety of internal features, such as pitting, holes, build-up, and wall loss due to wear and corrosion. However, one limitation of MFC tools is that they can only detect features on the inner casing wall. Their measurement resolution is directly related to the number of fingers, the inside diameter of the casing and the axial sampling rate. In addition, MFC tool measurement is affected by scale build-up or debris on the casing inner wall. In general, the principle of this technique and the tool's measurement capability remain largely the same, though post-processing of the measurement data may vary among different logging service vendors. MFC tools can be used in either gas- or liquid-filled wellbores. In addition to wall loss inspection, MFC log data can be used to estimate local casing trajectory changes and deformations, such as casing buckling, shear and collapse deformations [3,4,5].

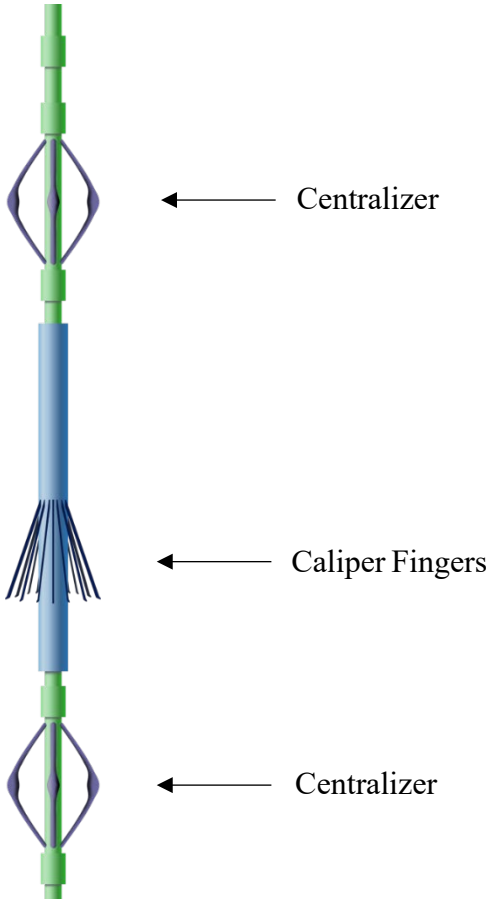

Figure 1 – Schematic of MFC Tool

Based on the findings from the preceding PRCI casing logging tool test project, interpretation of metal loss on the inner surface of the casing can be affected by the tool calibration and assumptions used by each vendor [2]. For example, if the metal loss calculation is based on the nominal casing dimensions, the casing manufacturing tolerances including diameter and ovality can introduce significant errors in metal loss depth calculation. In addition to manufacturing tolerances, in-situ pipe deformation may also introduce errors in estimating the metal loss when it is assumed that the casing is undeformed. Therefore, a more advanced interpretation algorithm is required to improve the accuracy of metal loss estimation. The calculation would need to consider variation of the radius and ovality at each reading location due to manufacturing tolerance or in-situ deformation.

The limitations of the MFC tools suggest that they are not suitable for comprehensive casing corrosion assessments. However, they can be used as a screening tool to obtain an estimate of casing corrosion condition on the inner surface of well tubulars. In many cases, the MFC tools are used along with other casing logging tools to assist interpretation of casing conditions [5,6,7].

4.1.2 - Ultrasonic Testing (UT) Tool

The UT tool provides a direct measurement of the pipe inner radius and wall thickness (WT) based on the transit time and resonant frequency of the echo of the ultrasonic signal emitted from the transducer. The resonance response can also be used to interpret the quality of the bond between

the pipe and the surrounding cement [8]. Figure 2 shows how the ultrasonic signal is interpreted to obtain several measurements of the casing and cement bond conditions. In general, the principle of this technique remains the same among various logging service vendors.

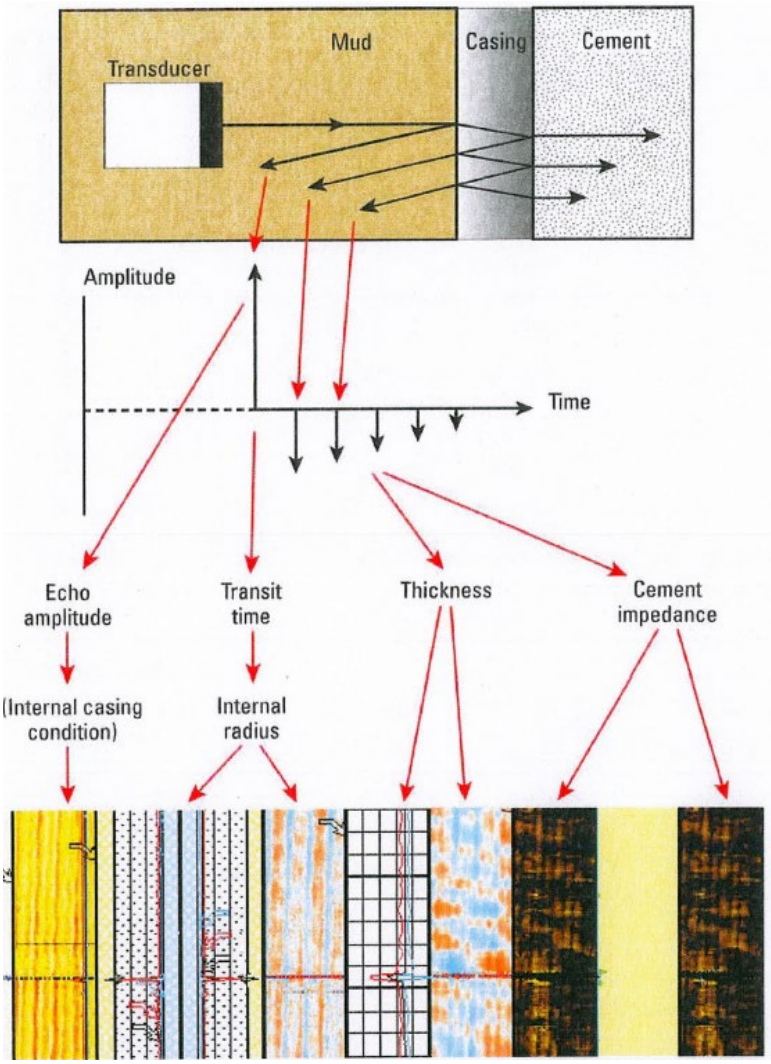

Figure 2 – UT Signal Analysis [9]

Compared to other types of casing corrosion logging tools, UT tools require the well to be filled with a fluid media to transmit the ultrasound from the tool to the pipe. The UT tool can only log the innermost pipe string, and the measurement is not affected by any metal parts on the outside of the casing.

The preceding PRCI casing logging tool test project evaluated several versions of commercial UT tools [2]. The following findings were obtained from the test results:

- The UT tool can provide qualitative information about the casing inner wall surface condition (e.g. roughness) and quantitative estimates of the casing WT. The metal loss is estimated by the deviation of the remaining WT from the original WT;

- Tool performance can vary significantly among vendors and tool models. The axial and circumferential resolution of the tools were found to have a great impact on the tool's detection capability and corrosion feature sizing accuracy. In general, higher sampling rates along both axial and circumferential directions result in an increase of the metal loss feature sizing accuracy. The circumferential sampling rate is typically a design feature of the specific tool, while the axial sampling rate varies with the logging speed; and
- The algorithm implemented by the vendor to interpret the ultrasonic signals can have a significant impact on the quality and accuracy of the interpreted results of the metal loss features.

4.1.3 - Magnetic Flux Leakage (MFL) Tool

MFL technology has been widely used in many industries to detect corrosion-induced metal loss in steel structures, such as pipelines, storage tanks and downhole tubulars. Figure 3 illustrates the technology principle of the MFL tool. The MFL tool creates a magnetic circuit to create a magnetic flux in the pipe wall. Any feature (e.g. corrosion pits, dents) or geometrical irregularity (e.g. metal loss or metal gain due to attached hardware) will cause the magnetic flux to leak from the steel. The leaked magnetic flux will be detected by the sensors mounted on the MFL tool and the signal can be analyzed to estimate the extent of the metal loss or gain. Since the primary MFL measurement does not distinguish if the corrosion features are on the internal or external surfaces of the pipe, many MFL tools also include additional components to conduct high frequency eddy current measurements. A dedicated transmitter generates a high frequency electromagnetic field, which creates eddy currents in the pipe. As the high frequency electromagnetic field can only penetrate into the near (internal) surface of the pipe, the response of the high frequency eddy current can then be used to distinguish if metal loss features are on the internal or external surface of the pipe.

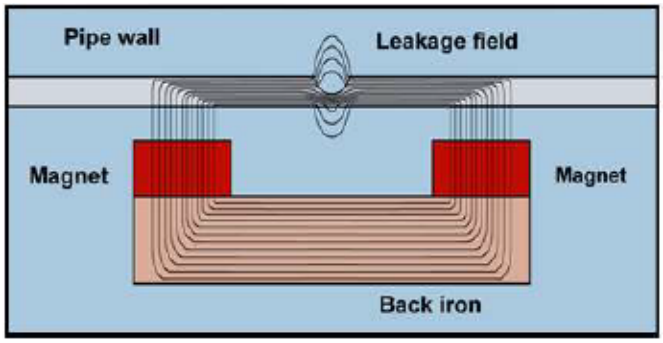

Figure 3 – Illustration of MFL Technology [5]

The preceding PRCI casing logging tool test project evaluated several versions of commercial MFL tools from different vendors [2]. In general, the test program found that, although different vendor tools rely on the same measurement principle, significant variations exist in the tool performance and final deliverables among vendors. The tools with overall best performance can provide relatively high-quality results with quantitative measurement of metal loss. Unlike UT tools, MFL tools can operate in both gas- or liquid-filled wellbores.

4.1.4 - Magnetic Eddy Current (MEC) Tool

The MEC technology is provided by one vendor (referred to as Vendor-C in this report) and this technology is relatively new to downhole casing corrosion inspection. A prototype MEC tool was

tested in the preceding PRCI casing logging evaluation project [2]. Based on the information provided by the vendor, the MEC tool is based on the eddy current testing technology that is well established for inspecting metallic components for surface flaws in the aviation and automotive industries. Although the general setup of the MEC tool is similar to the more widely used MFL tools, the MEC tool measures the impedance change of the coil in the tool for both the far-side (e.g. pipe external surface) and near-side (e.g. pipe internal surface) features. Figure 4 shows a schematic of the measurement principle of the MEC tool.

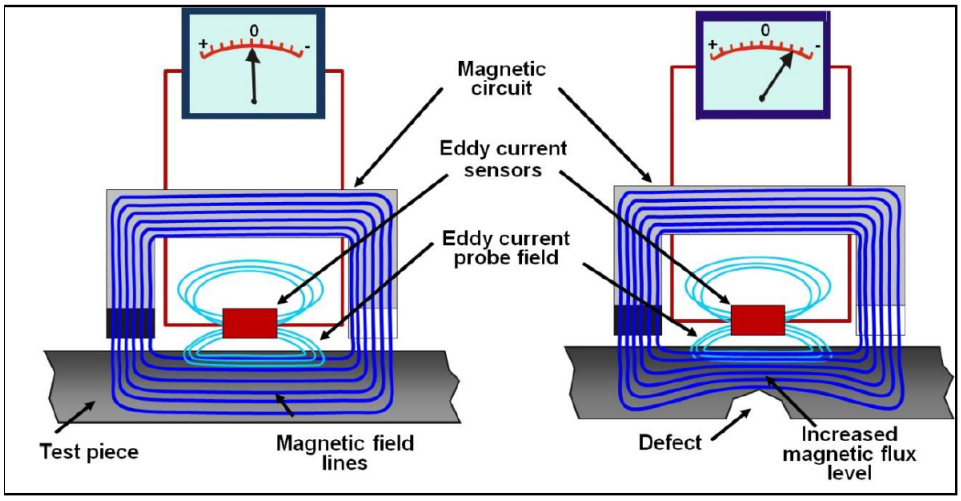

Figure 4 – Measurement Principle of the MEC Tool (from Vendor-C Logging Test Report)

As described in the vendor logging test report, the near-side measurement of this MEC tool is based on the standard eddy current measurement technique (e.g. like that used in many MFL tools for internal surface feature detection). For far-side feature measurement, the MEC tool creates a magnetic field to enable deeper penetration of the eddy current. In addition, metal loss will also cause the magnetic flux lines to concentrate and change the local magnetic permeability. The permeability change will induce an impedance change in the coil and create a signal that can be measured to detect the features on the pipe exterior. As pointed out in the vendor report, the MEC tool requires a lower magnetic field (~ 3 kA/m) than typical MFL tools (minimum 10 kA/m) to discriminate other magnetic permeability-related signals (e.g. stresses or material inhomogeneity). According to the vendor's statement, the MEC tool's lower magnetic field requirement allows inspection of smaller pipe sizes or greater WT.

Based on the preceding test program, the MEC tool was found to be able to provide a comprehensive assessment (e.g. location, size and depth) of corrosion-induced metal loss on casing specimens. This tool exhibited good performance in probability of detection (POD) and sizing accuracy and, therefore, was selected for further evaluation in this project. Details of the tool test are described in Section 5 of this report. Since the MEC tool tested in this project was the prototype version without a liquid seal, it could only operate in gas-filled wellbores.

4.1.5 - Electromagnetic (EM) Tool

Figure 5 shows a schematic of an EM logging tool. The transmitter is excited by alternating current and generates an EM field. The EM field induces eddy currents in the pipe wall. The distribution

and strength of the eddy current depends on both geometric and electromagnetic properties of the pipe, as well as the presence of metal loss features. The response of the magnetic field associated with the eddy current is then measured by the receivers mounted on the tool and interpreted to obtain the local average pipe WT. Note that this is different from MFL tools, which use the measured magnetic flux anomalies to detect metal loss features.

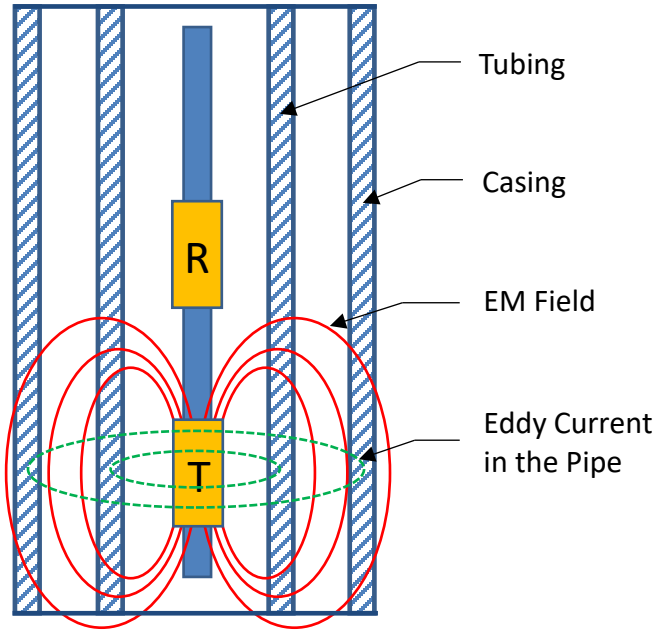

Figure 5 – Schematic of the EM Logging Tool

EM tools are the only technology that are capable of inspecting through multiple casing strings. Significant variations in the configurations of the EM tools exist among vendors. Some EM tools measure the total WT of all layers of casing strings [10]. When using multiple frequencies and different transmitter-receiver pairs, response from individual casing strings can be measured and interpretated to estimate the WT separately [11,12]. Some EM tools operate by generating pulsed eddy currents and analyze the decay response in the time domain [11,13], while others operate with continuously transmitting EM signal and analyze the response in the frequency domain [12].

The unique multi-layer measurement capability of the EM technology has attracted great attention in recent years. Most importantly, it eliminates the need to pull the tubing string for casing logging, offering the opportunity to significantly reduce the cost for casing inspection. An additional benefit is that it offers the benefit of inspecting surface casing without excavation [14].

The majority of the public literature on EM tools is based on case studies, mostly by individual vendors and operators. A few quantitative evaluation programs of EM tools were identified in the literature and are described below. In addition, findings from the preceding PRCI casing logging test project [2] are also presented as additional reference.

Petroleum Development of Oman (PDO) EM Tool Evaluation Program

In 2016, the Petroleum Development of Oman (PDO) conducted a comprehensive yard test to evaluate the capability of EM corrosion logging technology [15]. Multiple service providers anonymously participated in this test program. The vendors claimed their tools were able to quantitatively estimate the WT for each casing string ("layer") for up to three layers of concentric casing strings. The logging tool test setup included four sets of multiple layers (two or three layers) of concentric casing samples. The casing samples were setup horizontally and the logging tools were pulled through the inner casing during the logging test. Multiple machined features with varying size, geometry and orientation were made on the casing samples, as shown in Figure 6.

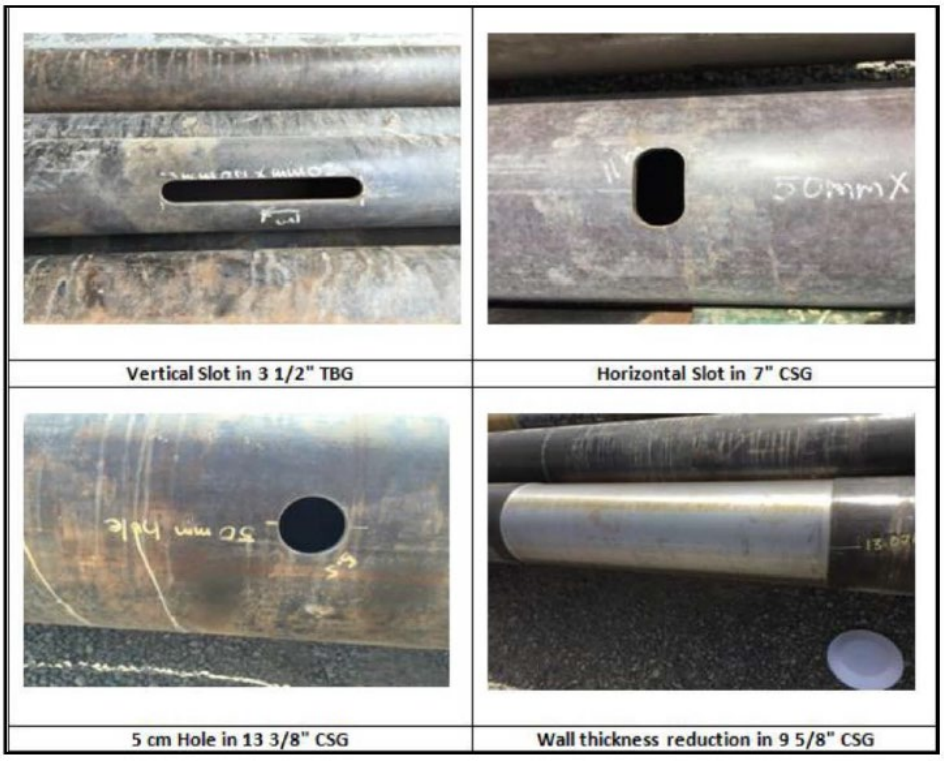

Figure 6 – Examples of Machined Features in PDO Test Program [15]

The test program led to some key findings:

- The final WT estimates were found to be sensitive to the data processing and interpretation by the individual interpreter, despite general consistency in raw data from the different tools;
- The per-layer WT estimation uncertainty was found to be around ±10%;
- The accuracy of WT estimation decreases from the first layer to the outermost layer due to signal deterioration, interference of previous layers and low signal-to-noise ratio when further from the tool;
- The EM log was found to be very sensitive to tubular eccentricity and magnetized material, which can result in misleading interpretation; and
- EM log technology is most suitable for generic corrosion investigation and is not applicable for detecting discrete features (e.g. holes, localized pitting, tiny full-wall penetration). For

example, holes as large as 2 in (5 cm) in diameter machined on all casing layers were not detected by the tools tested.

PRCI Casing Corrosion Logging Tool Test Program

Two versions of commercial EM tools from one commercial vendor were tested in the previous PRCI casing corrosion logging tool evaluation project [2]. The test results from these tools led to the following findings:

- The tools can provide a total WT measurement through multiple layers of casing strings. However, these tools do not measure casing WT in each separate layer; and
- The EM tools cannot perform comprehensive casing corrosion assessments for isolated local metal loss features because the tools do not provide the information required for remaining burst strength calculation (specifically depth, length and width measurements of discrete features).

Therefore, the two independent studies on EM tools resulted in a key conclusion that these tools are not suitable for inspecting discrete corrosion features. The same statement was also made by Mishkhes et al. [16] and Jain et al. [17].

Individual EM Tool Test

In addition to the two independent studies, a pull test was performed by Fouda et al. [12] to quantitatively evaluate the performance of their EM tool. Figure 7 shows the picture of the test setup with pipe specimens lying horizontally in a yard. Relatively large metal loss features (axial length of 2 to 10 ft and wall loss of 7.6% to 65%) were made on five concentric layers of casing strings in the outer diameter (OD) range of 2-7/8 in to 18-5/8 in. It was noted in the paper that the EM tool tested used continuous wave eddy current (EC) technique and conducted the measurement in the frequency domain. The author stated that this technique yields higher signal-to-noise ratios, especially for long-spaced receivers, which provide high quality measurement for outer pipes. The metal loss measurements by the EM tool were compared with the more accurate measurement by UT thickness gauge. The quantitative sizing accuracy evaluation led to a few key findings:

- The average error was found to be less than 7% of the WT;
- Some larger errors were identified due to factors including small features (axial length < 2 ft) and overlapping features at multiple pipes at the same axial location; and
- Pipe eccentricity also introduced some errors.

Figure 7 – Yard Test Setup of EM Tool [12]

Based on the findings described above, it was concluded that EM tools have the ability to measure the WT of multiple layers of casing strings, either separately for each layer or the total thickness for all layers, depending on the specific vendor tool configurations. However, these tools cannot differentiate whether the metal loss is around the entire circumference of the pipe or within a local area. Therefore, EM tools provide low resolution measurements of WT that may be used for estimating general casing wall loss. However, EM tools are not suitable for detailed remaining strength assessments that require detailed dimensions of metal loss features.

Various approaches have been proposed where a combination of several logging tools were used to assist evaluation of WT of multiple layers of casing strings by EM tools. For example, a combination of UT and EM tools can be used to inspect both tubing and casing separately, as described by Zaini et al. [18] and Valstar [7], where the external casing WT can be estimated by subtracting the tubing thickness (measured by the UT tool) from the total thickness (measured by the EM tool). Alaref et al. [6] used an EM tool, along with MFC, cement bond, noise and temperature logging tools, to assess well integrity. Kantyukov et al. [19] used a combination of EM, noise, temperature and pulsed neutron logs to diagnose the integrity of UGS wells.

The EM logging technology is continuously evolving. Further study and quantitative evaluation of different versions of EM tools are warranted to provide useful information for operators to help make informed decisions about the most appropriate tools to be used. The outcome of the evaluation program would also benefit service providers in terms of making improvements to their tools to better serve the industry's need.

4.2 - Remaining Burst Strength Prediction Methods

Various remaining burst strength prediction methods for corroded pipes are available and have been adopted by several industry standards. Most of the existing methods are based on the general form of equation shown in Equation (1).

$$S_F = S_{flow} \frac{1 - \frac{A}{A_0}}{1 - \frac{1}{M}\left(\frac{A}{A_0}\right)} \tag{1}$$

where

S_F is the nominal pipe body hoop stress limit at failure,
S_{flow} is the flow stress as a function of yield strength and/or ultimate strength,
A is the cross-section area of the metal loss,
A_0 is the nominal cross-section area of the pipe wall, and
M is the Folias factor to account for the stress concentration due to the bulging effect at the metal loss location.

Note that both A and A_0 are perpendicular to the primary load (e.g. hoop stress when the pipe is subjected to pure internal pressure). In addition, the longitudinal length (L) of the metal loss is often incorporated in the burst models through a non-dimensional parameter ($\frac{L}{\sqrt{Dt}}$) that also accounts for the fact that the 'length effect' is influenced by both the outer diameter (D) and wall thickness (t) of the pipe. The length parameter is often used in various methods as a threshold for how the cross-section area of the metal loss should be estimated. Equation (1) reflects the impact of the metal loss on the nominal hoop stress limit at ductile rupture.

The relationship between the internal pressure and the nominal pipe hoop stress is based on the Barlow's equation (see Equation (2)). The different methods use either the nominal OD or mid-wall diameter in the burst prediction model.

$$P_F = \frac{2S_F}{D/t} \tag{2}$$

Note that these methods are all based on the assumption that the primary failure mode is ductile rupture. These methods are only applicable when the following conditions are satisfied:

- The metal loss features are blunt (i.e. no crack-like elements) and the material is fully ductile. If these constraints do not apply, failure may be precipitated by fracture, which depends on material toughness, and capacity should therefore be assessed using a fracture mechanics approach;
- The primary load is internal pressure, while other loads, such as axial tension/compression, bending, external pressure and shear, are relatively insignificant. Excessive loads other than internal pressure could result in different pipe failure modes (e.g. necking, buckling, collapse), which require evaluation using different methods;

- The pipe has no significant cross-sectional deformation, such as dents, which may cause a significant change in the stress distribution compared to a non-deformed pipe; and
- The maximum depth of the metal loss does not exceed approximately 80% to 85% of the nominal WT.

This section describes the details of several models that are commonly used to assess corroded pipes in various industries. The ability to account for additional axial loads in remaining burst strength calculations offered by selected models are also briefly described.

4.2.1 - ASME B31G Method

The ASME B31G method is one of the most popular methods for determining the remaining strength of corroded pipelines. It is referred to as the "Original B31G" in the Level 1 evaluation procedure described in ASME B31G [20]. The ASME B31G method uses a hoop stress failure limit defined as:

$$S_F = S_{flow}\frac{1-\frac{2}{3}\left(\frac{d}{t}\right)}{1-\frac{2}{3}\frac{1}{M}\left(\frac{d}{t}\right)} \qquad \text{for } \left(\frac{L}{\sqrt{Dt}}\right)^2 \le 20 \tag{3}$$

$$S_F = S_{flow}\left(1-\frac{d}{t}\right) \qquad \text{for } \left(\frac{L}{\sqrt{Dt}}\right)^2 > 20 \tag{4}$$

where $S_{flow} = 1.1\sigma_{SMYS}$ (recommended to keep consistency with the earlier edition)

$$M = \sqrt{1+0.8\left(\frac{L}{\sqrt{Dt}}\right)^2} \tag{5}$$

Note that Equation (3) assumes a parabolic shape for the metal loss cross-section area, where *d* is the maximum depth of the metal loss.

ASME B31G also notes three options of flow stress definition that may be used, but does not prescribe the conditions in which each method should be used. Note that S_{flow} was defined as 1.1 × specified minimum yield strength (SMYS) in previous editions of B31G, and this definition is recommended to be used in the Level 1 assessment. In addition, S_{flow} shall not exceed the specified minimum tensile strength (SMTS).

4.2.2 - Modified ASME B31G Method

The modified B31G method [20] was developed with the intention to slightly reduce the conservatism in the original B31G method. The hoop stress failure limit is defined as:

$$S_F = S_{flow}\frac{1-0.85\left(\frac{d}{t}\right)}{1-0.85\frac{1}{M}\left(\frac{d}{t}\right)} \tag{6}$$

where

$$S_{flow} = \sigma_{SMYS} + 10 \text{ ksi (based on statistical fit to line pipe test database)} \quad (7)$$

$$M = \sqrt{1 + 0.6275\left(\frac{L}{\sqrt{Dt}}\right)^2 - 0.003375\left(\frac{L}{\sqrt{Dt}}\right)^4} \quad \text{for } \left(\frac{L}{\sqrt{Dt}}\right)^2 \leq 50 \quad (8)$$

$$M = 0.032\left(\frac{L}{\sqrt{Dt}}\right)^2 + 3.3 \quad \text{for } \left(\frac{L}{\sqrt{Dt}}\right)^2 > 50 \quad (9)$$

4.2.3 - CSA Method

A variation on the modified B31G model is provided in Canadian Standards Association (CSA) Z662-19 Annex O [21] for use in reliability-based integrity assessment of pipelines. The hoop stress failure limit is defined as:

$$S_F = S_{flow}\frac{1 - \left(\frac{d_{ave}}{t}\right)}{1 - \frac{1}{M}\left(\frac{d_{ave}}{t}\right)} \quad (10)$$

where

M has the same definitions as Equations (8) and (9),
d_{ave} is the average metal loss depth, which in the absence of a depth profile is assumed to be related to the maximum depth by:
$d_{ave} = \frac{1}{b}d$ (b is the maximum-to-average ratio with a mean of 2.08), and (11)

$S_{flow} = 0.9\sigma_u$, if SMYS > 35 ksi (σ_u is the ultimate tensile strength) (12)

4.2.4 - RSTRENG Effective Area Method

The RSTRENG effective area method was developed simultaneously with the modified ASME B31G method by Battelle and is documented in ASME B31G [20]. The RSTRENG effective area method requires a river bottom profile of the corroded area through a more accurate characterization of the corrosion feature. This is typically done by performing corrosion depth measurement along several axial profiles on the pipe and combining the measurements to obtain the most critical thickness profile (CTP) of the metal loss area. Calculation of the failure pressure for each possible subsection of the total feature profile is conducted using Equation (13) iteratively to obtain the minimum predicted failure pressure. The RSTRENG effective area method often provides a less conservative burst pressure prediction than the modified B31G method. The hoop stress failure limit is defined as:

$$S_F = S_{flow}\frac{1-\frac{A^i}{A_0^i}}{1-\frac{1}{M^i}\left(\frac{A^i}{A_0^i}\right)} \tag{13}$$

where

A^i is the cross-section area of the metal loss for subsection *i* within the CTP,
A_0^i is the nominal cross-section area of the pipe wall for subsection *i* within the CTP,

$$S_{flow} = \sigma_{SMYS} + 10 \text{ ksi} \tag{14}$$

$$M^i = \sqrt{1 + 0.6275\left(\frac{L}{\sqrt{Dt}}\right)^2 - 0.003375\left(\frac{L}{\sqrt{Dt}}\right)^4} \quad \text{for } \left(\frac{L}{\sqrt{Dt}}\right)^2 \le 50 \tag{15}$$

$$M^i = 0.032\left(\frac{L}{\sqrt{Dt}}\right)^2 + 3.3 \quad \text{for } \left(\frac{L}{\sqrt{Dt}}\right)^2 > 50 \tag{16}$$

4.2.5 - LPC-1 / BS 7910 / DNVGL-RP-F101 Methods

The Line Pipe Corrosion (LPC) method was developed through a group sponsored project led by Germanischer Lloyd. This study led to further development of the methods incorporated into the British standard BS 7910 [22] and DNVGL recommended practice DNVGL-RP-F101 [23].

The Level 1 assessment model in the LPC method (referred to as LPC-1) has a form similar to the ASME B31G and the modified ASME B31G models. In addition, there is also a slight difference between the LPC-1, BS 7910 and DNVGL-RP-F101 models in terms of the flow stress definition. The hoop stress failure limit is estimated as:

$$S_F = S_{flow}\frac{1-\left(\frac{d}{t}\right)}{1-\frac{1}{M}\left(\frac{d}{t}\right)} \tag{17}$$

where

$$M = \sqrt{1 + 0.31\left(\frac{L}{\sqrt{Dt}}\right)^2} \quad \text{for all lengths} \tag{18}$$

$$S_{flow} = \sigma_{SMTS} \quad \text{LPC-1 (for } \frac{d}{t} \le 0.85\text{)} \tag{19}$$

$$S_{flow} = (\sigma_{SMYS} + \sigma_{SMTS})/2 \quad \text{BS 7910 (for } \frac{d}{t} \le 0.8\text{)} \tag{20}$$

$$S_{flow} = \sigma_{SMTS} \qquad \text{DNVGL-RP-F101 (for } \frac{d}{t} \leq 0.85) \tag{21}$$

The burst pressure is then estimated as:

$$P_F = \frac{2S_F}{(D-t)/t} \tag{22}$$

Note that the mid-wall diameter was used instead of the OD in the pressure versus hoop stress equilibrium condition in Equation (22). Note also that a factor of 1.05 is applied to the predicted burst pressure in DNVGL-RP-F101 to get the best estimate, based on the comparison with the lab test results.

Biaxial Stress Effect in BS 7910

BS 7910 [22] provides a method for evaluating the biaxial (i.e. axial and hoop) stress effect based on the Tresca yield criterion. For a local thinned area (LTA) in a cylinder, the hoop stress is estimated by Equation (23).

$$\sigma_{ref2} = \frac{1 - \frac{1}{M}\left(\frac{d}{t}\right)}{1 - \left(\frac{d}{t}\right)}\sigma_2 \tag{23}$$

where σ_2 is the hoop stress in the cylinder (without metal loss).

The axial stress can be estimated by:

$$\sigma_{ref1} = \frac{\pi\left(1 - \frac{d}{t}\right) + 2\frac{d}{t}sin\left(\frac{c}{D}\right)}{\left(1 - \frac{d}{t}\right)\left[\pi - \left(\frac{c}{D}\right)\frac{d}{t}\right]}\sigma_1 \tag{24}$$

where

c is the circumferential width of the metal loss area, and
σ_1 is the axial stress in the pipe body.

The reference stress solution is taken as:

$$\sigma_{ref} = \begin{cases} max\left(\sigma_{ref1}, \sigma_{ref2}\right) & \text{for } \sigma_1 \geq 0 \text{ and } \sigma_2 \geq 0 \\ \sigma_{ref2} - \sigma_{ref1} & \text{for } \sigma_1 < 0 \text{ and } \sigma_2 > 0 \end{cases} \tag{25}$$

A safety factor is then applied to the reference stress and checked against the flow stress (i.e. $(\sigma_{SMYS} + \sigma_{SMTS})/2$). The LTA is acceptable if the resulting reference stress is less than the flow stress.

Biaxial Stress Effect in DNVGL-RP-F101

DNVGL-RP-F101 [23] also provides a method for assessing corrosion features subjected to combined internal pressure and axial compressive stress. However, it is noted in the recommended practice that validation of this method is not as comprehensive as that of the method for assessing corrosion features under internal pressure only. This method uses a single factor, H_1, to account for the axial compressive load effect by:

$$S_{comp} = H_1 \cdot S_F \tag{26}$$

where

$$H_1 = \frac{1 + \frac{\sigma_L}{f_u}\frac{1}{A_r}}{1 - \frac{1}{2A_r}\frac{1 - \left(\frac{d}{t}\right)}{1 - \frac{1}{M}\left(\frac{d}{t}\right)}} \tag{27}$$

$$A_r = 1 - \frac{d}{t}\theta \tag{28}$$

$$\theta = \frac{c}{\pi D} \tag{29}$$

σ_L is the axial compressive stress in the pipe body,
f_u is the tensile strength to be used in the design (i.e. a function of σ_{SMTS}, temperature derating value and material strength factor), and
c is the circumferential length (width) of the metal loss area.

The predicted failure pressure is taken as the minimum of the prediction values for the internal pressure only and combined loading conditions.

The recommended practice also notes that it is not necessary to include the axial compressive stress effect if it is within the following limit:

$$\sigma_L > -0.5 f_u \frac{1 - \left(\frac{d}{t}\right)}{1 - \frac{1}{M}\left(\frac{d}{t}\right)} \tag{30}$$

4.2.6 - API 579-1 Method

API 579-1/ASME FFS-1 Fitness-For-Service [24] Part 5 (Assessment of Local Metal-loss) provides methods for the assessment of local metal loss in pressure vessels, piping, storage tanks, etc. Although the standard was developed for use in the refining and petrochemical industry, the assessment methods were established on a similar technical basis as other remaining burst strength prediction methods described in this section and, therefore, are considered in this study. API 579-1

includes three assessment levels, with Level 1 and Level 2 assessment methods relying on analytical equations, and Level 3 assessment normally requiring numerical analysis. This section includes a brief description of the Level 1 and Level 2 assessment methods, both of which include assessment of the axial stress effect for cylindrical shell component.

Level 1 Assessment Method

The Level 1 method is based on a similar form as ASME B31G and other methods, and uses the minimum remaining WT to determine the remaining strength factor (*RSF*):

$$RSF = \frac{R_t}{1 - \frac{1}{M_t}(1 - R_t)} \tag{31}$$

where R_t is the remaining thickness ratio (defined as the percentage of the minimum remaining WT over the original WT) and M_t is the Folias factor for the cylindrical shell defined in a complex form shown in Equation (32).

$$\begin{aligned} M_t = {} & 1.0010 - 0.014195\lambda + 0.29090\lambda^2 - 0.096420\lambda^3 + 0.020890\lambda^4 \\ & - 0.0030540\lambda^5 + 2.9570(10^{-4})\lambda^6 - 1.8462(10^{-5})\lambda^7 \\ & + 7.1553(10^{-7})\lambda^8 - 1.5631(10^{-8})\lambda^9 + 1.4656(10^{-10})\lambda^{10} \end{aligned} \tag{32}$$

where λ is the longitudinal flaw length parameter defined as:

$$\lambda = \frac{1.285s}{\sqrt{D_i t}} \tag{33}$$

where D_i is the inside diameter and *t* is the original WT.

The reduced maximum allowable working pressure ($MAWP_r$) can be calculated by:

$$MAWP_r = RSF \cdot \frac{St}{R_i + 0.6t} \tag{34}$$

where *S* is the allowable stress and R_i is the inside radius. Since API 579-1 does not specify the allowable stress for casing, the flow stress definitions considered in other remaining burst strength models may be used.

In addition, API 579-1 also requires evaluation of the circumferential length of the metal loss for cylindrical shells. However, the evaluation follows an extremely conservative approach by assuming a uniform wall loss using the minimum remaining WT in calculating the longitudinal stress. Therefore, this approach seems to be inappropriate for the purpose of this study. Note that significant revisions were made in assessing the circumferential extent of the LTA between the 2007 version and the 2016 version of the API 579-1.

Level 2 Assessment Method

The Level 2 assessment method follows a similar approach as the RSTRENG effective area method to determine the RSF for each possible subsection of the total metal loss profile using the following equation:

$$RSF^i = \frac{1 - \left(\frac{A^i}{A_o^i}\right)}{1 - \frac{1}{M_t^i}\left(\frac{A^i}{A_o^i}\right)} \tag{35}$$

where

M_t^i is the folias factor for subsection *i* determined using Equation (32),
A^i is the cross-section area of the metal loss for subsection *i* within the LTA, and
A_o^i is the original cross-section area of the pipe wall for subsection *i* within the LTA.

The minimum value of the RSF for all subsections is used in the assessment. Therefore, this method requires characterization of the details of the metal loss profile.

For cylindrical structures, the circumferential stress in the LTA can be calculated by:

$$\sigma_{cm} = \frac{P}{RSF}\left(\frac{D_i}{D - D_i} + 0.6\right) \tag{36}$$

where P is the internal pressure and D is the OD.

The Level 2 method also provides a procedure to evaluate the circumferential extent of the metal loss feature (i.e. longitudinal stress effect). For cylindrical structures, the longitudinal stress in the LTA is calculated by:

$$\sigma_{lm} = M_s^C \left\{\frac{A_w}{A_m - A_f}P + \frac{F}{A_m - A_f} + \frac{y}{I_{\bar{X}}}[F\bar{y} + (\bar{y} + b)PA_w + M_x] + \frac{x}{I_{\bar{Y}}}M_y\right\} \tag{37}$$

where

$$M_s^C = \frac{1 - \frac{1}{M_t^C}\frac{d}{t}}{1 - \frac{d}{t}} \tag{38}$$

$$M_t^C = \frac{1.0 + 0.1401(\lambda_c)^2 + 0.002046(\lambda_c)^4}{1.0 + 0.09556(\lambda_c)^2 + 0.0005024(\lambda_c)^4} \tag{39}$$

$$\lambda_c = \frac{1.285c}{\sqrt{Dt}} \tag{40}$$

M_s^C is the Folias factor based on the circumferential extent of the LTA for a surface flaw,
M_t^C is the Folias factor based on the circumferential extent of the LTA for a through-wall flaw,
λ_c is the circumferential flaw length parameter,
c is the circumferential length of the local metal loss area,
A_w is the effective area on which pressure acts,
A_m is the cross-section area of the cylindrical structure, and
A_f is the cross-section area of the region of local metal loss.

The terms $\frac{y}{I_{\bar{X}}}[F\bar{y} + (\bar{y} + b)PA_w + M_x]$ and $\frac{x}{I_{\bar{Y}}}M_y$ in Equation (37) account for the axial stress due to bending moments. The details of these two terms can be found in API 591-1. In general, Equation (37) calculates the axial stress using the fundamental elasticity solutions for beams, along with the Folias factors accounting for the local stress condition within the metal loss area.

In addition, the API 579-1 also provides an equation to calculate the shear stress component, s, then the VME can be calculated by:

$$\sigma_{eq} = (\sigma_{cm}^2 - \sigma_{cm}\sigma_{lm} + \sigma_{lm}^2 + 3s^2)^{0.5} \tag{41}$$

The VME is compared to the flow stress. A failure is predicted to occur if the VME is equal to or larger than the flow stress.

This approach was adopted in previous research conducted by Francini et al. [25] to investigate the axial load effects on the remaining strength of corroded casing. Based on a review of the report by Francini et al., it appears that the Folias factor M_s^C in Equation (37) was not included in Francini et al.'s model and the reason is unclear.

5 - Casing Corrosion Logging Tool Evaluation

5.1 - Overview

The preceding PRCI casing corrosion logging tool test program evaluated the performance of several casing corrosion logging techniques and tools [2]. Five vendors participated in the logging tool test program. Five logging techniques (i.e. MFC, UT, MFL, MEC and EM), represented by a total of 11 tools, were tested. The test setup included a 4.5 inch casing string and a 7.0 inch casing string in a concentric configuration. Prior to the test, all vendors were provided with only basic information about the general test well setup (tubing and casing size, weight, grade, total length, dual string configuration, etc.) that was necessary for their test planning. Details of the metal loss features were not disclosed, making it a true "blind" test that eliminated any potential bias. Upon completion of the test program, three tools that demonstrated overall better performance than others were selected for further test evaluation in this project. This test program included three of the most common casing sizes (4.5 inch, 5.5 inch and 7.0 inch) used in depleted reservoir storage wells.

Table 2 lists the three logging tools selected for this project's testing program. As per the agreement with the vendors, each of the vendor tools is referenced based on the generic technology and vendor names were kept anonymous. For consistency, the vendor ID and tool name remained the same as in the preceding PRCI project. Further details of the three logging tools are described in Appendices B, C and D.

Table 2 – Participating Vendors and Logging Tools

Vendor	Logging Tool
B	Ultrasonic Tool – 2 (UT-2)
C	Magnetic Eddy Current (MEC) tool
D	Magnetic Flux Leakage (MFL) tool

5.2 - Test Setup and Procedure

5.2.1 - Test Setup

Figure 8 shows the well completion setup for the logging tool test. The three casing strings were supported from the hanging plate in a parallel configuration. This setup allowed vendors to log three casing strings without changing the test setup and it maximized the project execution efficiency. The casing strings were hung in C-FER's Deep Well Simulator (DWS), a cased wellbore that is 2 ft in diameter and 150-ft deep. Non-magnetic spacers were attached between the casing strings, as well as between the casing strings and the DWS casing to ensure at least 4 in of separation to eliminate the chance of interference with magnetic-based logging tools. The vertical test well setup closely represents field condition and allows vendors to run their tools conveniently using wireline trucks. In addition, the vertical test setup also minimizes concerns such as impact of tool de-centralization on performance.

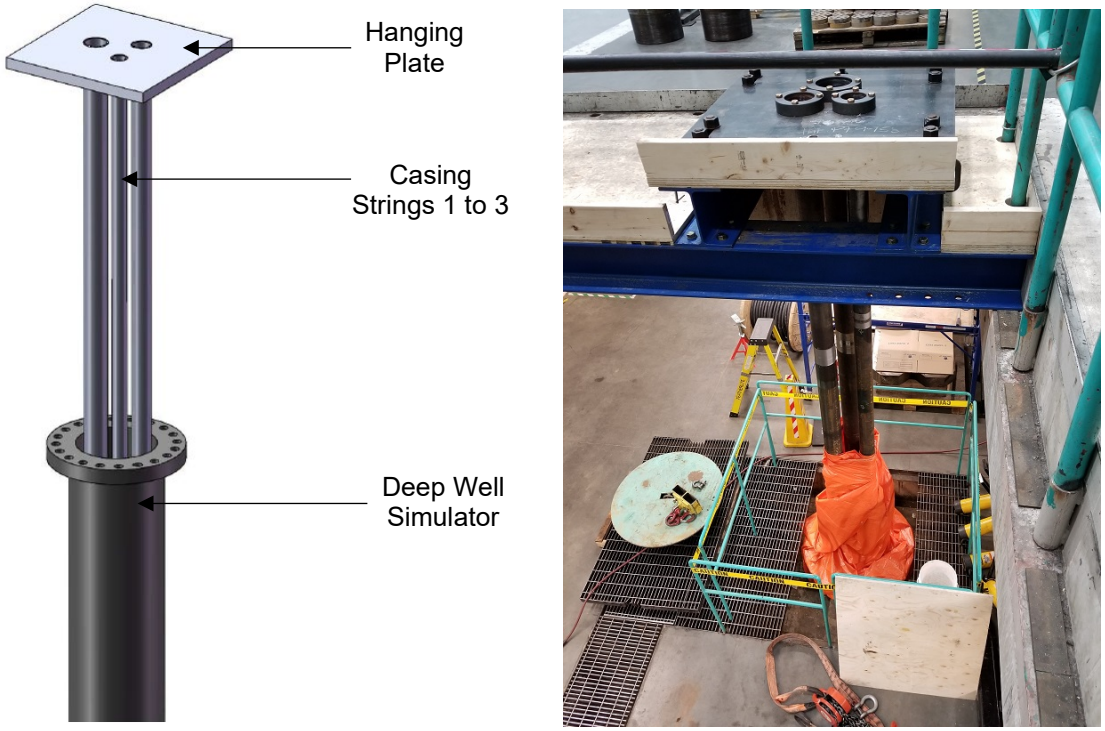

Figure 8 – Casing Corrosion Logging Tool Test Well Setup

Figure 9 illustrates the details of the casing joints, which included a combination of new joints with artificial metal loss features (blue) and used joints with natural corrosion features (orange). Selected casing joints used in the previous PRCI logging tool test program were reused in this project. Additional casing joints with artificial features were added in this project. As a result, this test program includes a variety of metal loss features covering a wide spectrum of corrosion features.

For easy reference, each casing joint ID was labelled by its OD and joint number. For example, “4.5in-JT#1” refers to the 4.5 inch casing joint number 1. Each artificial feature was labelled by “Dx”, where x is the feature number. As a result, each artificial feature can be uniquely identified by a combination of the casing joint ID and the feature ID. For example, “4.5in-JT#1-D1” refers to the feature “D1” on casing joint “4.5in-JT#1”.

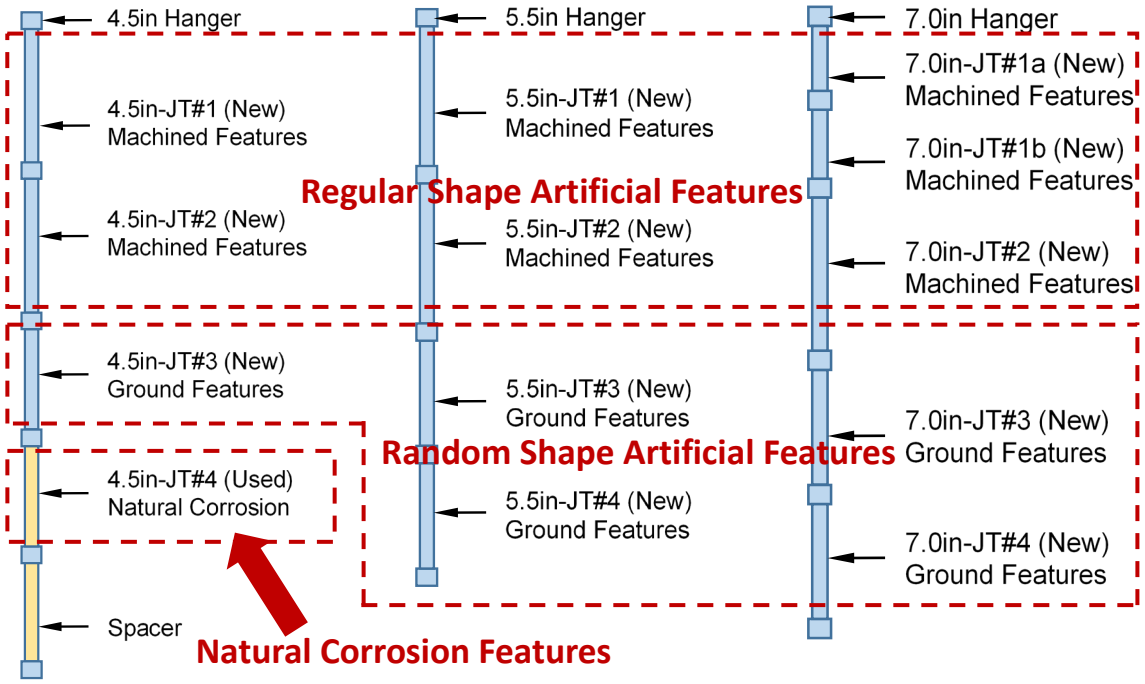

Figure 9 – Test Well Casing Joint Configurations

5.2.2 - Specimen Preparation

Regular Shape Artificial Features

A variety of artificial features were made by machining metal loss into the casing external surface, resulting in regular shape metal loss profiles. These features were designed to cover a wide range of feature categories defined by the Pipeline Operators' Forum [26], as shown in Figure 10. The maximum depths of these features are in the range of 10% to 70% of pipe WT. Figure 11 shows a few examples of the regular shape features. Details of the feature information are presented in Appendix A, including the feature design parameters, the distribution over the feature categories and pictures.

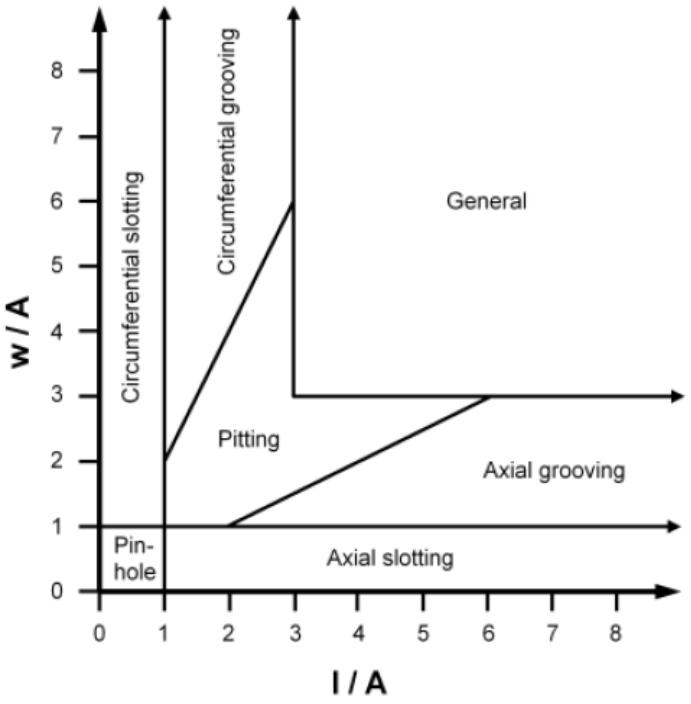

Figure 10 – Surface Dimensions of Metal Loss Features per Dimension Class [26]

Pinhole

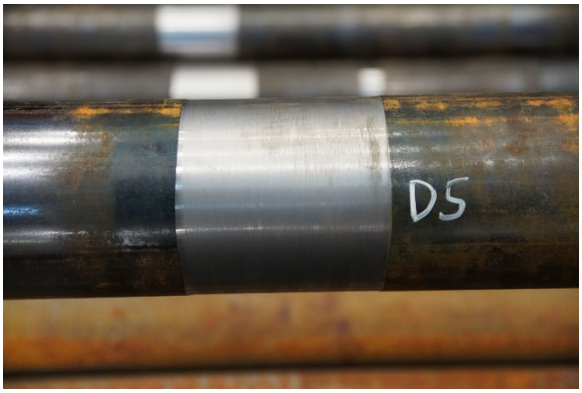

General Corrosion

Pitting

Circumferential Grooving

Pitting Cluster

Axial Grooving

Figure 11 – Regular Shape Artificial Feature Examples

The actual dimensions (length, width and maximum depth) of these features were hand measured at C-FER's lab. An ultrasonic thickness probe was used to measure the pipe WT surrounding the features. A pit gauge was used to measure the maximum wall loss of small pit-type features (where the area was too small to allow ultrasonic measurement). The feature length and width were measured using a digital caliper. These hand measurements were considered more accurate than the logging tools and, therefore, were used as the basis for sizing accuracy assessment for the corrosion logging tools in this test program.

Random Shape Artificial Features

In addition to the regular shape features, various metal loss features were manually created using a hand-held grinder, resulting in random shape profiles. These random shape features were also designed to cover a wide range of feature categories defined by the Pipeline Operators' Forum [26]. Most features have lengths and widths on the order of a few inches. The maximum depths of these features are in the range of 20% to 70% of the pipe WT, with most within the deep range of 50% to 70%. Details of these features are presented in Appendix A, including the distribution over the feature categories and example pictures.

The random shape features were laser scanned to capture the details of their profiles. The laser scan (LS) data were analyzed using C-FER's in-house feature mapping application to characterize the feature sizes as per the Pipeline Operators' Forum specifications [26], as shown in Figure 12. Furthermore, feature clusters were defined as per the flaw interaction rule (i.e. features that are within a distance of three-times the pipe WT are considered within a cluster) as specified in ASME B31G [20]. The LS results were verified using pit gauge for selected features to ensure the accuracy was sufficient for sizing accuracy assessment for corrosion logging tools.

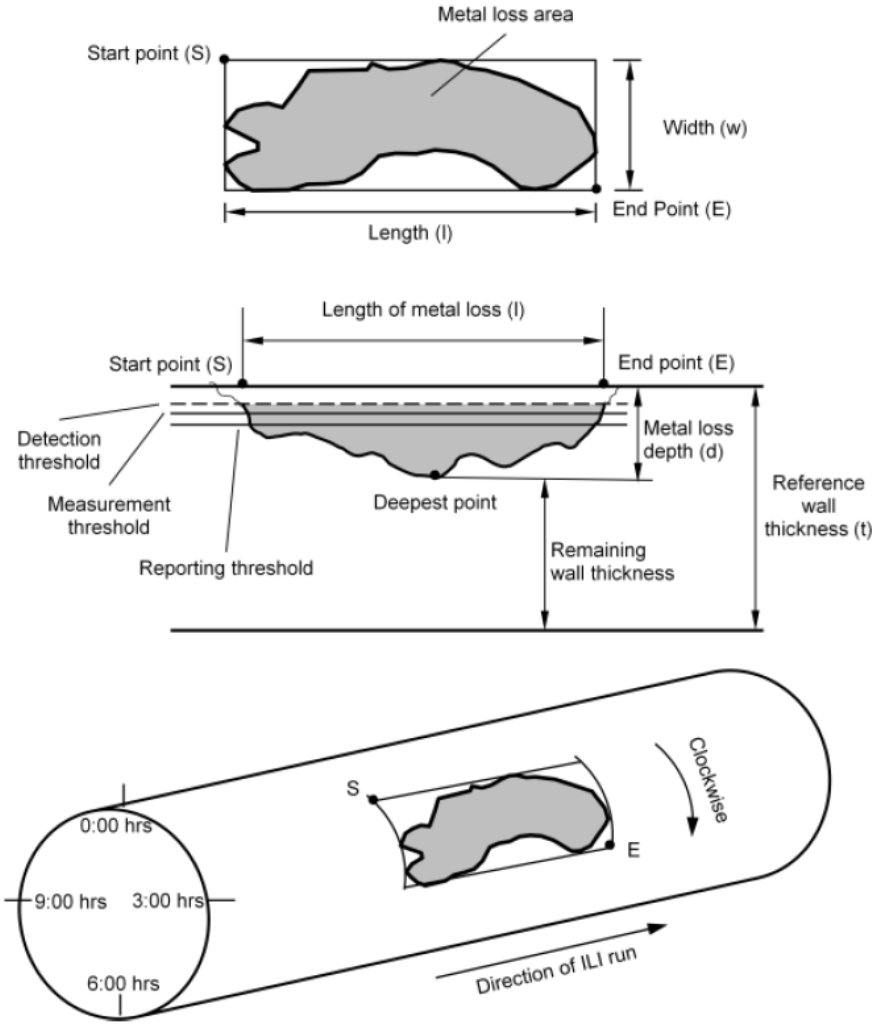

Figure 12 – Illustration of Parameters Describing Location and Dimensions of Metal Loss Feature [26]

Figure 13 shows an example of a random shape feature. The depth contour plot of this feature, analyzed from the LS data, is shown in Figure 14, where the color contour represents the amount of metal loss in terms of the percentage of casing WT. A 5% wall loss depth cutoff was used to remove minor fluctuations of the pipe surface profile. Each individual feature is enclosed by a red rectangle and the feature cluster is enclosed by a blue rectangle. The length and width of the feature or cluster is indicated by the size of the rectangle. The feature analysis results based on LS data were used to benchmark the logging tool test results in the subsequent tool performance evaluation. In addition, the green line in the contour plot represents the river bottom of the feature cluster. The river bottom profile is plotted in Figure 15. Further details for the random shape features are summarized in Appendix A.

Figure 13 – Random Shape Metal Loss Feature Example (4.5in-JT#3-D3)

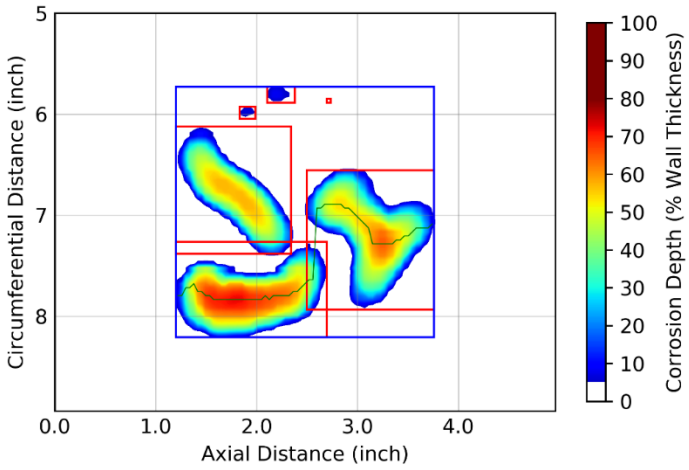

Figure 14 – Metal Loss Contour Plot from LS (4.5in-JT#3-D3)

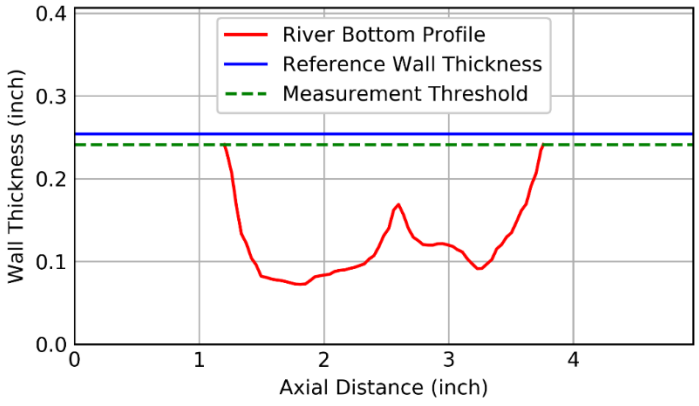

Figure 15 – Metal Loss River Bottom Profile from LS (4.5in-JT#3-D3)

Note that, upon completion of the logging tool test, Joints 4.5in-JT#3, 5.5in-JT#3 and 7.0in-JT#3 were cut into lengths to prepare burst test specimens in the subsequent full-scale test. Details of each of the metal loss features in the burst test specimens are summarized in Appendix E.

Natural Corrosion Features

The joint 4.5in-JT#4 was used in the preceding PRCI casing logging tool test program. It was supplied by PRCI and was pulled from a UGS well that had reportedly been in service since the 1940s. This joint was previously laser scanned and the natural corrosion features characterized.

Figure 16 shows an example of the natural corrosion features analyzed from the LS data. A 5% WT depth cutoff was applied to filter out minor imperfections in the pipe surface profile. Further details about these features can be found in the PRCI project report [2].

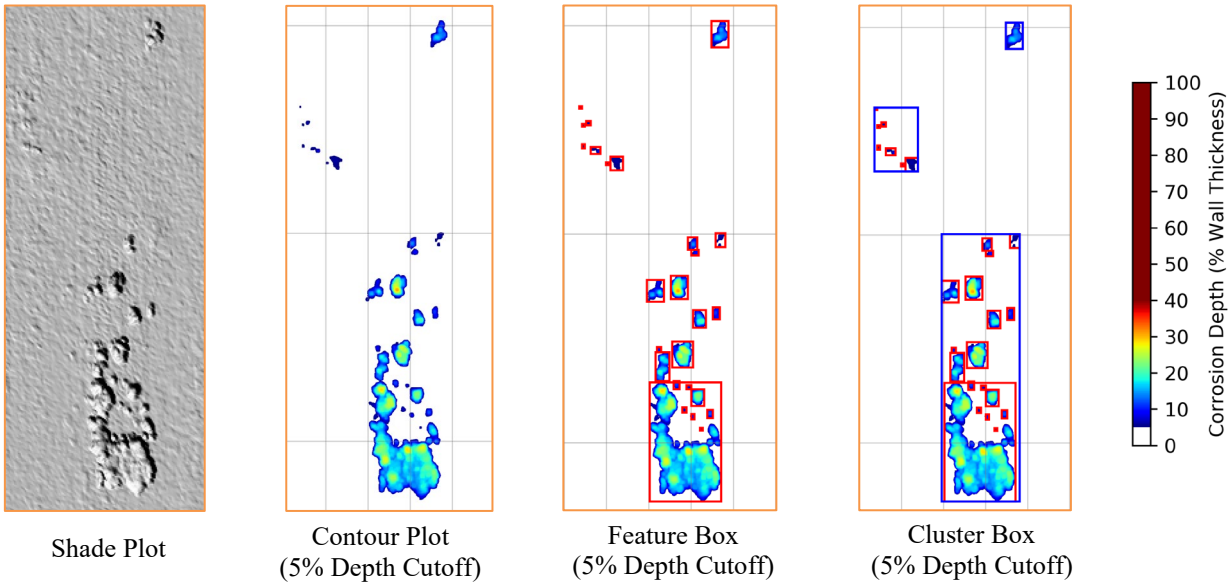

Figure 16 – Metal Loss Contour Plot Example of Natural Corrosion Features

5.2.3 - Casing Logging Tool Test

The logging tool tests were conducted in a sequence with one vendor at a time. Prior to each test, the vendor was provided with only basic information about the general test well setup (casing size, weight, grade, total length, casing string configuration, etc.) that was necessary for them to configure their tools for the test. Details of the metal loss features were not disclosed and, therefore, it was a true "blind" test for the vendors.

Figure 17 to Figure 19 show pictures of the logging tool test execution at C-FER's lab. The UT-2 and MFL tool tests were run by wireline trucks, while the MEC prototype tools were operated by an air winch. Each vendor test was completed within one or two days, depending on the logging speed and number of runs.

Figure 17 – Vendor-B's UT-2 Tool Test

Figure 18 – Vendor-C's MEC Tool Test

Figure 19 – Vendor-D's MFL Tool Test

5.3 - Tool Performance Evaluation

5.3.1 - Evaluation Approach

The logging tool performance evaluation followed the same approach as in the preceding PRCI casing logging test project [2]. Quantitative evaluation of tool performance included determination of the detection capability and sizing accuracy. The tool performance evaluation was performed separately for the regular shape artificial features, random shape artificial features and natural corrosion features.

For the regular shape artificial features, the pitting cluster (i.e. D11) was treated as a single feature instead of nine individual features, which otherwise would impose a significant weighting of the impact from this single feature on the overall performance of the tool. As such, the average size (length, width and depth) of the nine pits in the cluster was used in the sizing accuracy analysis. For the two artificial features with a pit inside an area of general corrosion (i.e. D4 and D8), the pit and the general corrosion were treated as two separate features.

The quantitative assessment of each tool's detection capability was based on two parameters: the POD, and the number of false detections. The POD is defined as the ratio between the number of detected features and the actual number of features. POD analysis was also performed for each feature category to assess the tool's response to various feature profiles.

The sizing accuracy assessment of the tool was performed by direct comparison between the reported dimensions from the logging tools and the actual dimensions (from hand measurement or LS) of the detected features. Unity charts, which contrast the relationships between the measured and actual dimensions of metal loss features, were used in the assessment. Note that the unity chart has been widely used in the pipeline industry for characterizing ILI tool sizing accuracy [1].

The metal loss feature size measurements (i.e. length, width, depth and pipe WT) conducted in C-FER's lab were considered highly accurate (with an error range of ±0.002 in) compared to the logging tools. Therefore, the effect of the lab measurement error on the logging tool sizing accuracy analysis is considered negligible. As such, any difference between the logging tool measurement and lab measurement were attributed to the logging tool sizing error. In the feature sizing accuracy analysis, all feature sizes based on lab measurements were referred to as "True Size". In the assessment, the logging tool measurements and the lab measurement (True Sizes) for each feature were represented along the y-axis and x-axis in the unity plot, respectively. The unity plot provides a quick visualization of how closely each logging tool's measurements agree with the lab measurements.

Figure 20 shows some examples of unity charts with relationships between the measured and actual dimensions of metal loss features for assumed inspection tools, including a hypothetical perfect tool (Figure 20a), and real tools with a combination of bias and scatter errors (Figures 20b through 20d). Since the hypothetical perfect tool has no measurement error, all measurement points stay on the unity line, as shown in Figure 20a. The Real Tool 1 shown in Figure 20b has scatter error but no bias error, and the slope of the linear regression line of the measurement data is close to that of the unity line. In Figure 13c, the linear regression line of Real Tool 2 has a lower slope than that of the unity line and a positive y-intercept. Therefore, Real Tool 2 tends to over-call the

feature size for small features and to under-call the feature size for large features. On the contrary, Real Tool 3 displayed in Figure 13d has a higher slope than that of the unity line and a negative y-intercept, and therefore tends to under-call small features while over-calling large features. When making decisions in casing integrity management, accurate sizing of deep features is of greater importance than for shallow features. Consequently, Real Tool 2 would lead to non-conservative decisions, while Real Tool 3 would result in conservative decisions.

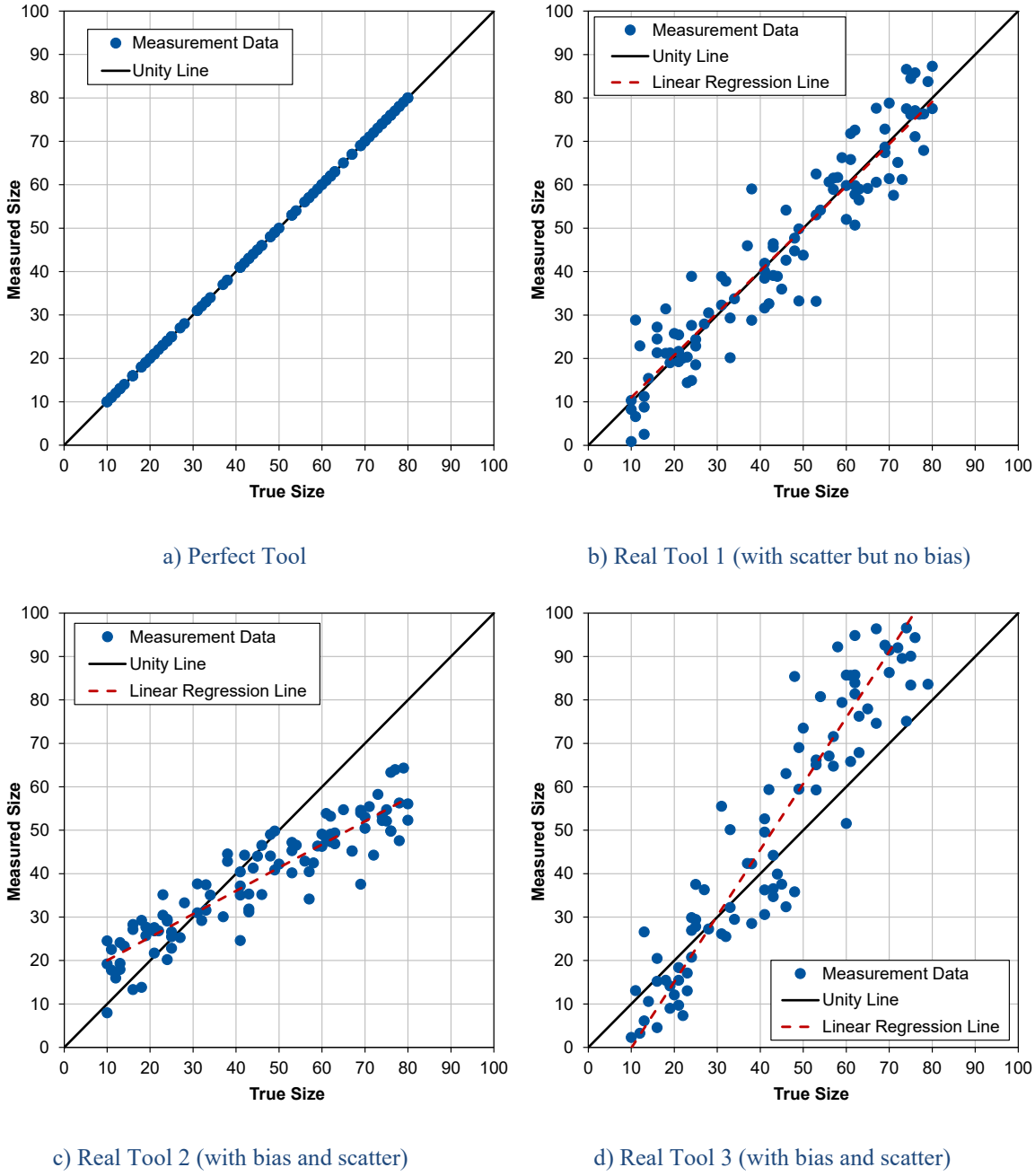

a) Perfect Tool

b) Real Tool 1 (with scatter but no bias)

c) Real Tool 2 (with bias and scatter)

d) Real Tool 3 (with bias and scatter)

Figure 20 – Unity Charts for Logging Tool Sizing Accuracy Evaluation

In addition, each tool's sizing accuracy was quantitatively evaluated using different error bands. Figure 21 shows an example unity chart with two error bands, where Error Band 1 is narrower than Error Band 2. The number of measurement points falling inside each error band relative to the total measurement points was defined as the percentage of detection. Therefore, a higher percentage of detection associated with a narrower error band indicates better sizing performance. The results were used to obtain a relative sizing accuracy performance comparison between the three logging tools tested.

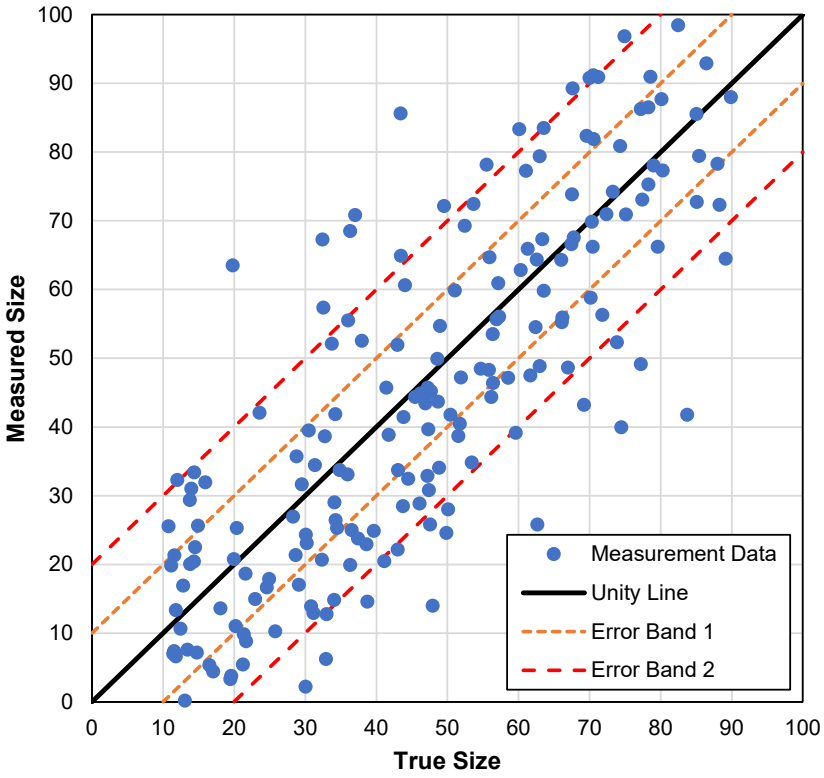

Figure 21 – Sizing Accuracy Evaluation Using Error Bands

5.3.2 - Tool Performance Results

Details of the logging tool test results are provided in Appendices B, C and D for each of the three tools. This section presents a comparison of various aspects of the performance for the three tools tested in this project. The tool performance evaluation is solely based on the results of this test program, which included a limited number of features. Additional testing with a larger feature population would help to increase the confidence level in the parameters derived to characterize tool performance.

Table 3 presents a summary of the POD and false detections of artificial features for the three logging tools. In general, all three tools showed an overall POD exceeding 80%. The UT-2 tool had the highest overall POD at 90%, and the MEC tool showed marginally higher POD than the MFL tool. All three tools showed a generally consistent response to the three different casing sizes.

In addition, it was noted that the MEC tool had a few false detections in the 4.5 inch casing joints, while the other two tools did not have any false calls.

Table 3 – Summary of POD and False Detection (Artificial Features)

Casing Size	Joint No.	Vendor-B (UT-2 Tool)		Vendor-C (MEC Tool)		Vendor-D (MFL Tool)	
		POD	Number of False Detections	POD	Number of False Detections	POD	Number of False Detections
4.5 inch	1	89%	0	89%	4	72%	0
	2	83%	0	83%	4	67%	0
	3	100%	0	100%	0	100%	0
	4	N/A	N/A	N/A	N/A	N/A	N/A
5.5 inch	1	87%	0	80%	0	80%	0
	2	87%	0	73%	0	80%	0
	3	100%	0	100%	0	100%	0
	4	100%	0	100%	0	100%	0
7.0 inch	1a & 1b	87%	0	87%	0	87%	0
	2	80%	0	73%	0	80%	0
	3	100%	0	86%	0	100%	0
	4	100%	0	88%	0	87.5%	0
Total		90%	0	85%	0	83%	0

The POD was further analyzed within each metal loss feature category to obtain an understanding of the tools' responses to different types of features. Figure 22 presents the POD values of the three tools within different categories for the regular shape artificial features. The results indicate that all three tools had difficulty detecting small pinhole features, with the MEC tool performing slightly better than the other two tools. For larger feature sizes, all three tools showed good performance in POD. It was also noted that the MEC tool missed one-third of the axial grooving features. This is a concern as long axial grooves can significantly reduce the remaining burst strength of the casing.

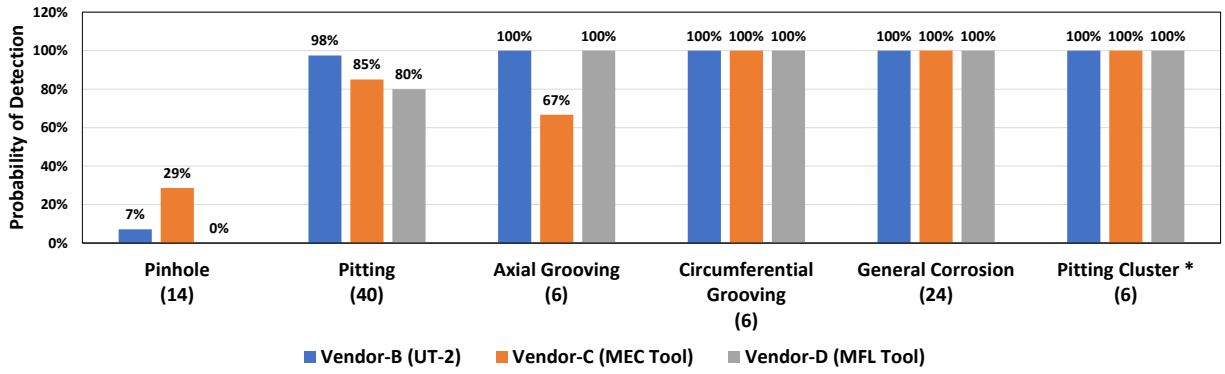

* Pitting cluster is not a feature category as per Pipeline Operators' Forum [26]. However, the pitting cluster is treated separately, as a special case, in this assessment.
** The number in the bracket indicates the total number of features in that category.

Figure 22 – POD for Various Feature Categories (Regular Shape Artificial Features)

All three tools were able to detect most natural corrosion features with significant wall loss. However, the natural corrosion features reported by each tool tended to have some large discrepancy in dimensions (length and width) with the LS results, possibly due to the tools' limited resolution or potentially different feature clustering rule used by each vendor (see Appendices B to D for details). Therefore, only feature depth results were analyzed.

Figure 23 compares the depth sizing accuracy of the three tools for artificial features. Vendor-B's UT-2 tool showed the highest accuracy for sizing the metal loss depth over a wide range of features and casing sizes. However, the remaining WTs of some deep features were below the UT-2 tool's lower bound thickness measurement limit (0.15 in). This caused a reduction of the depth sizing accuracy performance, especially for the random shape artificial features on the 4.5 inch casing, as noted in Figure 23. Details about the features that fall below the UT-2 tool's measurement limit can be found in Appendix B.

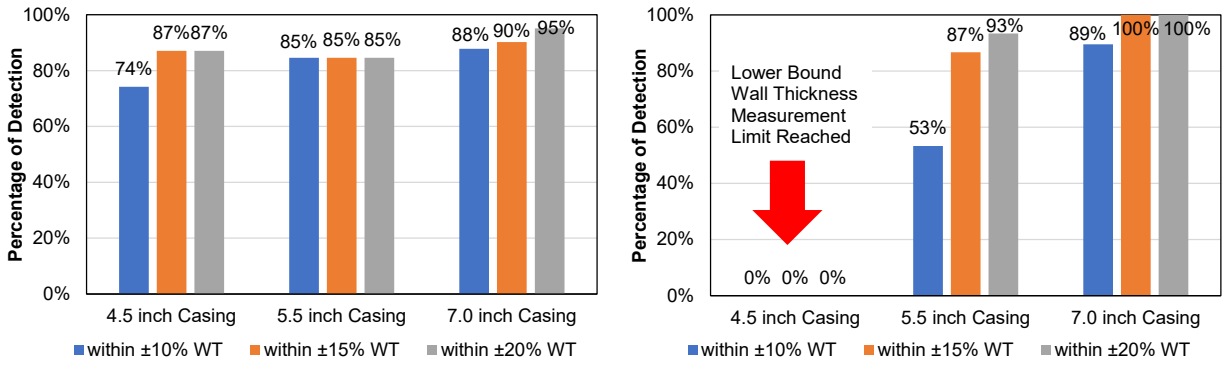

Vendor-B's UT-2 Tool

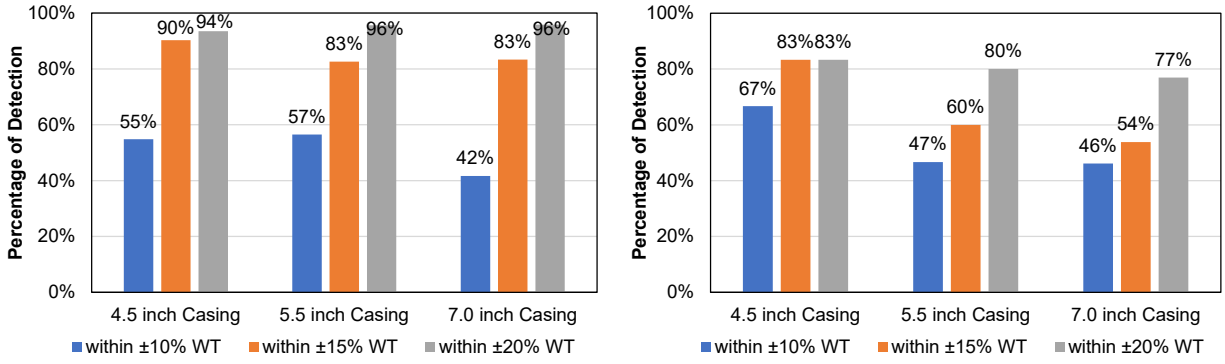

Vendor-C's MEC Tool

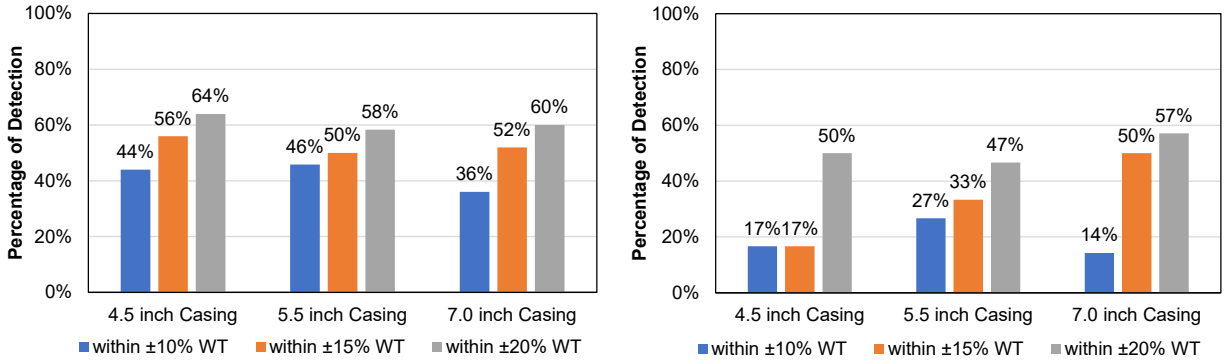

Vendor-D's MFL Tool

Regular Shape Features

Random Shape Features

Figure 23 – Tool Depth Accuracy for Artificial Features

Figure 24 compares the length sizing accuracy of the three tools for artificial features. For regular shape features, Vendor-C's MEC tool appears to show marginally better accuracy than Vendor-B's UT-2 tool, and both had slightly better accuracy than Vendor-D's MFL tool. For random shape features, all three tools seem to demonstrate comparable length sizing accuracy performance.

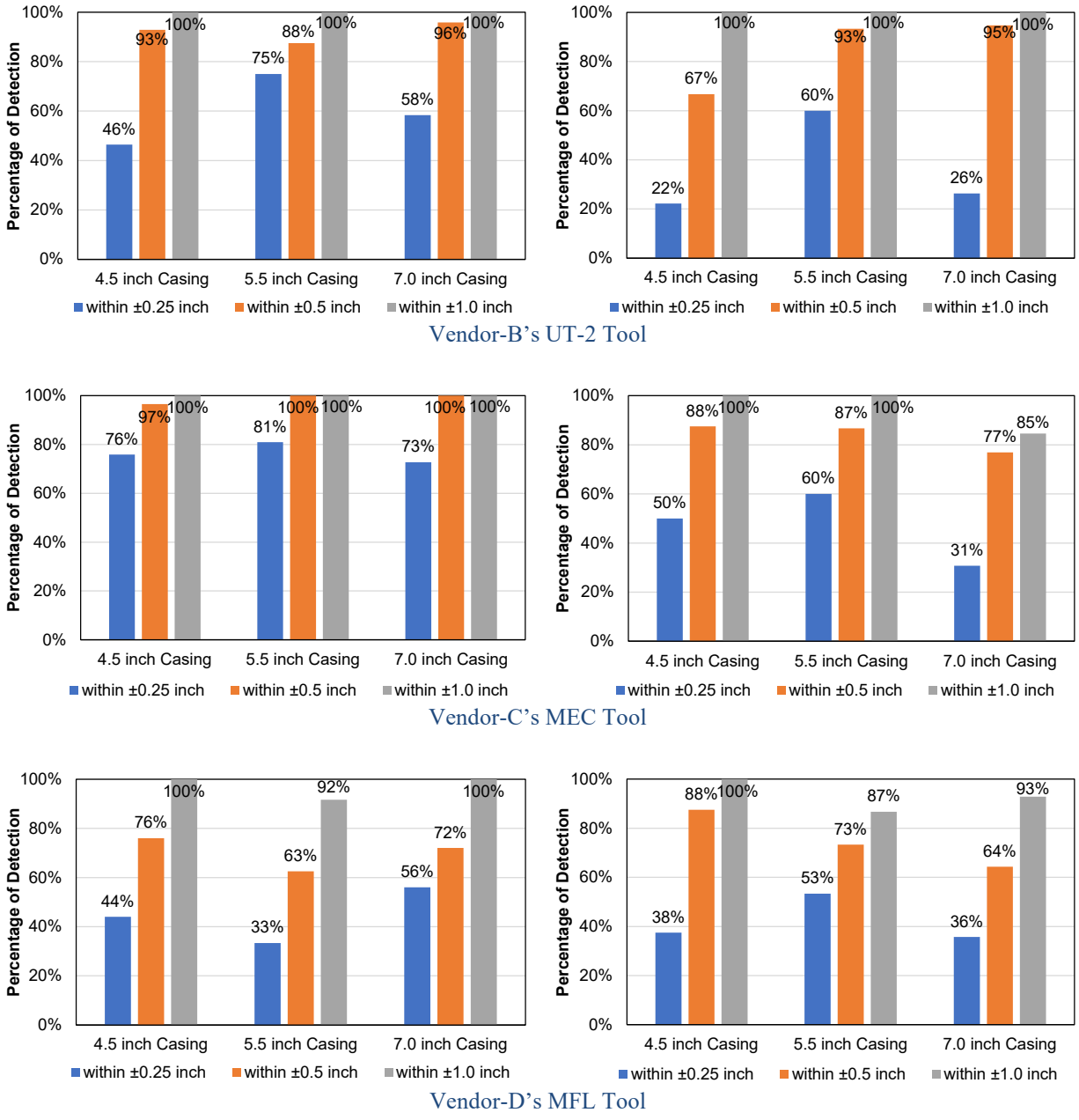

Figure 24 – Tool Length Accuracy for Artificial Features

Figure 25 compares the width sizing accuracy of the three tools for artificial features. Vendor-B's UT-2 showed significantly better width sizing accuracy than the other tools. However, note that,

after reviewing the test results, Vendor-C indicated that an error was found in estimating the feature width, which resulted in a poor width accuracy. This did explain the reason that the MEC tool had much better width accuracy performance in the preceding PRCI casing logging tool test [2] and inconsistent performance in this test. For random shape features, both Vendor-B's UT-2 tool and Vendor-D's MFL tool had similar width accuracy performance. The width accuracy is often less critical than the depth and length, since most remaining burst strength models do not consider the feature width. Only a few models that account for axial stress effects include the feature width parameter (see Section 4.2).

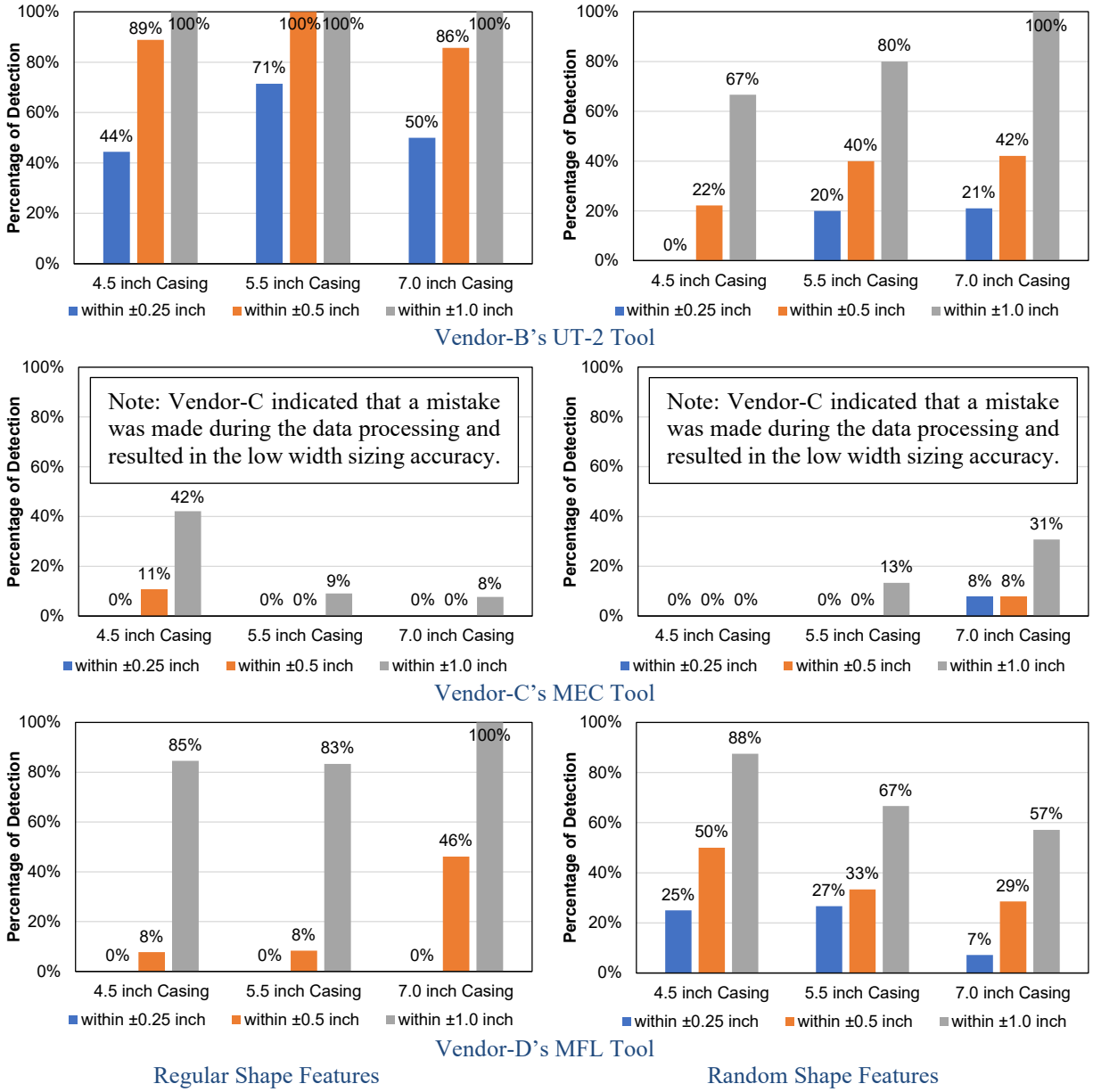

Figure 25 – Tool Width Accuracy for Artificial Features

Figure 26 presents unity plots for the maximum measured depths of the natural corrosion features for the three tools. The results show that Vendor-B's UT-2 tool tends to slightly over-call the feature depth, while the Vendor-D's MFL tool tends to slightly under-report the feature depth. Vendor-C's MEC tool showed larger deviation than the others, with a tendency of over-calling the depth. Since this casing joint was logged in the preceding PRCI casing logging tool test project [2], a further comparison of the tool response with the previous results are presented in Appendices B, C and D.

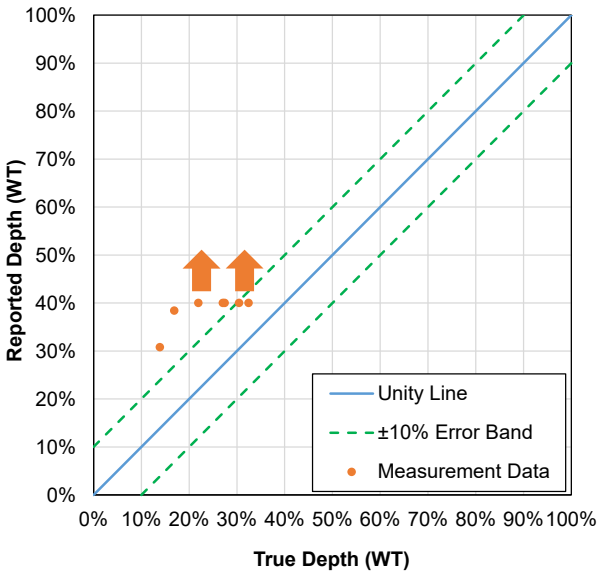

a) Vendor-B's UT-2 Tool

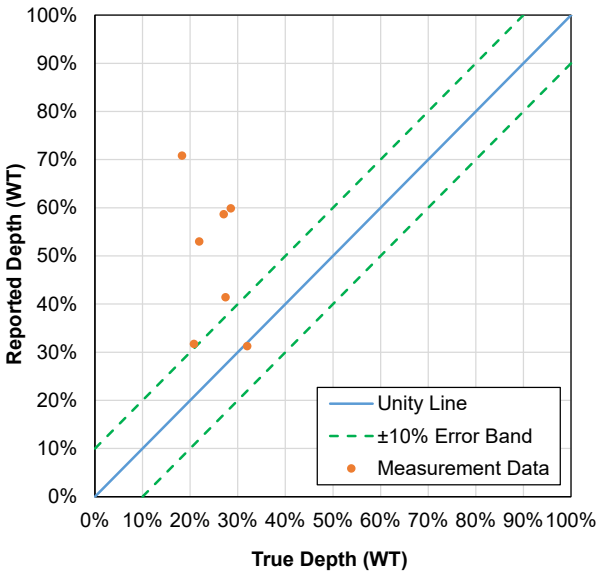

b) Vendor-C's MEC Tool

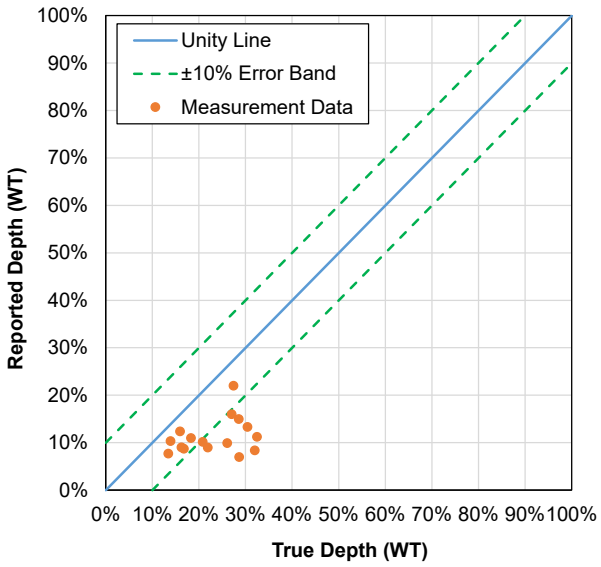

c) Vendor-D's MFL Tool

Figure 26 – Depth Unity Plots of Natural Corrosion Features

6 - Physical Test

6.1 - Coupon Tensile Test

The coupon tensile tests were initially conducted by a local material test lab following the ASTM A370 standard [27]. A review of the stress-strain curve results indicated that the accuracy was insufficient for the subsequent FEA task. In particular, the Young's modulus values determined from the stress-strain curve significantly deviated from the typical value of steel material (i.e. around 30,000 ksi at room temperature). Therefore, the coupon tests were repeated at C-FER's lab following the ASTM E111 standard [28], which is designed for measuring Young's modulus and has much more stringent specifications. In particular, the following key specifications were included in the coupon tests:

- As shown in Figure 27, rectangular coupons with thicknesses that were more than 80% of the original pipe wall were used to capture the average response of the pipe to account for potential non-uniform through-thickness properties of the casing material;
- Two Class B-1 extensometers [29], each with a 2-in gauge length, were placed on opposite sides of the coupon for simultaneous strain measurement, as shown in Figure 28;
- Prior to each test, an alignment check was performed by loading the coupon to a small portion of the yield limit (i.e. approximately 20% to 40%) and comparing the measurements between the two extensometers. The criterion specified by ASTM E111 [28] was followed (i.e. the strain increments between the initial and the final load measurement on opposite sides of the specimens should not differ from the average by more than 3%.);
- The data acquisition frequency was 4 Hz to ensure that a sufficient number of data points were collected in each test to capture accurate key information (e.g. enough data to determine Young's modulus, onset of yielding, onset of strain hardening); and
- All coupon tests were conducted with the load frame in strain-controlled mode at a constant strain rate of 0.3% per minute up to the ultimate tensile strength (UTS) point.

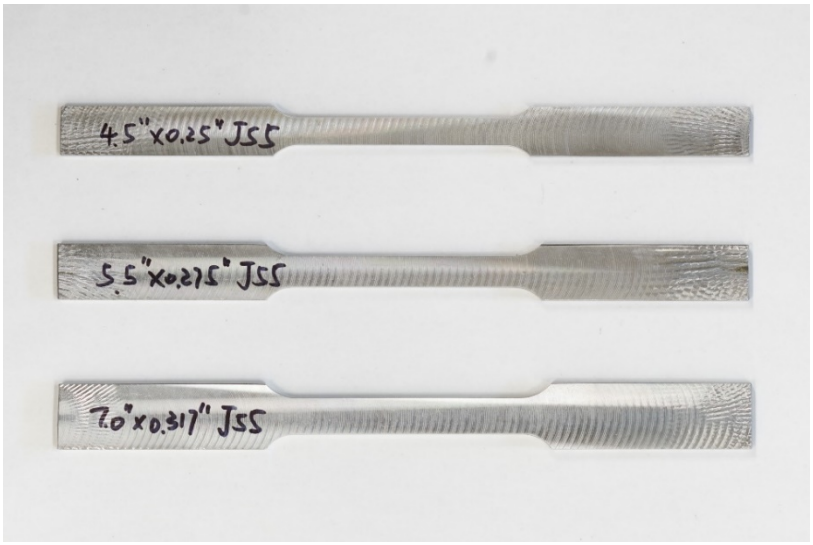

Figure 27 – Coupons for Tensile Tests at C-FER

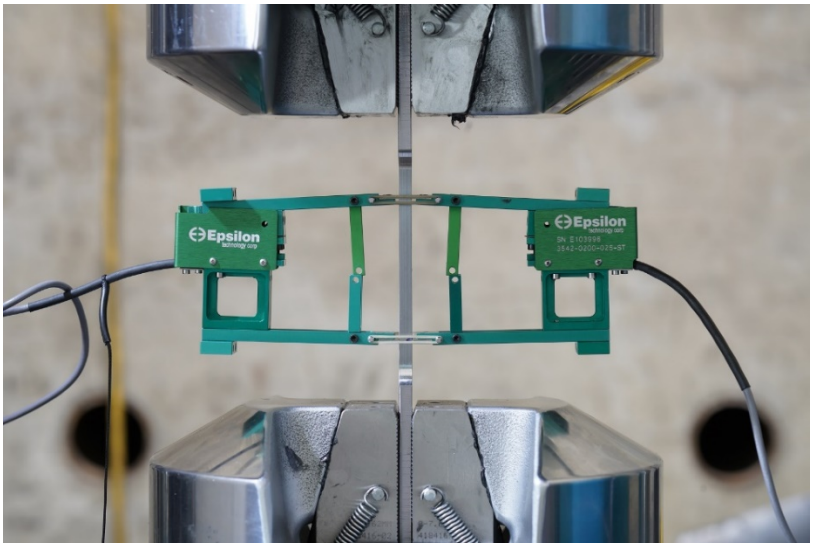

Figure 28 – C-FER Coupon Tensile Test Setup

In addition, these coupon tests also included characterization of the time-dependent response of the casing material, since this response will have an impact on casing burst strength [30]. After reaching the UTS, the coupon was held at a constant strain level for one hour to capture the stress relaxation response. After the one-hour hold period, the extensometers were removed, and the load frame was switched to stroke-control mode at about 10-times the strain rate used prior to UTS. Tests were continued at this higher strain rate until final specimen rupture. Note that characterizing the time-dependent material response was not included in the original work scope. However, due to its significant technical merit for future research (i.e. investigation of effects of sustained pressure on remaining burst strength of casing), it was added in this test program as part of C-FER's contribution to the project. It is expected that the stress relaxation data obtained from this project can be used for future research on remaining burst strength of corroded pipes.

Figure 29 presents the stress-strain curves obtained from the three coupon tests. Note that the stress drop at the constant strain levels at the end of the stress-strain curves represent the stress relaxation response over the one-hour hold period. Figure 30 shows a close-up view of the stress-strain curves within the elastic-plastic transition region. The high-accuracy coupon test results offered the opportunity to clearly identify that the J55 casing materials started to develop plastic deformation at around 40 ksi (i.e. the initiation of the non-linear stress-strain response beyond the proportional limit). However, note that these materials exceed the SMYS requirement of 55 ksi as per API 5CT specification [31]. By definition, the API yield strength (YS) for J55 casing grade is defined as the stress value at 0.5% engineering strain. The key mechanical properties were determined from the stress-strain curves and are summarized in Table 4.

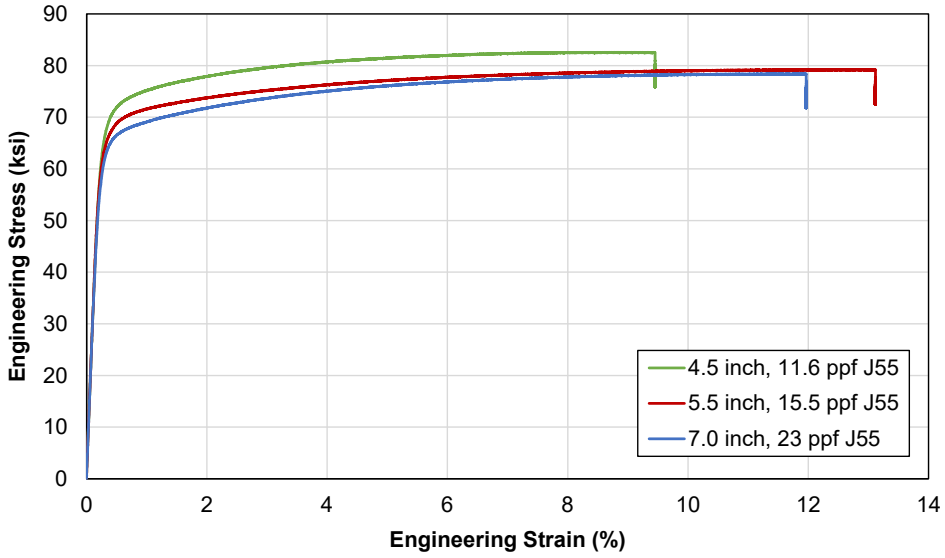

Figure 29 – Stress-strain Curves from C-FER Coupon Tensile Tests

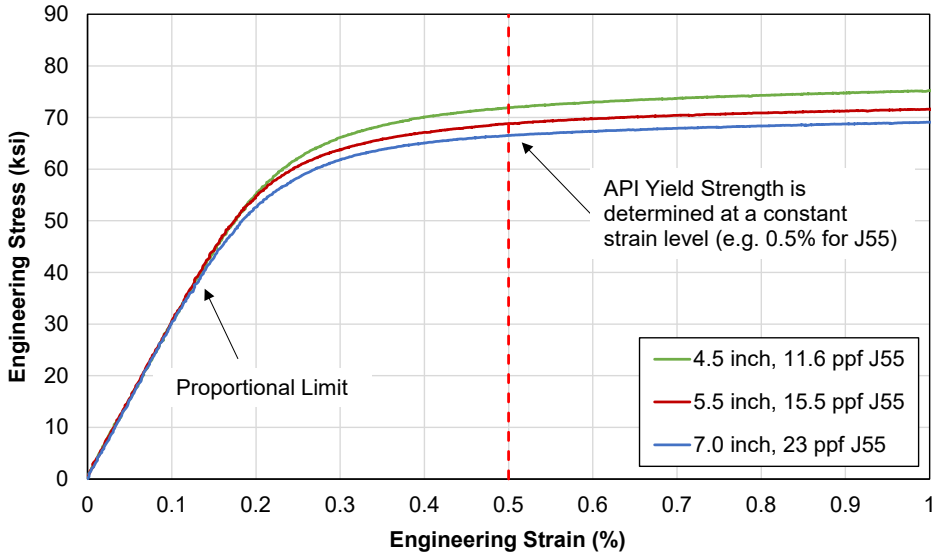

Figure 30 – Stress-strain Curves within the Elastic-plastic Transition Region

Table 4 – Key Mechanical Properties of Casing Specimens

	4.5 inch, 11.6 ppf J55	5.5 inch, 15.5 ppf J55	7.0 inch, 23 ppf J55
Young's Modulus (ksi)	29,600	29,600	29,900
API Yield Strength (ksi)	71.8	68.8	66.5
Ultimate Tensile Strength (ksi)	82.5	79.2	78.4

Figure 31 shows the stress relaxation response of the coupon materials over the one-hour hold period. Most importantly, the test results show that the UTS values for two of the three coupons dropped below the SMTS of 75 ksi for the J55 casing grade specified in API 5CT [31]. Although the 4.5-inch casing material sample remained above the minimum UTS of 75 ksi after one hour, the downward trend suggests that the UTS will eventually drop below the SMTS threshold. However, it's important to point out that such material behavior is not an indication of sub-standard casing products, since the UTS values exceed the SMTS per the tensile test procedure [27] specified by API 5CT [31]. The stress relaxation response reflects the time-dependent or strain-rate dependency of the casing material in its post-yield region [30]. This effect causes the material to show a reduction in post-yield strength as the strain rate decreases.

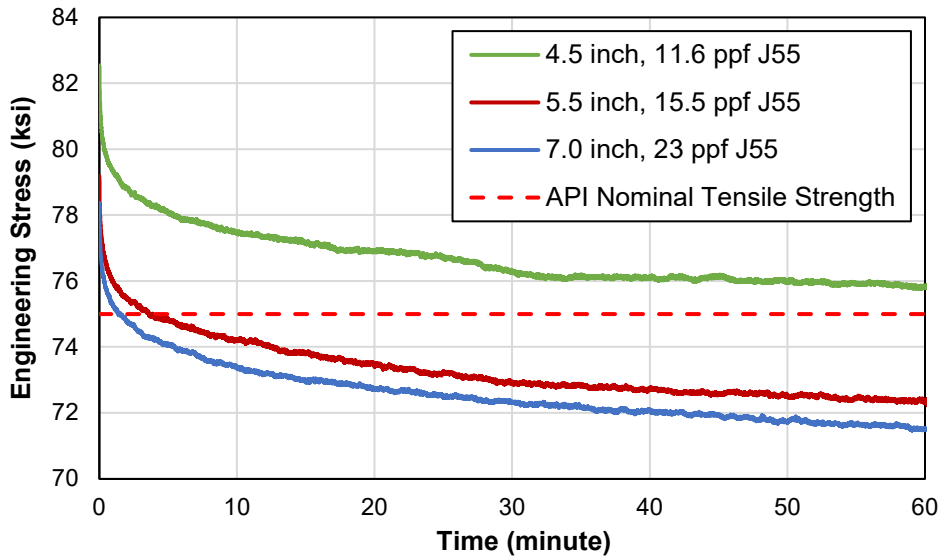

Figure 31 – Stress Relaxation Curves

Many lab tests, including coupon tests and burst tests, are typically conducted at relatively higher loading rates than that in UGS wells, where tubulars are typically subjected to lower loading rates and sustained pressure. Therefore, lab tests would often over-estimate the material strength and burst strength than what the casing may actually have in UGS wells. Therefore, further study is warranted to better understand the effects of slow loading rate and sustained pressure on casing burst strength in downhole conditions.

6.2 - Full-scale Burst Test

Figure 32 shows pictures of the burst test specimens with welded end caps installed. The unconstrained section (between the end caps) had a length of 4 to 5 ft (>8-times pipe OD), which exceeds the minimum length requirement for capped-end burst test specimens in API TR 5C3 Annex C [32]. This ensured that constraints from the welded end caps would have negligible effects on the burst strength of the specimens. As per the requirement in API TR 5C3 Annex C [32], the pressure transducer was installed on the opposite end of the specimen from the pressure supply to minimize recording the pressure spikes related to the pump stroking during testing.

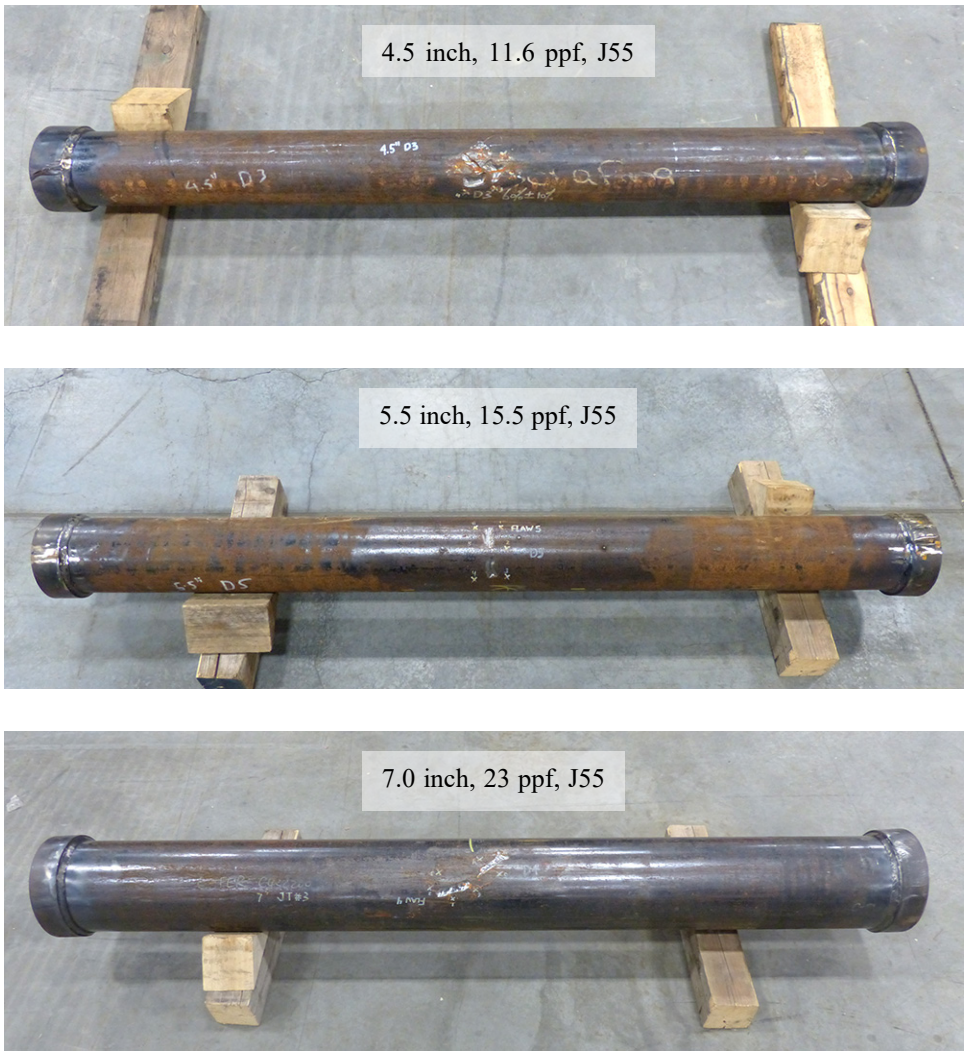

Figure 32 – Capped-End Burst Test Specimens

The full-scale burst tests were executed within an isolated blast containment chamber, as shown in Figure 33. The test chamber was filled with rigid foams to absorb the energy released upon specimen failure. The specimen was pre-filled with water, and entrained air was given time to dissipate from the solution and was vented off so that tests were performed with minimum trapped air inside the specimen. The pressure transducer was connected to a computer-based data

acquisition system (DAS) to record the water pressure during the test. The specimen pressure was manually increased at a nominal rate of 200 psi/minute. In most tests, the specimen leak or rupture was clearly identified by a sudden pressure drop. In one case (i.e. 4.5in-JT3-D5), a small leak developed, resulting in a small pressure drop (i.e. the pump was still able to maintain the specimen pressure). The test continued until a large pressure drop occurred. In the post-test diagnosis, the initial failure at the small leak was identified by a clear differential between the pump pre-charge pressure and the specimen pressure. Nonetheless, the small leak occurred at the peak pressure measured over the entire test. Figure 34 shows examples of failed burst test specimens: one showing a rupture and the other a leak failure mode. Table 5 to Table 7 summarize the burst test results. Details of each of the burst tests and photographs of the failed specimens are provided in Appendix E.

Figure 33 – Burst Test Chamber

a). Rupture (4.5in-JT#3-D1)

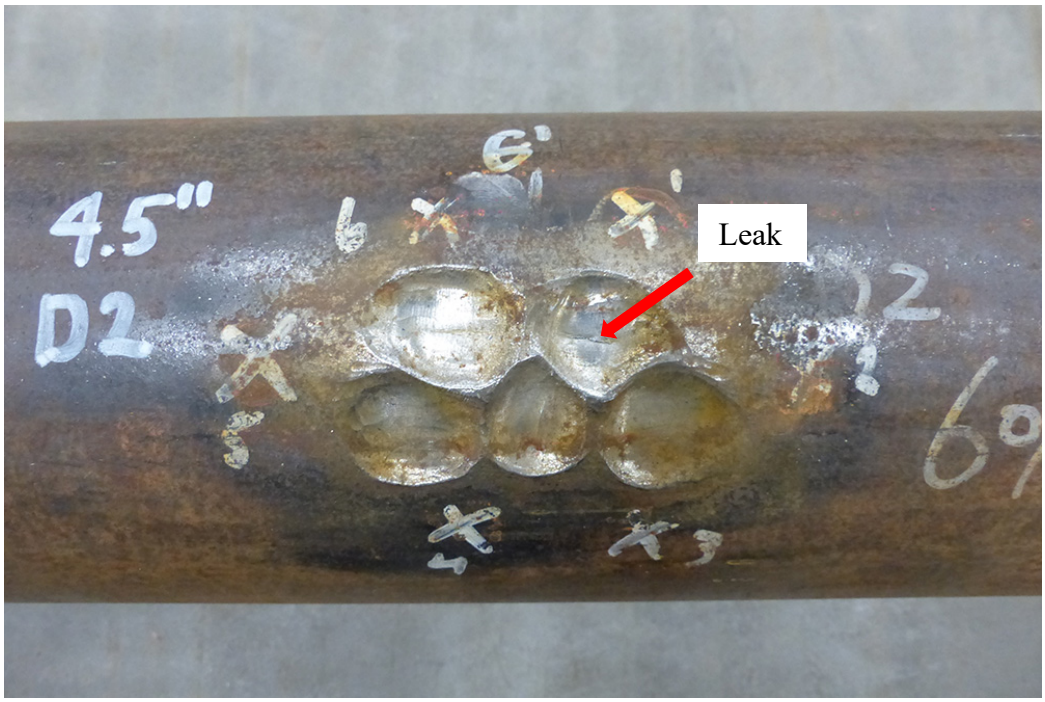

b). Leak (4.5in-JT#3-D2)

Figure 34 – Failed Burst Specimens

Table 5 – Burst Test Results of 4.5 inch, 11.6 ppf, J55 Casing Specimens

Specimen ID	Burst Pressure (psi)
4.5in-JT#3-D1	6,366
4.5in-JT#3-D2	8,116
4.5in-JT#3-D3	7,235
4.5in-JT#3-D4	7,504
4.5in-JT#3-D5	9,270
4.5in-JT#3-D6	6,625
4.5in-JT#3-D7	8,647
4.5in-JT#3-D8	8,432

Table 6 – Burst Test Results of 5.5 inch, 15.5 ppf, J55 Casing Specimens

Specimen ID	Burst Pressure (psi)
5.5in-JT#3-D1	6,080
5.5in-JT#3-D2	5,736
5.5in-JT#3-D3	6,948
5.5in-JT#3-D4	6,584
5.5in-JT#3-D5	8,085
5.5in-JT#3-D6	5,944

Table 7 – Burst Test Results of 7.0 inch, 23 ppf, J55 Casing Specimens

Specimen ID	Burst Pressure (psi)
7.0in-JT#3-D1	6,135
7.0in-JT#3-D2	5,823
7.0in-JT#3-D3	6,900
7.0in-JT#3-D4	6,287
7.0in-JT#3-D5	7,310
7.0in-JT#3-D6	5,802

7 - Finite Element Analysis

Advanced FEA was performed to predict the burst strength of the 20 burst test specimens. Analyses were conducted under both capped-end condition and the in-situ downhole load condition with locked-in axial strain. Analyses under the capped-end condition were calibrated with the physical burst test results to establish the appropriate failure criterion for predicting the burst strength. Once the failure criterion was identified, additional analyses were performed under the in-situ load conditions to investigate the impact of the axial constraint provided by the well cement on casing burst strength.

7.1 - Finite Element Model

FEA models of the casing burst test specimens were generated using the commercial FEA program Abaqus v2020, which possesses various advanced non-linear analysis capabilities, such as large deformation and material plasticity that were required in this study.

The LS measurements of the metal loss profiles were converted into solid computer-aided design (CAD) models using the commercial software DS SolidWorks. The CAD models were then imported into Abaqus CAE to generate the finite element models of the casing burst test specimens. Three-dimensional 20-node quadratic brick elements (C3D20R) were used. The mesh size within the local metal loss region was in the range of 0.02 to 0.04 inch. In addition, the local metal loss region was meshed with four layers of elements along the thickness direction to capture the local through-wall non-uniform stress and strain distributions. In regions away from the local metal loss, a mesh size up to 0.5 to 1.0 inch (along the casing axial direction) was used, with two layers of elements in the pipe thickness direction. Mesh sensitivity analysis was performed to ensure the mesh sizes were sufficient to produce converged results. Figure 35 shows an example of the FEA model of the 4.5 inch casing with the metal loss feature 4.5in-JT#3-D1.

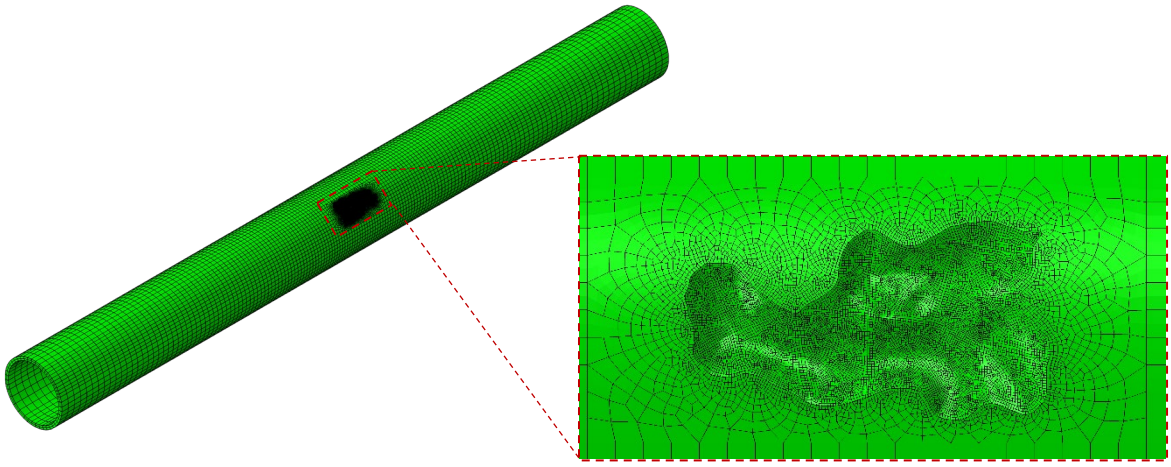

Figure 35 – Casing Specimen FEA Model Mesh Example (4.5in-JT#3-D1)

The engineering stress-strain curves obtained from the coupon tests described in Section 6.1 were converted to true stress-strain curves to define the J55 casing material models. The material models

were based on an elastic-plastic constitutive relationship with an isotropic hardening rule. The default von Mises yield criterion and associated flow rule were used. Since converting the engineering stress-strain curve to the true stress-strain curve becomes invalid after the coupon necking point (i.e. at the UTS), no further strain hardening was considered beyond the UTS point. Geometric non-linearity was enabled in all analyses.

7.2 - Load Scenarios

7.2.1 - Capped-End Load Condition

Under the capped-end pure internal pressure load scenario, the axial stress (σ_1) and hoop stress (σ_2) in a thin wall pipe body can be approximated by Equations (42) and (43), respectively.

$$\sigma_1 \approx \frac{P\pi D^2/4}{\pi D t} = \frac{PD}{4t} \tag{42}$$

$$\sigma_2 \approx \frac{PD}{2t} \tag{43}$$

where

D is the pipe OD,
t is the pipe WT, and
P is the internal pressure.

Therefore, the stress ratio between the axial and hoop components is approximate 0.5.

In the capped-end analysis cases, two hemispherical end caps were attached on both ends of the casing model. An internal pressure was gradually applied on the inner surfaces of the casing pup and the two end caps. Figure 36 shows an example of the capped-end burst test specimen model.

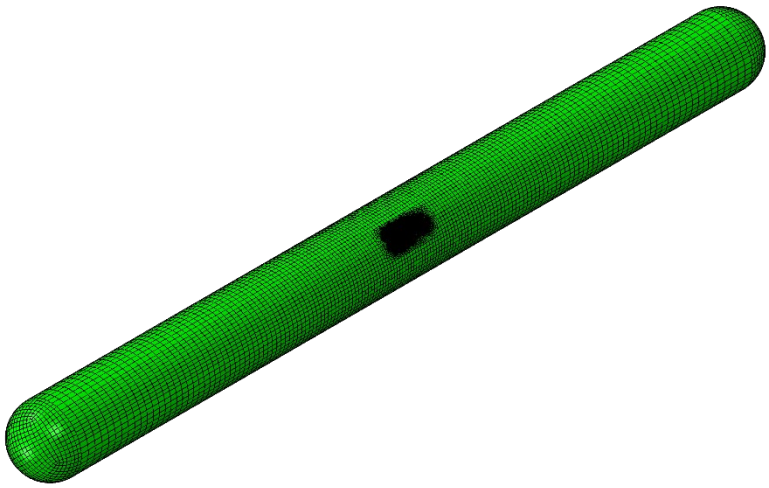

Figure 36 – Capped-End Casing Specimen FEA Model

7.2.2 - In-situ Load Condition

Well construction imposes various loads on the casing string, such as the hanging weight, buoyancy force and bending load induced by the wellbore curvature. These forces imposed on the casing string during installation and cementing are generally "locked-in" to the string once the cement has set and cured. Since additional stress components induced by these in-situ loads will have an effect on the onset of yielding and post-yield response of the casing materials (i.e. based on various multiaxial yielding criteria), it is expected that these in-situ casing loads would also affect the burst strength of the casing.

The in-situ loads were estimated considering the load and boundary conditions that are reasonably representative of the downhole conditions in a UGS well. Based on the feedback from members of the underground storage technical committee at PRCI, a maximum true vertical depth (TVD) of 8,000 ft and a maximum well curvature (dogleg severity (DLS)) of 3°/100 ft were assumed in estimating the in-situ loads.

Maximum Compressive Load

The maximum compressive load typically occurs at the bottom of the well, where the casing hanging weight is zero and the maximum buoyancy force is present. The "locked-in" maximum buoyancy force acting on the bottom of the cemented casing string can be estimated by Equation (44):

$$F_{bu} = (\rho_c h_c + \rho_d h_d)\frac{\pi}{4}D^2 - \rho_w h \frac{\pi}{4}{D_i}^2 \tag{44}$$

where

D is the casing OD,
D_i is the casing inside diameter,
ρ_c is the cement slurry hydrostatic pressure gradient (outside the casing),
ρ_d is the drilling fluid hydrostatic pressure gradient (outside the casing),
ρ_w is the displacement fluid hydrostatic pressure gradient (inside the casing),
h_c is the final vertical depth interval of the cement,
h_d is the final vertical depth interval of the drilling fluid (if not fully cemented to surface), and
h is the TVD of the well ($h = h_c + h_d$).

The cement slurry hydrostatic pressure gradient was assumed to be 0.736 psi/ft, and both the drilling fluid and displacement fluid hydrostatic pressure gradients were assumed to be 0.433 psi/ft.

Since the cement slurry has a higher pressure gradient than the drilling fluid, a casing string fully cemented to the surface ($h_d = 0$ and $h = h_c$) would have the highest buoyancy force at the bottom. Using the assumed well TVD of 8,000 ft and the casing nominal dimensions, the maximum buoyancy forces and the resulting compressive stress values at the bottom of the casing string were estimated and are listed in Table 8. In addition, the corresponding axial compressive strains were also calculated using a Young's modulus of 30,000 ksi and based on the uniaxial compressive stress alone. Note that neglecting the internal and external pressure conditions in this scenario results in higher (conservative) axial compressive strain estimates (i.e. due to Poisson's effect).

Maximum Tensile Load

The maximum tensile load in a casing string is typically located at the top of the well and can be estimated by Equation (45):

$$F_T = F_h - F_{bu} \tag{45}$$

where

F_h = total casing hanging weight in air, and
F_{bu} = maximum buoyancy force on the casing in the wellbore from Equation (44).

The casing hanging weight, F_h, is given by Equation (46):

$$F_h = W_c h \tag{46}$$

where W_c is the casing weight per unit length.

From Equation (45), a partially cemented casing string would have a higher tensile load at the top of the well than a fully cemented casing string (i.e. the maximum buoyance force of a partially cemented casing string at the bottom of the well would be smaller). Based on the well configuration of some existing depleted reservoir UGS wells, an assumed worst-case scenario with a casing string only cemented over the bottom 2,000 ft section was considered to determine the maximum casing tensile load. Using nominal casing dimensions, weight and assumed pressure gradients, the maximum tensile loads calculated using Equations (44) to (46) are listed in Table 8.

Well Curvature

The maximum axial strain induced by well curvature can be estimated by:

$$\varepsilon_a = \frac{D}{2}\kappa \tag{47}$$

where D is the casing OD and κ is the curvature (defined as the reciprocal of the local radius of the casing trajectory). Note that a conversion is required to calculate κ from the wellbore curvature defined in DLS.

The maximum axial stress and strain due to curvature are dependent on the casing diameter, but are independent of the casing weight. Using the assumed maximum well DLS of 3°/100 ft and the casing nominal dimensions, the maximum induced longitudinal strain and the corresponding stress (with assumed uniaxial strain) were calculated and are listed in Table 8.

Table 8 – Estimated Locked-in Loads in the Casing Strings

Casing String		4.5 inch, 11.6 ppf	5.5 inch, 15.5 ppf	7.0 inch, 23.0 ppf
Maximum Compressive Load (Casing Cemented to Surface)	**Force (lbf)**	-50,115	-73,227	-116,341
	Stress (ksi)	-15.0	-16.2	-17.5
	Strain	-0.050%	-0.054%	-0.058%
Maximum Tensile Load (Casing Cemented up to 6,000 ft)	**Force (lbf)**	71,599	93,966	137,624
	Stress (ksi)	21.5	20.8	20.7
	Strain	0.072%	0.069%	0.069%
Maximum Curvature	**Stress (ksi)**	2.9	3.6	4.6
	Strain	0.010%	0.012%	0.015%

The longitudinal stress induced by wellbore curvature was found to be much lower than the maximum tensile and compressive stresses at the top or bottom of the well. Considering that wellbore curvature typically does not coincide with the location of maximum tension or compression along the well casing, the curvature-induced loads were not considered in the analysis. Therefore, the in-situ load analyses considered two scenarios:

- The maximum locked-in axial compressive strain at the bottom of the well, and
- The maximum locked-in axial tensile strain at the top of the well.

The analysis was performed in two steps. In the first step, the initial axial strain was applied to the casing model, and the model was allowed to deform radially and circumferentially. In the second step, an internal pressure was gradually applied on the inner surface of the casing, while both ends of the model were axially constrained to simulate the in-situ cement confinement condition. For conservatism, the potential benefit of cement radial confinement to casing burst strength was not considered in the analysis. The generalized Hooke's law establishes the relationship between the axial strain and the three principal stress components in the pipe body. An incremental form of this relationship can be expressed by Equation (48):

$$\dot{\varepsilon_a} = \frac{1}{E}[\dot{\sigma_a} - \nu(\dot{\sigma_h} + \dot{\sigma_r})] \tag{48}$$

where

$\dot{\varepsilon_a}$ is the axial strain increment,
$\dot{\sigma_a}$ is the axial stress increment,
$\dot{\sigma_h}$ is the hoop stress increment,
$\dot{\sigma_r}$ is the radial stress increment,
E is the Young's modulus, and
ν is the Poisson's ratio.

For a thin wall pipe, the radial stress component is much smaller than the axial and hoop stress components. Therefore, in an axially constrained pipe ($\dot{\varepsilon_a} = 0$), the ratio between $\dot{\sigma_a}$ and $\dot{\sigma_h}$ is approximately equal to ν (~ 0.3 for steel).

Figure 37 presents an example of various stress paths of a 4.5 inch, 11.6 ppf casing string to illustrate the load scenarios discussed in this section. The example assumes a maximum internal pressure of 3,000 psi, which is representative of the operating condition in a typical depleted reservoir UGS well. The maximum locked-in tensile and compressive stresses in Table 8 were considered. Two additional scenarios, including an axially constrained condition with zero initial strain (i.e. a neutral point that exists somewhere between the top and bottom of the casing string) and a capped-end load condition (i.e. the physical burst test condition in this project), are also included for comparison purposes. A VME envelope based on the proportional limit of 40 ksi (see Section 6.1) is also plotted in Figure 37 for reference. As shown in Figure 37, under the normal operating condition in an UGS well, the stress state within the casing pipe body can vary significantly along the depth of the well. Therefore, it is critically important to understand if lab tests conducted with the capped-end load condition can still closely represent the burst strength of casing under the in-situ conditions.

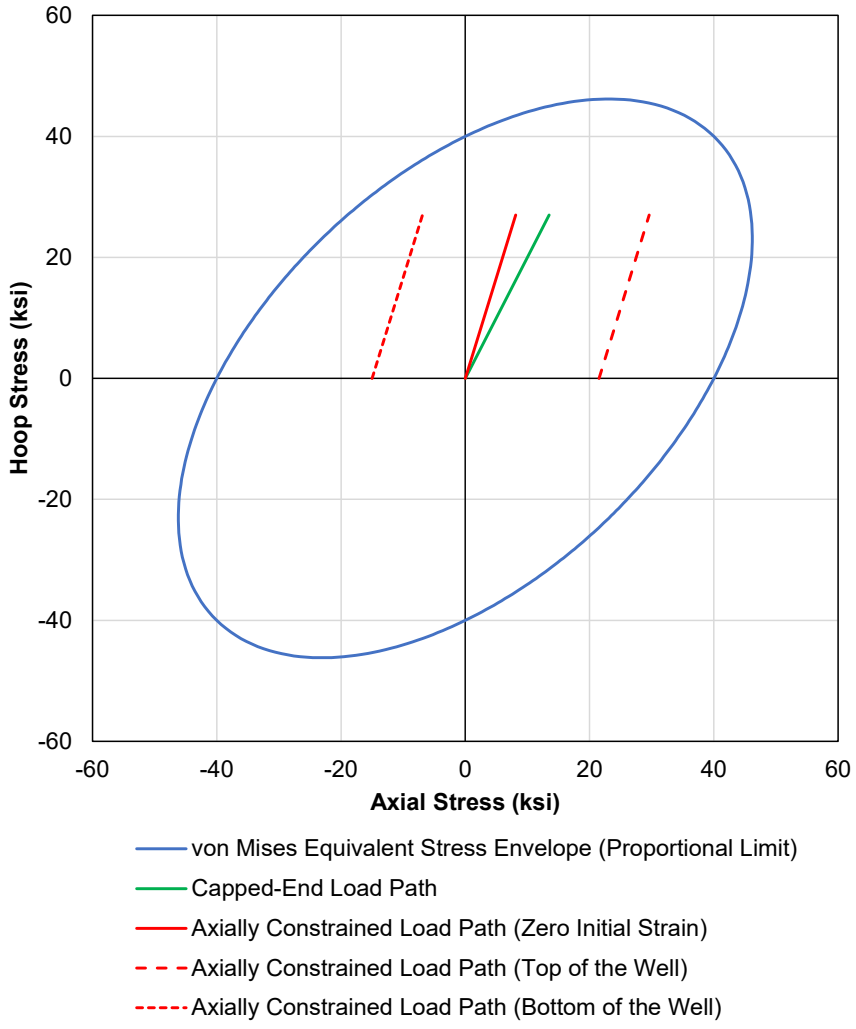

Figure 37 – Stress Paths of a 4.5 inch, 11.6 ppf Casing String in the UGS Well

7.3 - Failure Criterion

7.3.1 - von Mises Equivalent Stress Criterion

Many previous studies with FEA prediction of burst pressure of corroded pipes have used failure criteria that associate the VME in the corroded ligament with the material's true tensile strength [33,34,35]. Slight variations exist in these analyses, depending on whether the minimum, maximum or average value of the equivalent stress is used. The criterion adopted by BS 7910 Annex G [22] suggests that burst may be considered to occur when the average VME through the minimum ligament of the metal loss area equals the material's true tensile strength.

7.3.2 - Plastic Collapse Criterion

Another failure criterion is defined as the maximum load where local structural instability occurs due to large plastic deformation, which is usually referred to as plastic collapse. For a pipe under internal pressure load, local plastic collapse failure occurs when the rate of pipe cross-section

geometry change (i.e. diameter increase and wall thinning) induced by plastic deformation exceeds the rate of material strain hardening. Numerical methods, such as the "Riks" method in Abaqus [36], are often used to determine the maximum load capacity. This approach has been used to predict the burst capacity of uncorroded line pipe [37] and corroded line pipe [38].

Note that the objective of this study was to investigate the ultimate burst limit state of the metal loss features. Therefore, yielding of the undamaged pipe body was not considered as a failure.

7.3.3 - Failure Criteria Evaluation

Analyses under the capped-end condition were conducted to predict the burst capacity using the two failure criteria described above.

The prediction capability was quantitatively evaluated using the ratio of the predicted versus actual burst pressure (referred to as the predicted-to-actual pressure ratio or "prediction ratio" in the following text). A ratio equal to one indicates a perfect prediction and any deviation from one represents the model error. For each set of FEA results, the predicted-to-actual pressure ratio was determined for all 20 test cases. In addition, a mean value and a coefficient of variation (COV) were determined for each set of predicted-to-actual pressure ratios. The difference between the mean value and one represents the bias error of the prediction. The COV represents the ratio of the standard deviation to the mean, and is a measure of the scatter and reflects the level of random error of the prediction. Therefore, a prediction model with the best prediction capability should have a mean predicted-to-actual pressure ratio closest to one and the lowest COV. The bias error of the prediction model can be corrected by applying a multiplicative factor calibrated with statistically significant test data. However, the random error cannot be removed and it is a critical measure of the model's prediction capability.

In analyses using the VME failure criterion, burst failure was predicted when the maximum VME through the minimum ligament of the metal loss area equaled the material's true tensile strength, following the approach used by Chauhan et al. [33].

Figure 38 presents a summary of the prediction ratios for the 20 burst test specimens under capped-end condition. The dashed lines represent the mean value of the prediction ratios. The VME criterion was found to significantly under-estimate the burst pressure, which is reflected by a low prediction ratio mean of 0.886. The plastic collapse criterion was found to slightly over-estimate the burst pressure, but with a much better prediction ratio mean of 1.017. Additional evidence in the literature regarding the prediction performance of the two criteria in FEA were also identified:

- FEA on the remaining burst strength of metal loss features conducted in a PHMSA project DTPH56-14-H-00003 [38] had a similar finding that the "Riks" method in Abaqus resulted in better agreement with the full-scale test results of line pipe burst test specimens.
- FEA-predicted burst pressure based on the VME criterion by Chauhan et al. [33] was found to be on average 20% less than the actual capped-end burst test results on 5.5 inch and 7.0 inch casing specimens with metal loss.

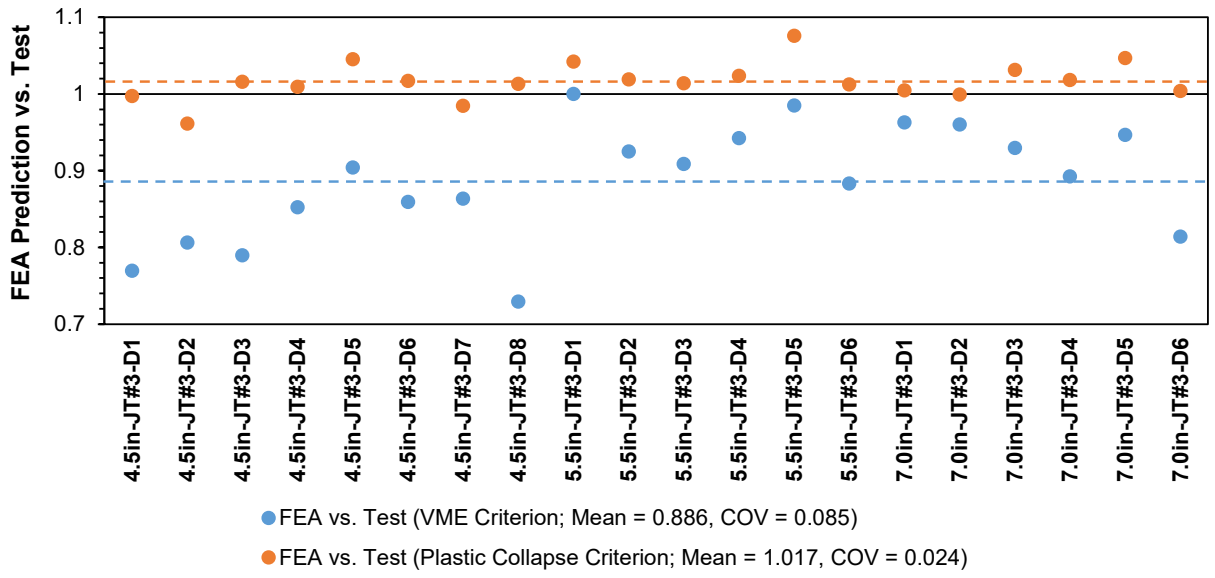

Figure 38 – FEA Prediction Accuracy (Capped-end Condition)

The COV values also suggest that the plastic collapse criterion resulted in a much narrower scatter than that using the VME criterion (0.024 versus 0.085). The comparison provides clear evidence that the plastic collapse criterion is more suitable than the VME criterion in FEA prediction of the remaining burst strength of casing with blunt metal loss. As such, the plastic collapse criterion was selected for additional FEA on casing remaining burst strength under in-situ load conditions. In addition, the small COV of the FEA prediction ratios is also an indication of highly consistent full-scale burst test results. The small random error in the FEA prediction was likely due to a combination of material property variations, uncertainty in the measurement of the metal loss profile, and variation in the local strain rate within the metal loss region in each burst test (see Section 6.1 for further discussion of the strain rate impact on burst strength).

In fact, the plastic collapse criterion has been widely adopted in analytical models to predict the ultimate ductile rupture strength of uncorroded pipes [39,40]. In addition, these studies also suggested that prediction of ductile rupture based on the von Mises yield theory tends to over-estimate the burst pressure when compared with physical burst tests. This also agrees with the slight over-estimation from the FEA results in this study (a mean predicted-to-actual pressure ratio of 1.017). Note that, as described in Section 7.1, the material constitutive model used in this FEA study was based on the von Mises yield criterion and associated flow rule. Since no further strain hardening was considered beyond the UTS point in the material model, this resulted in a slightly lower predicted burst pressure (i.e. the plastic strain in the remaining ligament of the metal loss region was found to exceed the plastic strain at the UTS point). As a result, the mean predicted-to-actual pressure ratio was only marginally higher than one.

Additionally, note that the material ductility has a critical role in ductile rupture. Better understanding of the material properties and burst failure mode (ductile versus brittle) of vintage casings that have been in service over several decades in existing UGS wells seems warranted, since they

could have a significant impact on the prediction capability of FEA and existing remaining burst strength models.

7.4 - Analysis Results

7.4.1 - Capped-End Scenario

This section presents examples to illustrate the FEA results for the capped-end load scenario. Figure 39 shows the relationship between the internal pressure and plastic strain within the critical remaining ligament of the metal loss feature 4.5in-JT#3-D1. Based on the plastic collapse criterion, the predicted burst pressure of 6,348 psi is the peak pressure in the curve, which occurs at ~55% plastic strain. If the VME criterion is used, the burst pressure would be predicted as 4,899 psi, which occurs at ~7.4% plastic strain. Note that the actual burst pressure from the burst test was 6,366 psi.

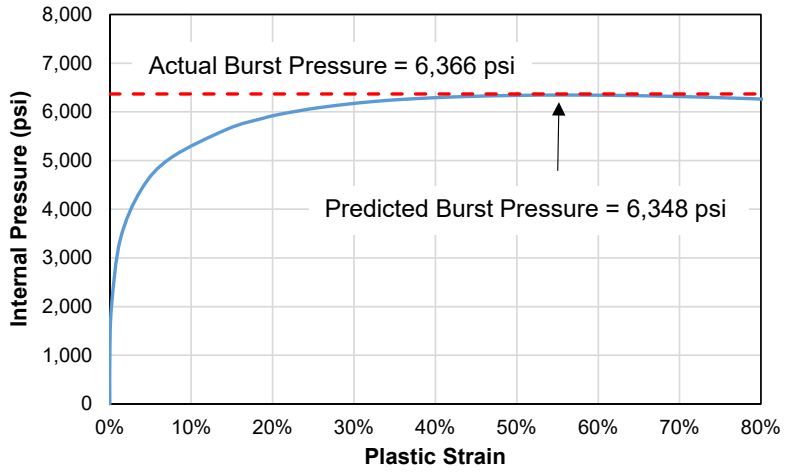

Figure 39 – Internal Pressure versus Plastic Strain in Metal Loss Feature (4.5in-JT#3-D1)

Figure 40 shows the VME distribution within the metal loss region at the peak pressure for the feature 4.5in-JT#3-D1, where significant stress concentration occurred within the metal loss region. Figure 41 shows the equivalent plastic strain distribution within the metal loss region at the peak pressure for the feature 4.5in-JT#3-D1. The plastic strain plot clearly shows the initiation of local necking along the large plastic strain band, represented by the red color. The predicted necking location was found to coincide with the final rupture failure in the physical burst test (see Appendix E).

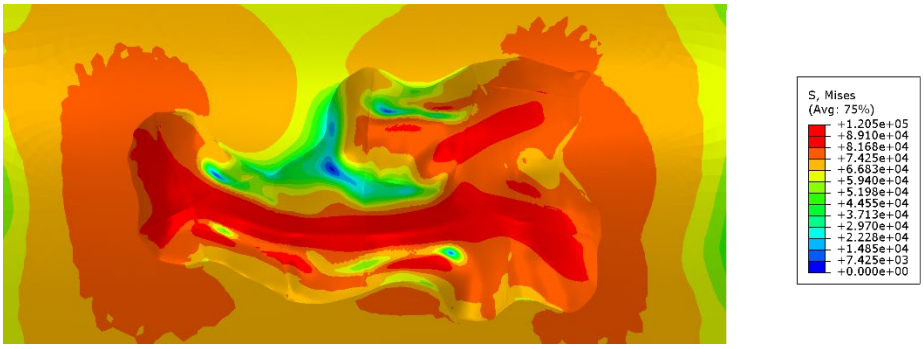

Figure 40 – Equivalent Stress Distribution at Peak Pressure (4.5in-JT#3-D1)

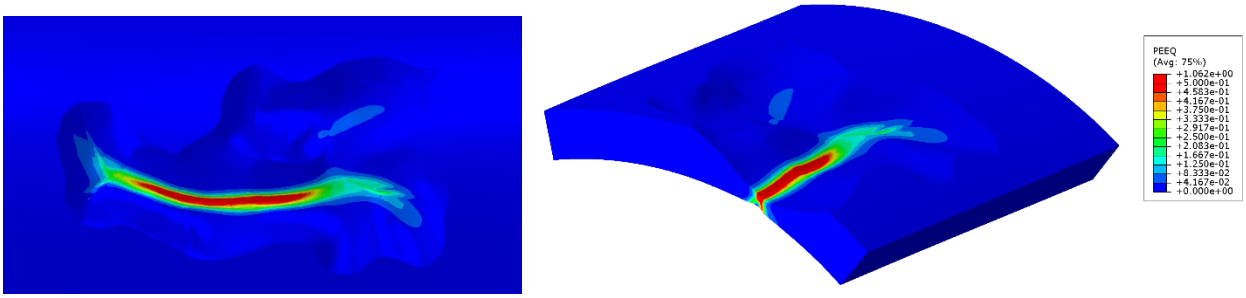

Figure 41 – Plastic Strain Distribution at Peak Pressure (4.5in-JT#3-D1)

Figure 42 shows another example of the VME distribution within the metal loss region at the peak pressure for the feature 4.5in-JT#3-D2, where significant stress concentration occurred within the metal loss region. Figure 43 shows the equivalent plastic strain distribution within the metal loss region at the peak pressure for the feature 4.5in-JT#3-D2. A localized severe plastic strain region is identified within one of the metal loss pits, indicated by the red color. Again, the predicted necking location was found to coincide with the final failure location in the physical burst test (see Appendix E). In addition, the physical test showed a leak instead of rupture, which agrees with the localized plastic strain in the FEA prediction.

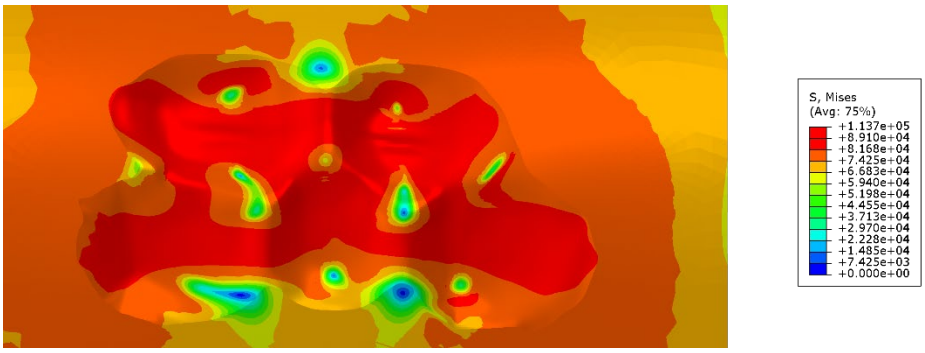

Figure 42 – Equivalent Stress Distribution at Peak Pressure (4.5in-JT#3-D2)

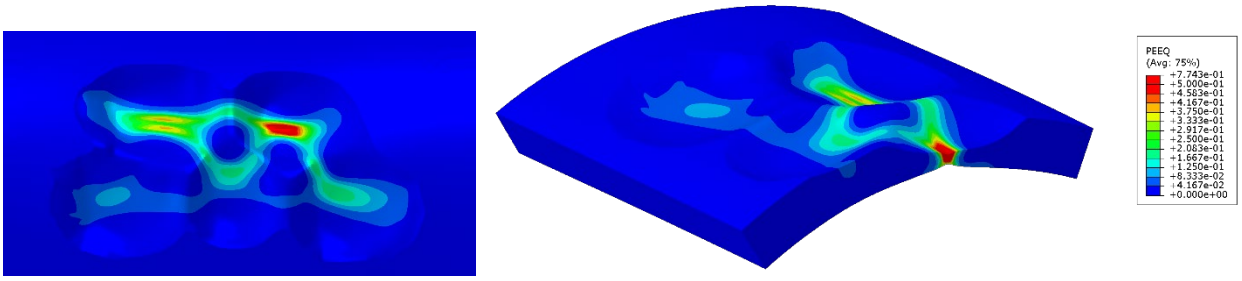

Figure 43 – Plastic Strain Distribution at Peak Pressure (4.5in-JT#3-D2)

Additional FEA results of the plastic strain distribution in the metal loss region at the peak pressure for all 20 burst test specimens are presented in Appendix E. These results demonstrate good agreement between the FEA prediction and the physical burst test in terms of the predicted large plastic strain zones and the actual failure location in the tests (leak or rupture). The one exception is feature 4.5in-JT#3-D7 where the actual failure did not occur at the predicted maximum plastic strain location. This could be due to local variations in material properties or inaccuracies in feature dimensions. In addition, all of the full-scale burst test specimens showed signs of necking and/or significant plastic deformation at the failure location, which confirms the plastic collapse failure mode.

Note that the predicted plastic strain within the necking region in the metal loss area is well beyond the plastic strain at the UTS point. This is different from the capped-end ductile rupture of uncorroded pipe, where plastic collapse occurs with the maximum plastic strain at a level prior to the UTS point [39,40]. The difference is associated with the local stress and strain distribution at the failure location between the two scenarios. For the uncorroded pipe, the longitudinal variations of the stress and strain distributions are relatively small. Therefore, an elastic-plastic analysis (by analytical models or FEA) on a 2D pipe model can provide a solution of the plastic strain at ductile rupture under the capped-end condition, which occurs prior to the UTS point. For the corroded pipe, the reinforcement from the uncorroded pipe body around the metal loss area would have a significant impact on the local stress/strain response within the metal loss region and its final plastic collapse under internal pressure loading. The uncorroded pipe body around the local metal loss area allows stress redistribution as large plastic strain develops within the critical region of the metal loss. The stress redistribution and strain hardening in the surrounding uncorroded pipe body provide additional pressure resistance, even the plastic strain within the metal loss region becomes quite high (i.e. well beyond the material's UTS point and initiation of local necking). As a result, the internal pressure can continue increasing until the pipe reaches its peak pressure capacity, which is the moment of plastic collapse. Further details of the local stress and strain within the metal loss region are discussed in the next section.

7.4.2 - In-situ Load Scenario

Figure 44 to Figure 46 present a summary of the FEA results of the predicted remaining burst pressures for all 20 casing specimens, including the capped-end and in-situ load conditions. In addition, the physical burst test results are also presented for reference. The impact of the in-situ load condition on the burst strength was statistically evaluated using the mean and COV of the ratios of the FEA-predicted pressures between the in-situ load scenario and the capped-end scenario.

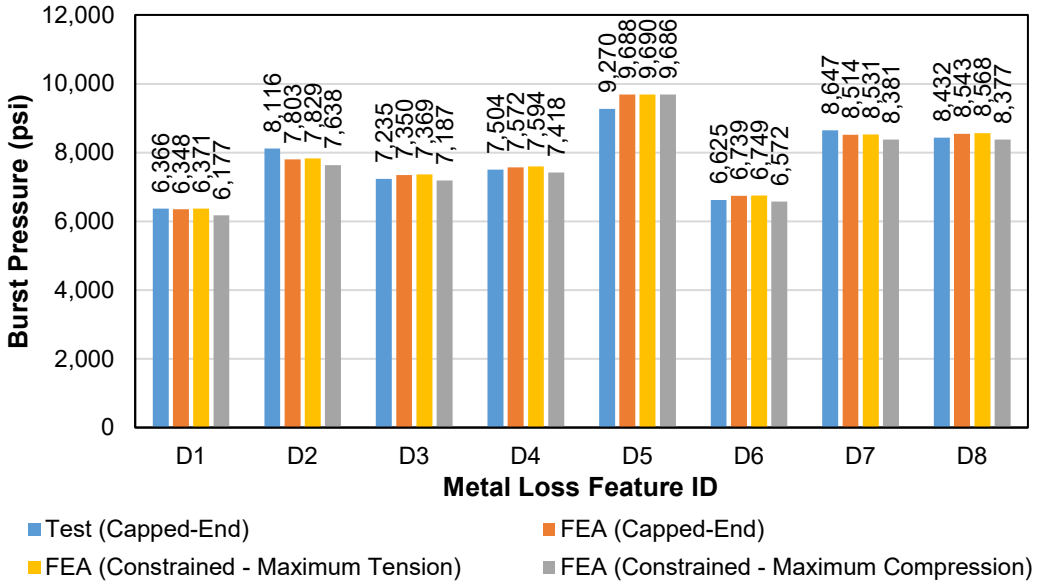

Figure 44 – Test versus FEA-predicted Burst Pressure (4.5in-JT#3)

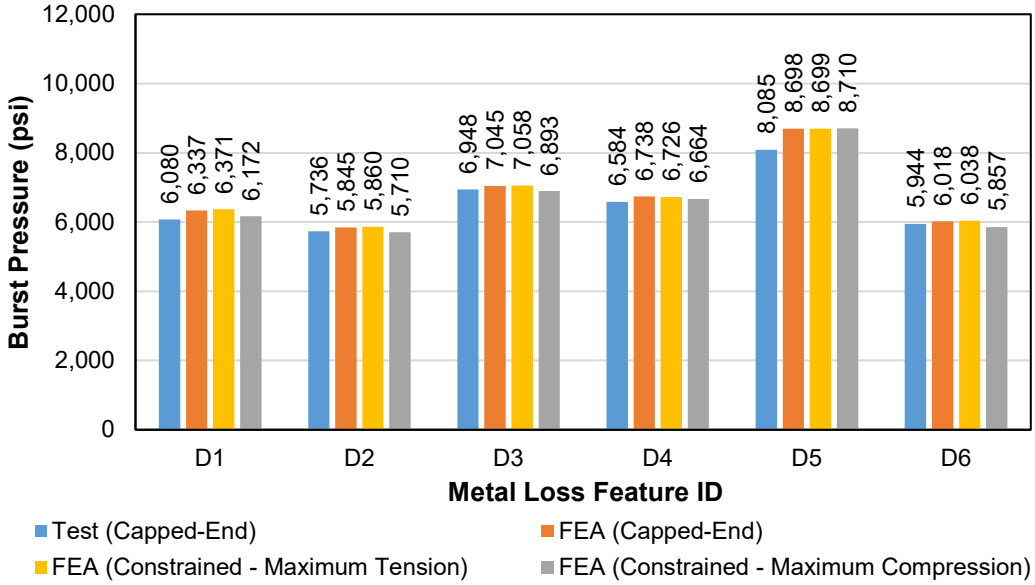

Figure 45 – Test versus FEA-predicted Burst Pressure (5.5in-JT#3)

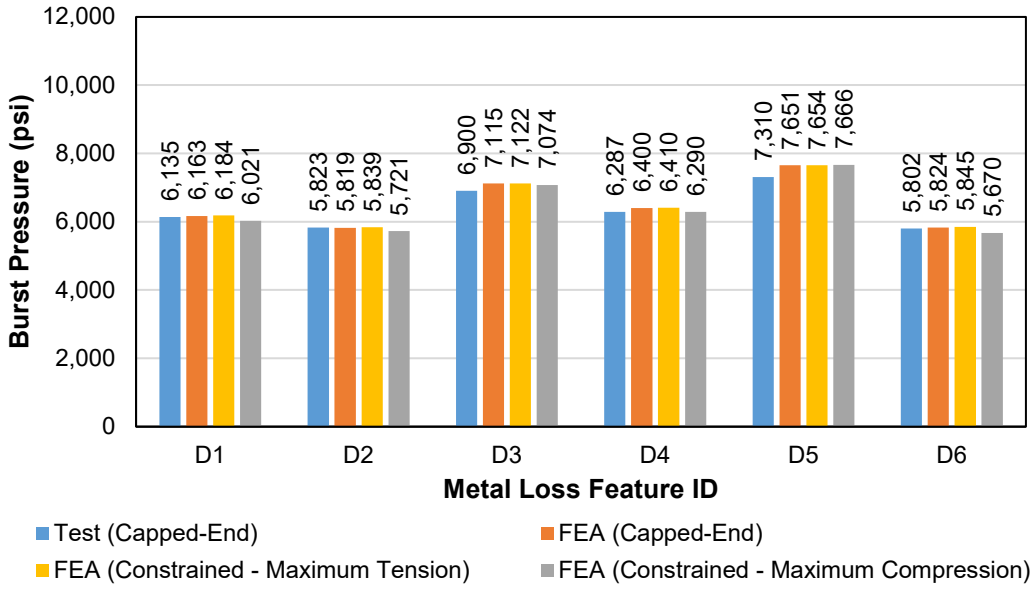

Figure 46 – Test versus FEA-predicted Burst Pressure (7.0in-JT#3)

The maximum locked-in initial compressive strain was found to result in a marginal reduction of the burst strength compared to the capped-end condition (mean = 0.983 and COV = 0.010). The effect of the maximum locked-in initial tensile strain was found to have a negligible impact on the burst strength (mean = 1.002 and COV = 0.002).

A similar finding was reported in a previous US DOT PHMSA sponsored project by Liu et al. [38]. Their study was based on FEA and full-scale burst tests of corroded line pipe under very high compressive strain (up to 2.3%). The results showed that the burst pressure reduction due to longitudinal compressive strain was small. In addition, the study also indicated that axial compressive strain has a greater influence on the burst pressure of specimens with longitudinal grooves than those with other types of metal loss features.

A further investigation was undertaken to examine the stress condition within the metal loss region under different load scenarios. Figure 47 shows an example of the two primary stress components (axial and hoop) at a critical location within the necking region of the metal loss feature 4.5in-JT#3-D1. Note that the radial stress and the three shear stress components were found to be about an order of magnitude smaller than the primary stress components and, therefore, are not included in this discussion. The analysis results at the same location for the three load scenarios (capped-end, fixed axial strain with pre-tension and pre-compression) are included in the same chart for comparison. The three key material parameters, i.e. the proportional limit, the API YS and the UTS, are plotted with VME envelopes as references to illustrate the boundaries between the elastic, elastic-plastic transition and large plastic deformation regions. At the peak pressure of over 6,000 psi, the pipe body stress exceeded the proportional limit in all three cases. Since the incremental plastic strain between the proportional limit and the API YS is relatively small (see Section 6.1), the slope of the stress paths in the pipe body stayed more or less constant (i.e., an axial versus hoop stress ratio of 0.5 for capped-end condition and 0.3 for axially constrained condition). However, the stress paths in this particular metal loss feature in all three cases followed an

initial slope close to that in the axially constrained condition within the elastic region, and finally converged to the capped-end stress path.

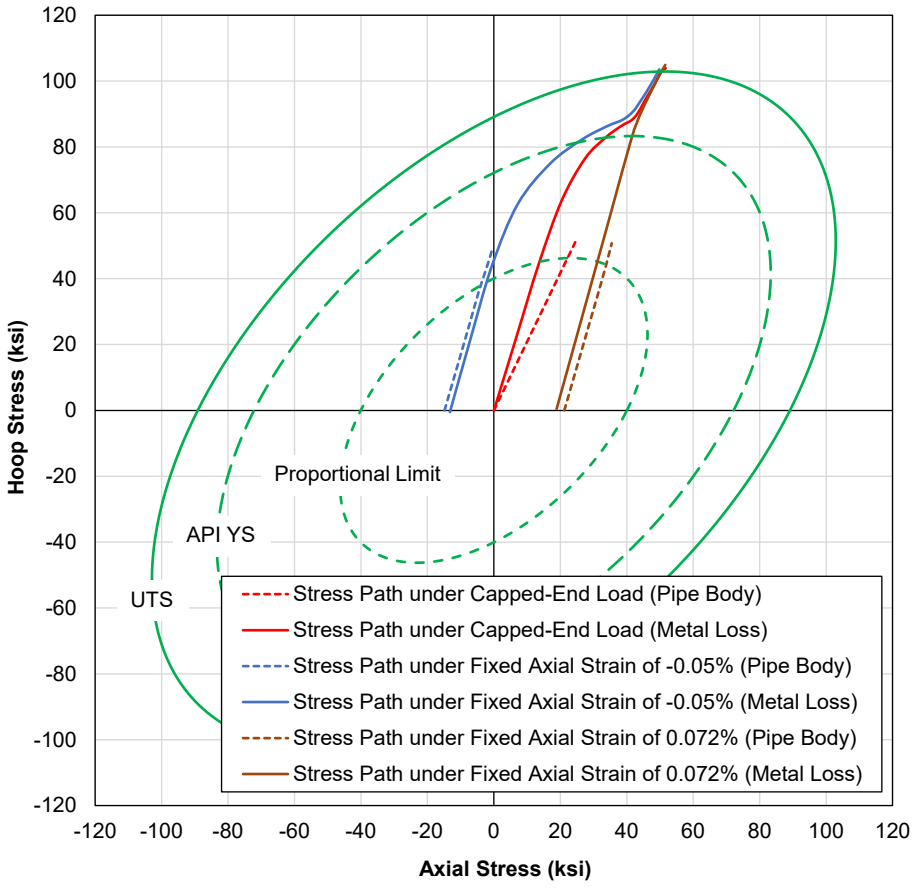

Figure 47 – Stress Paths in the Metal Loss Region in Burst Analysis (4.5in-JT#3-D1)

Under the axially constrained condition, the deviation of the stress path after the onset of yielding and its convergence towards the final capped-end stress path are driven by the plastic deformation following the associated flow rule, and can be demonstrated by classical elasticity and plasticity theories. In all three cases, the local metal loss region is constrained by the more rigid surrounding pipe body, which affects the axial stress transferred from the pipe body into the metal loss region. Therefore, the initial slope of the stress path (i.e. within the elastic range) within the metal loss region does not necessarily follow that in the uncorroded pipe body, and it is highly dependent on the local metal loss geometry and the constraint condition from the surrounding pipe body. After yielding, the stress and strain within the metal loss region become more independent from the load condition in the surrounding uncorroded pipe. Therefore, further evolution of the stress and strain associated with large plastic deformation within the metal loss largely would follow an axially constrained condition, which finally converges to the capped-end stress path. Similar behavior of the local stress convergence within the metal loss was also observed in all other cases.

The convergence of the stress path after the elastic-plastic transition led to similar stress and strain states between the different load scenarios examined in this study. Since the plastic strain

development within the elastic-plastic transition region is relatively small, the effect of path dependency on the final plastic collapse (which occurs at a much higher plastic strain level) is small. Therefore, this explains the similar predicted burst pressure in the different load scenarios in this FEA study. Further discussion of this behavior and the small effect of pre-strains on ductile rupture strength of uncorroded pipe is described by Stewart et al. [39].

Note that most of the methods used to account for axial load effects described in Section 4.2 assume a proportional relationship of the axial stress between the metal loss region and the pipe body. However, the investigation of the local stress response within the metal loss region suggests that this assumption seems to be invalid, especially after the onset of yielding. Therefore, further study is required to validate these methods for calculating the remaining burst strength of corroded casing.

Nevertheless, considering the worst-case of the maximum locked-in compressive strain in the well, a relatively simple approach may use a pressure reduction ratio based on mean-minus-two-standard-deviations to adjust the predicted burst pressures. For example, based on the pressure ratio mean of 0.983 and a COV of 0.010 determined in this study, a correction factor of 0.963 may be applied to the remaining burst strength model calibrated with capped-end burst test data. From a statistical basis, this is associated with a probability of non-exceedance at 97.7%. Note that similar approaches using mean-minus-two-standard-deviations have been adopted by industry in cases such as the fatigue design S-N curves established in DNVGL-RP-C203 [41]. Certainly, further research, including additional FEA and full-scale validation tests over a wider range of corrosion metal loss features, is warranted to gain better understanding of the in-situ load impact and to improve the methodology to account for the in-situ load effect in predicting the remaining burst strength.

8 - Remaining Burst Strength Prediction Model Evaluation

8.1 - Model Evaluation Based on Current Tests

Results of the 20 capped-end burst tests were used to evaluate the predictive capability of various remaining burst strength prediction models previously developed for corroded pipelines described in Section 4.2. The metal loss profile inputs required for the remaining burst strength calculation are listed in Appendix E. Note that the majority of the prediction models described in Section 4.2 use SMYS and/or SMTS in the calculation. However, to evaluate the model prediction capacity, the actual YS and UTS obtained from the coupon tests were used instead in the burst strength calculations. Note that API 597-1 does not define the flow stress [9]. For this study, flow stress was defined as the average between the actual YS and UTS in the API 597-1 prediction, which was found to provide the best prediction against test data by Francini et al. [25]. Figure 48 shows the comparison between the predicted and actual burst pressure for the eight remaining burst strength prediction models. The FEA prediction of burst pressure (based on the plastic collapse criterion) is also included for comparison.

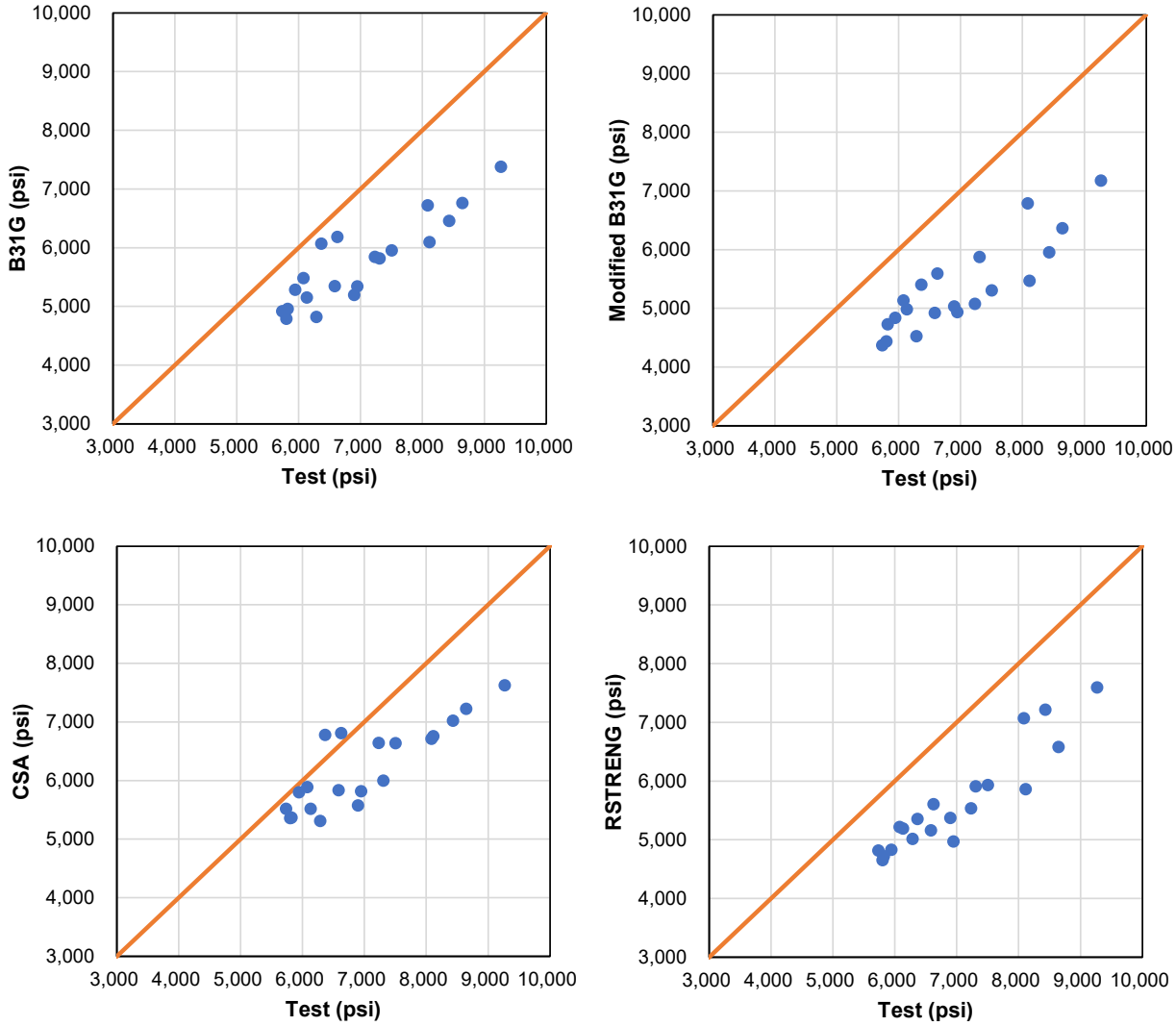

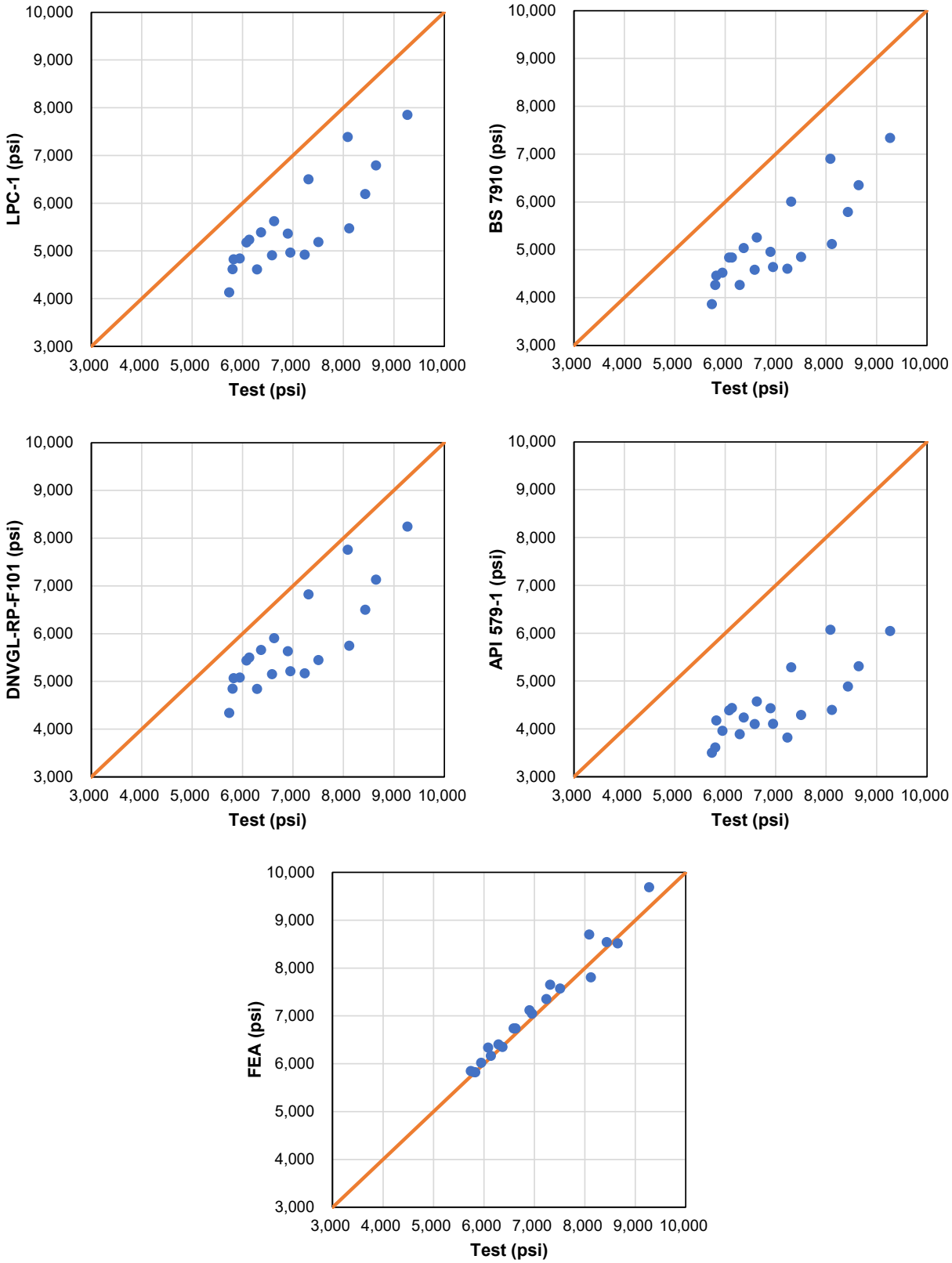

Figure 48 – Comparison of Predicted and Actual Burst Pressure

Following the same approach as described in Section 7.3.3, the model prediction capability was quantitatively evaluated using the predicted-to-actual pressure ratio. Figure 49 and Figure 50 present the mean value and COV for the eight remaining burst strength prediction models evaluated. Comparing the mean and COV values of the predicted-to-actual pressure ratio for all models leads to the following observations and conclusions:

- The FEA model demonstrated superior prediction capability due to its ability to capture the details of geometrical characteristics of the pipe and metal loss profile, as well as the elastic-plastic stress-strain relationship;
- All analytical models under-estimate the remaining burst strength by approximately 10% to 36%, as indicated by the mean predicted-to-actual pressure ratio;
- The CSA model showed the smallest bias error among the eight analytical models, with an average of ~10% under-estimation;
- The RSTRENG model showed the lowest COV among the eight analytical models based on the 20 burst tests. However, note that accurate characterization of the river bottom profile of metal loss features in the downhole environment is still a significant challenge. Further improvement in casing logging technology is required to effectively use the RSTRENG model for downhole applications;
- Considering models that could be used in downhole applications (i.e. excluding the RSTRENG model that is difficult to apply downhole), the ASME B31G and modified B31G models showed the lowest random error levels among the seven analytical models;
- Among the eight analytical models, the API 579-1 model showed both the largest bias error (i.e. lowest mean) and random error (i.e. largest COV); and
- Since the LPC-1, BS 7910 and the DNVGL-RP-F101 models share similar forms of equations, they showed similar random errors. The difference in the bias error among the three models resulted from the different flow stress definitions used.

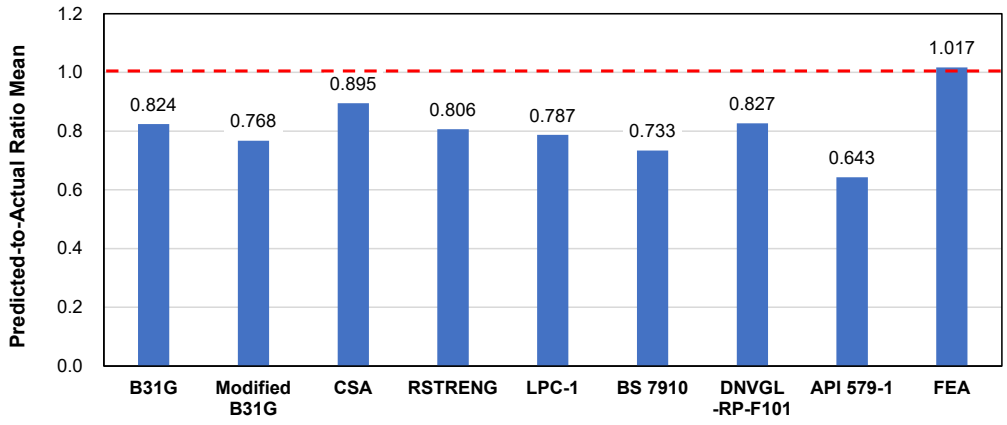

Figure 49 – Mean Value of the Predicted-to-Actual Pressure Ratio (C-FER Tests)

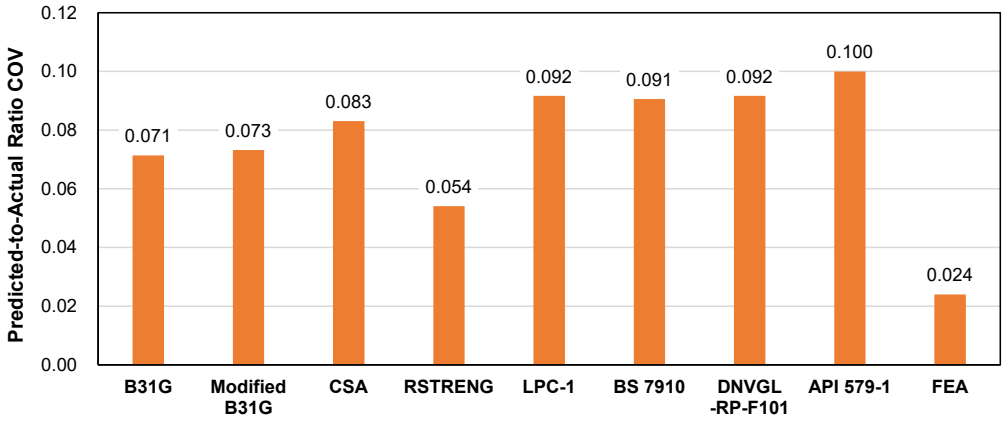

Figure 50 – COV of the Predicted-to-Actual Pressure Ratio (C-FER Tests)

Note that these remaining burst strength prediction models were developed based on extensive burst test data sets on line pipe samples that had D/t ratios exceeding 40 [42], whereas the casing specimens in this project ranged from 18 to 22. A careful review of these remaining burst strength prediction models indicates that the non-dimensional parameter $L/\sqrt{Dt}$ in various forms of the Folias factor can be re-formulated as $(L/t)/\sqrt{D/t}$. The component L/t is the ratio between the metal loss feature length and the pipe WT, and it reflects the geometric characteristic of the feature. On the other hand, the factor of the D/t ratio is implicitly included in the Folias factor. Therefore, the form of the Folias factor directly affects the burst pressure prediction capacity of the model for pipes with different D/t ratios. As a result, it is likely that the Folias factors calibrated based on large D/t line pipe samples are not suitable for these small D/t casing samples. Further adjustment of the Folias factors could be made to improve the model prediction accuracy.

Since this project included three different casing size and weight combinations, it provided an additional opportunity to investigate the impact of varying pipe D/t ratio on the remaining burst strength prediction model error. Figure 51 presents the relationship between the mean values of the predicted-to-actual pressure ratio and the casing D/t ratio for the three casing configurations tested in this project. The LPC-1, BS 7910, DNVGL-RP-F101 and API 579-1 models showed an improvement (increase) in the predicted-to-actual pressure ratio as the casing D/t ratio increases. The ASME B31G, the modified B31G, the CSA and the RSTRENG models do not appear to show a dependence on the pipe D/t. Since the number of tests are still quite limited, further investigation appears to be necessary to confirm if the pipe D/t ratio could affect model predication accuracy.

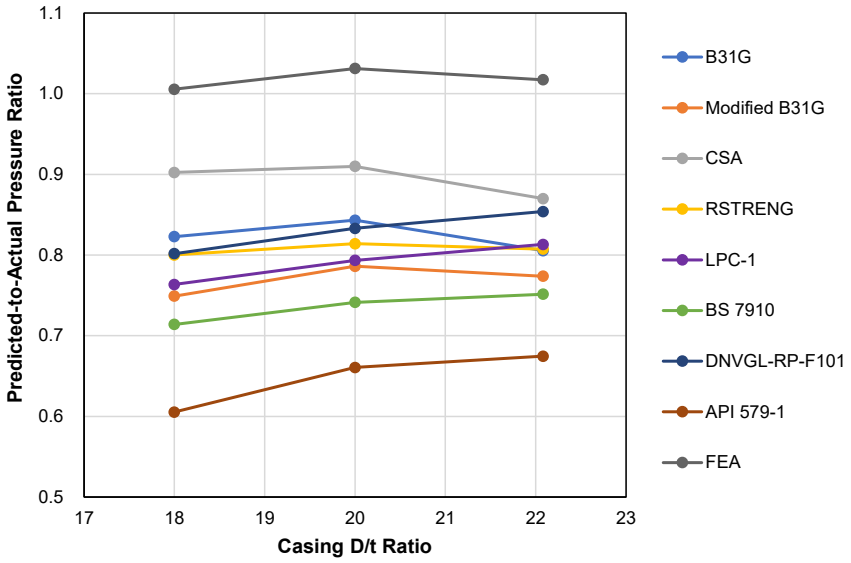

Figure 51 – Predicted-to-Actual Pressure Ratio (Mean Value) for Different Casing D/t Cases

8.2 - Model Evaluation Based on Previous Tests

Additional full-scale burst tests of casing samples with metal loss features have been previously conducted by Advantica [33] and Kiefner and Associates [25,43]. All of the Advantica burst tests were conducted under the capped-end condition. Review of the Advantica report indicates that seven out of the nine tests conducted in the project were valid (one test was terminated since the pump pressure limit was reached, and another test did not fail at the metal loss region) and, therefore, are used as additional data for the remaining burst strength prediction model evaluation. Table 9 lists the key information of the seven tests. Unfortunately, the YS and UTS for the 7.0 inch casing were not reported. Therefore, they were assumed to be the same as the 5.5 inch casing samples in this model evaluation. Note that the Advantica report indicates that all samples were J55 grade. The tests conducted by Kiefner and Associates are not included in this analysis as these tests included additional axial load or constraint that were not included in the current analysis.

Table 9 – Advantica Casing Burst Test Data [33]

Nominal OD (inch)	Nominal WT (inch)	Measured YS (psi)	Measured UTS (psi)	Feature Information*	Burst Pressure (psi)
5.5	0.275	55,000	110,800	single pit (diameter – 4t; depth – 80%t)	7,179
5.5	0.275	55,000	110,800	single pit (diameter – 6t; depth – 80%t)	7,048
5.5	0.275	55,000	110,800	single pit (diameter – 8t; depth – 80%t)	7,005
5.5	0.275	55,000	110,800	single pit (diameter – 2t; depth – 90%t)	8,745
7.0	0.317	N/A	N/A	single pit (diameter – 2t; depth – 60%t)	10,370
7.0	0.317	N/A	N/A	single pit (diameter – 2t; depth – 80%t)	9,819
7.0	0.317	N/A	N/A	single pit (diameter – 8t; depth – 60%t)	9,862

* t is the nominal WT of the casing.

Figure 52 and Figure 53 present the mean and COV of the predicted-to-actual pressure ratios from all remaining burst strength prediction models evaluated as applied to the Advantica test results. Note that the RSTRENG and FEA predictions were obtained directly from Advantica's report. In addition, as mentioned in Section 7.3.1, the FEA conducted by Advantica was based on the VME failure criterion (see Section 7.3 for detailed discussions). The following observations are made based on the model evaluation results:

- Models using the UTS as the flow stress showed a mean predicted-to-actual pressure ratio close to one (i.e. the CSA, LPC-1 and the DNVGL-RP-F101 models) primarily due to the high UTS of the casing samples;
- Models using the YS as the flow stress significantly under-estimated burst pressure. This is not surprising as the YS is only 50% of the UTS for these casing samples;
- All model predictions showed much higher COV of the predicted-to-actual pressure ratio than that determined based on the current tests;
- The differences in the model prediction performance appear to be significant between the Advantica test data set and the current test data set. However, the casing samples tested by Advantica had a much higher strain hardening property (i.e. a YS/UTS ratio of around 0.50) than the pipe materials in the current study (i.e. a YS/UTS ratio in the range of 0.85 to 0.87), which is likely to affect the prediction capabilities of the analytical models; and
- The Advantica FEA also under-predicted the burst pressure by ~20%, with a similar COV as other models. This is likely due to the VME criterion adopted in the modeling approach (see Section 7.3 for further discussions).

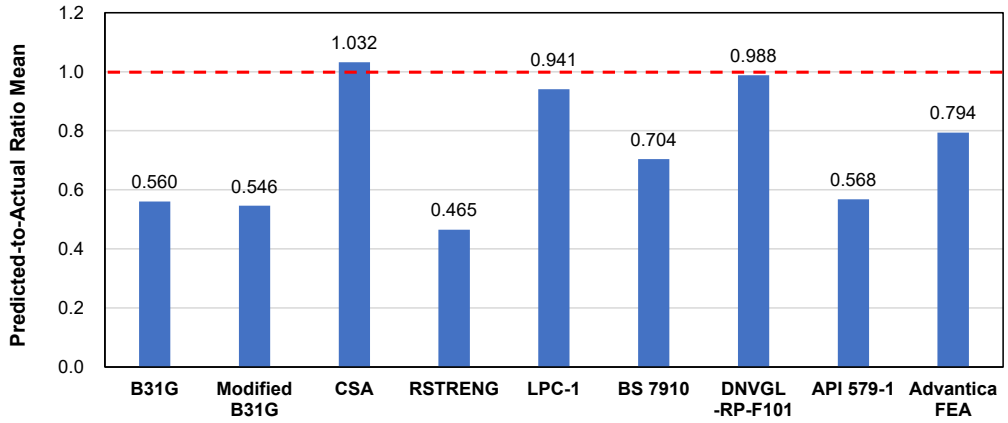

Figure 52 – Mean Value of the Predicted-to-actual Pressure Ratio (Advantica Tests)

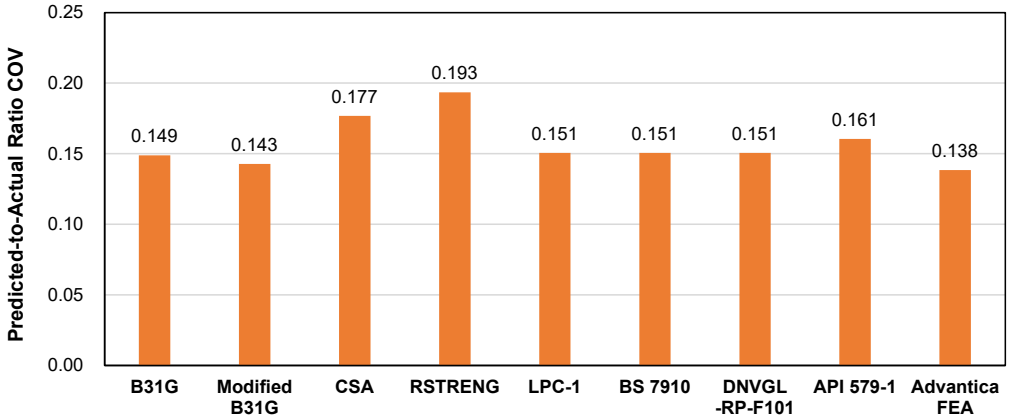

Figure 53 – COV of the Predicted-to-actual Pressure Ratio (Advantica Tests)

Based on the model prediction performance evaluation, further development of these remaining strength prediction models for downhole casing applications appears to be warranted. Specifically, the model improvement needs to focus on eliminating the excessive conservatism in burst strength calculations. For example, efforts could be focusing on modification of the Folias factors for the D/t range of casings that are commonly used in UGS wells. In addition, further development of advanced models may also consider including the strain hardening property of casing materials to capture the ductile rupture failure mechanism. Additional full-scale burst testing including other casing configurations (size, weight and grade) and a broader range of metal loss features representative of UGS well applications are critical for further development of the remaining burst strength prediction models.

9 - Framework for Reliability-based Casing Corrosion Management

9.1 - Overview

Casing reliability with respect to corrosion can be defined as the probability that a given length of casing will not experience loss of pressure containment due to corrosion damage within a specified period. As such, it is equal to the probability of corrosion failure subtracted from 1.0.

The probability of corrosion failure is calculated as the probability that the load effect will exceed the resistance capacity of the casing. Expressions that define the load effect and the resistance can be developed from basic physical and operational parameters of the casing using analytical models. The uncertainties associated with many of these basic parameters (i.e. random variations, measurement errors and modeling uncertainties) can be accounted for by characterizing the parameters using probability distributions. So-called limit state functions can be formulated from the load and resistance functions, which serve to define the combinations of basic parameters that would be expected to lead to casing failure. Standard methods are available to calculate failure probabilities from applicable limit state functions and the probability distributions associated with the basic input parameters.

This section first undertakes to explain why a reliability-based approach for casing integrity management is advantageous and then outlines a framework for the reliability assessment of downhole casing containing corrosion damage, based on metal loss feature data obtained from high-resolution casing integrity logs. It concludes with a simple demonstration analysis.

9.2 - The Argument for Employing a Reliability-Based Approach

Casing corrosion assessment processes are intended to provide information that will facilitate management of the potential for corrosion-induced failure, either by casing burst or leak. Remaining burst strength prediction models typically assume that failure occurs when the stress level in the casing material surrounding a metal loss feature exceeds the stress level that will result in material failure. The time to failure by burst is dependent on the existing feature size, the operating pressure, the mechanical and geometric properties of the casing, and the feature depth and length growth rates. Failure by leak requires through-wall feature growth. The time to failure by leak is independent of operating pressure and casing properties, being entirely dependent on casing wall thickness, the maximum feature depth and feature depth growth rate.

Maintaining integrity with respect to corrosion-induced leak or burst, when high-resolution casing logging data is available, involves the following key steps:

1) Identify and size significant features,

2) Project feature growth with time, and

3) Assess the remaining life of features and remediate as required.

This relatively straightforward, sequential approach to corrosion management is, however, complicated by the fact that each step in the process is associated with significant uncertainty. Consider the following:

- The actual size of metal loss features is uncertain because random measurement error is associated with the feature sizing information obtained from casing integrity logs and it is not possible to obtain direct measurement of downhole corrosion features to calibrate log results;
- The complexities and uncertainties associated with corrosion growth mechanisms imply that both the likelihood of further growth for a given feature and the rate of such growth for that feature are uncertain; and
- The time to feature remediation or time to re-inspection, as dictated by the time required for significant features to grow to a failure-critical size, is influenced by the sources of uncertainty described above, the added uncertainty associated with the accuracy of the adopted casing burst capacity prediction model, and the uncertainties associated with both the maximum operating pressure and the casing material properties.

A range of methods and models have been developed for assessing and managing corrosion integrity in pipelines and many of these methods are directly applicable to downhole casing. For simplicity, these different methods can be classified as either deterministic or probabilistic approaches that differ based on how the sources of analysis uncertainty are addressed. The key features inherent in each approach are described below as they pertain to the way in which casing integrity with respect to failure by burst is addressed.[1]

Deterministic methods address analysis uncertainties implicitly by employing conservative values for selected analysis inputs and by incorporating a safety factor on the calculated nominal burst capacity. The casing strength, for example, is typically assumed to be equal to the specified minimum value, which can be interpreted to be a conservative lower limit on the likely capacity of the steel in a given joint of casing. The uncertainties inherent in the remaining inputs to the burst calculation (i.e. uncertainties in feature size and growth rate, and the accuracy of the chosen burst capacity prediction model) are addressed through the safety factor applied to the predicted burst capacity.

The assessment approach, when employing a deterministic method, ensures that the factor of safety with respect to burst, as calculated for a given feature at a given point in time, is greater than or equal to the prescribed value. The margin of safety that is implicit in a deterministic assessment is controlled by the choice of the safety factor with a higher prescribed safety factor (SF), achieving a higher margin of safety against failure by burst.

A probabilistic approach, on the other hand, explicitly considers all significant sources of analysis uncertainty. The uncertain inputs to the burst capacity estimate are treated as random quantities, which are characterized by probability distributions that define both the range of values that each parameter can assume, and the likelihood associated with each value within the possible range.

[1] Integrity with respect to failure by leak is addressed by these methods in a similar manner, but, for clarity and simplicity of presentation, the focus of the discussion is confined to integrity with respect to burst.

The deterministic model that predicts nominal burst capacity is replaced with a probabilistic model that incorporates one or more model error terms, which explicitly acknowledge the potential for the chosen model to either over- or under-predict the true burst capacity. Using standard structural reliability methods, the description of the set of conditions that would lead to burst failure (i.e. the burst limit state function) is combined with probabilistic characterizations of all uncertain inputs to the burst calculation to produce an estimate of the probability of burst failure. A necessary refinement for time-dependent damage mechanisms, such as corrosion, is acknowledgment that feature size will increase with time. By treating feature size as a function of time, the analysis can be configured to provide an estimate of the probability of failure (POF) as a function of time.

The assessment approach, when employing a probabilistic method, ensures that the probability of corrosion feature failure by burst, as calculated for a given feature at a given point in time[2], is less than or equal to the prescribed maximum allowable value. The margin of safety that is implicit in a probabilistic assessment is controlled by the choice of the maximum allowable POF. To achieve a higher margin of safety against burst failure, one would adopt a lower value for the maximum allowable POF.

A conceptual illustration of the difference between a deterministic approach and a probabilistic approach to corrosion feature assessment is shown in Figure 54, assuming that the casing operating pressure is defined in terms of a maximum operating pressure (MOP).[3]

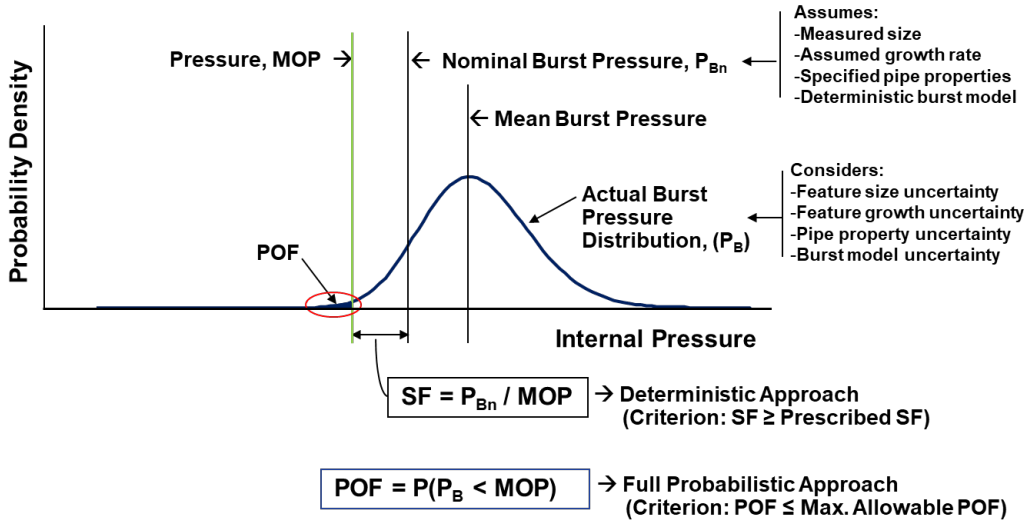

Figure 54 – Conceptual Illustration of the Difference between Deterministic and Probabilistic Methods for Assessing Failure by Burst

A summary of the key characteristics of each approach, together with a list of advantages and disadvantages, is as follows:

[2] For simplicity and consistency of presentation, the discussion of the probabilistic approach assumes a feature-specific burst assessment criterion. Note that the assessment criterion need not be feature-specific and, in the interest of risk consistency, a criterion based on feature aggregation is preferred (see Section 9.3.3).
[3] The illustration provided in Figure 54 makes the simplifying assumption that operating pressure is effectively deterministic. A full-probabilistic approach can address operating pressure uncertainty.

- ***Deterministic Approach***: This approach manages the potential for burst by ensuring that the calculated nominal burst pressure for a feature exceeds the MOP by not less than a prescribed amount (i.e. the safety factor). It manages the potential for leak by ensuring that the feature depth does not exceed a threshold depth, defined as a fraction of the nominal WT.

  Advantages: - Methods are generally well established and easy to understand.

  Disadvantages: - Sources of analysis uncertainty are not explicitly considered (they are, however, implicitly addressed through conservative specification of selected calculation inputs and the application of a safety factor to the burst capacity).

- ***Probabilistic Approach:*** This approach manages the potential for burst by limiting the likelihood that the operating pressure will exceed the calculated actual burst pressure at a feature, based on a probabilistic analysis that treats all burst model input parameters (including the accuracy of the burst model itself) as random quantities. It manages the potential for leak by limiting the likelihood that feature depth will grow to exceed the casing WT.

  Advantages: - All significant sources of analysis uncertainty are explicitly considered.
  - The calculated POF has a physical interpretation, and both the calculated value and the adopted probability threshold can be benchmarked using historical data.
  - POF thresholds can be chosen to achieve safety and/or environmental risk consistency.

  Disadvantages: - Methods are less established and implementation is more complex.
  - Characterization of significant sources of analysis uncertainty is required.
  - Consensus on POF thresholds has yet to be achieved.

In support of a move towards broader use of probabilistic assessment methods for casing corrosion integrity management, a reliability-based assessment framework is described in the subsections that follow. This assessment framework is an adaptation of the reliability-based design and assessment (RBDA) framework previously developed for pipelines by C-FER under PRCI sponsorship [44,45,46]. The framework description provided herein is intended to promote a better understanding of what is required to carry out a probabilistic assessment of casing corrosion integrity and how the results can be used for decision-making.

9.3 - Casing Corrosion Reliability Assessment Framework

9.3.1 - Overview

The major steps in the proposed reliability-based corrosion assessment framework are shown in Figure 55.

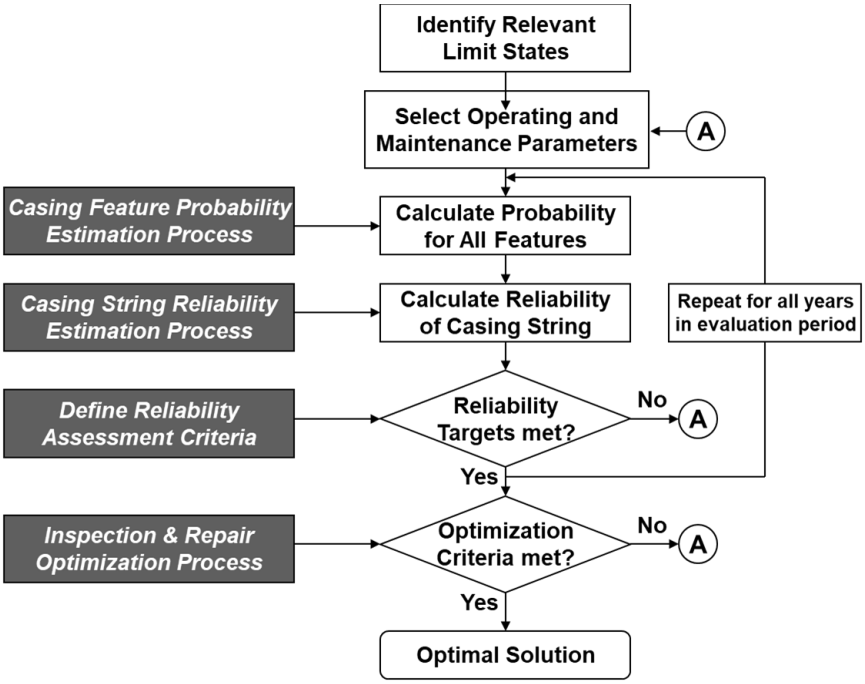

Figure 55 – Steps to Carry Out Reliability-based Casing Corrosion Integrity Management

As identified in Figure 55, the main process elements required to implement the methodology are:

1. ***Casing Feature Probability Estimation***: The process of calculating the probability and mode of failure for individual features identified through inspection, giving due consideration to all sources of uncertainty that can have a significant impact on the probability estimate, including the uncertainties inherent in the inspection data and casing material properties, and the models used to predict failure based on the inspection data.
2. ***Casing String Reliability Estimation***: The process of developing meaningful measures of casing string reliability based on the mode-specific POF estimates generated for individual features detected by inspection.
3. ***Definition of Reliability Assessment Criteria***: The process of establishing reliability targets for a given casing string that must be met or exceeded to ensure that adequate levels of safety and/or environmental protection are maintained throughout the time period of interest.
4. ***Inspection and Repair Optimization:*** The process of developing and analyzing candidate feature repair and re-inspection options to identify the preferred casing integrity management strategy.

9.3.2 - Casing Feature Probability Estimation

Failure due to corrosion can occur in one of two ways: either the corrosion feature penetrates the casing wall, resulting in a leak; or the casing wall experiences material failure (usually plastic collapse) at the feature location prior to the feature penetrating the wall, resulting in a burst. The distinction is important because the consequences of failure associated with each failure mode can be dramatically different and this has significant implications when establishing tolerable POF levels.

In the context of structural reliability analysis, a mathematical expression that defines the set of conditions that result in failure is an example of a *limit state function*. A failure limit state function is written such that it assumes a negative value for any set of conditions that would result in failure.

The limit state function for corrosion failure due to leak is

$$g_1 = t - d_{\max} \tag{49}$$

where t is the WT and d_{max} is the maximum feature depth.

The general form of the limit state function for corrosion failure due to burst is

$$g_1 = r_a - P \tag{50}$$

where r_a is the pressure resistance of a part through-wall corrosion feature and P is the internal pressure. The estimated pressure resistance is typically defined as a function of selected geometric and material properties of the casing and geometric parameters of the corrosion feature. In developing a model for the burst capacity of corroded casing, it is important to formally acknowledge the uncertainty inherent in the adopted failure prediction model (i.e. the model error) since this prediction uncertainty will have a significant influence on the failure probability estimates developed using the model. Examples of quantifying the prediction model uncertainties are illustrated in Section 8 of this report.

The preceding information indicates that, in general terms, each limit state function, $g(\boldsymbol{x})$, is defined as a mathematical function of a set of basic random variables, $\boldsymbol{x} = x_1, x_2, \ldots, x_n$, such that $g(\boldsymbol{x}) \leq 0$ if failure occurs, and $g(\boldsymbol{x}) > 0$ if failure does not occur. Given this, and considering, for now, a single limit state in isolation, the POF, p_f, associated with that limit state can be expressed mathematically as

$$p_f = p(g(x) \leq 0 \tag{51}$$

However, the POF due to corrosion is a function of time because the extent of corrosion damage increases with casing age. The values of selected random variables associated with a given corrosion limit state function, specifically feature depth and/or length, must, therefore, be defined as functions of time.

For example, the maximum feature depth, which is a random variable in the limit state function for small leak failure (see Equation (49)), must be defined as a function of time. Assuming, for illustration purposes, that the rate of depth growth is taken to be independent of the current feature depth, an expression for the maximum depth as a function of time, τ, is given by

$$d_{\max(\tau)} = d_{\max}(0) + d_{\max}\tau \tag{52}$$

where $d_{\max}(0)$ is the current maximum depth and $d_{\max}$ is the rate of growth in maximum depth.

Denoting a time-dependent limit state function by $g(\boldsymbol{x}, \tau)$, the POF by time τ is given by

$$P(\tau) = p(g(x,\tau) \leq 0 \tag{53}$$

This probability can be used to calculate the POF during a specific time interval (τ_1 to τ_2), given that the feature survives to the beginning of this interval, using the following relationship [47]:

$$p_f(\tau_1,\tau_2) = p_f(\tau_1 < \tau < \tau_2 | \tau > \tau_1) = \frac{P(\tau_2) - P(\tau_1)}{1 - P(\tau_1)} \tag{54}$$

If the time interval is taken as one year, and assuming that the feature is safe at time $\tau = 0$, it can be shown, using Equation (54), that the annual POF in the n^{th} year is given by

$$p_f(n) = \frac{P(n) - P(n-1)}{1 - P(0)} \tag{55}$$

The annual probability of feature failure in any given year can, therefore, be calculated by first solving Equation (53), at appropriate points in time, and then inserting the results into Equation (55).

In general, where only a single time-dependent limit state function is involved, Equation (53) can be solved using various analytical methods (e.g. First and Second Order Reliability Methods, FORM and SORM) or numerical techniques (e.g. Monte Carlo simulation). However, where multiple failure limit states are involved, as is the case for corrosion, the solution of Equation (53) is significantly complicated by the way that the limit states interact. Analytical methods for reliability solving Equation (53), when multiple interacting limit states are involved, have yet to be identified; however, simulation-based methods can be employed to obtain a solution.

9.3.3 - Casing String Reliability Estimation

At a location where a single corrosion feature is known to exist, the reliability, with respect to corrosion, is defined as the probability that the feature will not fail within a specified period. It is related to the probability of feature failure by

$$R = 1 - p_f \tag{56}$$

For a linear system, such as a casing string, which will typically contain many corrosion features distributed along the length of the string, it is more appropriate to define the reliability as the probability that the entire string will not fail due to corrosion damage within a specified time period. As such, the relevant probability is the total POF for all corrosion features associated with the casing string under consideration.

Adopting one year as the reference time, the reliability per year for a casing string containing *n* corrosion features is

$$R = 1 - \sum_{i=1}^{n} p_{fi} \tag{57}$$

where p_{fi} is the annual POF of the i^{th} feature contained in the casing string under consideration.[4]

The key to reliability assessment based on this approach is the establishment of defensible reliability thresholds (or reliability targets), above which continued casing operation is deemed acceptable.

Assuming that appropriate reliability targets, R_T, can be established for a given casing string, it follows that acceptable operating conditions are confirmed with respect to corrosion if the following check is satisfied for all years within the time period of interest:

$$1 - \sum_{i=1}^{n} p_{fi} \geq R_T \tag{58}$$

If this reliability check is recast in terms of a maximum allowable failure probability per year, p_{max}, which is related to the prescribed reliability target by

$$R_T = 1 - p_{max} \tag{59}$$

then the basic reliability check becomes

$$p_t \leq p_{max} \tag{60}$$

where p_t is the total annual probability of casing string failure given by

$$p_t = \sum_{i=1}^{n} p_{fi} \tag{61}$$

Also, if a risk-consistent approach to corrosion integrity assessment is to be employed (see also Section 9.3.4), where risk is defined as failure probability multiplied by the consequence of failure, then separate reliability checks will be required for leak and burst failures. This is because the failure-mode-specific reliability targets (or maximum allowable failure probabilities) for a specific casing string, as determined from a prescribed threshold risk level for the casing, will differ due to the significant differences in failure consequences between failure modes. For similar reasons, a distinction between large leak and rupture failures may also be warranted.

The reliability-based approach to corrosion integrity assessment can, therefore, be employed to determine when (i.e. how many years after the last inspection) the reliability check given by Equation (60) is no longer satisfied (see Figure 56). The rationale behind feature repair, as a component of a viable corrosion management strategy, is that re-inspection will be required before the reliability check is no longer satisfied, and the time over which the reliability check is satisfied can be

[4] Note that Equation (57) is an approximation because it does not explicitly reflect the potential for multiple feature failures within the reference time period. However, in the context of a reliability-based assessment of corrosion integrity, where the annual POF for individual corrosion features is meant to be very small, the simplified formulation provides a very close approximation to the true reliability for the length of casing under consideration.

extended if the failure probability associated with selected features is eliminated by repairing the casing at those feature locations (see Figure 57). Staged or delayed repair is conceivably permissible because features that are candidates for repair prior to re-inspection need not be repaired until just before the estimated casing failure probability exceeds the maximum allowable level.[5]

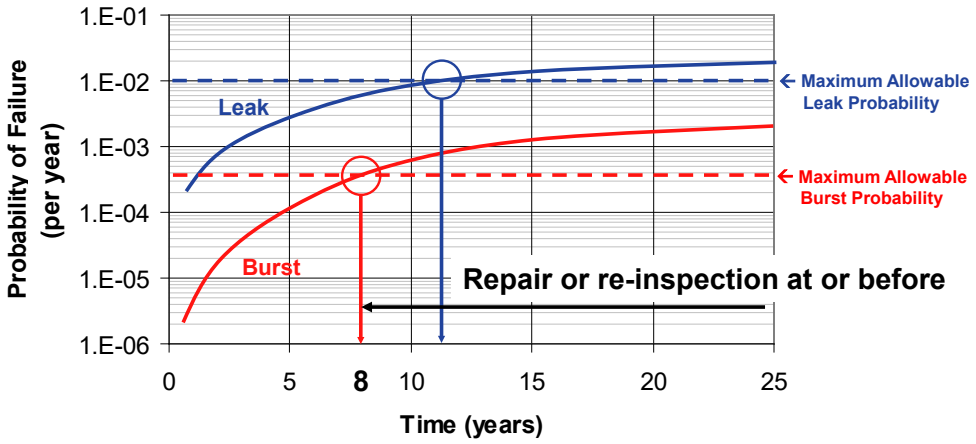

Figure 56 – Casing String Reliability Assessment – Without Repair

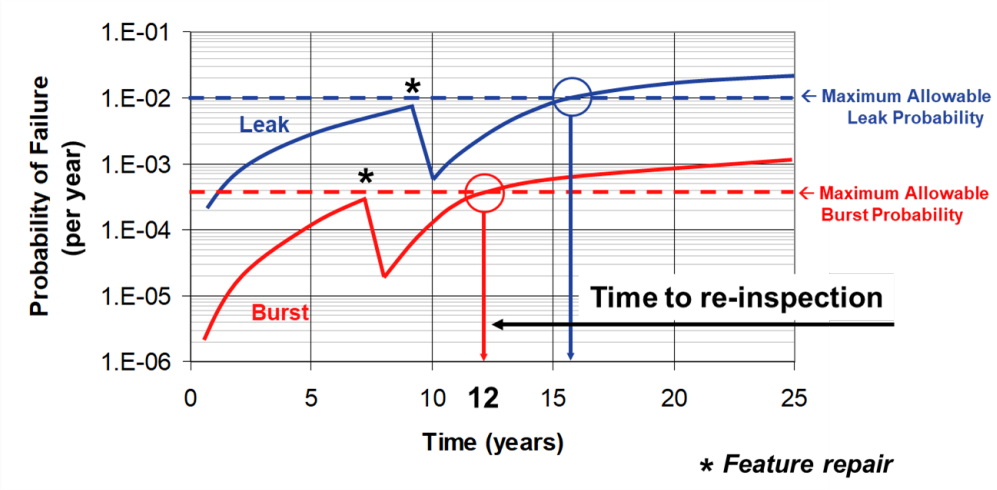

Figure 57 – Casing String Reliability Assessment – With Repair

[5] The corrosion management process, as described herein, assumes that, within the time period of interest, the well operating conditions (e.g. internal pressure) and environmental conditions (e.g. corrosion growth rates) will not change significantly, and that the reliability of the casing string in question will be controlled by the POF associated with the features that existed in the string at the time of the last inspection. In this context, checks should be undertaken to ensure that, within the time period of interest, the impact of the initiation and the growth of new corrosion features is negligible, otherwise the potential contribution to the POF within a given evaluation length should be given explicit consideration.

9.3.4 - Reliability Assessment Criteria

As previously discussed, a reliability-based approach to integrity management requires that a casing string be maintained to ensure that the calculated level of reliability meets or exceeds a prescribed threshold value, referred to as the reliability target, and a complementary statement of the same requirement is that a casing string must be maintained such that the total annual probability of casing failure does not exceed a prescribed limiting value, referred to as the maximum allowable failure probability. If it is assumed that casing reliability must be maintained to ensure adequate levels of public safety and environmental protection, the determination of appropriate reliability targets (or maximum allowable probabilities of failure) for a given casing string can be approached in one of two ways:

- ***Inference-based approach***: This approach assumes that the reliability of a given casing string is to be maintained at or above the level that can be shown to be associated with a similar reference casing, which is deemed, by inference, to afford an adequate level of protection to people and/or the environment. In this case, the reliability target is equal to the calculated level of reliability associated with the reference casing string.

- ***Risk-based approach****:* This approach assumes that the reliability of a given casing string is to be maintained such that a predefined level of public safety and/or environmental protection is met or exceeded. In this case, the reliability target is calculated using a risk-based approach that is based on direct application of explicit relationships that quantitatively reflect the potential impact of casing failure on people and/or the environment.

An inference-based approach generally requires the selection and characterization of an appropriate reference casing string, followed by the calculation of the reliability associated with the reference string, which is then assumed to define an acceptable reliability level. The allowable level of damage that is to be associated with the reference casing string must be shown to be acceptable based on current practices, past experience or some other performance metric, and it is left to the proponent of the inference-based approach to explicitly define this damage-extent based on their preferred approach.

Assuming that an allowable damage-extent can be defined, the reliability estimation process previously described can be used to calculate the failure-mode-specific levels of reliability associated with the reference casing sting, and these reference reliability levels can then be taken as acceptable values for the mode-specific reliability thresholds.

Alternatively, a simplified inference-based approach to establishing reliability thresholds could involve assuming that, in general, the past performance of casing strings in service is broadly acceptable. Historical incident data could then be used to determine the average annual casing failure rate and the mode-specific (i.e. leak versus burst) failure rates could be adopted as the reliability thresholds. Note that defensible application of this approach requires that stakeholders agree that past performance is in fact acceptable.

A risk-based approach to establishing reliability assessment criteria, on the other hand, follows directly from the basic definition of risk, $\bar{R}$, which is given by

$$\bar{R} = p_t \times C \tag{62}$$

where p_t is the total annual probability of casing failure and C is a measure of the failure consequences. Based on Equation (62), the maximum allowable value of p_t , previously defined as p_{max}, is given by

$$p_{max} = \frac{\bar{R}_{max}}{C} \tag{63}$$

where $\bar{R}_{max}$ is the maximum tolerable level of risk.

To be able to use this approach to determine the reliability threshold (or the maximum allowable annual failure probability), a tolerable risk level must, therefore, be established, and an appropriate consequence model is required to relate failure to the potential outcome.

If multiple aspects of risk need to be addressed (for example, if public safety risk and the risk of environmental damage need to be considered), then multiple measures of risk may have to be considered. This implies that more than one measure of tolerable risk level will have to be established and consequence models capable of assessing the magnitude of failure impact in appropriate terms will also be required.

9.3.5 - Inspection and Repair Optimization

The longer that casing re-inspection is deferred, the more the remaining features will grow and the greater the likelihood that additional features will require remediation to avoid exceeding the prescribed failure probability limits. This implies that progressively longer times to the next casing inspection are associated with the requirement of progressively more feature repairs. Each candidate time to next inspection, and the associated set of required feature repairs, constitutes a viable maintenance option in the sense that each option satisfies the reliability requirements up until re-inspection is performed. However, it is not obvious which option is preferred. (Is it better to remediate a few features and re-inspect sooner or remediate more features and re-inspect later?) Complicating the analysis is that casing re-inspection requires well re-entry, the act of which itself poses an additional threat to well integrity. In addition, casing repairs can often require a second well entry, following well entry for inspection, to facilitate casing repairs.

To address the implications of the competing factors outlined above, a comparative reliability assessment is generally required to determine the preferred course of action. Specifically, candidate casing reliability management scenarios must be defined in terms of whether casing repairs are to be performed and, if so, how many repairs are to be made. Each scenario must then be analyzed to determine the number of years of casing operation that can be achieved before well entry is again required to ensure that casing reliability is being maintained.

Assuming that reliability thresholds are available, the optimal course of actions is the lowest cost option that meets or exceeds the prescribed criteria over the remaining operating life of the well, taking into account both the reliability enhancements achieved through periodic casing inspection and repair, and the additional point-in-time reliability detriments introduced every time the casing is to be re-inspected and casing repairs are to be made.

Note that, if reliability thresholds are not yet available, the preferred course of action is the one shown to maximize the reliability of the well over its remaining operating life time, again taking into account that both the reliability enhancements achieved through periodic casing inspection and repair, and the reliability detriments introduced by casing re-inspection and repair activities.

The above suggests that true optimization of casing integrity through periodic well entry, casing inspection and repair must also explicitly evaluate the likelihood of well failure during well entry. While outside the scope of these guidelines, guidance for evaluating the potential for well failure during well entry is available in a study titled "Risk Assessment and the Treatment of Wells" carried out by C-FER for the US DOT's Pipelines and Hazardous Materials Safety Administration [48].

9.4 - Demonstration Analysis

9.4.1 - Overview

To illustrate the application of the reliability assessment framework described in Section 9.3, the process, as described, was used to generate reliability estimates over time for a hypothetical 7-inch diameter casing string in a 50-year-old natural gas storage well operating at a maximum pressure of 2,000 psi.

The analysis assumes that casing corrosion data is available from a recent inspection performed using a high-resolution logging tool and this information is used to estimate the annual probability of casing failure by leak or burst over the course of a 20-year evaluation period. The effect of repairing selected metal loss features following inspection is illustrated in remediation scenarios that involve re-calculating the annual mode-specific casing failure rates associated with the remaining corrosion feature population.

9.4.2 - Analysis Inputs and Assumptions

The required operating parameters, geometric parameters, material properties and any associated uncertainties for the assumed 7.0 inch, 23 ppf J55 casing are summarized in Table 10. The probabilistic characterizations of the various uncertainty parameters are considered typical based on C-FER internal data and public information.[6]

The metal loss information available from the hypothetical casing inspection is assumed to include maximum feature depth (expressed as percent WT) and feature length. Feature width, while often reported, is not explicitly considered by the chosen burst prediction model. The casing string is assumed to contain 10 metal loss features (see Table 11). Note that features D8, D9 and D10 correspond to actual metal loss features contained in three burst test specimens (see Appendix E).

[6] API TR 5C3 Annex F [32], which provided the WT and YS uncertainty parameters in the demonstration analysis, provides a summary of statistical distributions of several key pipe body parameters based on an extensive industry survey. Characterization of the statistical data of these pipe body parameters was part of an effort by API to develop a new probabilistic approach to determine casing collapse ratings. Nonetheless, these data were directly collected from several major pipe manufacturers and are representative of the majority of the casing products. However, pipe manufacturing technology and processes are continuously evolving, so current product characteristics may not represent the casing products in UGS wells that were constructed several decades ago.

The analysis also assumes, based on C-FER's experience to date, that, for illustration purposes, a representative feature sizing tolerance for a such a tool is ±20% of WT for depth measurement and ± 0.8 in for length measurement, both at an 80% certainty level.

The burst prediction model used as the basis for the burst limit state function in the probabilistic analysis is a model developed by C-FER that is referenced in Annex O of CSA Z662-19 [21], a deterministic version of which is also discussed in Section 4.2.3. This model estimates burst pressure based on the reported feature axial length and the average depth. Where maximum feature depth is provided instead of average depth, as is the case for the assumed casing logging tool, a conversion from maximum to average feature depth is required. Analysis by C-FER of metal loss feature depth profiles for a wide range of pipeline corrosion features supports defining this ratio by a probability distribution, which is also provided in Table 10. In addition, a burst model error characterization is incorporated in the probabilistic analysis, which includes both additive and multiplicative error terms (see Table 10). Note that this model error characterization is based on analysis of actual versus predicted burst pressures for a range of real metal loss features in line pipe. While it has not been demonstrated to be directly applicable to downhole casing, it is considered a reasonable basis for model error characterization in this illustrative analysis.

Lastly, the analysis assumes that resident metal loss features are increasing in depth due to corrosion growth at a linear rate and that deeper features are likely associated with higher average corrosion rates than shallower features. This analysis assumes no significant length growth. Borrowing from methods often employed for assessing corrosion growth in pipelines, where feature data from only a single ILI run is available, it is further assumed that all reported metal loss features have been growing in depth for one-half of the life of the casing (which conservatively increases the growth rate prediction in comparison to assuming growth from time of casing installation). On this basis, the mean annual growth rate for each feature is taken to be equal to the measured feature dimension divided by one-half of the casing age (i.e. assumed growth period is 25 years). Growth rate uncertainty is introduced in the analysis by acknowledging that the reported feature dimensions are subject to the sizing error implied by the assumed tool sizing tolerance.

Table 10 – Input Parameters for Casing Reliability Analysis

Parameter	Units	Mean	Standard Deviation	Distribution Type
Diameter	inch	7	N/A	Deterministic
Wall thickness	inch	0.319	0.0083	Normal
Maximum pressure	psi	2,000	N/A	Deterministic
Yield strength	ksi	67.65	4.86	Normal
Tensile strength	ksi	84	2.52	Normal
Max. depth measurement error	inch	0.0	0.024	Normal
Length measurement error	inch	0.0	0.307	Normal
Maximum-to-average feature depth ratio	N/A	2.16	1.03	Log Normal (shift = 1.0)
Burst model error term, e1	N/A	1.04	N/A	Deterministic
Burst model error term, e2	N/A	–0.000556	.00147	Normal

Table 11 – Corrosion Feature Sizes for Hypothetical Casing String

Feature	Feature Depth (%WT)	Feature Length (inch)
D1	40%	0.79
D2	30%	0.79
D3	20%	7.87
D4	20%	1.38
D5	12%	4.72
D6	5%	3.15
D7	5%	0.79
D8 (7.0in-JT#3-D1)	47%	4.57
D9 (7.0in-JT#3-D2)	47%	6.34
D10 (7.0in-JT#3-D3)	50%	3.58

9.4.3 - Selection of Reliability Criteria

For this demonstration analysis, the historical rate of failure of casing strings in US UGS wells, as developed and reported by deWolf et al. [49], and interpreted by C-FER [48], was used to define the broadly acceptable levels of casing string reliability with respect to leak and burst failure.

These reliability thresholds, expressed as maximum allowable values for the annual casing leak and burst failure probability, rounded to single digit precision, are 1×10^{-4} failure per year for small leak and 1×10^{-5} failure per year for burst.

9.4.4 - Analysis Results and Discussion

Based on the input parameters described in Section 9.4.2, the annual POF by leak and burst, for each reported feature in the casing string, was calculated for a 20-year period starting from the year of inspection. The individual feature-specific probability estimates were then aggregated to produce failure-mode-specific casing failure rates over the same period. The projection of the aggregated annual corrosion leak and burst probabilities for all reported features in the casing string are shown in Figure 58. The figure also shows the leak and burst reliability thresholds (i.e. maximum allowable failure probabilities), developed as described in Section 9.4.3.

The intent of the demonstration analysis is to determine the extent of feature remediation required to achieve an acceptable level of casing reliability up until the time of next casing inspection. This is demonstrated by showing when the predicted annual leak and burst failure rates are less than or equal to the prescribed respective threshold values. The results can be interpreted to mean that re-inspection is required in the year prior to that in which one or both failure probability limits thresholds are exceeded.

The Base Case analysis results shown in Figure 58 indicate that, without feature repair, the casing will be operating at a reliability level that satisfies neither the leak nor burst criteria (i.e. both annual failure probabilities exceed the prescribed limits in the first year following inspection).

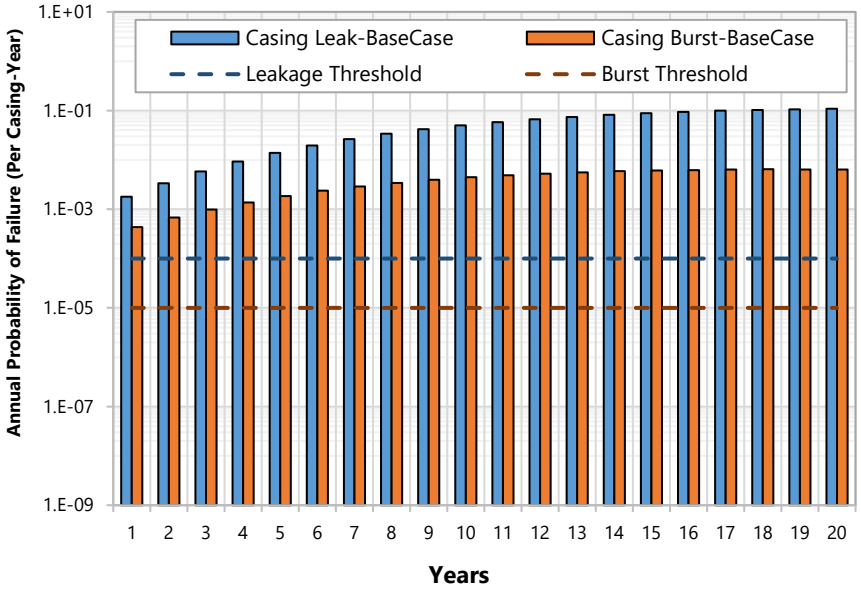

Figure 58 – POF versus Time for Base Case: No Feature Remediation

Remediation Scenario 1, shown in Figure 59, involves removal of three features following inspection. This corresponds to the minimum number of casing repairs required to achieve the acceptable operating reliability level following the initial inspection and repair cycle. However, this scenario is shown to meet the reliability criteria for only one year.

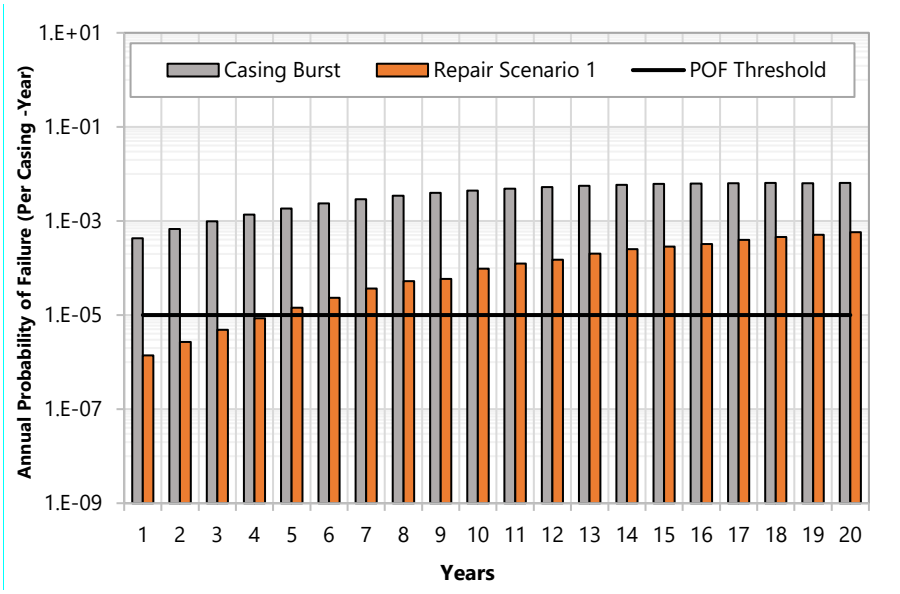

a) POF with Respect to Burst Threshold

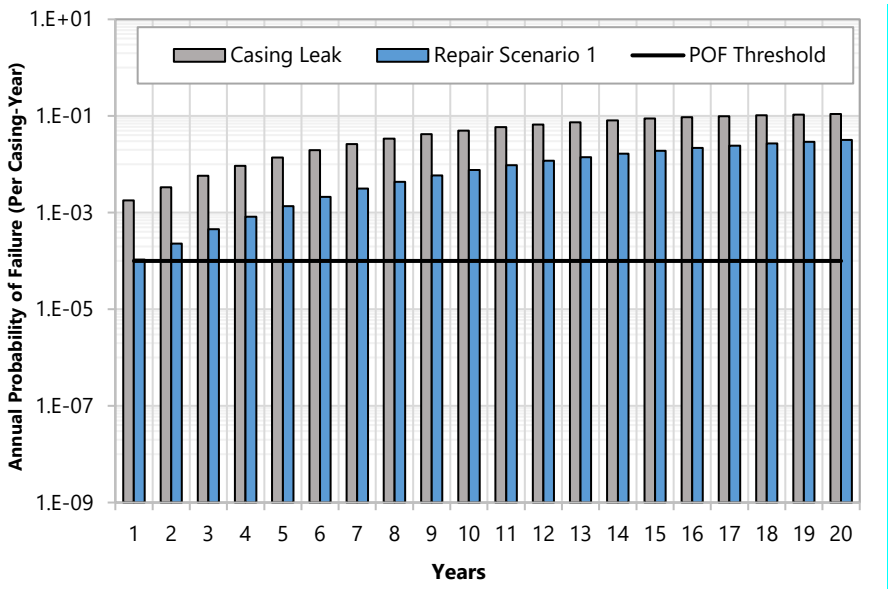

b) POF with Respect to Leakage Threshold

Figure 59 – Casing POF for Remediation Scenario 1: Removal of D8, D9 and D10

Remediation Scenario 2, shown in Figure 60, involves the removal of four features. This more aggressive repair strategy is shown to achieve adequate casing reliability for four years, meaning that re-inspection and potential further casing remediation is required before the start of year five.

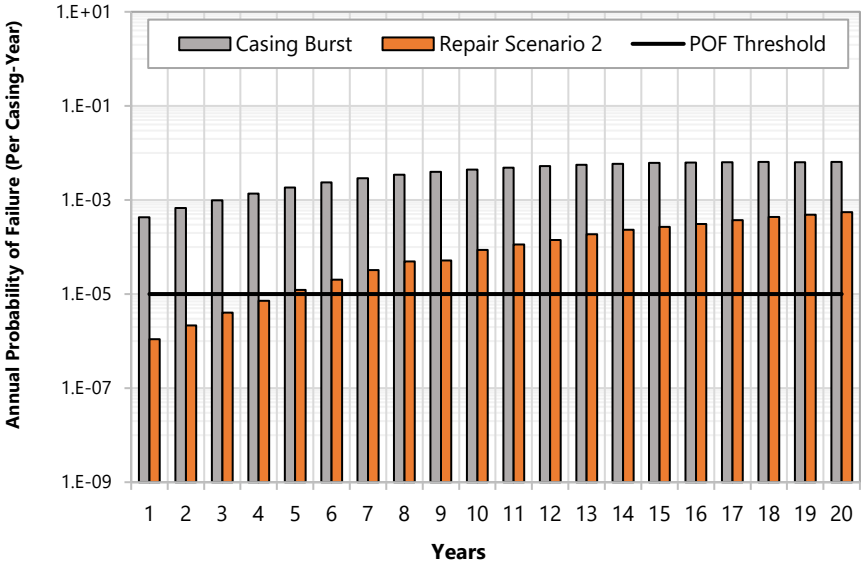

a) POF with Respect to Burst Threshold

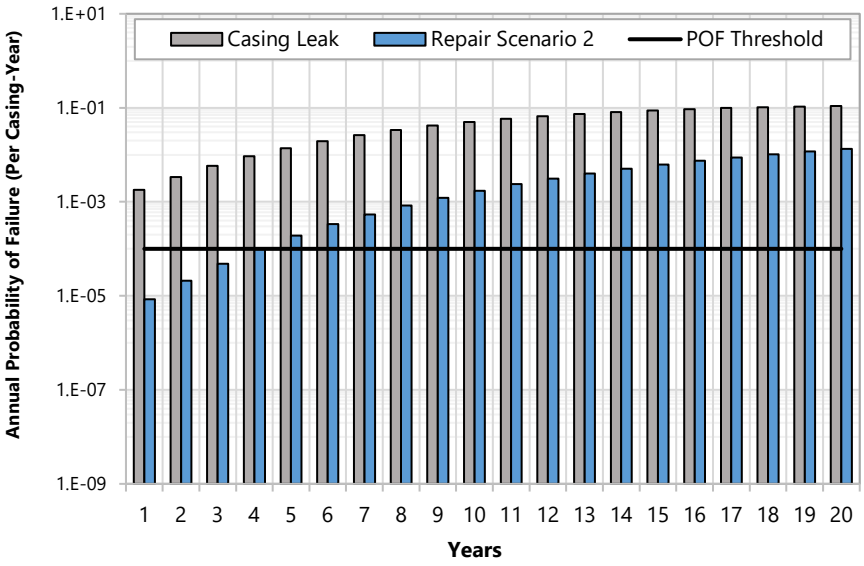

b) POF with Respect to Leakage Threshold

Figure 60 – Casing POF for Remediation Scenario 2: Removal of D1, D8, D9 and D10

Remediation Scenario 3, shown in Figure 61, involves the removal of six features and is shown to achieve adequate casing reliability for eight years.

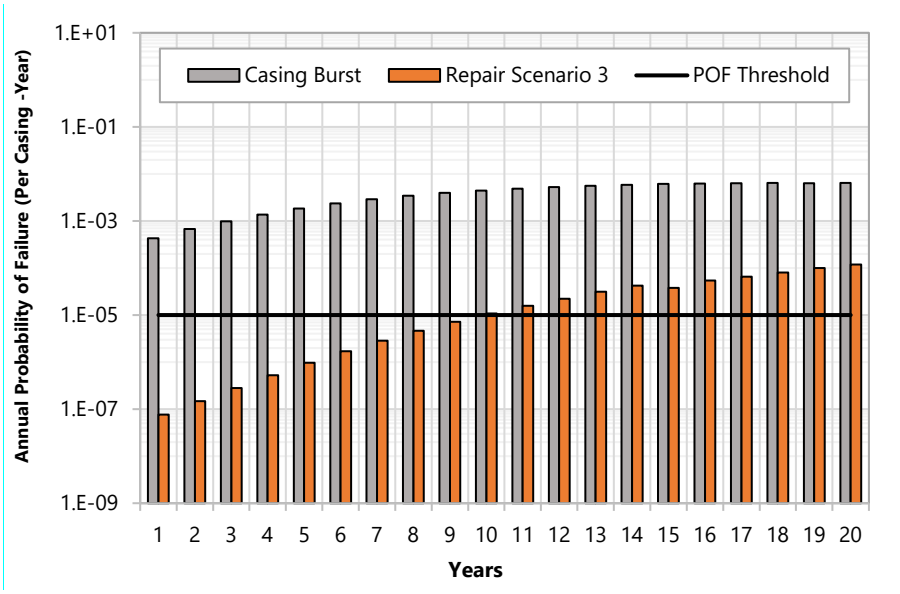

a) POF with Respect to Burst Threshold

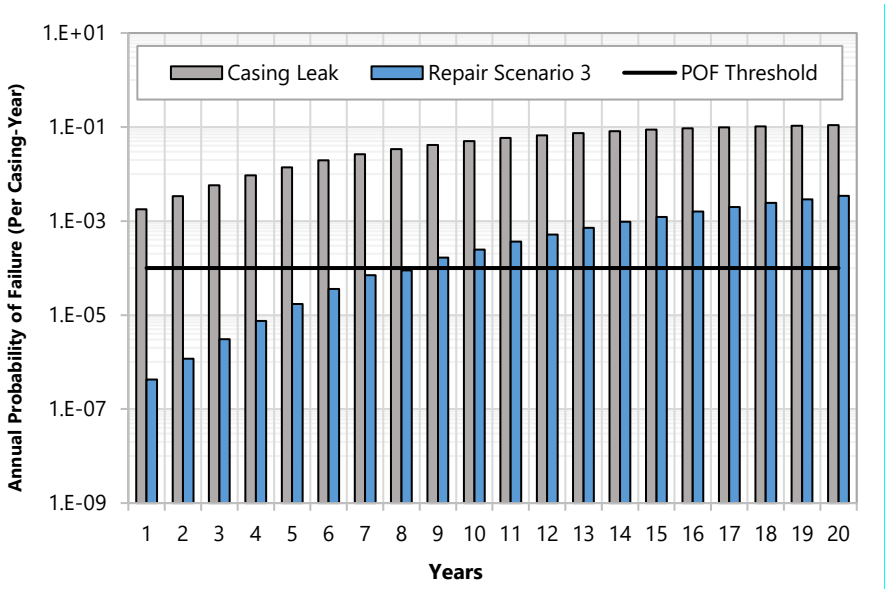

b) POF with Respect to Leakage Threshold

Figure 61 – Casing POF for Remediation Scenario 3: Removal of D1, D2, D3, D8, D9 and D10

Lastly, Remediation Scenario 4, shown in Figure 62, involves removal of eight features following inspection and this repair strategy is shown to achieve adequate casing reliability for 15 years.

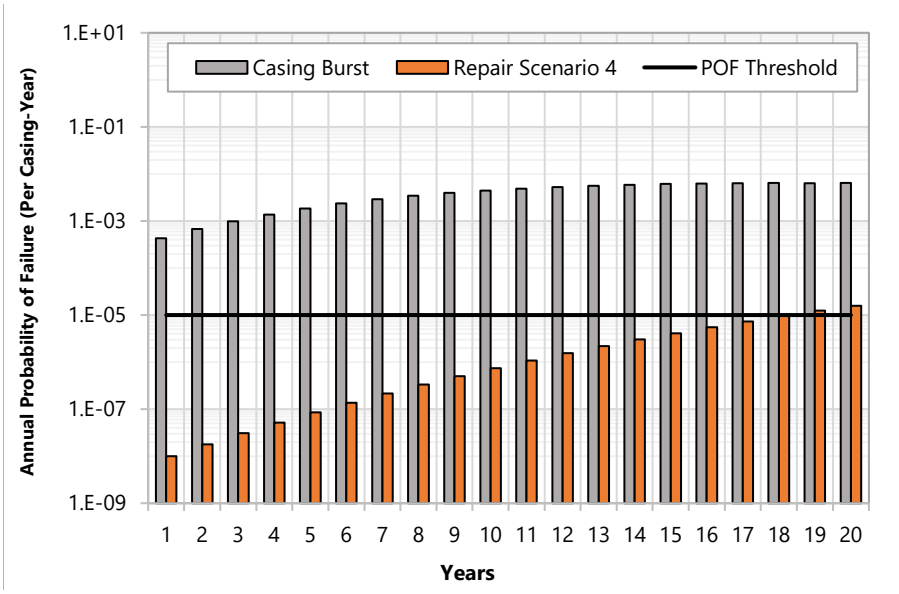

a) POF with Respect to Burst Threshold

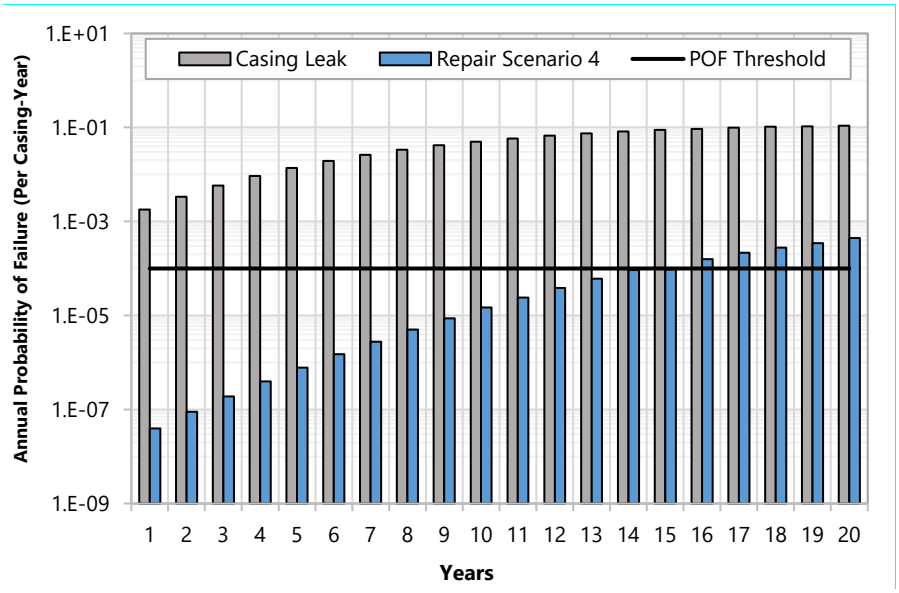

b) POF with Respect to Leakage Threshold

Figure 62 – Casing POF for Remediation Scenario 4: Removal of D1, D2, D3, D4, D5, D8, D9 and D10

Collectively, the Base Case and Remediation Scenario analyses described herein demonstrate that the proposed probabilistic assessment process can be used to determine whether casing reliability without feature remediation will be acceptable going forward and, if so, for how long. It also provides the means to determine which metal loss features need to be remediated to achieve acceptable casing reliability for a range of candidate times to next inspection.

Note that the demonstration analysis is artificial in the sense that it involves a very limited number of corrosion features sized to illustrate various aspect of the methodology. However, the process as described can readily be scaled up to address more realistic situations (i.e. significantly larger feature populations) and it can be adapted to include separate evaluations of different casing depth regions that should perhaps be assessed against different reliability thresholds that would depend on depth-dependent differences in leak and/or burst consequences.

9.4.5 - Summary

A reliability-based assessment framework is described that addresses issues of key importance with respect to casing corrosion integrity management based on high-resolution integrity logs, including: feature-specific probability estimation; the treatment of inspection-related uncertainties; appropriate measures of casing reliability; the development of reliability assessment criteria; and the relationship between measured casing damage severity, the extent of repair and the required time to next inspection.

The use of the proposed framework is illustrated with an analysis of a hypothetical casing string for which high-resolution metal loss corrosion data is assumed to be available. The demonstration analysis shows how casing log data can be used to estimate casing reliability as a function of time, how selected corrosion feature remediation affects the reliability projections and how this information can be used to support the determination of the required time to next inspection.

Note that the determination of how many features should be remediated and when the casing should be re-inspected will depend on many factors, not the least of which is recognition that follow-on well entry for casing feature repair, and later well entry for re-inspection and possibly further casing repair, will introduce additional well risk. The optimal mitigation strategy will balance the risk reduction achieved by casing feature remediation against the risk increase associated with additional well entry for casing feature remediation and/or re-inspection. A framework for managing the overall well risk with due consideration of the additional well risk posed by well entry is provided in a companion research project carried out for PHMSA titled “Risk Assessment and Treatment of Well Entry Risk” [48].

10 - Summary of Findings and Developments

This multi-phase study resulted in the following key findings and developments:

Casing Corrosion Logging Technologies:

Findings on the performance of casing corrosion logging technologies are made based on the collective information from this and the preceding PRCI logging tool test projects, as well as the literature review.

- Significant variations exist among different casing corrosion logging technologies. Understanding the benefits and limitations of each technology is critical for selecting the most appropriate technology for the intended application;
    - Commercial tools based on UT and MFL technologies generally have the capability to conduct high-resolution inspection of isolated casing corrosion features. However, note that significant variations can exist among vendor deliverables and tool performance even for tools using the same technology. Therefore, communication between operators and logging service providers is critical to ensure that the final deliverable meets the operational and regulatory requirements. In the pipeline industry, API Standard 1163 [1] suggests that pipeline operators co-operate with service providers to choose the proper inspection technology that meets the operator's goals and objectives. The operator shall provide information on the physical characteristics and constraints of the pipeline to service providers, and the service provider shall state whether the chosen ILI system can meet the written performance specification. The same information exchange should also apply to downhole casing inspections;
    - The prototype tools based on the MEC technology tested in this project also demonstrated good performance that is comparable to commercial logging tools using other technologies. Further commercialization of this technology to supplement existing casing corrosion logging technologies is recommended;
    - The MFC tool physically measures the casing inner wall profile, which may be used to diagnose casing deformation and metal loss due to internal corrosion. The MFC tool cannot inspect metal loss on the outer surface of the casing. The sizing accuracy of MFC tools is directly related to the casing diameter and the measurement resolution (i.e. the number of caliper fingers and axial sampling rate). In addition, it appears that nominal casing dimensions are often assumed in interpretating MFC logs for metal loss estimation, which can introduce significant error. Therefore, the MFC tools may be used as an initial screening tool to obtain an estimation of internal corrosion and deformation of casing strings. Due to several limitations, MFC logs are not recommended for comprehensive casing corrosion assessments;
    - Tools based on EM technologies can conduct through-tubing corrosion logging. The literature review indicated that significant variations exist among vendor tools, including tool configurations, operating modes and measurement capabilities. An important limitation of EM tools is that they can only estimate the average wall loss of the casing strings along the entire circumference, and they are not suitable for characterizing discrete corrosion features. In addition, there is a lower threshold of detection that limits these tools in detecting minor metal loss features. Nevertheless, additional investigation

involving quantitative lab test evaluations is warranted to better understand the capability of these tools; and
    - Well logging using multiple tools with different technologies can help minimize measurement uncertainties; and
- Unlike the ability to evaluate ILI tool performance by excavating the pipe and directly measuring selected features by hand, it is extremely difficult to validate casing corrosion logging tool performance in real wells. This and the preceding PRCI casing logging tool test projects demonstrated that lab tests can be an efficient approach to collect high quality data for quantitative evaluations of corrosion logging tools.

Remaining Burst Strength Prediction of Corroded Casing:

- All burst test specimens in this project showed a plastic collapse failure mode in the blunt metal loss regions, with either a small leak or ductile rupture;
- All analytical remaining burst strength prediction models under-estimate the remaining burst strength by approximately 10% to 36% based on the current physical test results;
- Among the analytical prediction models reviewed (excluding the RSTRENG model), the ASME B31G and modified B31G remaining burst strength prediction models were found to have the lowest random error levels for the 20 burst test results obtained in this project;
- The LPC-1, BS 7910, DNVGL-RP-F101 and the API 579-1 models appeared to show that the prediction accuracy varies with the casing D/t ratio;
- FEA prediction using the actual stress-strain relationship and the metal loss profile was found to achieve good agreement with the physical burst test results. Particularly, the failure criterion based on plastic collapse was found to significantly improve the prediction accuracy compared to the VME failure criterion;
- The downhole in-situ load conditions, such as the locked-in axial load, was found to have a marginal impact on the remaining burst strength of casing. This effect can be accounted for with an empirical factor applied to the remaining burst strength predictions. Additional study is required to further validate the findings of the locked-in axial load effect; and
- The casing material showed time-dependent stress-strain response in the post-yield region in modified coupon tests that included an extended hold period at high stress. Therefore, the casing burst strength obtained from lab tests (under a relatively high strain rate) would overestimate the actual burst strength in the UGS well, where the casing is under sustained pressure (i.e. extremely low strain rate). Further investigation of the strain-rate effect on the remaining burst strength of corroded casing is warranted to ensure appropriate safety margins are considered in predicting the remaining burst strength.

Reliability-based Casing Corrosion Management Framework:

- A reliability-based assessment framework is described that addresses issues of key importance with respect to casing corrosion integrity management based on high-resolution integrity logs, including: feature-specific probability estimation; the treatment of inspection-related uncertainties; appropriate measures of casing reliability; the development of reliability assessment criteria; and the relationship between measured casing damage severity, the extent of repair and the required time to next inspection.

- The use of the proposed framework is illustrated with an analysis of a hypothetical casing string for which high-resolution metal loss corrosion data is assumed to be available. The demonstration analysis shows how casing log data can be used to estimate casing reliability as a function of time, how selected corrosion feature remediation affects the reliability projections and how this information can be used to support the determination of the required time to next inspection.

11 - Recommendations for Future Work

Based on the outcomes of this research program, the following recommendations are made for future work:

Casing Corrosion Logging Tool Evaluation and Improvement:

- Further lab test evaluation of high-resolution casing logging tools is recommended to improve the understanding of logging tool response to a broader range of casing metal loss features. Additional metal loss features with complex profiles should be included in the test. The expanded test data sets would form the basis for determining parameters that describe the uncertainties associated with logging tool performance, which can be implemented into the quantitative reliability-based casing corrosion management system;
- Industry should consider developing a more rigorous downhole corrosion logging system qualification guideline. The guideline could be based on guidelines used in the pipeline industry, such as API Standard 1163 [1], but will be specially designed to meet the unique conditions for downhole applications. This guideline would facilitate a more standardized workflow and consistent deliverables from service providers, and would minimize the gaps between the stated logging tool performance and operators' expectations;
- Industry should consider a comprehensive lab test evaluation of through-tubing logging tools. It is expected that this test program would invite multiple through-tubing logging tool vendors with a mix of tool configurations and sensing technologies. The through-tubing tool test program should include specially designed severe metal loss features that fall within the detection range of the tools. The outcome of the test program would provide a quantitative comparison of the performance of the various tools. Most importantly, the test program would help operators establish appropriate expectations for tool performance and make informed decisions to use through-tubing tools for monitoring or screening purposes.

Improvement of Remaining Burst Strength Prediction Models for Corroded Casing:

The studies performed in this and previous projects all suggest that the remaining burst strength prediction models developed for pipelines have the tendency to under-estimate the burst strength of casing. Further improvement of remaining burst strength prediction models for downhole casing is warranted. The following are recommendations for future projects:

- Additional full-scale burst testing should be conducted for casing specimens with a broader range of metal loss features and additional casing grades that are used in UGS wells. The burst test program should consider both capped-end condition and axially constrained condition (i.e. representative of downhole condition). Burst tests under axially constrained condition are expected to validate the findings in this study and to help establish a methodology to appropriately account for the impact on remaining burst strength calculation;
- Advanced FEA should be conducted with the full-scale burst tests to further validate the plastic collapse failure criterion identified in this study. The high accuracy predication capability of the advanced FEA would model a broader range of scenarios (e.g. a variety of metal loss features, casing configurations and in-situ load conditions), while minimizing the number of

physical burst tests. The validated FEA approach would reduce the number of tests required to calibrate remaining burst strength prediction models;

- Based on a combination of expanded physical burst tests and FEA cases, further study should be performed to improve the accuracy of remaining burst strength prediction models for downhole casing applications. In addition, new models should be developed that incorporate the post-yield stress-strain relationship and a plastic collapse failure mechanism;
- Additional study is required to understand the mechanical properties and the burst failure of vintage casings in existing UGS wells. Special attention should be paid to the ductility of vintage casing materials and their burst failure mode (i.e. ductile versus brittle), which could have a significant impact on the prediction capability of existing remaining burst strength prediction models; and
- Industry should investigate the strain-rate effect on the remaining burst strength of corroded casing. The strain rate effect should be properly accounted for in calibration tests and analysis of remaining burst strength prediction models.

Identification and Mitigation of Other Downhole Threats

- Further research is recommended to identify and better understand additional downhole threats that may compromise casing integrity in UGS wells. For critical threats identified, the research effort should focus on selecting proper inspection tools and mitigation strategies. The additional downhole threats include, but are not limited to:
  - potential environmental assisted cracking in casing pipe body and threaded connections that can significantly reduce the casing strength;
  - casing deformation (e.g. parting, collapse, formation movement, buckling) that could occur in weak formation, tectonically active areas and salt cavern storage wells; and
  - long-term casing connection sealability and structural integrity, especially for wells using API connections and/or wells subjected to high-frequency temperature and pressure cycles; and
- Additional studies should investigate issues related to cement integrity and remediation methods to help improve the overall UGS well integrity.

Further Development of Reliability-based Casing Corrosion Management Framework

The framework developed and described in this work provides a means to utilize casing inspection data obtained from high-resolution downhole integrity logs to estimate casing reliability (i.e. annual probability of failure) and predict how the reliability will change (i.e. probability of failure will increase) with time due to corrosion feature growth. It also provides a means to relate feature characteristics (i.e. depth, length and growth rates) and candidate remediation strategies to the required time to next inspection, provided a reliability threshold (i.e. limit on allowable probability of failure) can be defined.

However, there is as yet no consensus on the maximum allowable probability of casing failure. To facilitate broader use of the proposed reliability-based framework, additional work is required to develop consensus-based casing reliability thresholds, with due consideration of casing failure mode (i.e. leak versus burst). And to the extent that the reliability thresholds should also reflect the consequences of casing failure, a risk-consistent approach to the development of reliability

thresholds is warranted that requires higher reliability thresholds (i.e. lower allowable failure probabilities) for casings where the consequences of failure are higher.

Lastly, note that the optimal casing corrosion management strategy will balance the risk reduction achieved by casing feature remediation against the risk increase associated with additional well entry for casing feature remediation and/or re-inspection. While a framework for managing the overall well risk with due consideration of the additional well risk posed by well entry is provided in a companion research project carried out for PHMSA titled “Risk Assessment and Treatment of Well Entry Risk” [48], further work is required to directly incorporate these considerations into the casing corrosion management framework.

12 - Final Financial Section

The cost of this fixed-price project was 50% funded by the Government, with the other 50% cost-shared by the Project Team as identified on Page iv. Project expenses and billings were in strict accordance with the terms and conditions of Agreement #693JK31810014. The final invoice, representing 100% completion, will be submitted through the final quarter, June 30, 2021. There are no prior discrepancies or variances in contributions to reconcile.

13 - Acknowledgement

C-FER sincerely acknowledges and appreciates the support and technical advice provided by the members of the underground storage technical committee at PRCI. C-FER would also like to thank Ms. Zoe Shall (Program Manager, Integrity & Inspection and Underground Storage at PRCI) for the direction and oversight provided throughout the execution of this program. Special thanks are also extended to the logging service vendors for their participation in the test program and contribution of their valuable knowledge towards this research project.

14 - Referenced Publications

1. AMERICAN PETROLEUM INSTITUTE (API). In-line Inspection Systems Qualification. 2nd ed. Washington, DC: American Petroleum Institute, Apr.2013. API Standard 1163.
2. TAO, Gang. *Casing Corrosion Logging Tool Test*. Chantilly, VA: Pipeline Research Council International, 2019. PRCI Final Report PR-244-16704-R01.
3. WAGG, Brian, Maurice SLACK, Trent KAISER and Duane DEGEER. Identification of Casing String Failure Modes Using Caliper Data. *Geothermal Resources Council Transactions*. 1997, vol. 21, September/October, pp. 129-133.
4. WAGG, B., J. XIE, S. SOLANKI and S. ARNDT. Evaluating Casing Deformation Mechanisms in Primary Heavy Oil Production. *Proceedings of the 1999 SPE International Thermal Operations and Heavy Oil Symposium.* Richardson, TX: Society of Petroleum Engineers, 17-19 Mar. 1999. SPE 54116.
5. KAMGANG, Sebastien, Rodney FOSTER, Amer HANIF and Craig JOHNSON. Innovative Cement and Casing Corrosion Evaluation Technologies Provide Reliable Well Integrity Information in Natural Gas Storage Wells. *Proceedings of the SPWLA 58th Annual Logging Symposium*. Houston, TX: Society of Petrophysicists and Well Log Analysts, 17-21 Jun. 2017.
6. ALARF, Omar, Marvin ROURKE, Murat KHABIBULLIN and Alfir YAKUPOV. Comprehensive Well Integrity Solutions in Challenging Environments Using Latest Technology Innovations. *Proceedings of the Offshore Technology Conference Asia*. Houston, TX: Offshore Technology Conference, 22-25 Mar. 2016. OTC-26560-MS.
7. VALSTAR, Dirk. Acquiring a Baseline Casing Thickness Log For Future Corrosion Monitoring Without Pulling The Tubing. *Proceedings of the SPWLA 61st Annual Logging Symposium.* Houston, TX: Society of Petrophysicists and Well Log Analysts, 24 Jun.-29 Jul. 2020.
8. KHALIFEH, Mahmoud, Dave GARDNER and Muhammad Yassar HADDAD. Technology Trends in Cement Job Evaluation Using Logging Tools. *Proceedings of the Abu Dhabi International Petroleum Exhibition & Conference*. Richardson, TX: Society of Petroleum Engineers, 13-16 Nov. 2017. SPE 188274.
9. AMERICAN PETROLEUM INSTITUTE (API). *Cement Sheath Evaluation*. 2nd ed. Washington, DC: American Petroleum Institute, Sep, 2008. API Technical Report 10TR1.
10. BRILL, Thilo Michael, Cindy DEMICHEL, Edward Andrew NICHOLS and Fernando Zapata BERMUDEZ. Electromagnetic Casing Inspection Tool for Corrosion Evaluation. *Proceedings of the International Petroleum Technology Conference*. Richardson, TX: Society of Petroleum Engineers, 15-17 Nov. 2011. IPTC-14865-MS.
11. YU, Yanxiang, William REDFIELD, Nicholas BOGGS, Kuang QIN, Marvin ROURKE and Jeff OLSON. An Advanced Technique for Simultaneous in Situ Inspection of Multiple Metallic Tubulars. *Proceedings of the SPE/ICoTA Well Intervention Conference and Exhibition*. Richardson, TX: Society of Petroleum Engineers, 26-27 Mar. 2019. SPE 194269.
12. FOUDA, Ahmed, Junwen DAI and Yunyun HU. Multi-Tubular Electromagnetic Corrosion Inspection Tool – Performance Demonstration using Yard Testing. *Proceedings of the Abu Dhabi International Petroleum Exhibition & Conference*. Richardson, TX: Society of Petroleum Engineers, 9-12 Nov. 2020. SPE 202718.

13. JAIN, S., A. AL HAMADI, H. SARADVA, J. ASARPORTA, S. J. SPARKE, M. VOLKOV and H. ABU RAHMOUN. Well Integrity Management: Challenges in Extending Life of a Mature Gas Condensate Field – A Case Study. *Proceedings of the Abu Dhabi International Petroleum Exhibition & Conference*. Richardson, TX: Society of Petroleum Engineers, 13-16 Nov. 2017. SPE-188422-MS.
14. YUGAY, A., H. B. DAGHMOUNI, A.B. ALI, M. VOLKOV and S. J. SPARKE. Field Trial Results for 3rd Barrier Evaluation Using Technology of Individual Electromagnetic Metal Loss Logging Validated by Actual Excavations. *Proceedings of the Abu Dhabi International Petroleum Exhibition & Conference.* Richardson, TX: Society of Petroleum Engineers, 13-16 Nov. 2017. SPE-188258-MS.
15. MACKI, Ali Al, Albashir Al SALMI, Timothy DUGGAN, Eduardo DELGADO, Jackie KECHICHIAN, Hamood AL BUSAIDI and Nassar AL AZRI. Electromagnetic Corrosion Logs, Insights from Yard Test. *Proceedings of the Abu Dhabi International Petroleum Exhibition & Conference.* Richardson, TX: Society of Petroleum Engineers, 13-16 Nov. 2017. SPE-188672-MS.
16. MISHKHES, Abdulrahman T., Mohammad D. AL-AJMI, Nassar M. AL-HAJR, Fehead M. AL-SUBAIE and Muhammad F. FAYYAZ. Field Application of Electromagnetic Eddy Current Technology Enables Proactive Near Surface Casing Inspection. *Proceedings of the SPE Kingdom of Saudi Arabia Annual Technical Symposium and Exhibition.* Richardson, TX: Society of Petroleum Engineers, 25-28 Apr. 2016. SPE-182758-MS
17. JAIN, S., A. AL HAMADI, A. M. ALGHASRA, M. SAADA and A. H. AMIN. Well Integrity Management: Analysis of Multi-Barrier Corrosion in Mature Wells Using Advanced Magnetic Impulse Technology. *Proceedings of the Abu Dhabi International Petroleum Exhibition & Conference*. Richardson, TX: Society of Petroleum Engineers, 7-10 Nov. 2016. SPE-182968-MS.
18. ZAINI, A. Bin Ahmad, A. Md ALI, M. Abdul RAZAK, E. SAMAILE, Adil BUSAIDY and Wee Wei WA. Improved Casing Integrity Evaluation Enables Multiple Strings Metal-Loss Profilling in Aging Wells. *Proceedings of the Offshore Technology Conference Asia*. Houston, TX: Offshore Technology Conference; 22-25 Mar. 2016. OTC-26719-MS.
19. KANTYUKOV, R., D. GRISHIN, R. NIKITIN, A. ASLANYAN, I. ASLANYAN, R. MINAKHMETOVA and S. SOROKA. An Integrated Approach to the Integrity Diagnostics of Underground Gas Storage Wells. *Proceedings of the Abu Dhabi International Petroleum Exhibition & Conference*. Richardson (TX): Society of Petroleum Engineers, 13-16 Nov. 2017. SPE-188656-MS.
20. AMERICAN SOCIETY OF MECHANICAL ENGINEERS (ASME). *Manual for Determining the Remaining Strength of Corroded Pipelines: Supplement to ASME B31 Code for Pressure Piping*. New York, NY: American Society of Mechanical Engineers, 2012. ASME B31G-2012.
21. CANADIAN STANDARDS ASSOCIATION (CSA). *Oil and gas pipeline systems*. Toronto, ON: CSA Group. CSA Z662:19.
22. BRITISH STANDARDS INSTITUTION (BSI). *Guide to methods for assessing the acceptability of flaws in metallic structures*. London, UK: British Standards Institution, 2019. BS 7910:2019.

23. DNV GL AS. *Corroded pipelines*. Oslo, Norway: DNV GL AS, Sep. 2019. Recommended Practice DNVGL-RP-F101.
24. AMERICAN PETROLEUM INSTITUTE (API). *Fitness-For-Service*. Washington, DC: API Publishing Services, Jun. 2016. API 579-1/ASME FFS-1.
25. FRANCINI, Robert B., Jacob D. WAHL and Paul A. ZELENAK. *Effects of Tensile Loading on the Remaining Strength of Corroded Casing*. Worthington, OH: Kiefner and Associaties, Dec. 2008. Final Report, DOE Award No. DE-FC26-03NT41779.
26. PIPELINE OPERATORS FORUM. *Specifications and Requirements for in-line Inspection of pipelines* [online]. 2016.
27. ASTM INTERNATIONAL. *Standard Test Methods and Definitions for Mechanical Testing of Steel Products.* West Conshohocken, PA: ASTM International, 2020. ASTM A370-20.
28. ASTM INTERNATIONAL. *Standard Test Method for Young's Modulus, Tangent Modulus, and Chord Modulus.* West Conshohocken, PA: ASTM International, 2017. ASTM E111-17.
29. ASTM INTERNATIONAL. *Standard Practice for Verification and Classification of Extensometer Systems.* West Conshohocken, PA: ASTM International, 2016. ASTM E83-16.
30. TAO, Gang, Cam MATTHEWS and Adrian ADAMS. *Special Considerations for Well Tubular Design at Elevated Temperatures*. Proceedings of the IADC/SPE International Drilling Conference and Exhibition. Galveston, TX: IADC/SPE International Drilling Conference and Exhibition, 3–5 Mar. 2020. SPE-199570-MS.
31. AMERICAN PETROLEUM INSTITUTE (API). *Casing and Tubing*. 10th edition. Washington, DC: API Publishing Services, Jun. 2018. API Specification 5CT.
32. AMERICAN PETROLEUM INSTITUTE (API). *Calculating Performance Properties of Pipe Used as Casing or Tubing*. 7th edition. Washington, DC: API Publishing Services, Jun. 2018. API Technical Report 5C3.
33. CHAUHAN, V., R. GRANT and A. WOOD. *Well Bore Integrity - Development of Methods for Assessing Corrosion Metal Loss Defects in Casing Strings*. Des Plaines, IL: Gas Research Institute, Nov. 2004. GRI-05/0171.
34. LIU, J., V. CHAUHAN, P. NG, S. WHEAT and C. HUGHES. *Remaining Strength of Corroded Pipe Under Secondary (Biaxial) Loading*. Loughborough, UK: GL Industrial Services UK, Aug. 2009. Project #153J, Report No. R9068, US DOT Contract No. DTPH56-05-T0003.
35. BAO, Ji, Shulong ZHANG, Wenxing ZHOU and Shenwei ZHOU. Evaluation of Burst Pressure of Corroded Pipe Segments Using Three-Dimensional Finite Element Analyses. *Proceedings of the 2018 12th International Pipeline Conference*. New York: American Society of Mechanical Engineers, 24-28 Sep. 2019. IPC2018-78130.
36. DASSAULT SYSTEMES. SIMULIA User Assistance [online]. Paris: Dassault Systems, 2020.
37. ZHU, Xian-Kui and Brian N. LEIS. Theoretical and Numerical Predictions of Burst Pressure of Pipelines. *Proceedings of PVP2006-ICPVT-11: 2006 ASME Pressure Vessels and Piping Division Conference.* New York: American Society of Mechanical Engineers,23-27 July 2006.
38. LIU, M., H. ZHOU, B. WANG and Y. WANG. *Strain-Based Design and Assessment in Critical Areas of Pipeline Systems with Realistic Anomalies*. Washington, DC: Pipeline and

Hazardous Materials Safety Administration, 2017. US DOT Contract No. DTPH56-14-H-00003, Project #556.
39. STEWART, Graham, Frans J. KLEVER and David RITCHIE. An analytical model to predict the burst capacity of pipelines. *Pipeline Technology*. 1994, vol. v, pp. 177–188.
40. ZHU, Xian-Kui and Brian N. Leis. Evaluation of burst pressure prediction models for line pipes. *International Journal of Pressure Vessels and Piping.* 2012, vol. 89, pp. 85-97.
41. DNV GL AS. *Fatigue design of offshore steel structures*. Oslo, Norway: DNV GL AS, 2019. Recommended Practice DNVGL-RP-C203.
42. CHAUHAN, V. and J. BRISTER. *A Review of Methods for Assessing the Remaining Strength of Corroded Pipelines*. Loughborough, UK: GL Industrial Services UK, Nov. 2009. Report No. 6781, US DOT Contract No. DTPH56-05-T0003 – Project 153.
43. FRANCINI, R.B. and N.T. QUADE. *Extension of a Method to Validate the Remaining Strength of Corroded Casing to Additional Cases*. Worthington, OH: Kiefner and Associates, 2010. DOE Award No. DE-FC26-03NT41779.
44. STEPHENS, Mark and Maher NESSIM. A Comprehensive Approach to Corrosion Management Based on Structural Reliability Methods. *Proceedings of the 6th International Pipeline Conference*. New York: American Society of Mechanical Engineers, 25-29 Sep. 2006. IPC2006-10458.
45. STEPHENS, Mark and Albert VAN ROODSELAAR. Developments in reliability-based corrosion management and the significance of in-line inspection uncertainties. *Proceedings of the 7th International Pipeline Conference*. New York: American Society of Mechanical Engineers, 29 Sep.-3 Oct. 2008. IPC2008-64384.
46. STEPHENS, Mark, Maher NESSIM and Albert VAN ROODSELAAR. Reliability-based Corrosion Management – The Impact of Maintenance and Implications for the Time to Next Inspection. *Proceedings of the 8th International Pipeline Conference*. New York: American Society of Mechanical Engineers, 27 Sep.-1 Oct. 2010. IPC2010-31399.
47. MADSEN, H.O., S. KRENK and N.C. LIND. Methods of Structural Safety. Englewood Cliffs, NJ: Prentice-Hall Inc., 1986.
48. STEPHENS, Mark, Smitha KODURU, Josh VANI, Tyler PAXMAN and Chance WRIGHT. *Risk Assessment and Treatment of Wells*. Edmonton, AB: C-FER Technologies, Sep. 2020. Project no.: M251.
49. DEWOLF, Glenn, Katherine SEARCY, Douglas ORR and Christopher LOUGHRAN. *Risk Assessment Methodology for Accidental Natural Gas and Highly Volatile Liquid Releases from Underground Storage, Near-Well Equipment*. Chicago, IL: Gas Research Institute, May 2004. GRI-05/0172.

Appendix A - Artificial Metal Loss Feature Details

This appendix summarizes details of the artificial metal loss features made on the three sizes of casing strings:

- Table A.1 to Table A.3 list details of the design matrix of regular shape artificial features for the three sizes of casing strings;
- Figure A.1 presents the distribution of the regular shape artificial features over the different metal loss feature categories defined by the Pipeline Operators' Forum (2016);
- Figure A.2 shows examples of the regular shape artificial features machined on the casing joints;
- Table A.4 to Table A.6 list details of the characterized dimensions of the random shape artificial features for the three sizes of casing strings;
- Figure A.3 presents the distribution of the random shape artificial features over the different metal loss feature categories defined by the Pipeline Operators' Forum (2016); and
- Figure A.4 shows examples of the random shape artificial features machined on the casing joints.

Table A.1 – Design Matrix of Regular Shape Artificial Features for 4.5 inch Casing (Repeated on JT#1 and JT#2)

Feature ID	Feature Type	Design Value		
		Length (inch)	Width (inch)	Maximum Depth (%WT)
D1A	Pinhole	0.2	0.2	20%
D1B	Pitting	0.625	0.625	20%
D1C	Pitting	0.625	0.625	50%
D1D	Pitting	1.0	1.0	20%
D2	General corrosion	4.5	Full circumference	20%
D3	Pinhole	0.2	0.2	10%
D4	Pinhole and general corrosion	0.2 (pinhole) 4.5 (general corrosion)	0.2 (pinhole) Full circumference (general corrosion)	20% (pinhole) 10% (general corrosion)
D5	General corrosion	4.5	Full circumference	10%
D6	Pitting	0.625	0.625	70%
D7	Pitting	1.0	1.0	10%
D8	Pitting and general corrosion	1.0 (pitting) 4.5 (general corrosion)	1.0 (pitting) Full circumference (general corrosion)	20% (pitting) 10% (general corrosion)
D9	Circumferential grooving	0.625	Full circumference	20%
D10	Pitting	1.0	1.0	70%
D11	Pitting cluster (9 pits)	1.0	1.0	20%
D12	Axial grooving	4.5	0.625	20%
D13	Pitting	1.0	1.0	50%

Table A.2 – Design Matrix of Regular Shape Artificial Features for 5.5 inch Casing (Repeated on JT#1 and JT#2)

Feature ID	Feature Type	Design Value		
		Length (inch)	Width (inch)	Maximum Depth (%WT)
D1	Pitting	0.625	0.625	50%
D2	General corrosion	5.5	Full circumference	20%
D3	Pinhole	0.2	0.2	10%
D4	Pinhole and general corrosion	0.2 (pinhole) 5.5 (general corrosion)	0.2 (pinhole) Full circumference (general corrosion)	20% (pinhole) 10% (general corrosion)
D5	General corrosion	5.5	Full circumference	10%
D6	Pitting	0.625	0.625	70%
D7	Pitting	1.0	1.0	10%
D8	Pitting and general corrosion	1.0 (pitting) 5.5 (general corrosion)	1.0 (pitting) Full circumference (general corrosion)	20% (pitting) 10% (general corrosion)
D9	Circumferential grooving	0.625	Full circumference	20%
D10	Pitting	1.0	1.0	70%
D11	Pitting cluster (9 pits)	1.0	1.0	20%
D12	Axial grooving	5.5	0.625	20%
D13	Pitting	1.0	1.0	50%

Table A.3 – Design Matrix of Regular Shape Artificial Features for 7.0 inch Casing (Repeated on JT#1a/b and JT#2)

Feature ID	Feature Type	Design Value		
		Length (inch)	Width (inch)	Maximum Depth (%WT)
D1	Pitting	0.625	0.625	50%
D2	General corrosion	7.0	Full circumference	20%
D3	Pinhole	0.2	0.2	10%
D4	Pinhole and general corrosion	0.2 (pinhole) 7.0 (general corrosion)	0.2 (pinhole) Full circumference (general corrosion)	20% (pinhole) 10% (general corrosion)
D5	General corrosion	7.0	Full circumference	10%
D6	Pitting	0.625	0.625	70%
D7	Pitting	1.0	1.0	10%
D8	Pitting and general corrosion	1.0 (pitting) 7.0 (general corrosion)	1.0 (pitting) Full circumference (general corrosion)	20% (pitting) 10% (general corrosion)
D9	Circumferential grooving	0.625	Full circumference	20%
D10	Pitting	1.0	1.0	70%
D11	Pitting cluster (9 pits)	1.0	1.0	20%
D12	Axial grooving	7.0	0.625	20%
D13	Pitting	1.0	1.0	50%

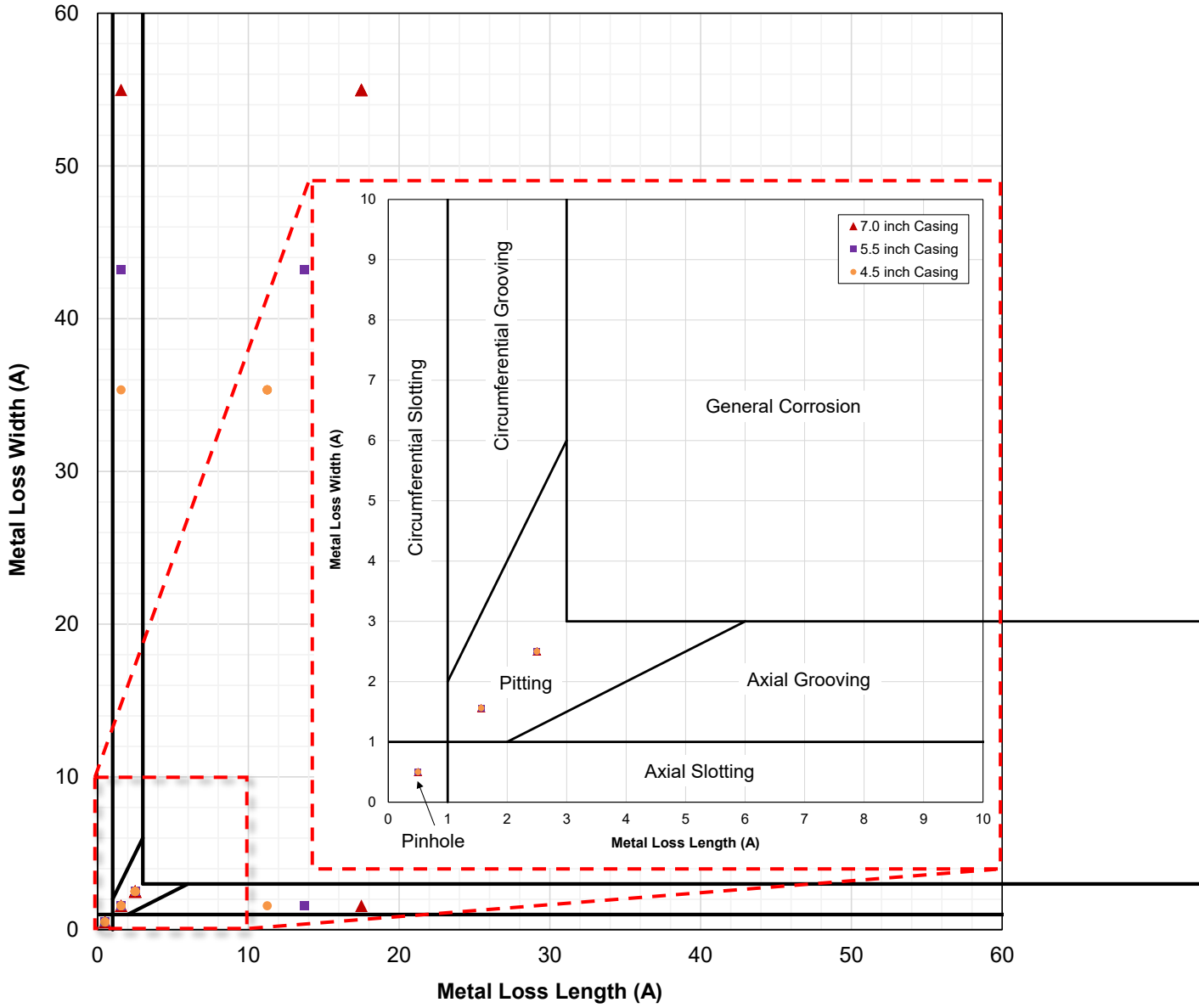

Figure A.1 – Regular Shape Artificial Metal Loss Feature Distribution


DIA


DIB


DIC


DID

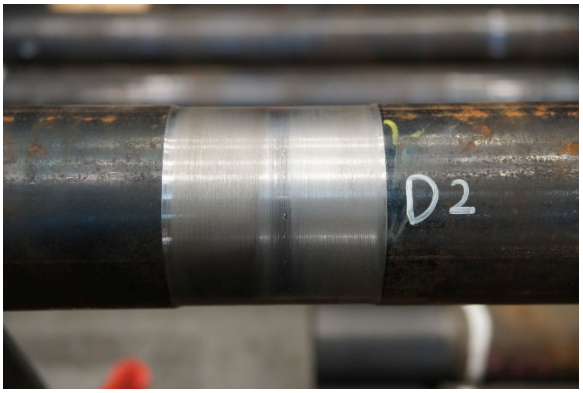
D2


D3


D4

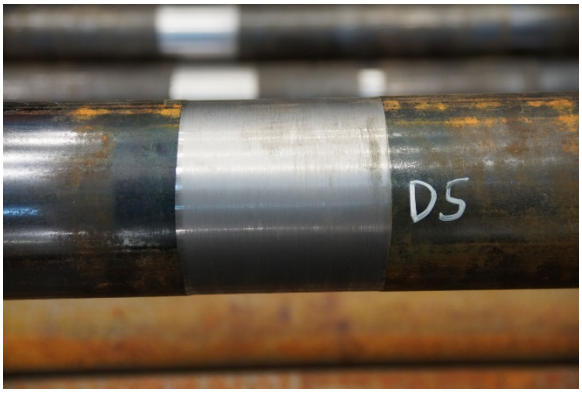
D5

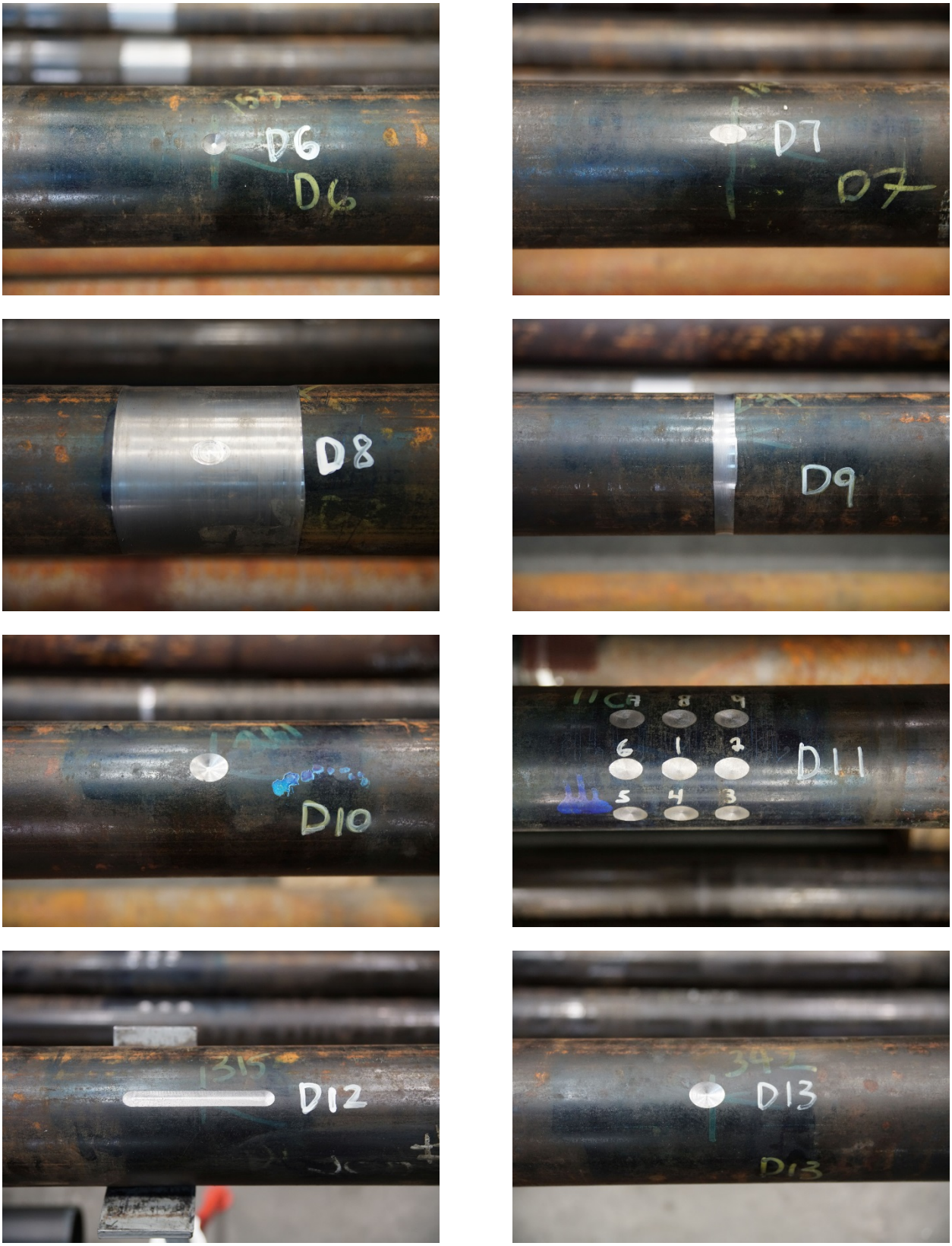

Figure A.2 – Regular Shape Artificial Features (Similar on 4.5 inch, 5.5 inch and 7.0 inch Casings)

Table A.4 – Random Shape Artificial Features on 4.5 inch Casing

Feature	Length (inch)	Maximum Depth (%WT)	Width (inch)	Burst Test
4.5in-JT#3-D1	2.56	68%	1.37	Yes
4.5in-JT#3-D2	2.80	65%	1.49	Yes
4.5in-JT#3-D3	2.56	72%	2.47	Yes
4.5in-JT#3-D4	3.50	63%	1.65	Yes
4.5in-JT#3-D5	1.10	66%	3.10	Yes
4.5in-JT#3-D6	2.95	63%	1.26	Yes
4.5in-JT#3-D7	1.85	62%	2.08	Yes
4.5in-JT#3-D8	2.24	63%	1.06	Yes

Table A.5 – Random Shape Artificial Features on 5.5 inch Casing

Feature	Length (inch)	Maximum Depth (%WT)	Width (inch)	Burst Test
5.5in-JT#3-D1	4.06	54%	2.01	Yes
5.5in-JT#3-D2	4.84	63%	2.56	Yes
5.5in-JT#3-D3	3.50	59%	2.44	Yes
5.5in-JT#3-D4	3.90	58%	3.62	Yes
5.5in-JT#3-D5	1.06	57%	3.94	Yes
5.5in-JT#3-D6	3.39	61%	1.18	Yes
5.5in-JT#3-D7	2.05	28%	1.30	No
5.5in-JT#4-D1	1.54	41%	0.67	No
5.5in-JT#4-D2	2.24	54%	1.46	No
5.5in-JT#4-D3	1.38	32%	1.26	No
5.5in-JT#4-D4	0.75	52%	1.46	No
5.5in-JT#4-D5	0.83	32%	0.75	No
5.5in-JT#4-D6	1.69	57%	1.65	No
5.5in-JT#4-D7	1.61	32%	1.69	No
5.5in-JT#4-D8	1.46	47%	1.73	No

Table A.6 – Random Shape Artificial Features on 7.0 inch Casing

Feature	Length (inch)	Maximum Depth (%WT)	Width (inch)	Burst Test
7.0in-JT#3-D1	4.57	47%	1.85	Yes
7.0in-JT#3-D2	6.34	47%	2.72	Yes
7.0in-JT#3-D3	3.58	50%	3.62	Yes
7.0in-JT#3-D4	5.16	54%	3.54	Yes
7.0in-JT#3-D5	1.57	53%	4.09	Yes
7.0in-JT#3-D6	3.15	64%	1.26	Yes
7.0in-JT#3-D7	2.28	22%	1.65	No
7.0in-JT#4-D1	1.73	44%	0.79	No
7.0in-JT#4-D2	2.24	63%	1.38	No
7.0in-JT#4-D3	1.89	34%	1.34	No
7.0in-JT#4-D4	1.02	51%	1.85	No
7.0in-JT#4-D5	0.83	38%	1.02	No
7.0in-JT#4-D6	1.50	54%	1.34	No
7.0in-JT#4-D7	2.24	37%	1.81	No
7.0in-JT#4-D8	1.22	50%	1.73	No

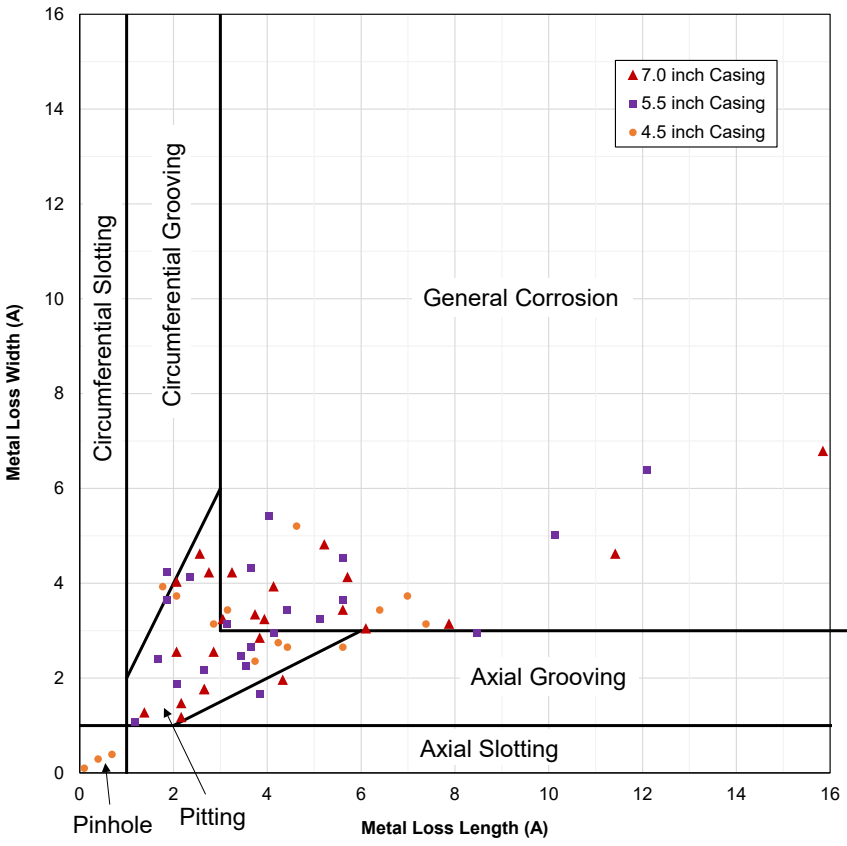

Figure A.3 – Random Shape Artificial Metal Loss Feature Distribution

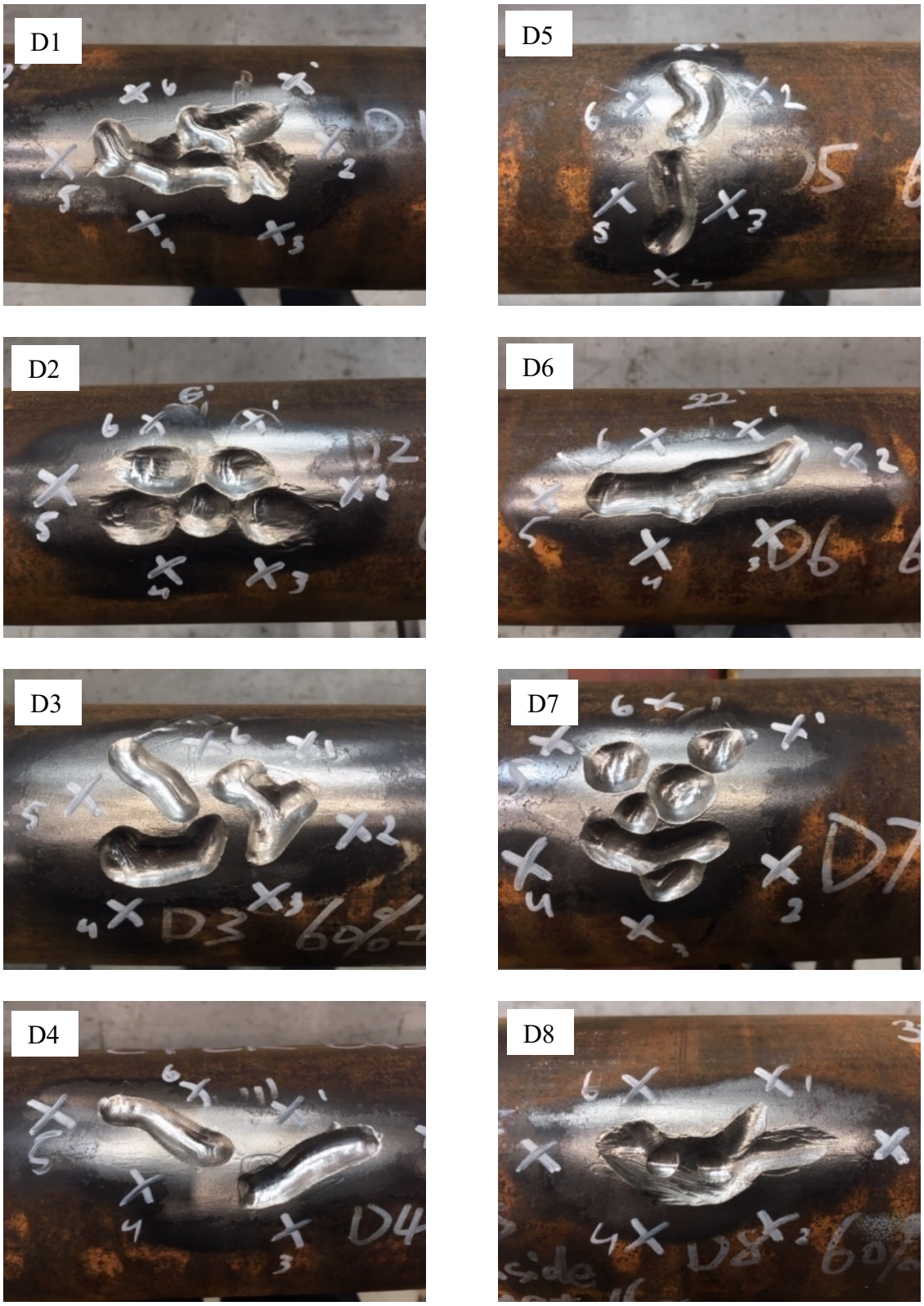

Figure A.4 – Random Shape Artificial Features (4.5in-JT#3)

Appendix B - Vendor-B's UT-2 Tool Test Results

B1 - Overview

B1.1 - Tool Features and Specifications

Vendor-B's UT-2 tool is a higher resolution ultrasonic tool that fires a 3 MHz pulse at every 2° along the circumferential direction, resulting in 180 samples per revolution. The vertical sampling interval can be either 0.2 or 1.5 inch. In this lab test project, the tool was operated at an axial sample interval of 0.2 in. The curvature of the tool's transducer creates a focused pulse, which allows the surveyed area to be as small as 1/8 in when the casing is 2 in away from the transducer. Note that the UT-2 tool is a dedicated casing thickness measurement tool and it does not have the ability to evaluate cement bond quality like some other UT tools. Table B.1 lists a summary of the tool specifications based on the information from Vendor-B.

Table B.1 – Vendor-B's UT-2 Tool Specifications

Casing Thickness Range	0.177 to 0.59 in
Casing Size Range	4-1/2 to 13-3/8 in
Vertical Resolution	0.2- or 1.5-in intervals
Circumferential Resolution	180 samples per revolution
Accuracy	Internal radius ±0.04 in; thickness ±4%
Logging Speed	3,000 ft/h (914 m/h); High resolution: 400 ft/h (122 m/h)
Maximum Temperature	350 ºF (177 ºC)
Maximum Pressure	20,000 psi (138 MPa)
Special Application	H_2S Service

B1.2 - Vendor Deliverables

Upon completion of the logging tool test, Vendor-B provided a summary of the key logging test results, including the various plots of measurements and a spreadsheet summary of identified metal loss features. Figure B.1 shows an example of the logging plots with various measurements. A metal loss feature on the external surface of the casing is clearly shown in the "Feature Amplitude" and "Thickness" plots. In addition, the results also include summaries of the internal radius (maximum, average and minimum) and WT (average and minimum) along the axial depth of the well.

Vendor-B provided a quantitative analysis of the identified features, including the location, length, width and remaining WT. In addition, Vendor-B also provided the river bottom profile for each reported feature. Using the nominal WT of the casing, the metal loss depth was also calculated. In the preceding PRCI project, Vendor-B commented in their report that the tool observed WT variation in the pipe samples, such that using the nominal WT for metal loss calculation would result in some error [2]. However, such error may be quantified and corrected using the direct WT measurement from the UT. Note that Vendor-B indicated that WT less than 0.15 in cannot be measured

by their tools and noted all measurements that reached this limit. These considerations have been accounted for in the subsequent tool sizing accuracy assessment.

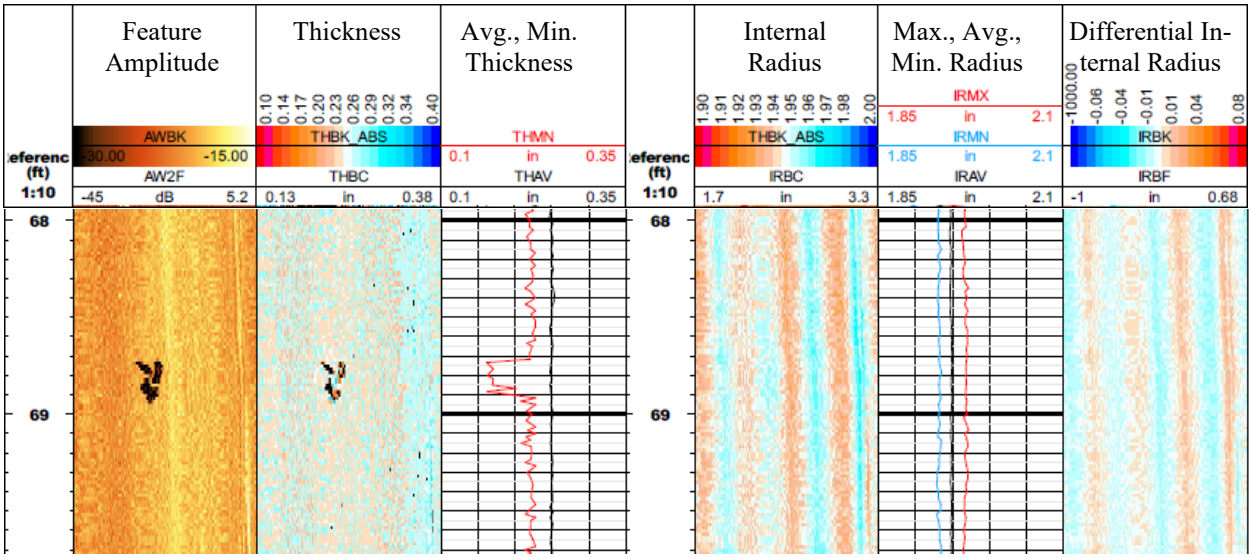

Figure B.1 – Vendor-B's UT-2 Tool Logging Chart Example

B2 – Performance Evaluation

A quantitative assessment of the tool's performance was conducted based on the reported features. The evaluation was performed separately for the regular shape artificial features, random shape artificial features and natural corrosion features. Note that, in the sizing accuracy analysis, the maximum feature length and width were considered. For relatively small features, including pinholes and pitting, the maximum depth was considered in the depth accuracy evaluation. For features other than pinholes and pitting, average thickness measurements reported by the tools were considered in the depth accuracy evaluation, since the minimum wall thickness measured by the tool appeared to be significantly less than the actual value.

Further review of the log charts indicated that the ultrasonic tools tend to underestimate the minimum WT of the pipe samples. This is shown in the pipe specimen regions with no metal loss features, where the minimum WT measured by the tools was less than the minimum allowable values (i.e. 87.5% of the nominal WT) specified by API Specification 5CT [31]. In reality, the actual WT tolerance of manufactured API casing is typically much less than the API specified value. In addition, C-FER's hand measurements conducted on a few metal loss features with full circumference metal loss also showed much less variance than the tools' log results. Further improvement of the WT measurement accuracy of the ultrasonic tools by Vendor-B appears to be warranted.

B2.1 - Detection Capability

B2.1.1 - Artificial Features

The features identified on all new casing joints were carefully reviewed and successfully matched with the known artificial features (i.e. by the axial location, circumferential location and general shape), including regular and random shape features. Due to the high sample rates (in both axial and circumferential directions) and the ability for direct WT measurement, the UT-2 tool was able to capture the details of the metal loss feature profile. Figure B.2 shows an example of a comparison between the UT-2 tool result and the LS result for a random shape artificial feature. The tool provided not only a 2D shape of the metal loss feature, but also a river bottom profile of the feature. The river bottom profile can be used to assess the remaining burst strength in some models described in Section 5.2. Evaluation of the accuracy of the river bottom profile warrants further study, which is out of the scope of the current project.

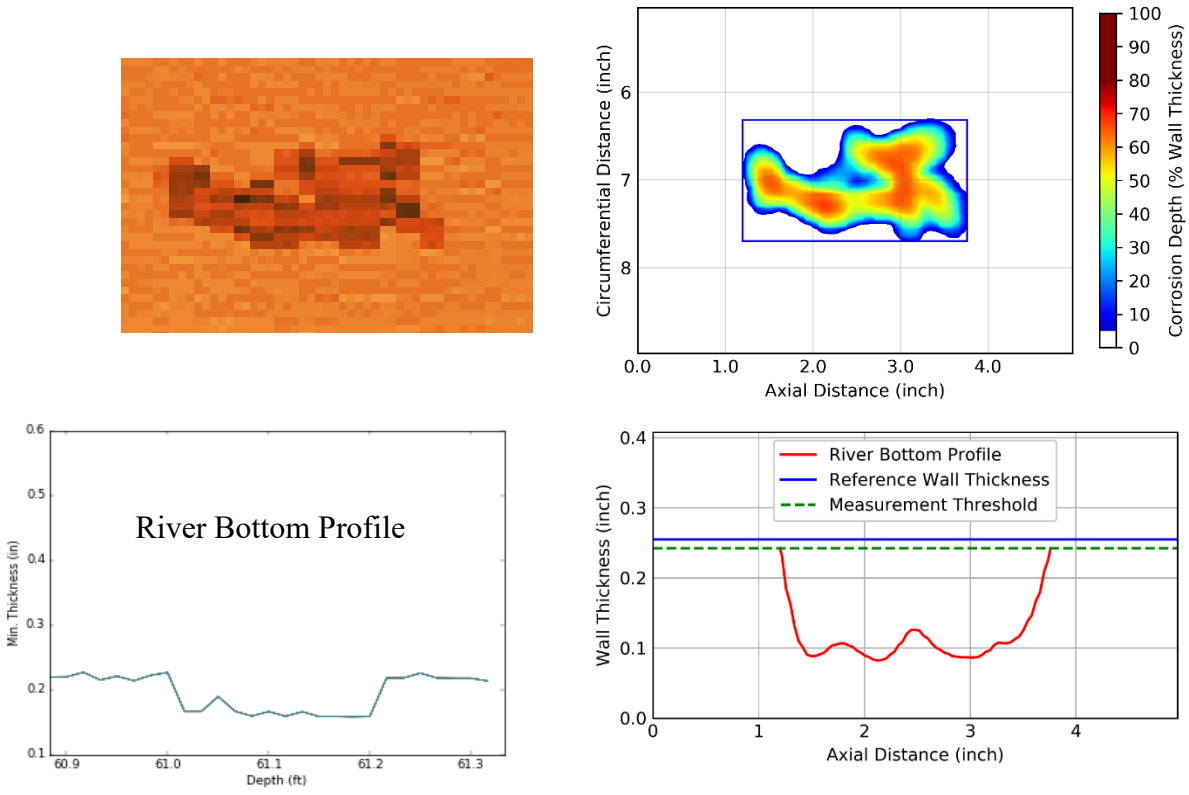

Feature Reported by UT-2 Tool LS Data

Figure B.2 – Matching Random Shape Artificial Feature for Vendor-B's UT-2 Tool

The detection capability of the tool was quantitatively evaluated by the POD. Table 19 lists the POD for each joint, as well as an overall POD for new casing joints. The tool showed consistent detecting capability for the artificial features over the three different casing sizes. In addition, the UT-2 tool did not report any false detections within these joints. The POD results are grouped by the feature categories classified by Pipeline Operators' Forum [26] to further investigate the tool response to different feature types. Note that only regular shape artificial features were considered.

As shown in Table B.3, the UT-2 tool had difficulty detecting the extremely small size pinholes (0.2 in diameter). However, the tool demonstrated good performance in detecting pitting and larger features.

Table B.2 – POD and False Detection for Vendor-B's UT-2 Tool (Artificial Features)

Casing Size	Joint No.	Total Number of Features	Number of Detected Features	POD	Number of False Detections
4.5 inch	1	18	16	89%	0
	2	18	15	83%	0
	3	8	8	100%	0
	4	N/A	N/A	N/A	N/A
5.5 inch	1	15	13	87%	0
	2	15	13	87%	0
	3	7	7	100%	0
	4	8	8	100%	0
7.0 inch	1a & 1b	15	13	87%	0
	2	15	12	80%	0
	3	7	7	100%	0
	4	8	8	100%	0
Total		134	120	90%	0

Table B.3 – Feature-classified POD for Vendor-B's UT-2 Tool (Regular Shape Artificial Features)

Feature Category	Total Number of Features	Number of Detected Features	POD
Pinhole	14	1	7%
Pitting	40	39	98%
Axial Grooving	6	6	100%
Circumferential Grooving	6	6	100%
General Corrosion	24	24	100%
Pitting Cluster *	6	6	100%

* Pitting cluster is not a feature category as per Pipeline Operators' Forum [26]. However, the pitting cluster is treated separately, as a special case, in this assessment.

B2.1.2 - Natural Corrosion Features

Matching of natural corrosion features was performed visually by comparing the feature pattern reported by the UT-2 tool to the LS results. As shown in Figure B.3, a generally good match was obtained for the corrosion feature pattern. The UT-2 tool was able to detect most of the features that have significant wall losses. It appears that Vendor-B used different clustering rules than that used in the LS data analysis. As a result, a quantitative assessment of the tool's detection capability (i.e. by POD) was not conducted.

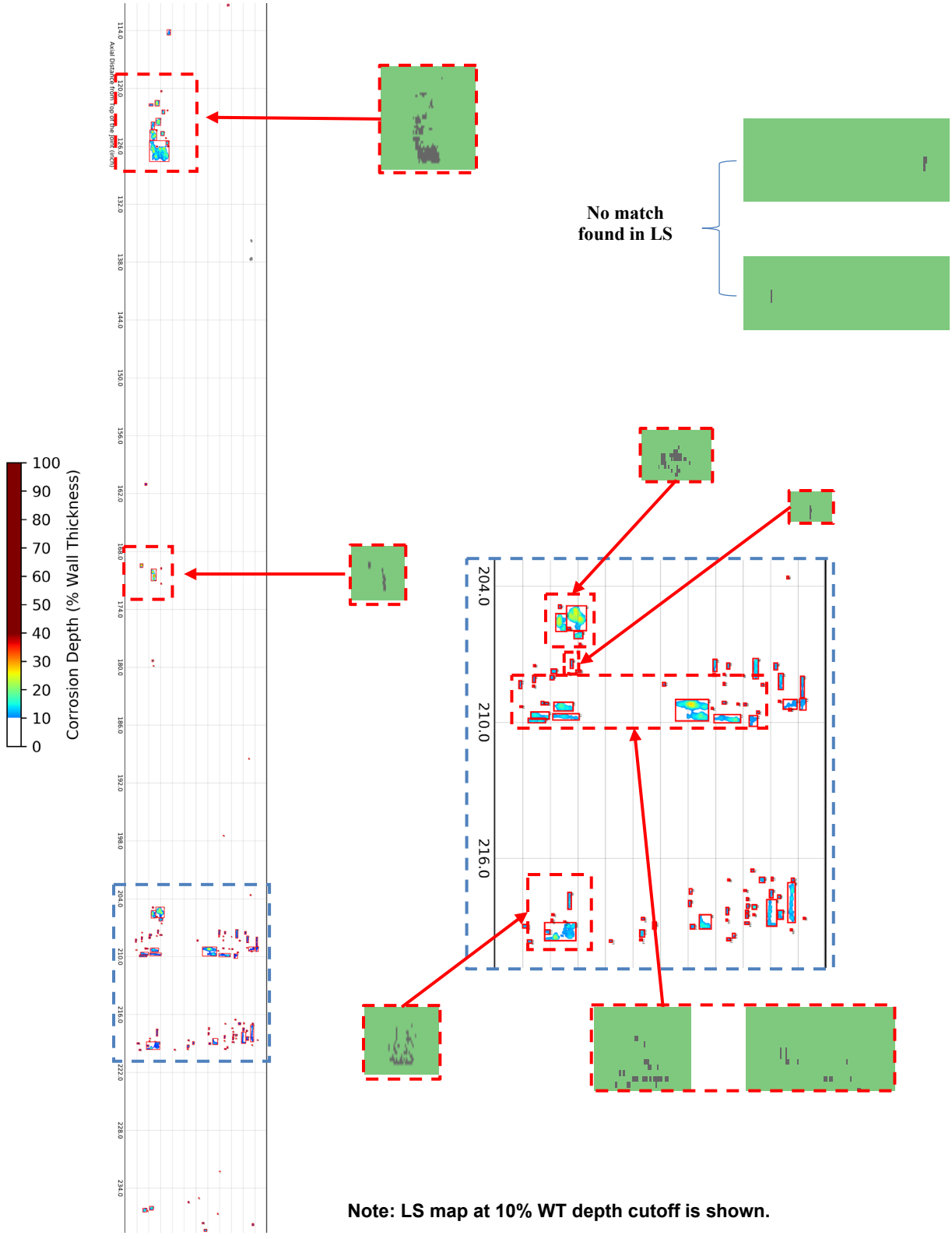

Figure B.3 – Natural Corrosion Feature Matching Examples for Vendor-B's UT-2 Tool (4.5in-JT#4)

B2.2 - Sizing Accuracy

The sizing accuracy analysis on the UT-2 tool was also performed separately on the artificial features and the natural corrosion features.

B2.2.1 - Artificial Features

Figure B.4 and Figure B.5 present the unity plots of the measured size versus the true size for the regular shape and random shape artificial features, respectively. A quantitative summary of the sizing accuracy with respect to various error bands is presented in Figure B.6. Note, in the depth unit chart, measurement data that reached the lower measurement limit of 0.15 in of the tool are marked with arrows indicating that the actual depth was possibly larger than reported. Based on the results, the following observations are made:

- This tool appears to have a generally consistent sizing accuracy response to the three different casing sizes;
- Except the lower bound WT measurement limit of 0.15 in, this tool did not show any obvious bias error in depth accuracy. In general, this tool demonstrated the best performance in the depth sizing accuracy among the three tools tested in the project;
- This tool appears to slightly under-report the length of both regular and random shape features; and
- The tool was found to consistently under-report the width of both regular and random shape features in this test. The finding was contradictory to the test results in the preceding PRCI project, where this tool showed excellent performance in width sizing accuracy (i.e. 89% for feature width within ± 0.25 in) due to its very high circumferential resolution (i.e. 180 samples per revolution). However, note that the width values of the feature population in the preceding test were all less than 1.0 in.

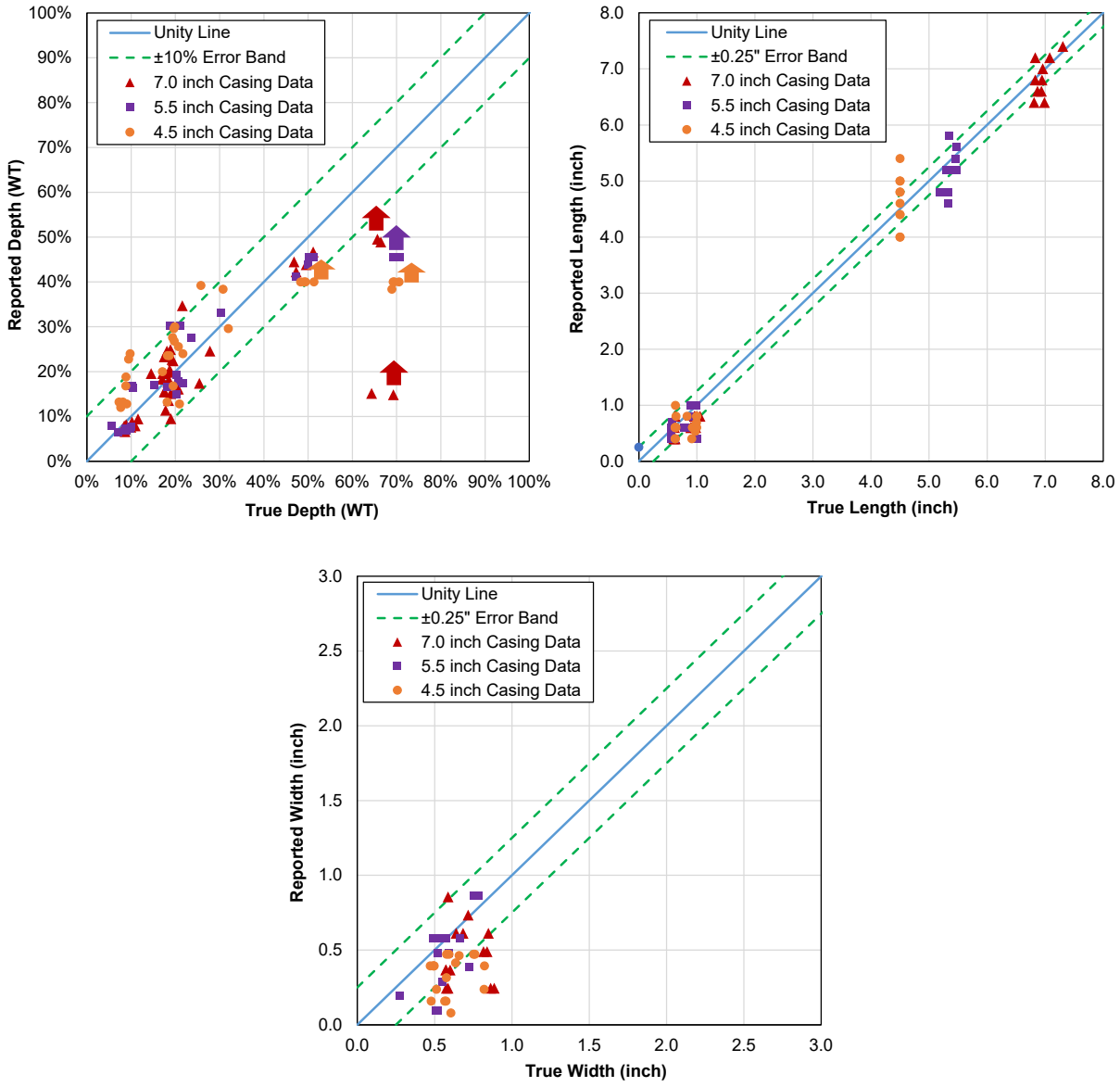

Figure B.4 – Unity Plots of Regular Shape Artificial Features Called by Vendor-B's UT-2 Tool

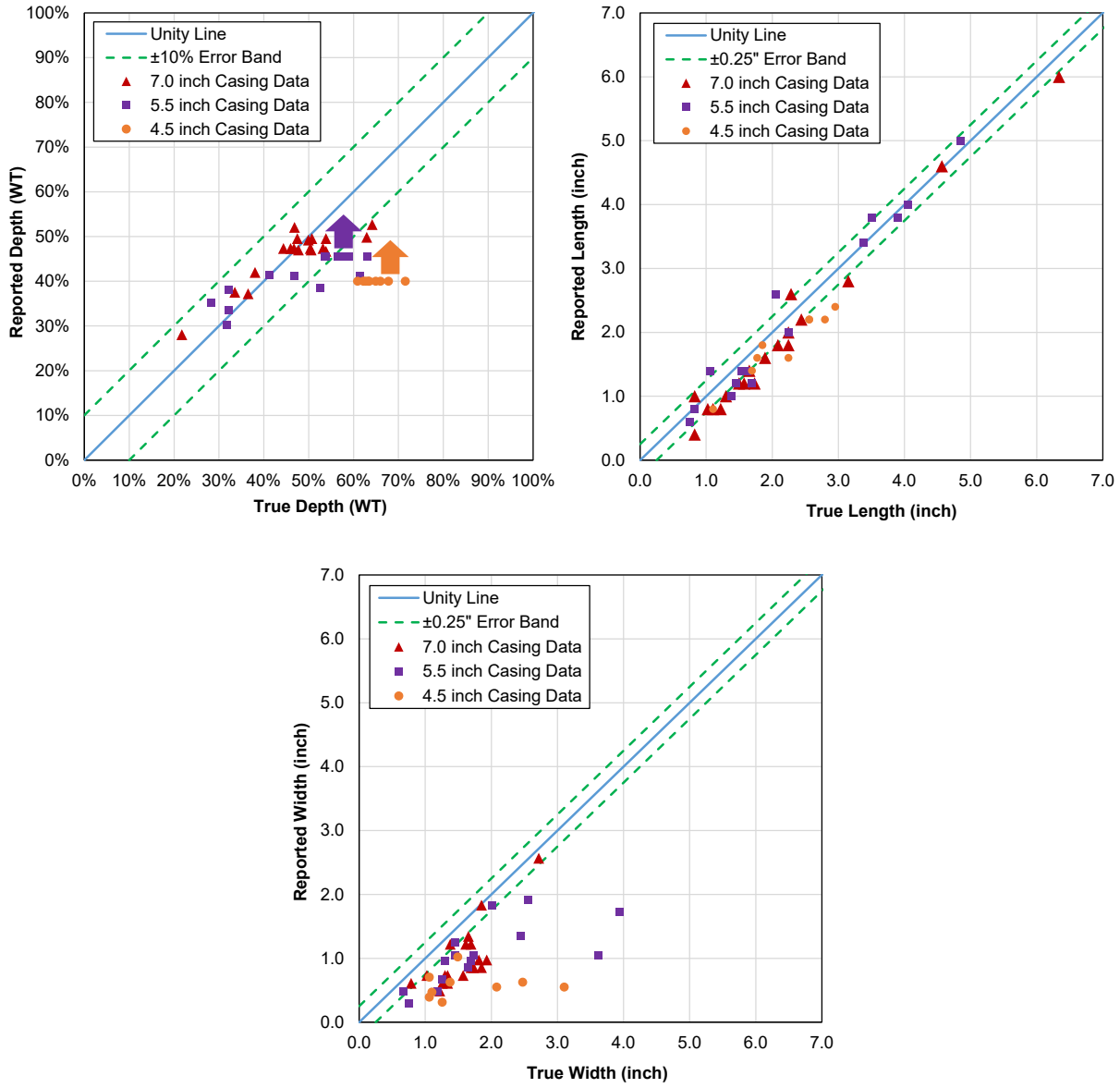

Figure B.5 – Unity Plots of Random Shape Artificial Features Called by Vendor-B's UT-2 Tool

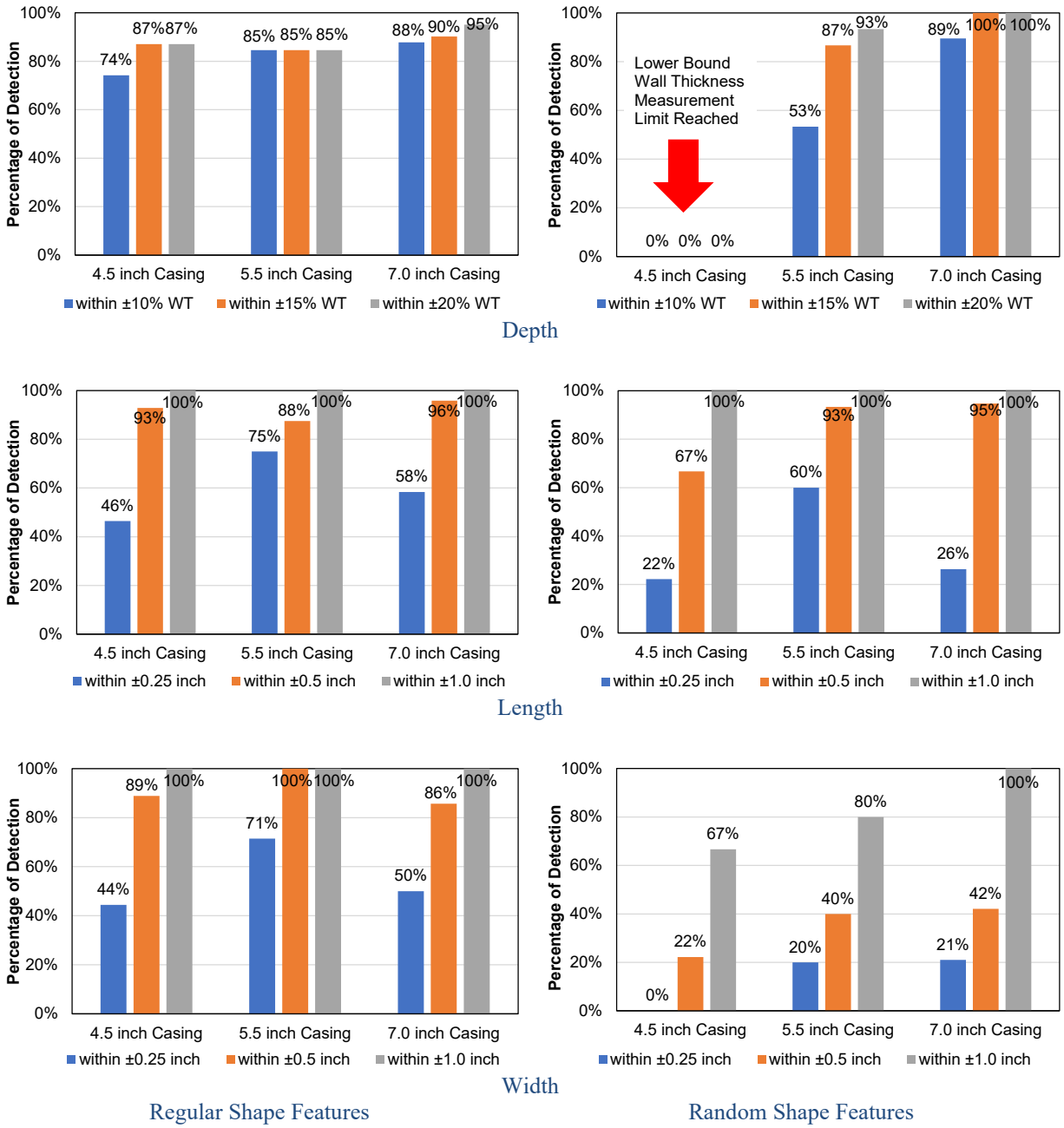

Figure B.6 – Vendor-B's UT-2 Tool Measurement Accuracy for Artificial Features

B2.2.1 – Natural Corrosion Features

It's unclear what criterion Vendor-B used to group the natural corrosion features into clusters. But the resulting shapes of these clusters were different from the LS results, where the clustering criterion was based on ASME B31G [20]. Due to this discrepancy, a sizing accuracy assessment on feature length and width was not performed. However, the depth sizing accuracy assessment was conducted using the maximum depth within the identified features. Since the same casing joint has also been logged in the preceding PRCI test project, the unity plots of the maximum depth from

both previous tests and the current tests are presented in Figure B.7. The number of features reported in the current tests was less than the previous one, mainly due to different clustering rules used by Vendor-B. Nonetheless, both tests showed similar tool response, where the depth was slightly over-called for the natural corrosion features that have metal loss less than 35% WT.

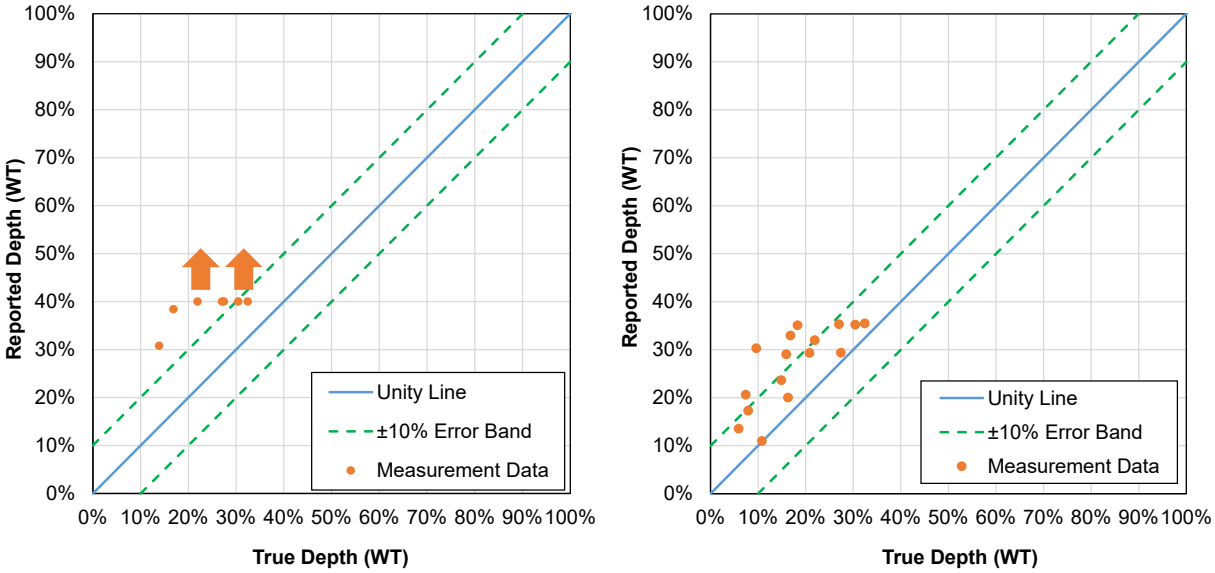

a) Current Test

b) Previous Test

Figure B.7 – Unity Plots of Natural Corrosion Features Called by Vendor-B's UT-2 Tool

Appendix C - Vendor-C's MEC Tool Test Results

C1 - Overview

C1.1 - Tool Features and Specifications

The MEC tools tested in this project are prototype tools that have not yet been commercialized. Vendor-C provided three tools, each of which was specifically designed for each of the three casing sizes. The 4.5 inch and 5.5 inch tools were equipped with 16 eddy current sensors to cover the full circumference of the pipe, while the 7.0 inch tool was equipped with 24 eddy current sensors. The distance of the sensor to the metal surface was set to be ~0.12 in (3 mm).

As the tools are prototypes and are not fully sealed, they cannot be operated in a fluid environment with their current design. The vendor did not provide any other operating specifications for these tools (temperature, pressure, resolution, etc.).

C1.2 - Vendor Deliverables

Upon completion of the logging test, Vendor-C submitted a detailed logging test report summarizing the technology of the MEC tool and the detected features. Figure C.1 and Figure C.2 present two examples from the vendor report showing the scan results for the casing joints with regular and random shape artificial features, respectively. As indicated in the vendor report, the color code in these charts is an amplitude-based conversion of the signal into feature depth, which, in most cases, is a good estimate of the true depth of the feature. The vendor report also provided a table summarizing the details of each individual feature.

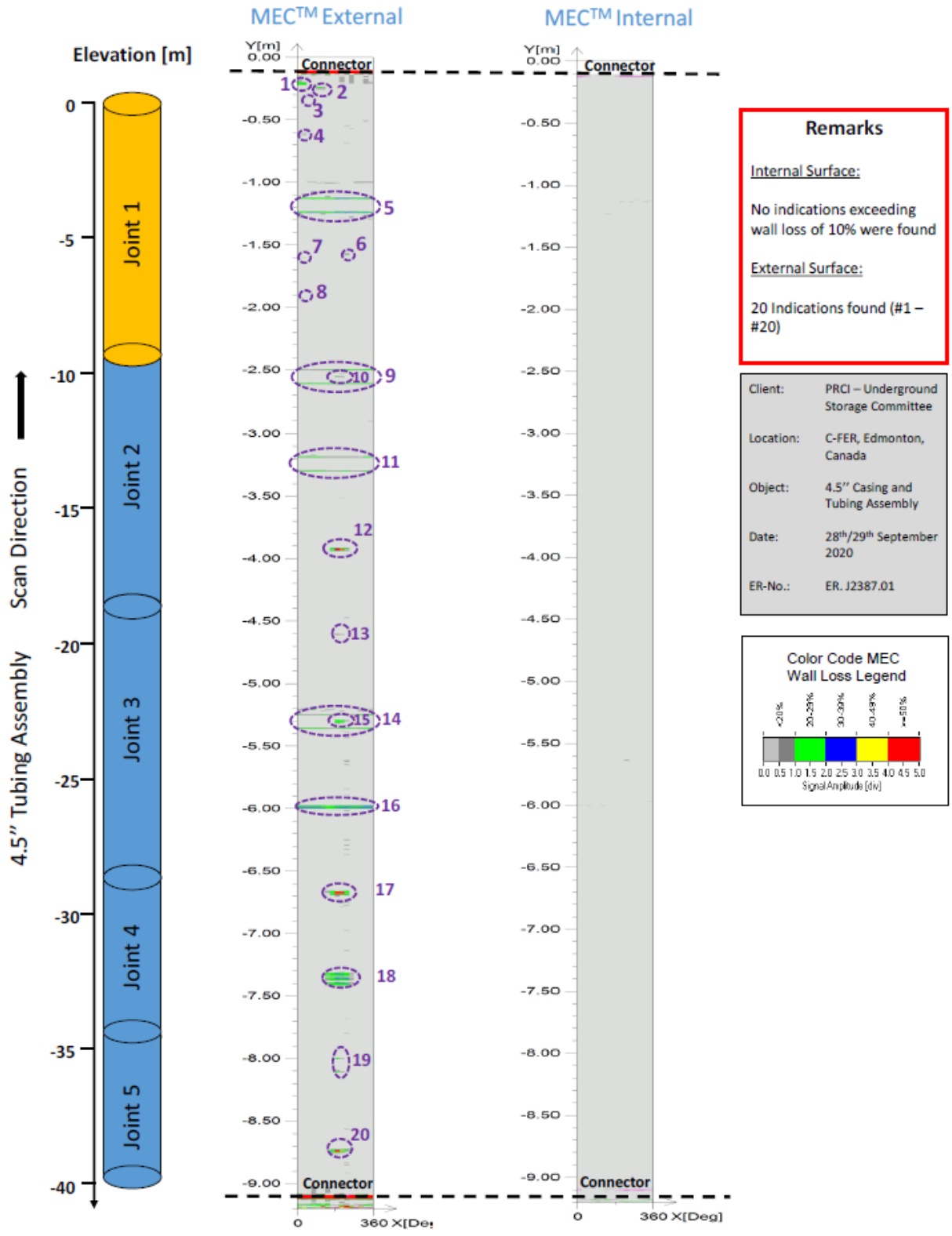

Figure C.1 – Scan of 4.5in-JT#1 with Regular Shape Artificial Features (from Vendor-C Report)

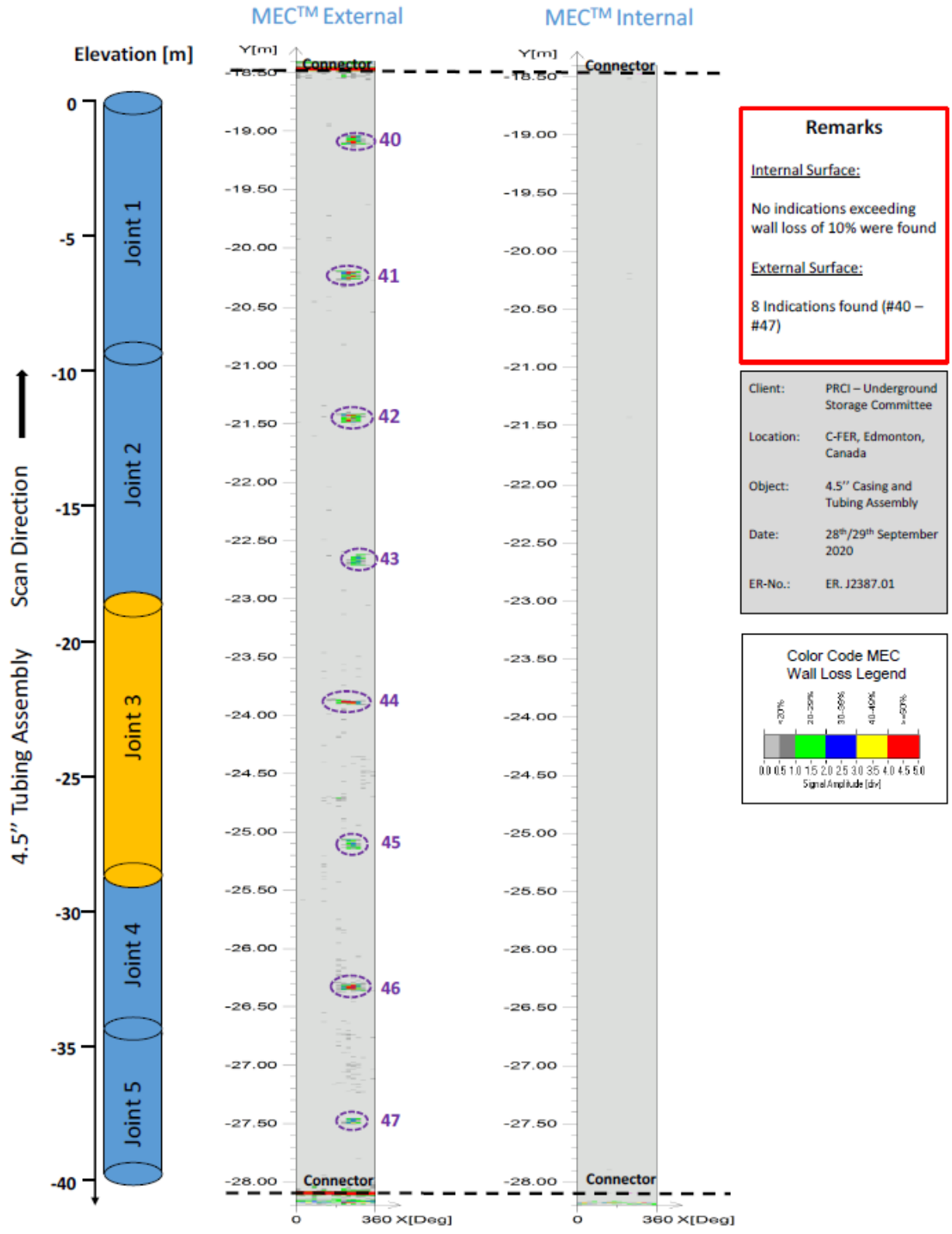

Figure C.2 – Scan of 4.5in-JT#3 with Random Shape Artificial Features (from Vendor-C Report)

C2 - Performance Evaluation

The MEC tools supplied by Vendor-C were able to provide a comprehensive assessment of the metal loss features on the casing, including location, size and maximum depth. Based on the list of the corrosion features identified, a quantitative assessment of the tool's performance was conducted. The evaluation was performed separately for the artificial features and the natural corrosion features. Note that, in the sizing accuracy analysis, the maximum feature length, width and depth were considered.

C2.1 - Detection Capability

C2.1.1 - Artificial Features

The tool identified features on all new casing joints were carefully reviewed and successfully matched with the known artificial features (i.e. by the axial and circumferential locations). The detection capability of Vendor-C's MEC tool was quantitatively evaluated by the POD.

Table C.1 lists the POD for each joint, as well as an overall POD for joints. In addition, this tool also reported some features in the 4.5 inch joints that do not actually exist. These called features were considered false detections and were also listed in Table C.1. Overall, the tool showed consistent detection capability for the artificial features over the three different casing sizes.

The POD results are grouped by the feature categories classified by the Pipeline Operators' Forum [26] to further investigate the tool response to different feature types. Note that only regular shape artificial features were considered. As shown in Table C.2, the tool performed well in detecting the majority of the small- to large-sized features. The extremely small size pinholes (0.2 inch diameter) were difficult to detect with this tool. However, when compared with other tools tested in this project, this tool showed a higher POD for these small pinholes, although at a relatively low POD of 29%. This tool also missed one-third of the axial grooving features, consistent with the results from the preceding PRCI test program [2]. Note that long and deep axial grooves can significantly compromise casing burst strength. Improvement in POD for axial grooving features by Vendor-C is certainly warranted. Also note that the tool did not detect the pitting cluster D11 (see Appendix A) as nine individual pitting features. Instead, the three pitting features at the same axial location were detected as one single circumferential grooving feature. Nonetheless, the pitting cluster D11 was considered successfully detected by the MEC tool.

Table C.1 – POD and False Detection for Vendor-C's MEC Tool (Artificial Features)

Casing Size	Joint No.	Total Number of Features	Number of Detected Features	POD	Number of False Detections
4.5 inch	1	18	16	89%	4
	2	18	15	83%	4
	3	8	8	100%	0
	4	N/A	N/A	N/A	N/A
5.5 inch	1	15	12	80%	0
	2	15	11	73%	0
	3	7	7	100%	0
	4	8	8	100%	0
7.0 inch	1a & 1b	15	13	87%	0
	2	15	11	73%	0
	3	7	6	86%	0
	4	8	7	88%	0
Total		134	114	85%	0

Table C.2 – Feature-classified POD for Vendor-C's MEC Tool (Regular Shape Artificial Features)

Feature Category	Total Number of Features	Number of Detected Features	POD
Pinhole	14	4	29%
Pitting	40	34	85%
Axial Grooving	6	4	67%
Circumferential Grooving	6	6	100%
General Corrosion	24	24	100%
Pitting Cluster *	6	6	100%

* Pitting cluster is not a feature category as per Pipeline Operators' Forum [26]. However, the pitting cluster is treated separately, as a special case, in this assessment.

C2.1.2 - Natural Corrosion Features

Matching of natural corrosion features was performed visually by comparing the feature pattern reported by the MEC tool to the LS results. As shown in Figure C.3, a generally good match was obtained for the corrosion feature pattern. The MEC tool was able to detect most features that have significant wall losses, but it also missed a few features that were relatively smaller in size. Most of the features reported by the tool enclosed several small features shown in the LS map. As a result, a quantitative assessment of the tool's detection capability (i.e. by POD) was not conducted.

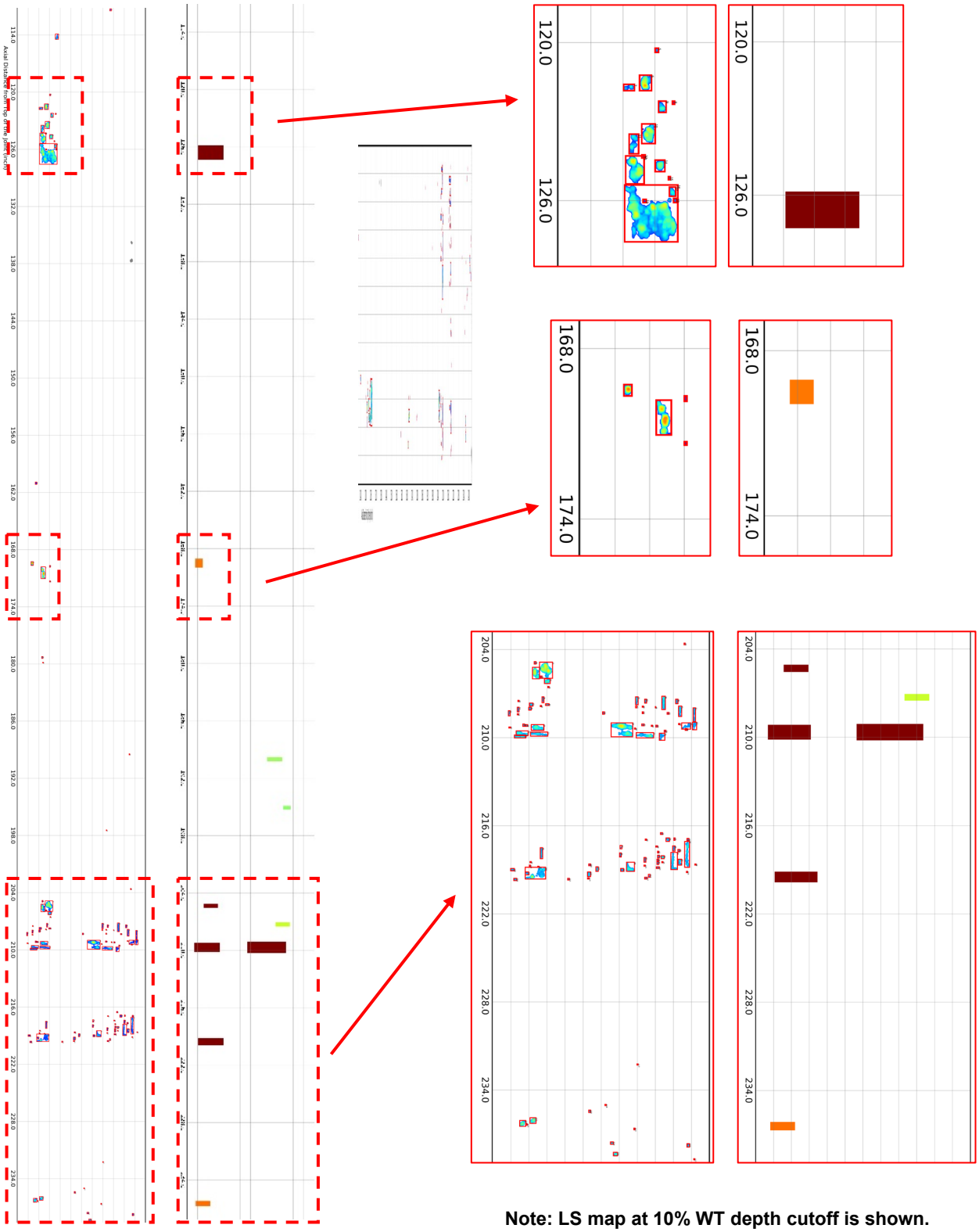

Figure C.3 – Natural Corrosion Feature Matching Examples for Vendor-C's MEC Tool (4.5in-JT#4)

C2.2 - Sizing Accuracy

C2.2.1 - Artificial Features

Note that the vendor reported the depth of the pits inside the general wall loss feature (i.e. features D4 and D8) as the percentage of the remaining wall instead of the total wall loss (the sum of the wall loss for both the general wall loss and the pit). This is due to the principle that the MEC tool detects relative WT change. Therefore, careful review of the results and appropriate engineering judgement must be made to avoid under-estimating corrosion wall loss. In the following depth sizing accuracy analysis, for pits inside the general corrosion areas, the reported relative wall loss of the pit was converted to the actual total wall loss.

Figure C.4 and Figure C.5 present the unity plots of the measured size versus the true size for the regular shape and random shape artificial features, respectively. A quantitative summary of the sizing accuracy with respect to various error bands is presented in Figure C.6. Based on the results, the following observations are made:

- This tool appears to have a generally consistent sizing accuracy response in the three different casing sizes;
- This tool tended to slightly over-call the feature depth if the value is less than 30% WT. For medium to deeper features (30% to 70% WT), there is no apparent bias error in the depth sizing accuracy;
- This tool did not show any apparent bias error in the length sizing accuracy. The tool showed slightly higher length sizing accuracy for regular shape features than random shape features; and
- Based on the initial report from the vendor, the tool significantly over-called the width of both regular and random shape features. A follow-up communication with the vendor indicated that a mistake was made during the data processing and it resulted in the low width sizing accuracy. This is actually consistent with the findings from the preceding PRCI project, where the MEC tool showed much better width sizing accuracy.

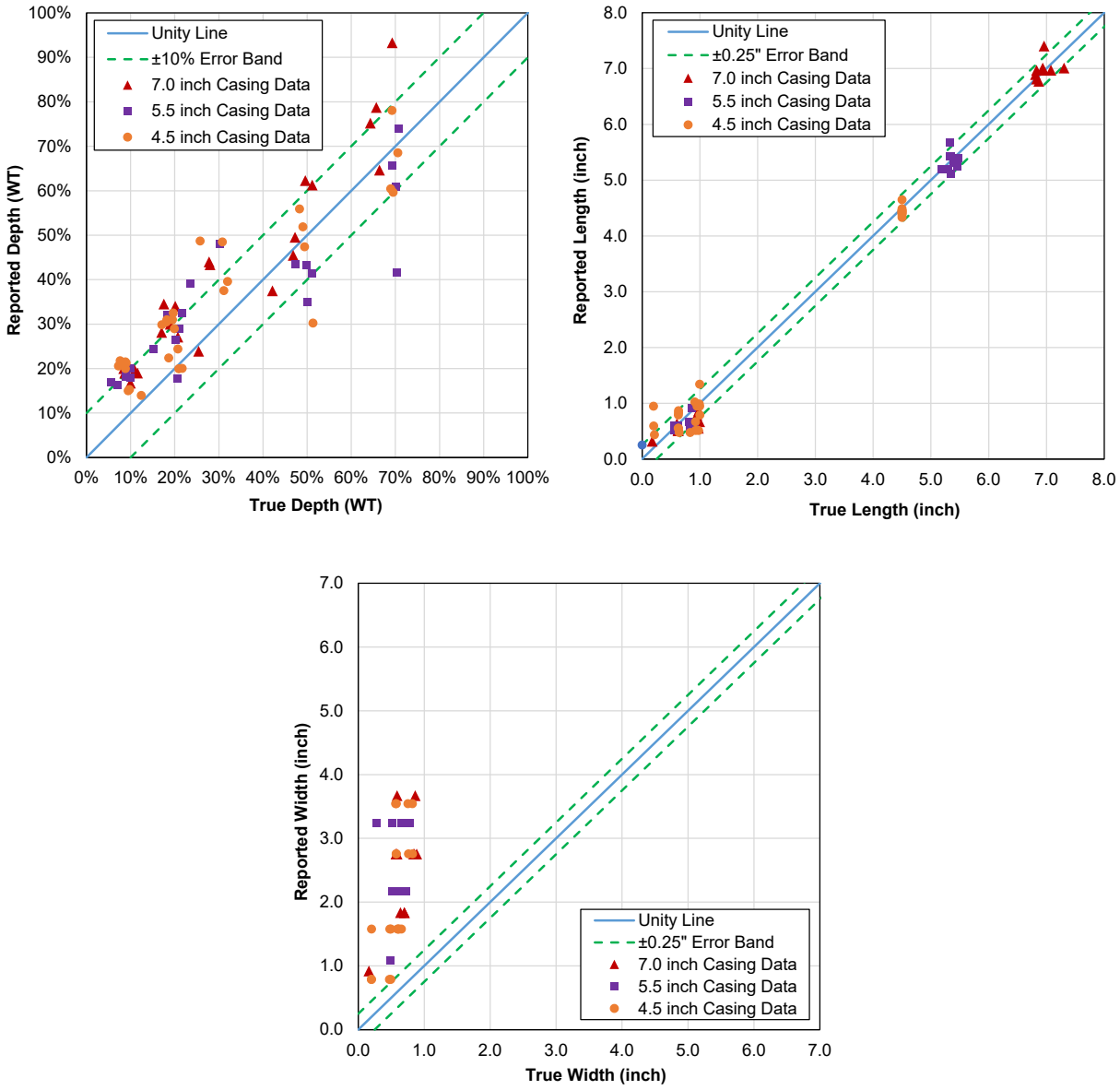

Note: Vendor indicated that a mistake was made during the data processing and it resulted in the low width sizing accuracy.

Figure C.4 – Unity Plots of Regular Shape Artificial Features Called by Vendor-C's MEC Tool

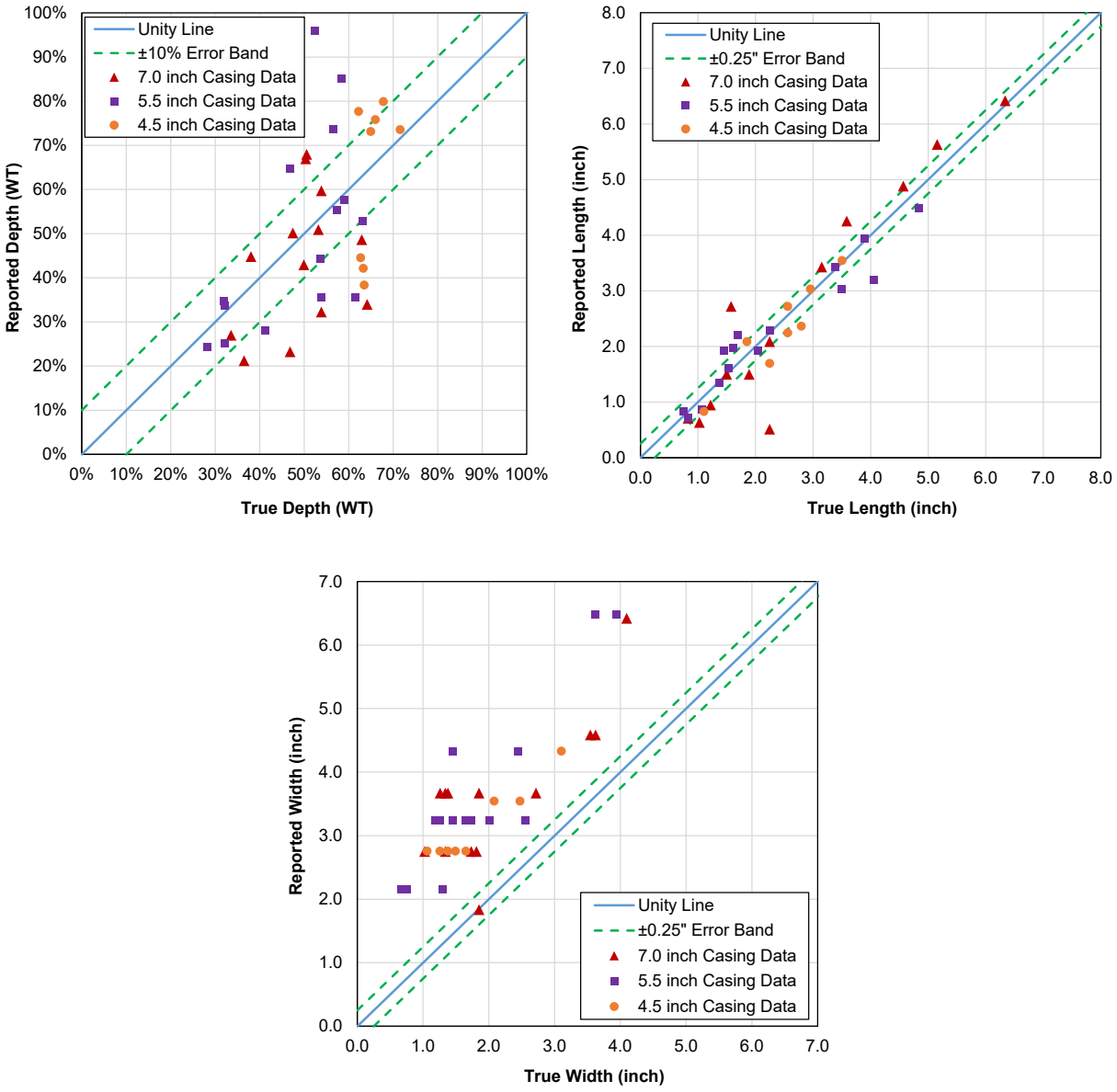

Figure C.5 – Unity Plots of Random Shape Artificial Features Called by Vendor-C's MEC Tool

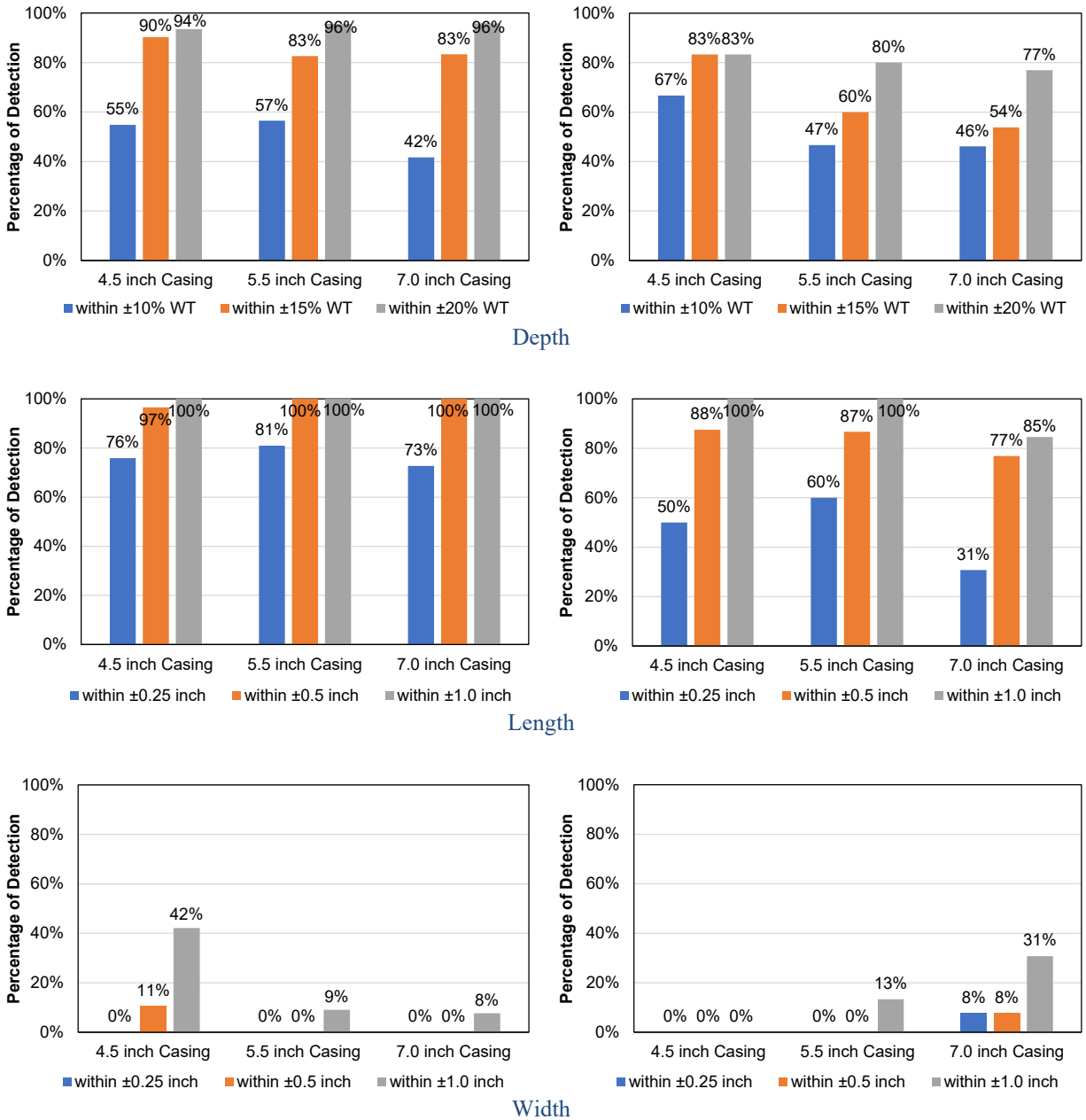

Note: Vendor-C indicated that a mistake was made during the data processing and resulted in the low width sizing accuracy.

Figure C.6 – Vendor-C's MEC Tool Measurement Accuracy for Artificial Features

C2.2.2 - Natural Corrosion Features

Each of the external metal loss features identified by the tool were successfully matched with the LS results through a manual process. However, the complexity of the natural corrosion profile created significant ambiguity in the actual feature size when matching the feature size indicated by the tool. In many cases, the tool identified feature was matched with a group of features (cluster)

from the LS results. Due to the size uncertainty during feature matching, evaluation of the sizing accuracy for length and width was found to be difficult. However, depth sizing accuracy was performed based on comparing the maximum feature depth reported by the tool and the LS results.

Figure C.7 presents the unity plots of the measured depth versus true depth for the detected features. The results suggest that this tool tends to over-call the depths of these natural corrosion features. It appears that there is a discrepancy in the tool's response in depth sizing accuracy between the artificial features and the natural corrosion features. Further investigation of this discrepancy and potential improvement of the tool for sizing natural corrosion features by Vendor-C is warranted.

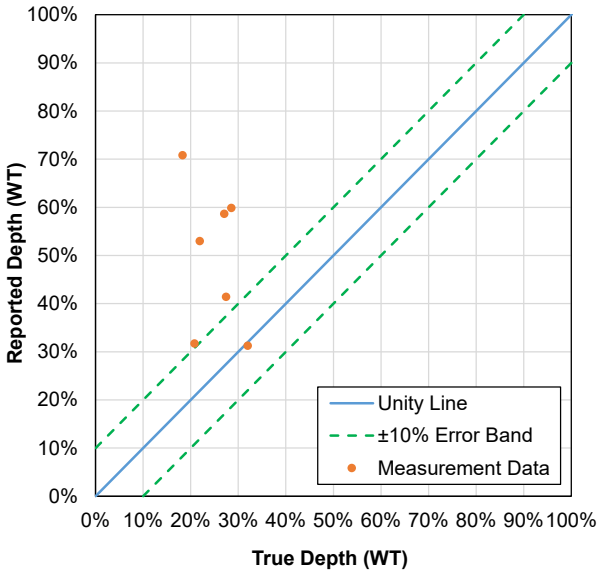

Figure C.7 – Unity Plots of Natural Corrosion Features Called by Vendor-C's MEC Tool

Appendix D - Vendor-D's MFL Tool Test Results

D1 - Overview

D1.1 - Tool Specifications

A summary of the Vendor-D's MFL tool specifications is shown in Table D.1, based on the publicly available information from Vendor-D.

Table D.1 – Vendor-D's MFL Tool Specifications

Measurable Casing Size	4.5 to 9.625 in
Vertical Resolution	±0.1 in (2.5 mm) under high resolution mode
Temperature Rating	350 ºF (177 ºC)
Pressure Rating	15,000 psi (103.4 MPa)

D1.2 - Vendor Deliverables

Upon completion of the logging tool test, Vendor-D provided a comprehensive logging test report that contained key information based on what the tool detected, including the overall casing configuration, various features (casing joints, collars, casing hardware, metal loss features, other anomalies, etc.). Various summary charts were also provided for the metal loss features. In addition, the report provided several remaining burst strength calculations (i.e. using Barlow, B31G, Modified B31G and Effective Area methods) based on the estimated metal loss feature geometries.

Table D.2 shows an example of a table provided in Vendor-D's logging test report summarizing all metal loss features in the 4.5 inch casing string detected by the tool. Figure D.1 presents an example plot from the vendor report on a feature size classification summary of the metal loss detected. The vendor further indicated that their report for this test program did not consider any wall loss threshold, while typically they don't report metal loss less than 15% to 20%.

Table D.2 – Metal Loss Feature Summary for the 4.5 inch Casing String (from Vendor-D MFL Tool Report)

Feature Type	Occurrences		
	Internal	External	Total
Pinholes	0	0	0
Pits	109	45	154
General	2	43	45
Axial Grooving	0	1	1
Axial Slotting	0	0	0
Circumferential Grooving	33	36	69
Circumferential Slotting	0	1	1
Total	**144**	**126**	**270**

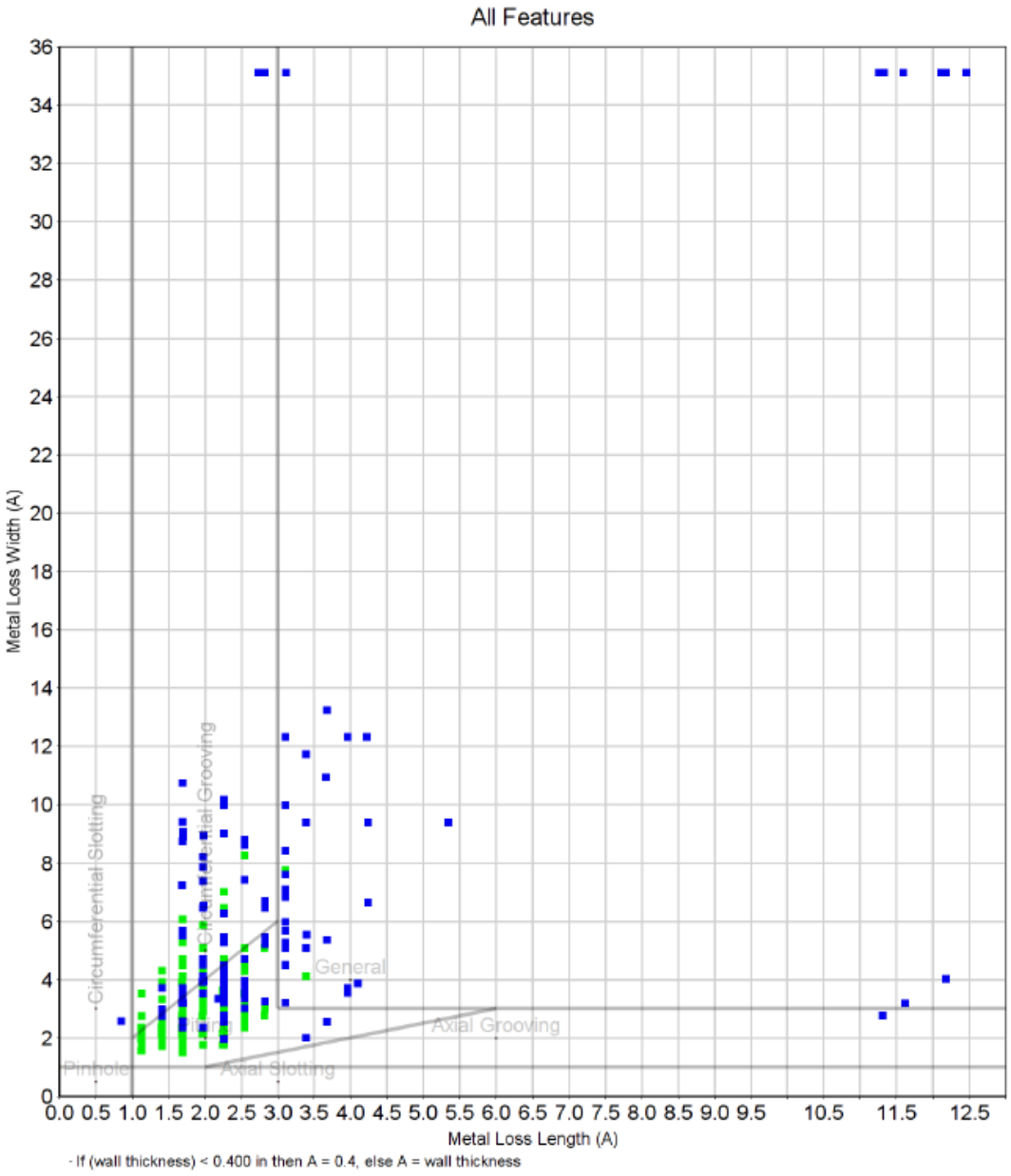

Figure D.1 – Metal Loss Feature Map for the 4.5 inch Casing String (from Vendor-D MFL Tool Report)

D2 - Performance Evaluation

The Vendor-D report provided a comprehensive description of the metal loss features on the casing, including size, maximum depth, location and type. Based on the list of the metal loss features identified, a quantitative assessment of the tool's performance was conducted. The evaluation was performed separately for the regular shape artificial features, random shape artificial features and natural corrosion features. Note that the maximum feature length, width and depth reported by Vendor-D were considered in the sizing accuracy analysis.

D2.1 - Detection Capability

D2.1.1 - Artificial Features

The tool-identified features on all new casing joints were carefully reviewed and successfully matched with the known artificial features (i.e. by the axial location). Figure D.2 to Figure D.4 show examples of comparisons between the MFL tool results and the LS results for the random shape artificial features. Since Vendor-D did not group features into clusters, the features called by the tool were grouped within a single cluster based on visual comparison with the LS result. The dimensions of the clusters were used in the subsequent sizing accuracy assessment. It appears that a random shape metal loss could result in multiple features called by the tool. Therefore, it seems that an appropriate clustering rule is required to further characterize the features for remaining strength estimation.

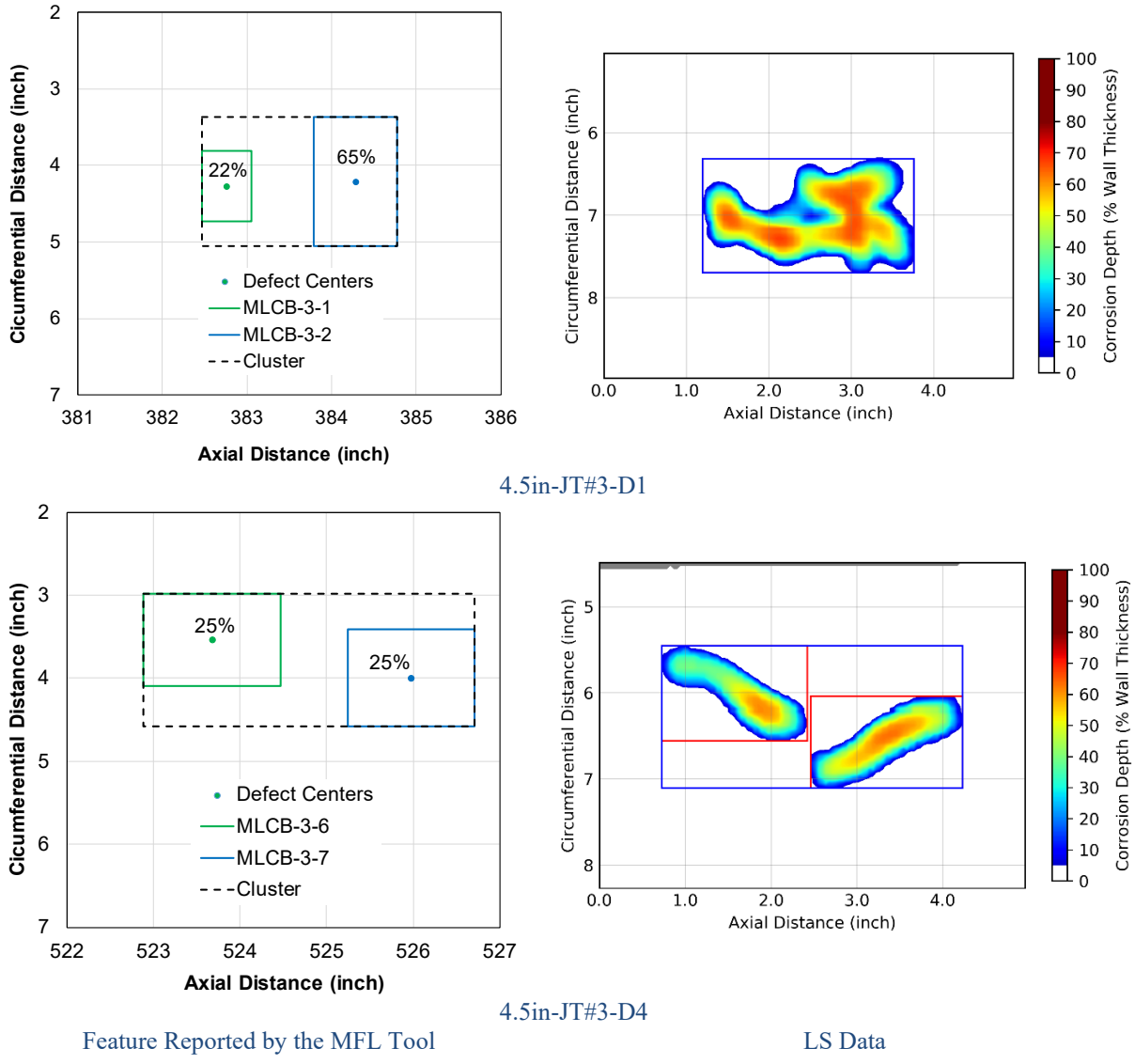

Figure D.2 – Matching Random Shape Artificial Feature for Vendor-D's MFL Tool (4.5in-JT#3)

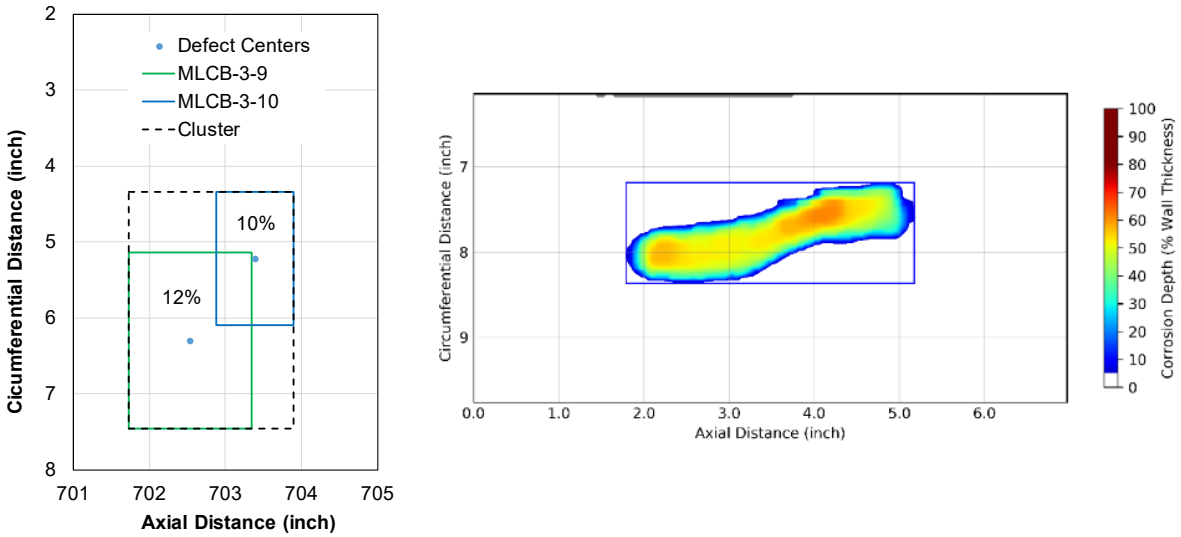

Feature Reported by the MFL Tool LS Data

Figure D.3 – Matching Random Shape Artificial Feature for Vendor-D's MFL Tool (5.5in-JT#3-D6)

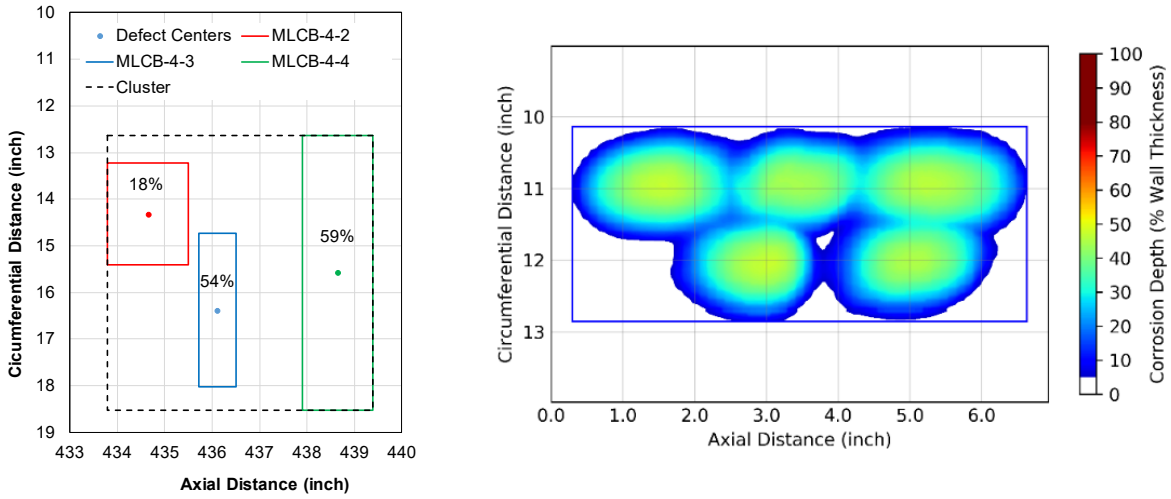

Feature Reported by the MFL Tool LS Data

Figure D.4 – Matching Random Shape Artificial Feature for Vendor-D's MFL Tool (7.0in-JT#3-D2)

The detection capability of Vendor-D's MFL tool was quantitatively evaluated by the POD. Table D.3 lists the POD for each joint, as well as an overall POD for new casing joints. Overall, the tool showed consistent detection capability for the artificial features over the three different casing sizes. In addition, the MFL tool did not report any false detections within these joints. The POD results are grouped by the feature categories classified by the Pipeline Operators' Forum [26] to further investigate the tool response to different feature types, as shown in Table D.4. Note that only regular shape artificial features were considered. Apparently, the extremely small sized pinholes (0.2 inch diameter) are below the detection limit of this tool. However, the tool demonstrated good performance in detecting pitting and larger features. Also note that the tool did not detect the pitting cluster D11 (see Appendix A) as nine individual pitting features. Instead, the three pitting

features at the same axial location were detected as one single circumferential grooving feature. Nonetheless, the pitting cluster D11 was considered successfully detected by the MFL tool.

Table D.3 – POD and False Detection for Vendor-D's MFL Tool (Artificial Features)

Casing Size	Joint No.	Total Number of Features	Number of Detected Features	POD	Number of False Detections
4.5 inch	1	18	13	72%	0
	2	18	12	67%	0
	3	8	8	100%	0
	4	N/A	N/A	N/A	N/A
5.5 inch	1	15	12	80%	0
	2	15	12	80%	0
	3	7	7	100%	0
	4	8	8	100%	0
7.0 inch	1a & 1b	15	13	87%	0
	2	15	12	80%	0
	3	7	7	100%	0
	4	8	7	87.5%	0
Total		134	111	83%	0

Table D.4 – Feature-classified POD for Vendor-D's MFL Tool (Regular Shape Artificial Features)

Feature Category	Total Number of Features	Number of Detected Features	POD
Pinhole	14	0	0%
Pitting	40	32	80%
Axial Grooving	6	6	100%
Circumferential Grooving	6	6	100%
General Corrosion	24	24	100%
Pitting Cluster *	6	6	100%

* Pitting cluster is not a feature category as per Pipeline Operators' Forum (2016). However, the pitting cluster is treated separately, as a special case, in this assessment.

D2.1.2 - Natural Corrosion Features

Matching of natural corrosion features was performed visually by comparing the feature pattern reported by the MFL tool and from the LS results. As shown in Figure D.5, a generally good match was obtained for the corrosion feature pattern. It clearly shows that the tool was able to detect most of the significant metal loss features (e.g. WT of ≥ 10%). In addition, the tool did not have any false calls. It appears that Vendor-D used different clustering rules than that used in the LS data analysis. As a result, a quantitative assessment of the tool's detection capability (i.e. by POD) was not conducted.

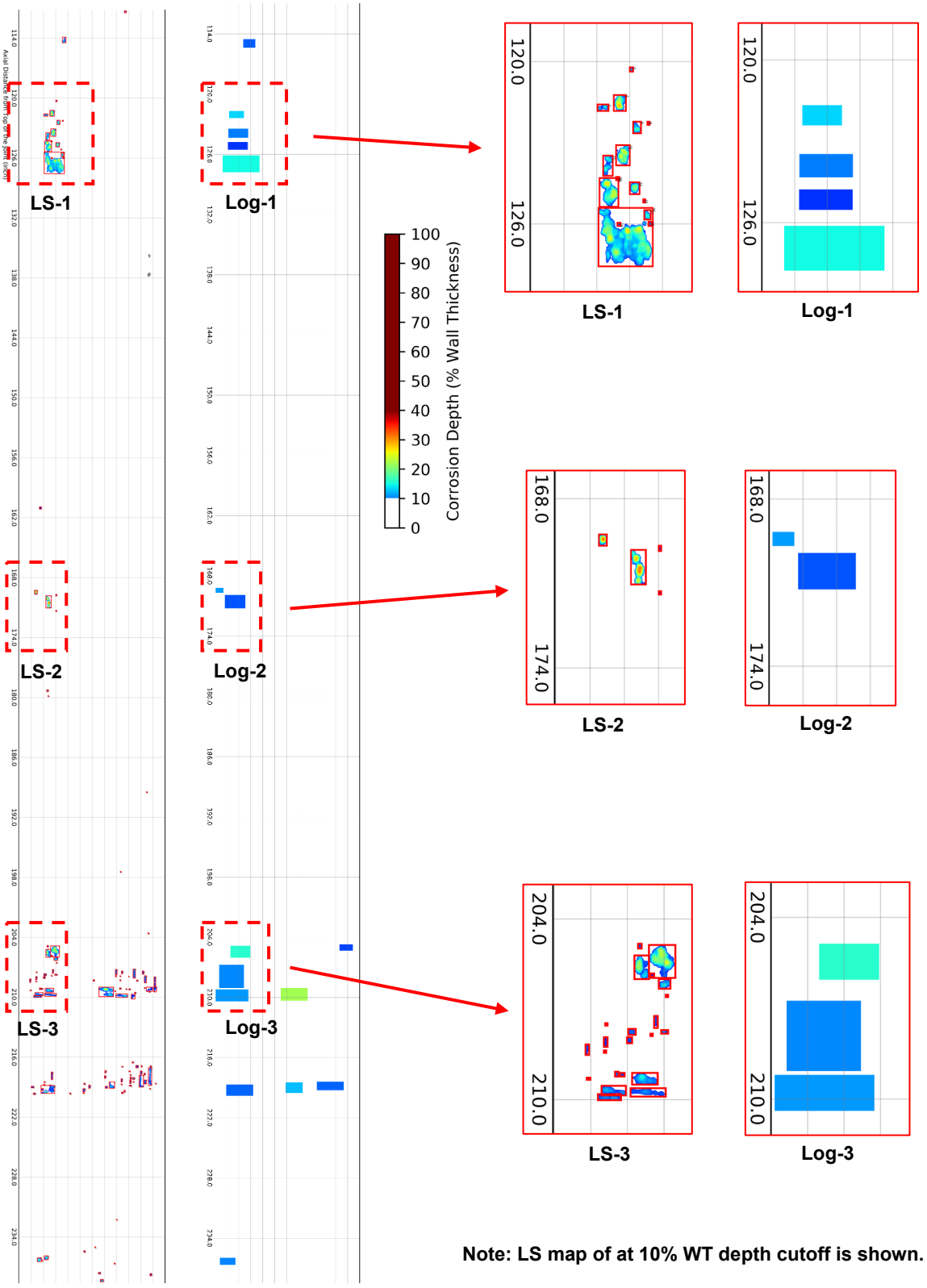

Figure D.5 – Natural Corrosion Feature Matching Examples for Vendor-D's MFL Tool (4.5in-JT#4)

D2.2 - Sizing Accuracy

D2.2.1 - Artificial Features

Note that the vendor reported the depth of the pits inside the general wall loss feature (i.e. features D4 and D8) as the percentage of the remaining wall instead of the total wall loss (the sum of the wall loss for both the general wall loss and the pit). This is due to the principle that the MFL tool detects relative WT change. Therefore, careful review of the results and appropriate engineering judgement must be made to avoid under-calling corrosion wall loss. In the following depth sizing accuracy analysis, for pits inside the general corrosion areas, the reported relative wall loss of the pit was converted to the actual total wall loss.

Figure D.6 and Figure D.7 present unity plots of the measured size versus the true size for the regular shape and random shape artificial features, respectively. A quantitative summary of the sizing accuracy with respect to various error bands is presented in Figure D.8. Based on the results, the following observations are made:

- This tool appears to have a generally consistent sizing accuracy response in the three different casing sizes;
- This tool tended to under-call the feature depth for both regular and random shape artificial features. Although a difference in the depth sizing accuracy is shown in Figure D.8, reviewing the unity plots suggests that the difference is primarily due to the difference of depth sample population (i.e. more features with medium to large depth in the random shape category than in the regular shape category). In addition, consistent depth sizing bias error was identified on certain regular shape artificial features reported by this tool:
    - This tool consistently over-called the depth of features D2 (full-circumferential general corrosion) and D9 (full-circumferential grooving) on all casing joints, as shown in Figure D.6. Note that the metal losses of features D2 and D9 are in the range of around 15% to 20% WT, while, for other full-circumferential metal loss features with metal loss of approximately 10% WT (i.e. D4, D5 and D8), the depth measure is within the 10% error band; and
    - The tool consistently under-called deep pitting features (i.e. ≥ 50% WT) on all casing joints, as shown in Figure D.6. In addition, the results suggest that the bias error increases with increasing pitting depth;
- This tool was found to slightly over-call the length of regular shape features, while slightly under-calling the random shape features. However, the length sizing accuracy response was generally consistent between the regular and random shape features; and
- The tool was found to consistently over-call the width of both regular and random shape features.

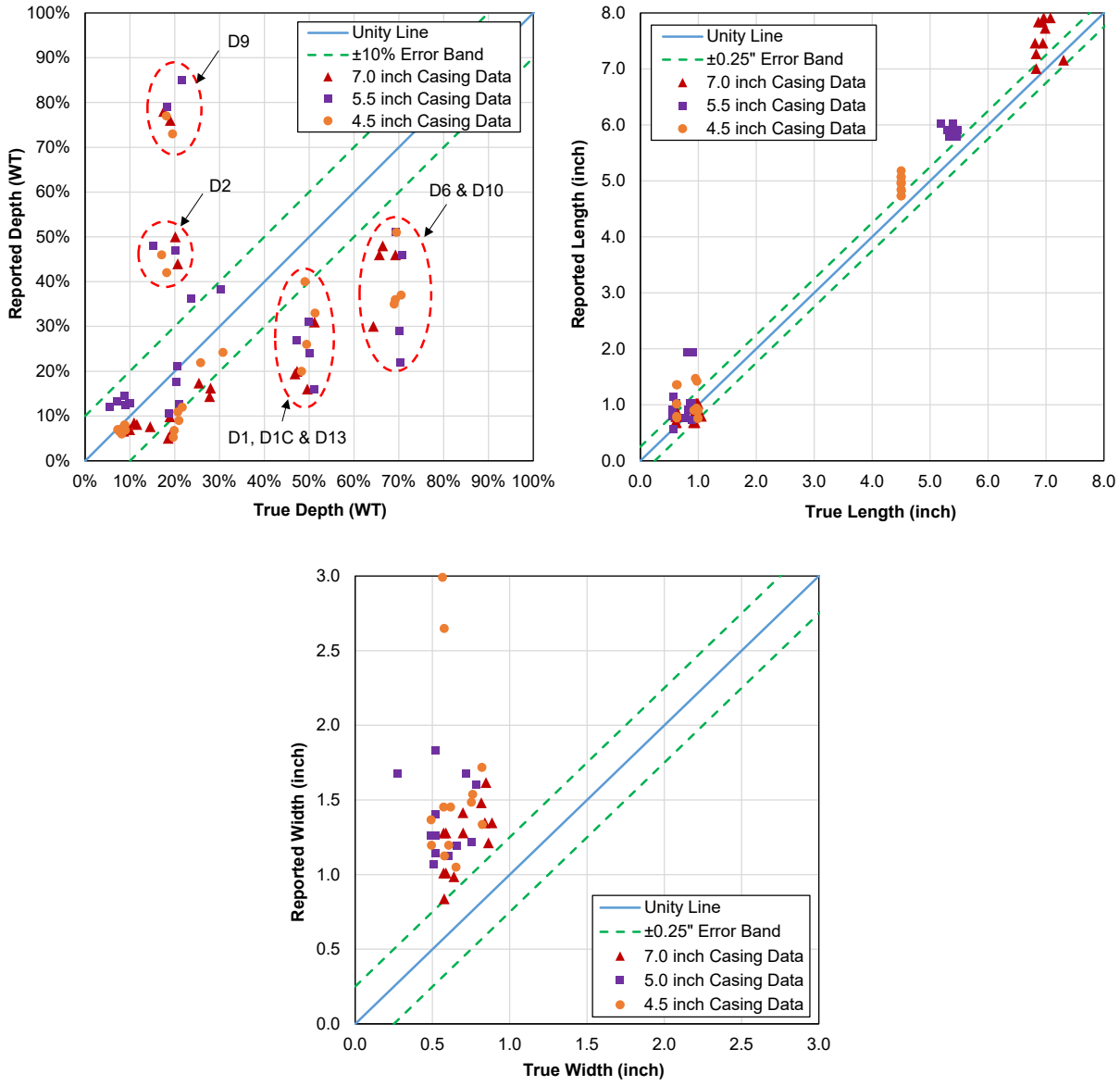

Figure D.6 – Unity Plots of Regular Shape Artificial Features Called by Vendor-D's MFL Tool

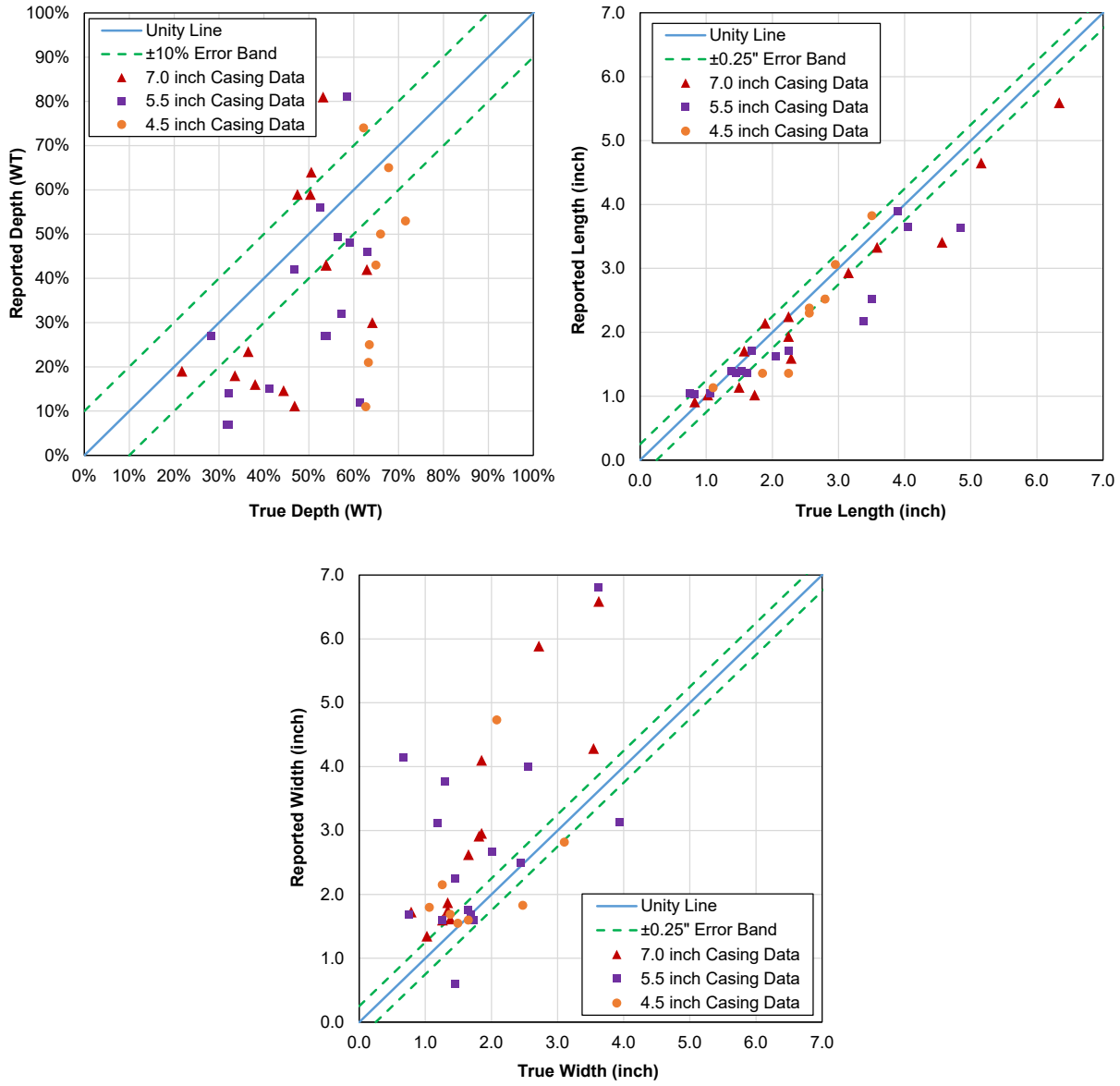

Figure D.7 – Unity Plots of Random Shape Artificial Features Called by Vendor-D's MFL Tool

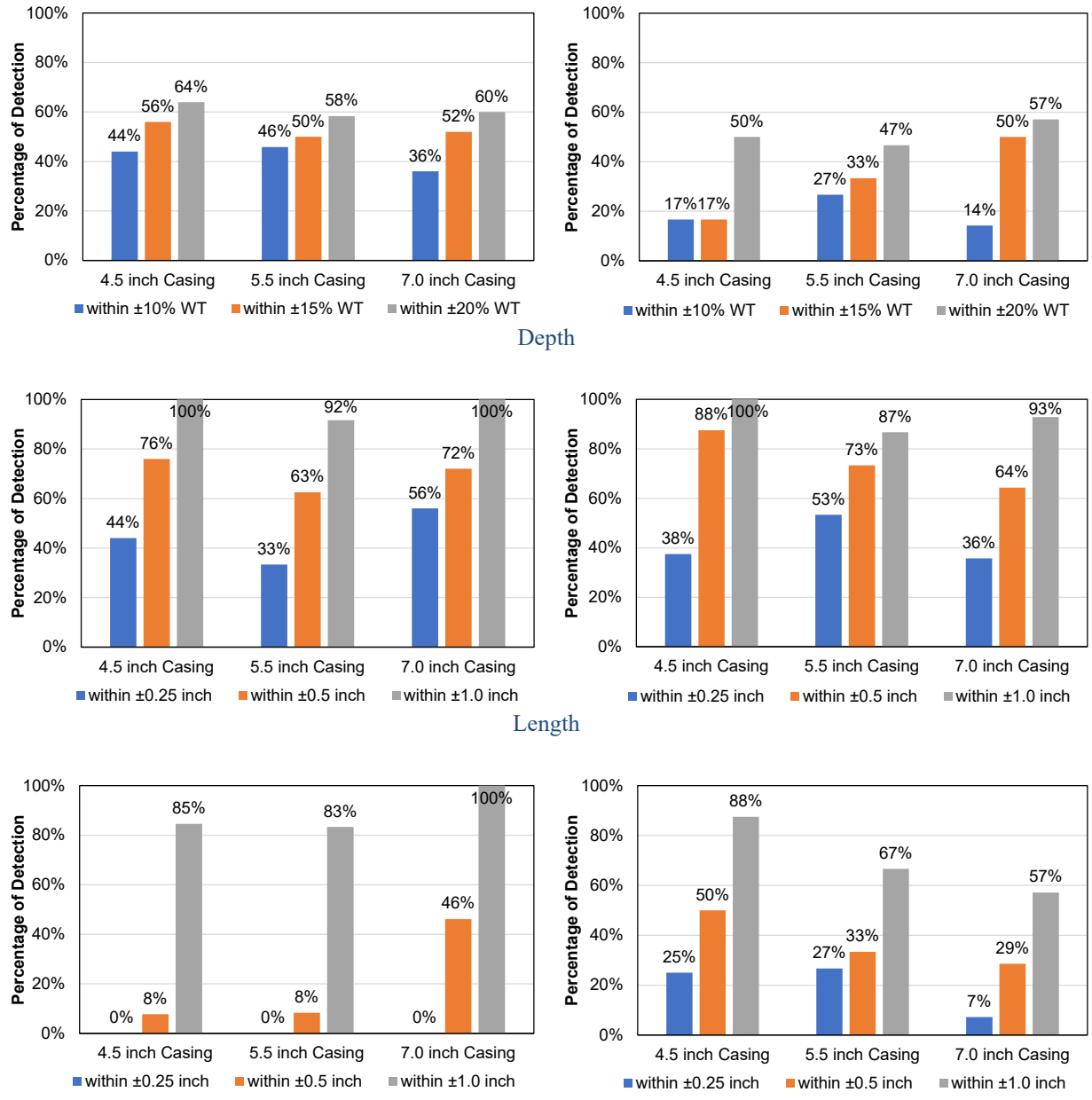

Figure D.8 – Vendor-D's MFL Tool Measurement Accuracy for Artificial Features

D2.2.2 - Natural Corrosion Features

Each of the external metal loss features identified by the tool were successfully matched with the LS results through a manual process. However, the complexity of the natural corrosion profile created significant ambiguity in the actual feature size when matching the feature size indicated by the tool. In many cases, the tool-identified feature was matched with a group of features (cluster) from the LS results. Due to the size uncertainty during feature matching, evaluation of the

sizing accuracy for length and width was difficult. However, depth sizing accuracy was performed based on the maximum feature depth between the tool and the LS results.

Figure D.9 presents the unity plots of the measured depth versus true depth for the detected features. Further review of the unity plots suggests that this tool tends to slightly under-call feature depths that are over ~20% WT, which is consistent with the findings for the artificial features (see Figure D.6 and Figure D.7).

Since the same casing joint has also been logged in the preceding PRCI test project, the maximum depth measurements from the previous test are also presented in Figure D.9 for comparison. In general, both tests showed similar tool response.

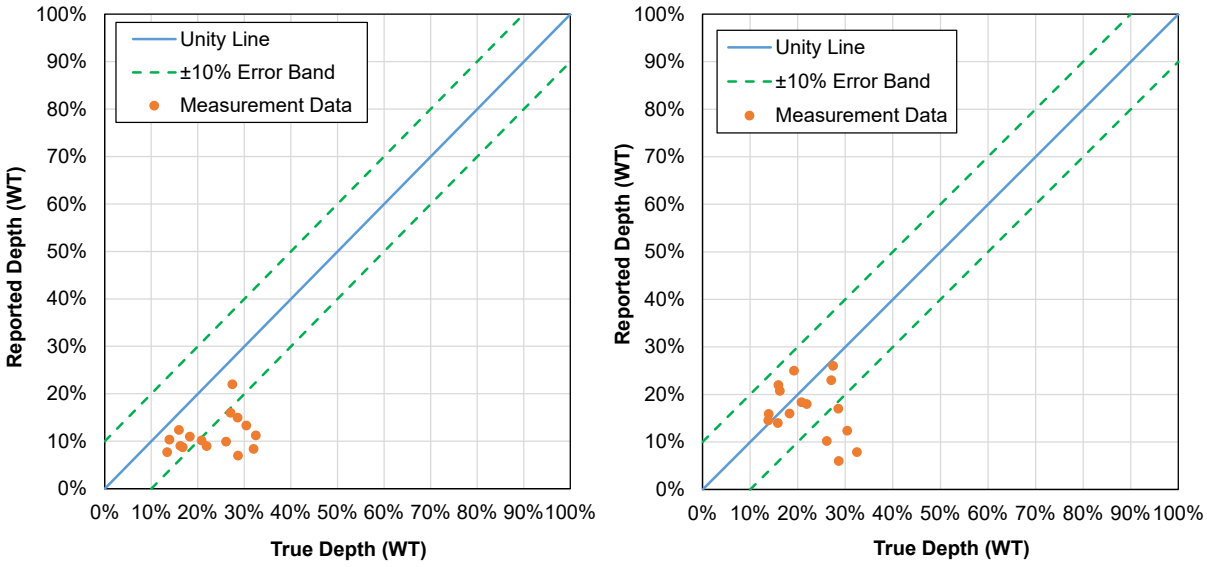

a) Current Test

b) Previous Test

Figure D.9 – Depth Unity Plots of Natural Corrosion Features Called by Vendor-D's MFL Tool

Appendix E - Burst Test Results

This appendix summarizes the details of the burst test specimens and test results, including the casing information, metal loss profiles, burst test results, the failed specimen pictures, and the FEA results showing the plastic strain distribution at the peak pressure.

Casing Information					
Outside Diameter	4.5 inch	Nominal Wall	0.25 inch	Material Grade	J55
Metal Loss Information					
Feature ID	4.5in-JT#3-D1				
Length	2.56 inch	Width	1.37 inch	Max. Depth	69%
Burst Strength (Physical Test)					
Load Condition	Capped-End				
Burst Strength	6,366 psi				

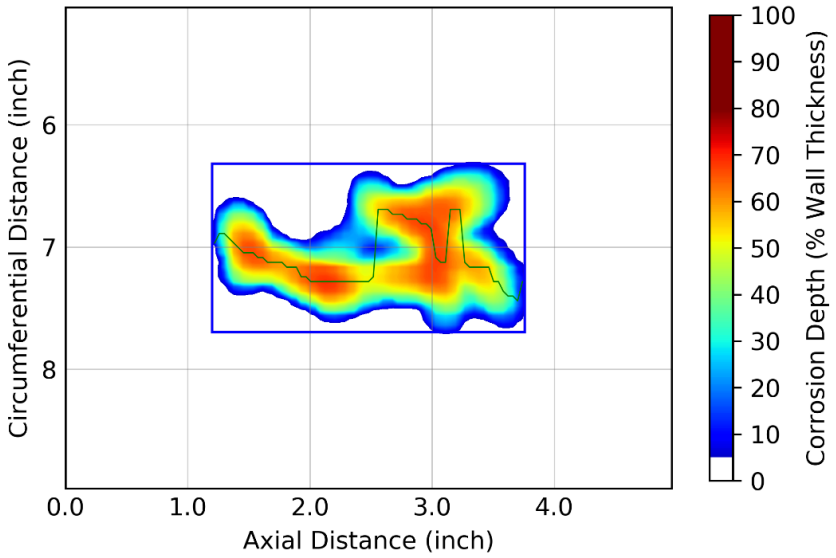

Figure E.1 – Laser Scan Plot (4.5in-JT#3-D1)

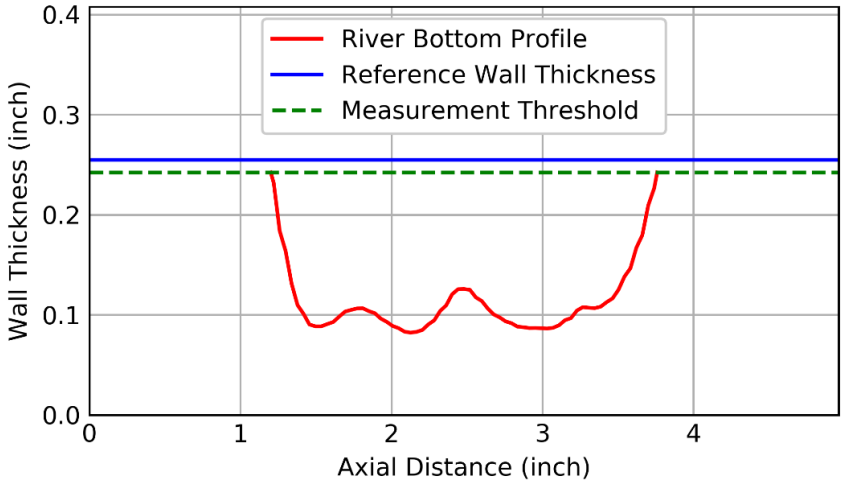

Figure E.2 – River Bottom Profile (4.5in-JT#3-D1)

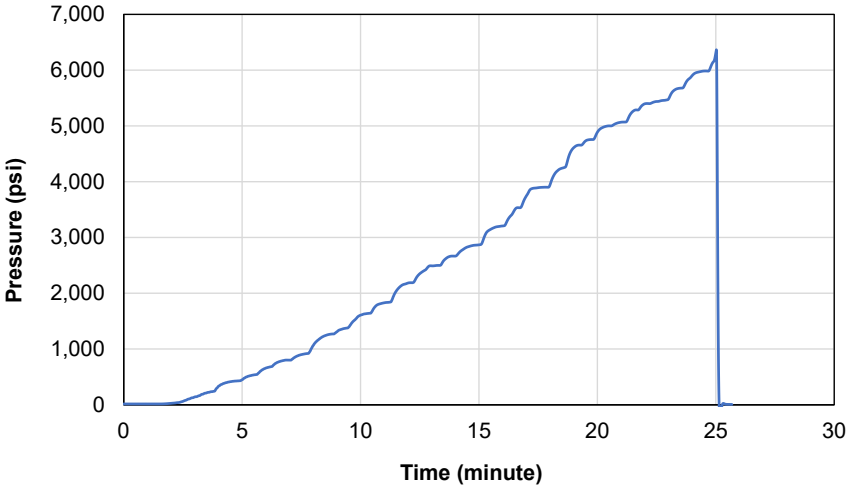

Figure E.3 – Burst Test Pressure versus Time (4.5in-JT#3-D1)

Figure E.4 – Failed Specimen (4.5in-JT#3-D1)

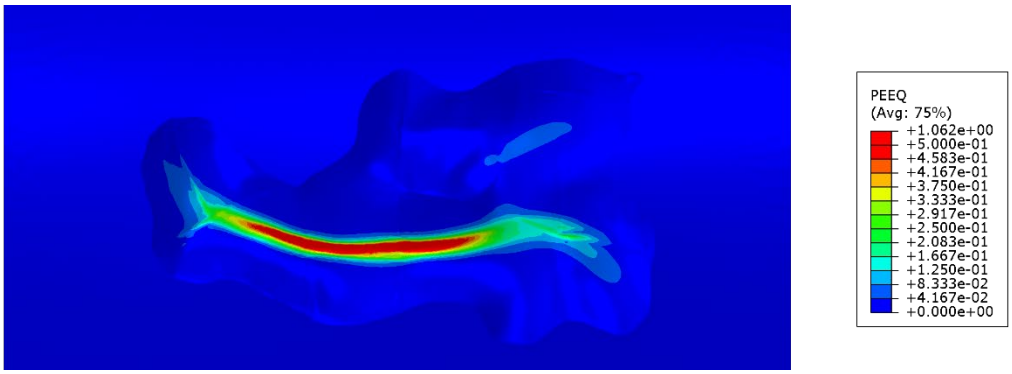

Figure E.5 – FEA Result - Plastic Strain at Peak Pressure (4.5in-JT#3-D1)

Casing Information					
Outside Diameter	4.5 inch	Nominal Wall	0.25 inch	Material Grade	J55
Metal Loss Information					
Feature ID	4.5in-JT#3-D2				
Length	2.80 inch	Width	1.49 inch	Max. Depth	66%
Burst Strength (Physical Test)					
Load Condition	Capped-End				
Burst Strength	8,116 psi				

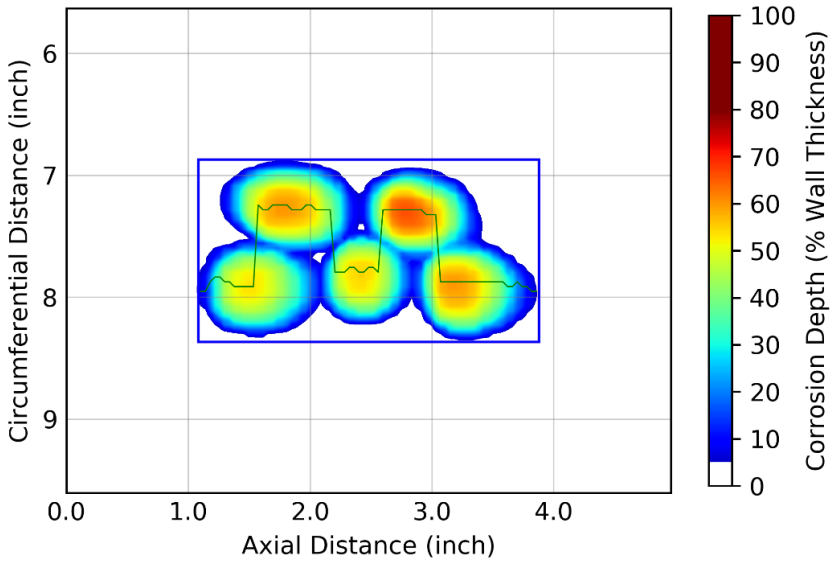

Figure E.6 – Laser Scan Plot (4.5in-JT#3-D2)

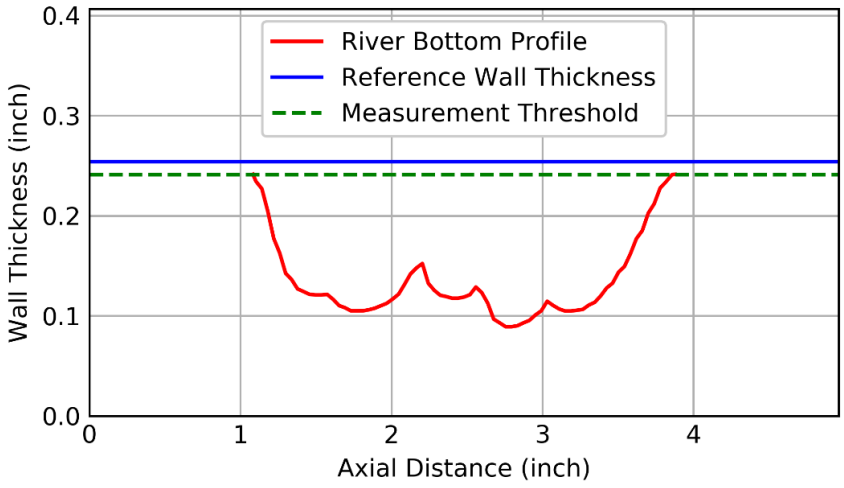

Figure E.7 – River Bottom Profile (4.5in-JT#3-D2)

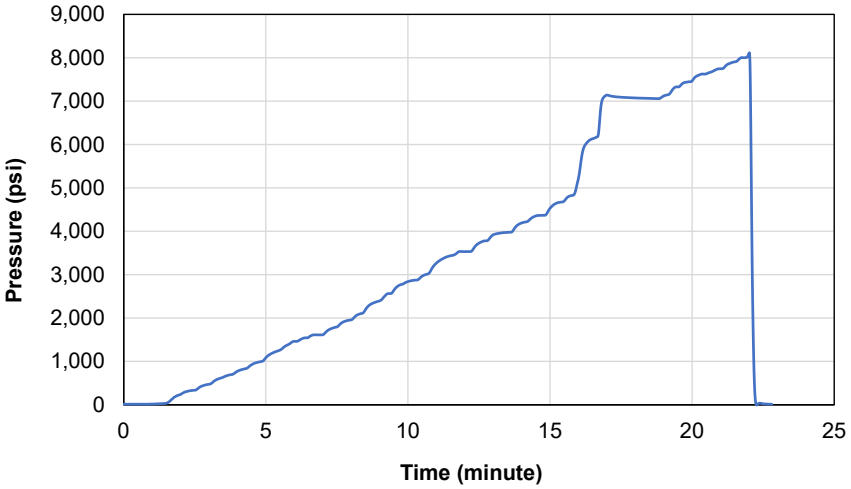

Figure E.8 – Burst Test Pressure versus Time (4.5in-JT#3-D2)

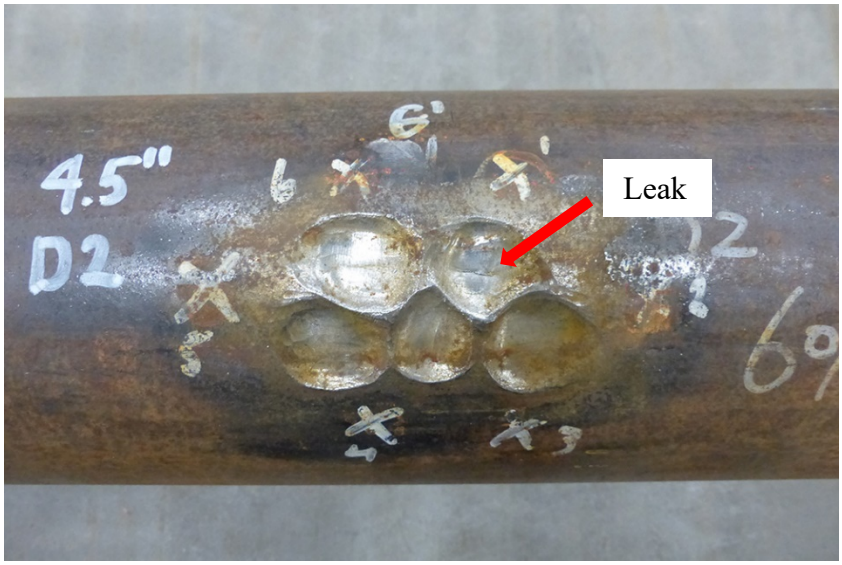

Figure E.9 – Failed Specimen (4.5in-JT#3-D2)

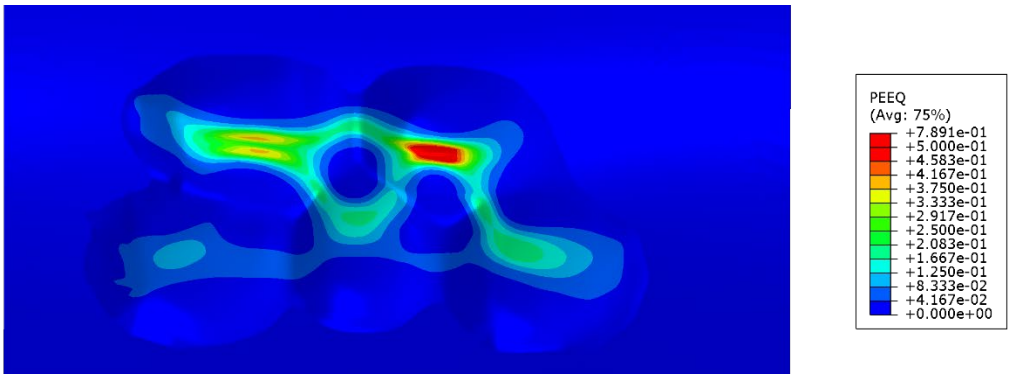

Figure E.10 – FEA Result - Plastic Strain at Peak Pressure

Casing Information					
Outside Diameter	4.5 inch	Nominal Wall	0.25 inch	Material Grade	J55
Metal Loss Information					
Feature ID	4.5in-JT#3-D3				
Length	2.56 inch	Width	2.47 inch	Max. Depth	73%
Burst Strength (Physical Test)					
Load Condition	Capped-End				
Burst Strength	7,235 psi				

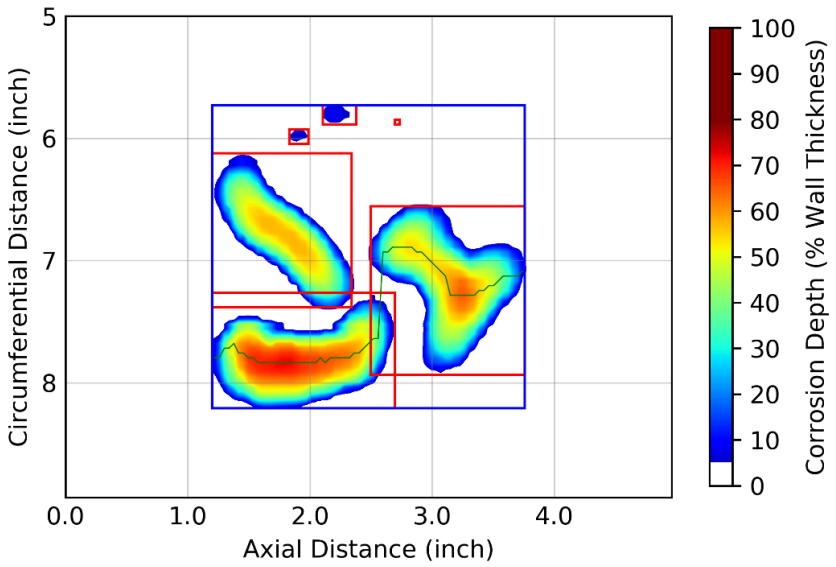

Figure E.11 – Laser Scan Plot (4.5in-JT#3-D3)

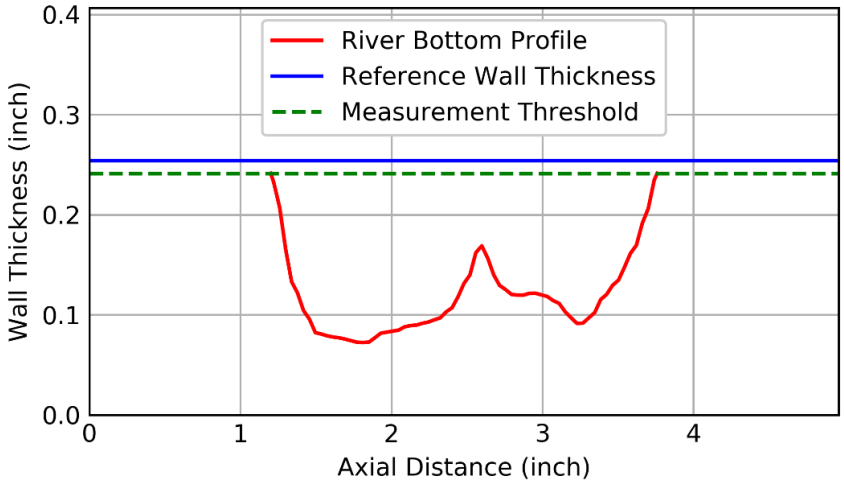

Figure E.12 – River Bottom Profile (4.5in-JT#3-D3)

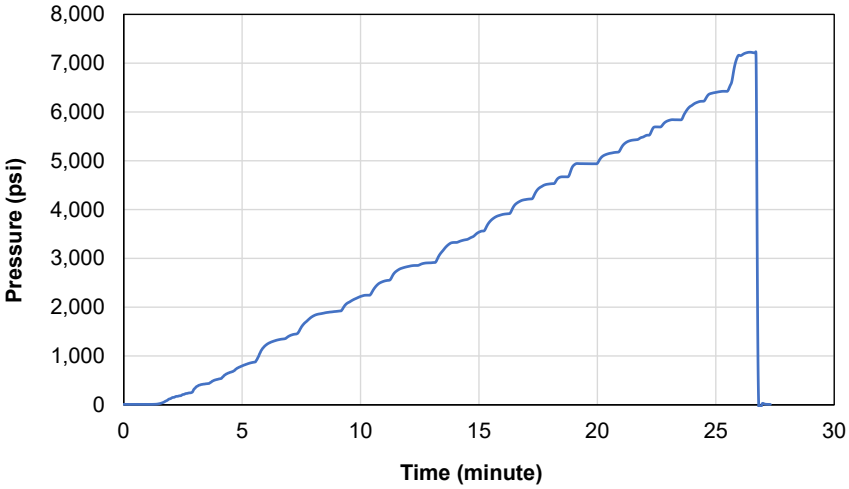

Figure E.13 – Burst Test Pressure versus Time (4.5in-JT#3-D3)

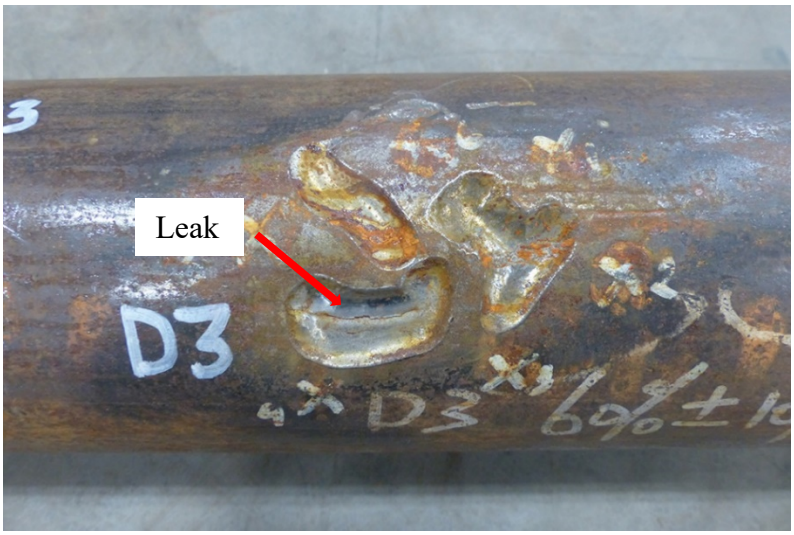

Figure E.14 – Failed Specimen (4.5in-JT#3-D3)

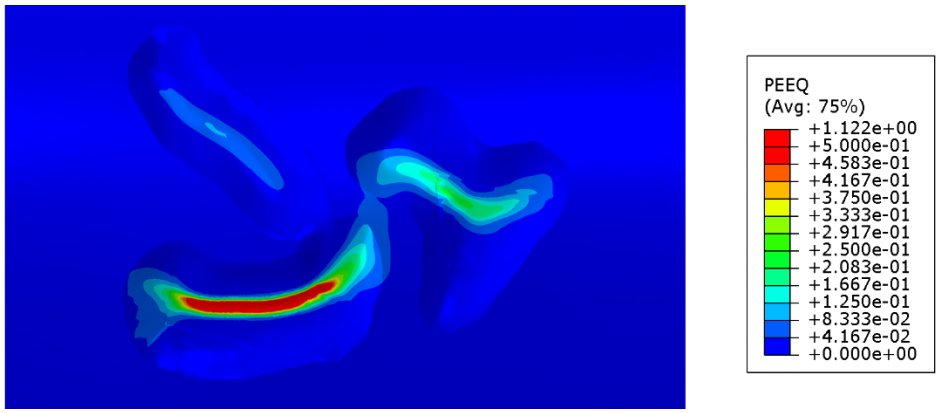

Figure E.15 – FEA Result - Plastic Strain at Peak Pressure (4.5in-JT#3-D3)

Casing Information						
Outside Diameter	4.5 inch	Nominal Wall	0.25 inch	Material Grade	J55	
Metal Loss Information						
Feature ID	4.5in-JT#3-D4					
Length	3.50 inch	Width	1.65 inch	Max. Depth	65%	
Burst Strength (Physical Test)						
Load Condition	Capped-End					
Burst Strength	7,504 psi					

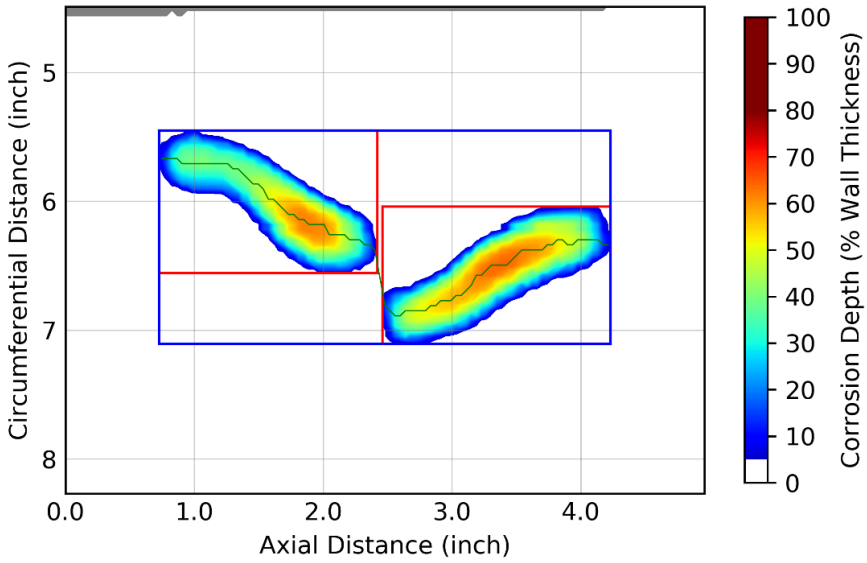

Figure E.16 – Laser Scan Plot (4.5in-JT#3-D4)

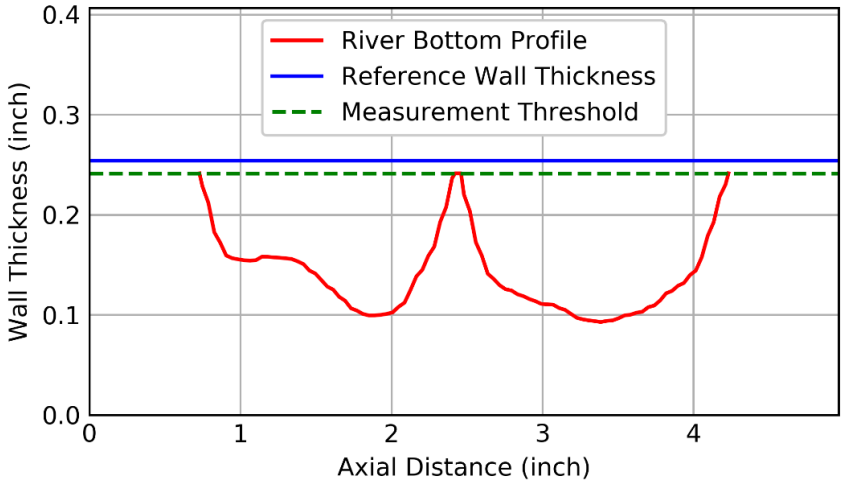

Figure E.17 – River Bottom Profile (4.5in-JT#3-D4)

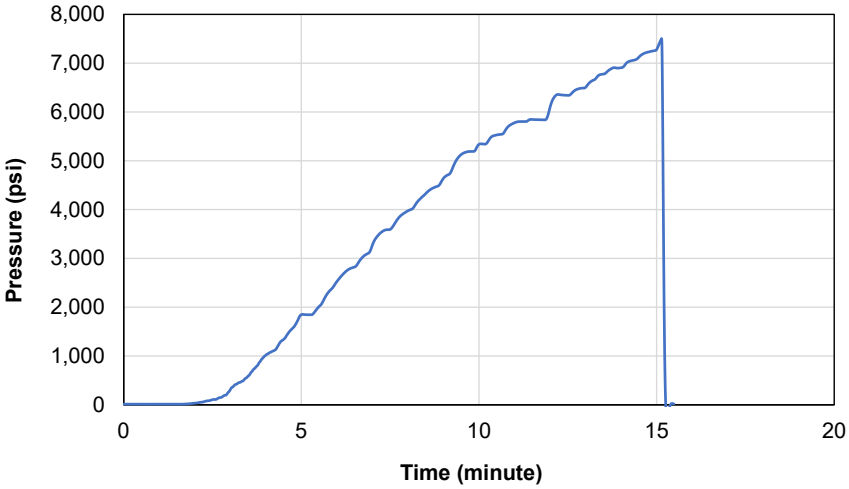

Figure E.18 – Burst Test Pressure versus Time (4.5in-JT#3-D4)

Figure E.19 – Failed Specimen (4.5in-JT#3-D4)

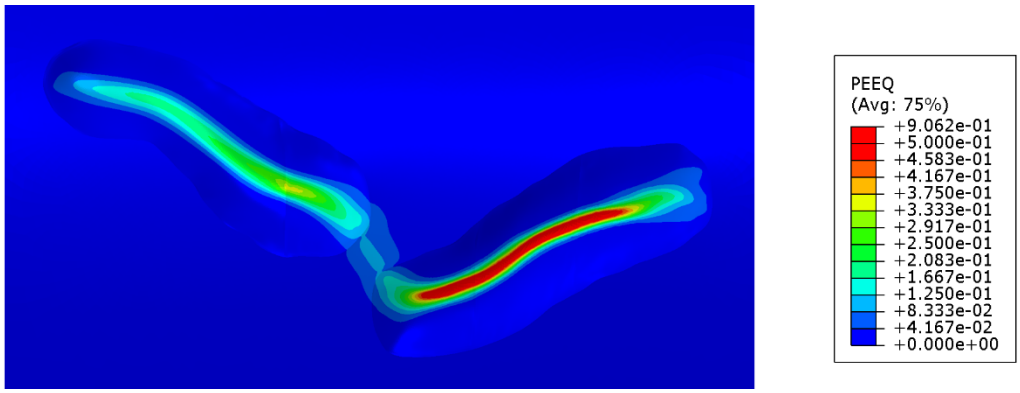

Figure E.20 – FEA Result - Plastic Strain at Peak Pressure (4.5in-JT#3-D4)

Casing Information					
Outside Diameter	4.5 inch	Nominal Wall	0.25 inch	Material Grade	J55
Metal Loss Information					
Feature ID	4.5in-JT#3-D5				
Length	1.10 inch	Width	3.10 inch	Max. Depth	67%
Burst Strength (Physical Test)					
Load Condition	Capped-End				
Burst Strength	9,270 psi				

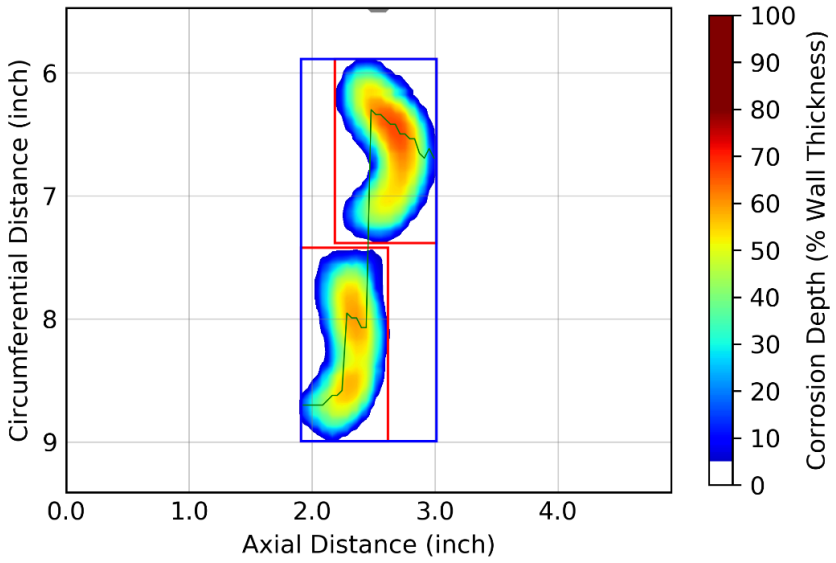

Figure E.21 – Laser Scan Plot (4.5in-JT#3-D5)

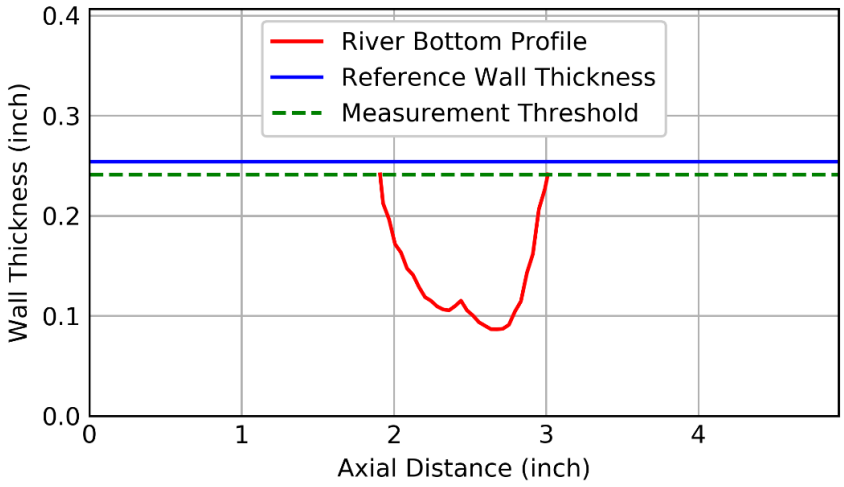

Figure E.22 – River Bottom Profile (4.5in-JT#3-D5)

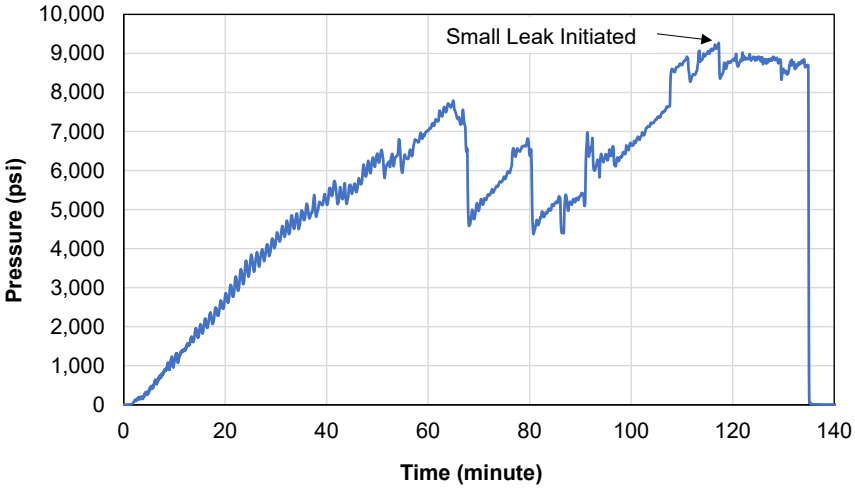

Figure E.23 – Burst Test Pressure versus Time (4.5in-JT#3-D5)

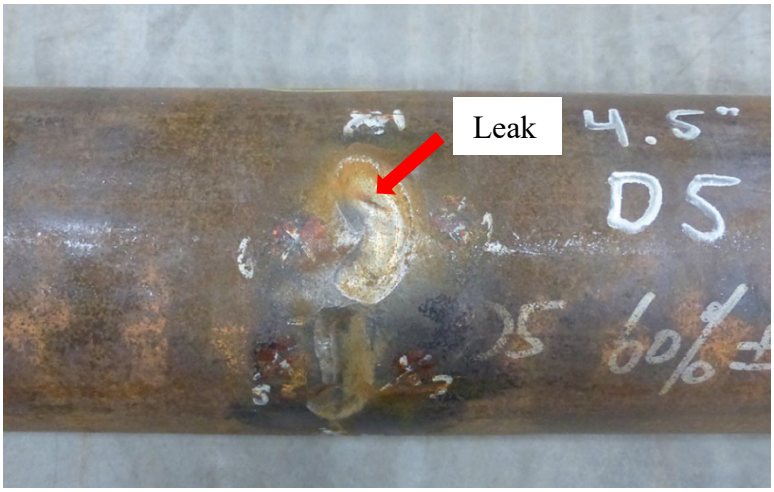

Figure E.24 – Failed Specimen (4.5in-JT#3-D5)

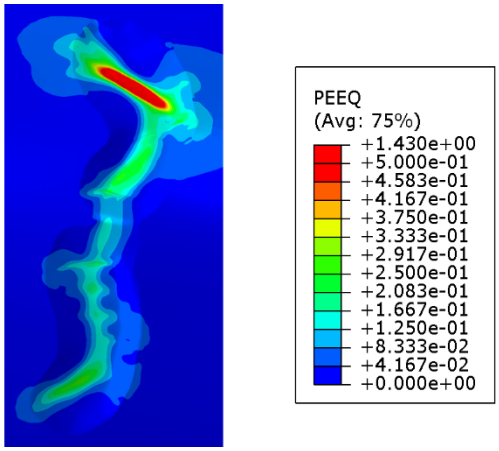

Figure E.25 – FEA Result - Plastic Strain at Peak Pressure (4.5in-JT#3-D5)

Casing Information					
Outside Diameter	4.5 inch	Nominal Wall	0.25 inch	Material Grade	J55
Metal Loss Information					
Feature ID	4.5in-JT#3-D6				
Length	2.95 inch	Width	1.26 inch	Max. Depth	64%
Burst Strength (Physical Test)					
Load Condition	Capped-End				
Burst Strength	6,625 psi				

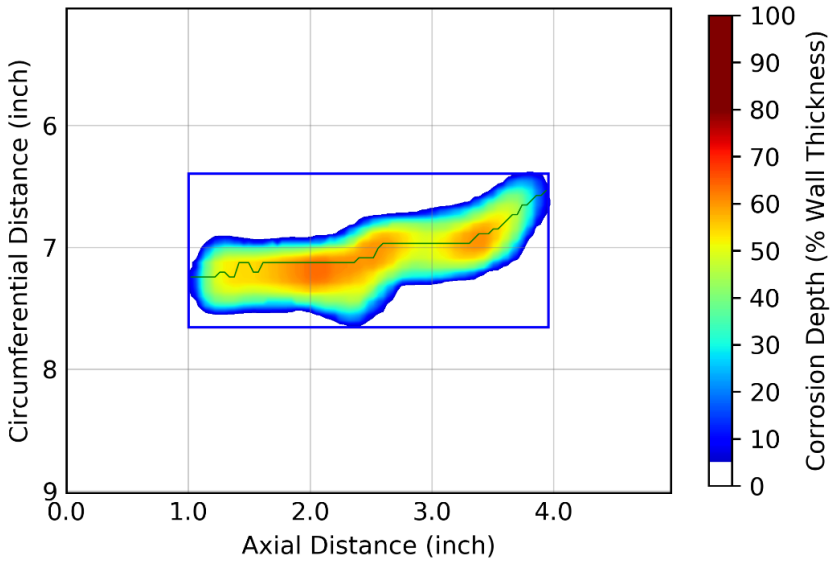

Figure E.26 – Laser Scan Plot (4.5in-JT#3-D6)

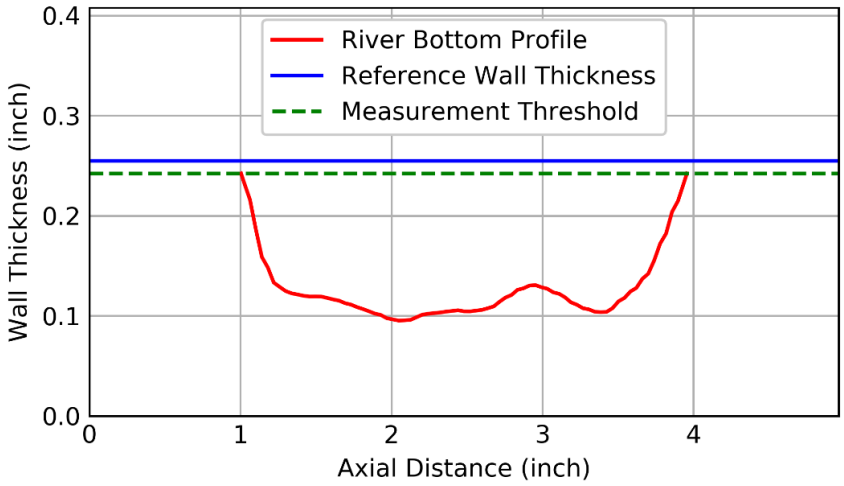

Figure E.27 – River Bottom Profile (4.5in-JT#3-D6)

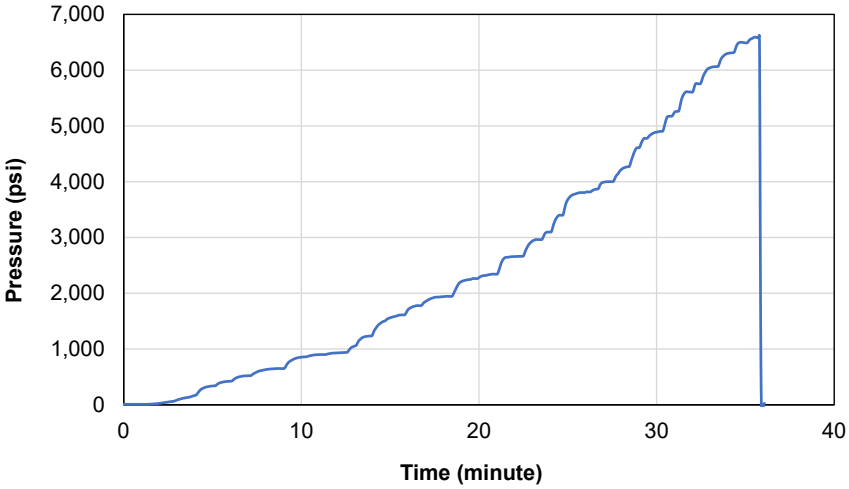

Figure E.28 – Burst Test Pressure versus Time (4.5in-JT#3-D6)

Figure E.29 – Failed Specimen (4.5in-JT#3-D6)

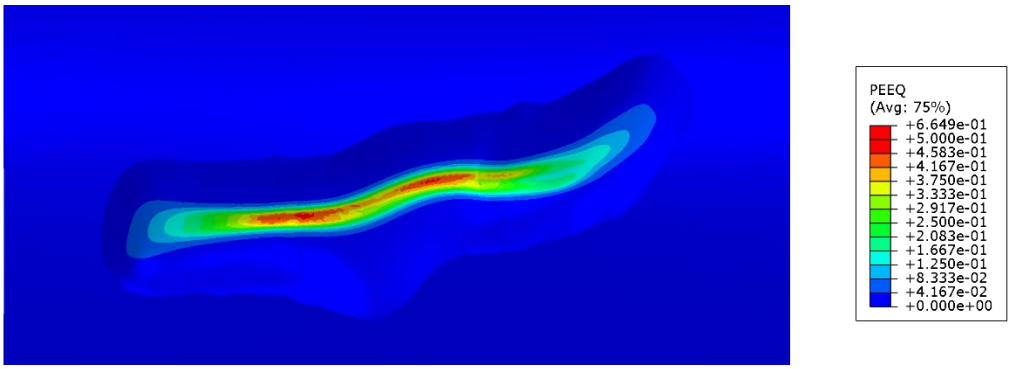

Figure E.30 – FEA Result - Plastic Strain at Peak Pressure (4.5in-JT#3-D6)

Casing Information					
Outside Diameter	4.5 inch	Nominal Wall	0.25 inch	Material Grade	J55
Metal Loss Information					
Feature ID	4.5in-JT#3-D7				
Length	1.85 inch	Width	2.08 inch	Max. Depth	63%
Burst Strength (Physical Test)					
Load Condition	Capped-End				
Burst Strength	8,647 psi				

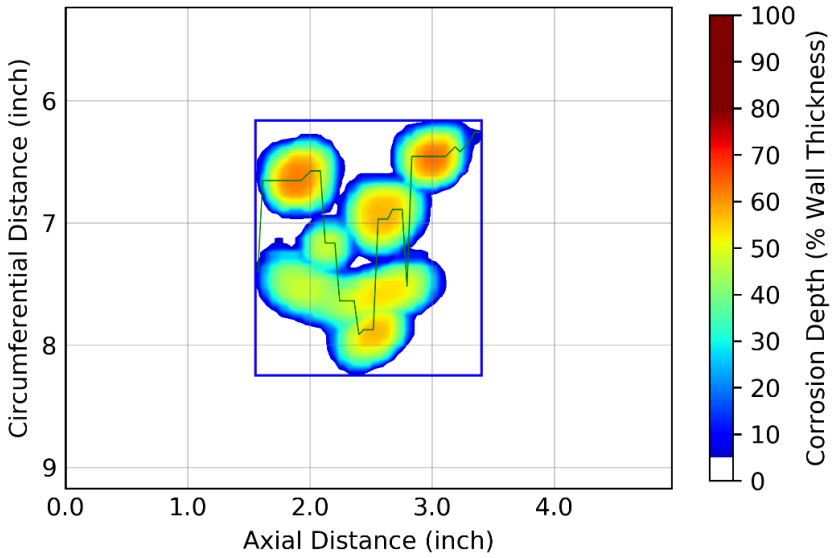

Figure E.31 – Laser Scan Plot (4.5in-JT#3-D7)

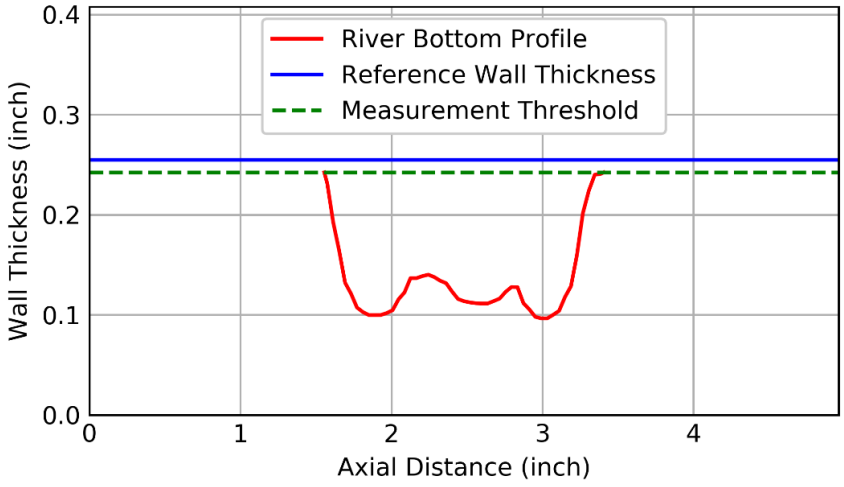

Figure E.32 – River Bottom Profile (4.5in-JT#3-D7)

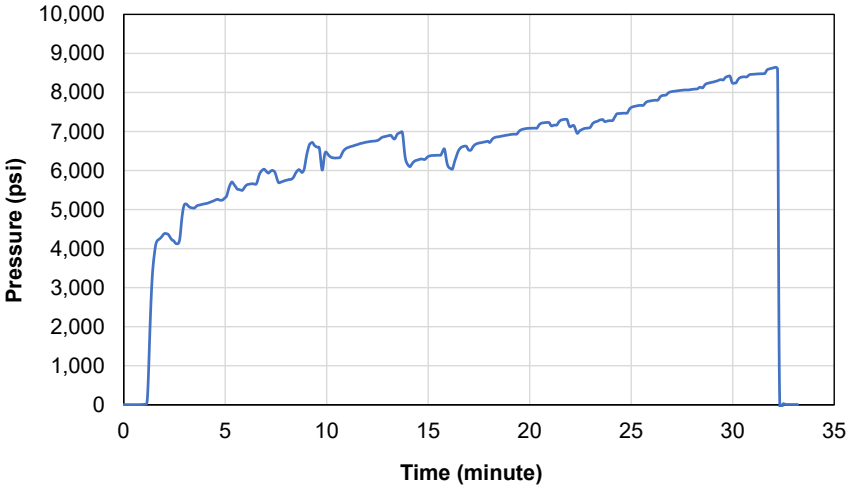

Figure E.33 – Burst Test Pressure versus Time (4.5in-JT#3-D7)

Figure E.34 – Failed Specimen (4.5in-JT#3-D7)

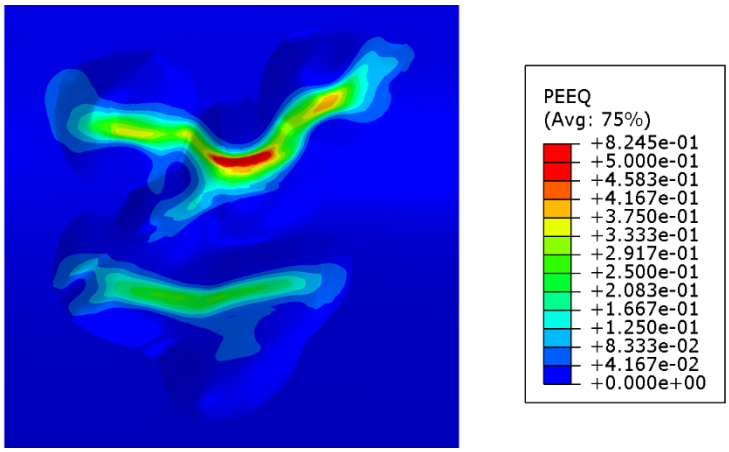

Figure E.35 – FEA Result - Plastic Strain at Peak Pressure (4.5in-JT#3-D7)

Casing Information					
Outside Diameter	4.5 inch	Nominal Wall	0.25 inch	Material Grade	J55
Metal Loss Information					
Feature ID	4.5in-JT#3-D8				
Length	2.24 inch	Width	1.06 inch	Max. Depth	65%
Burst Strength (Physical Test)					
Load Condition	Capped-End				
Burst Strength	8,432 psi				

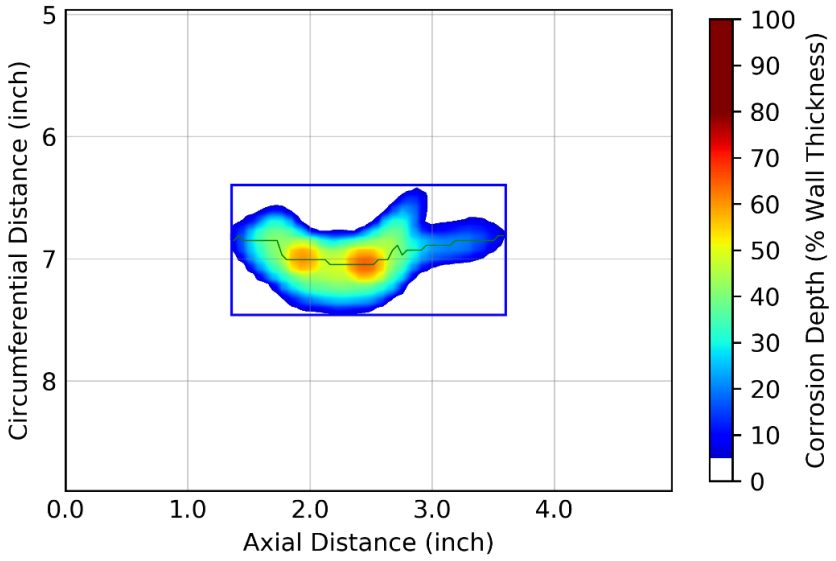

Figure E.36 – Laser Scan Plot (4.5in-JT#3-D8)

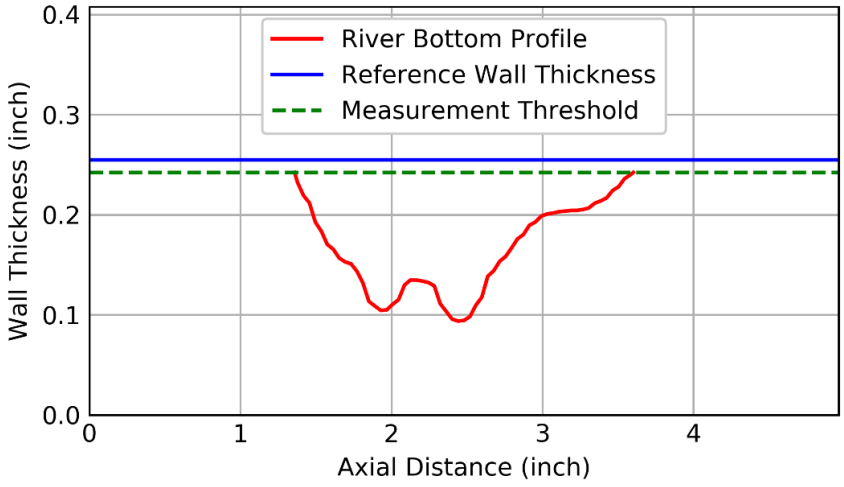

Figure E.37 – River Bottom Profile (4.5in-JT#3-D8)

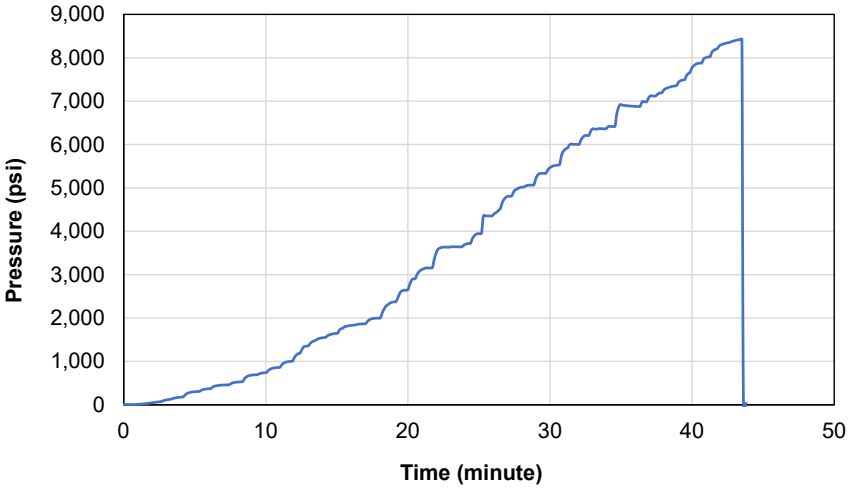

Figure E.38 – Burst Test Pressure versus Time (4.5in-JT#3-D8)

Figure E.39 – Failed Specimen (4.5in-JT#3-D8)

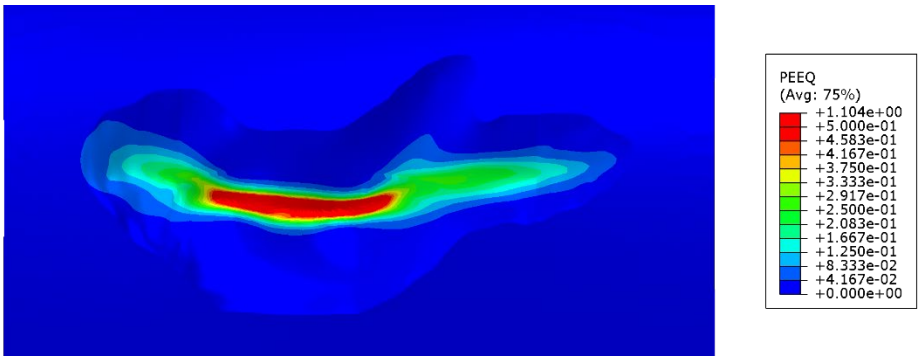

Figure E.40 – FEA Result - Plastic Strain at Peak Pressure (4.5in-JT#3-D8)

Casing Information					
Outside Diameter	5.5 inch	Nominal Wall	0.275 inch	Material Grade	J55
Metal Loss Information					
Feature ID	5.5in-JT#3-D1				
Length	4.06 inch	Width	2.01 inch	Max. Depth	54%
Burst Strength (Physical Test)					
Load Condition	Capped-End				
Burst Strength	6,080 psi				

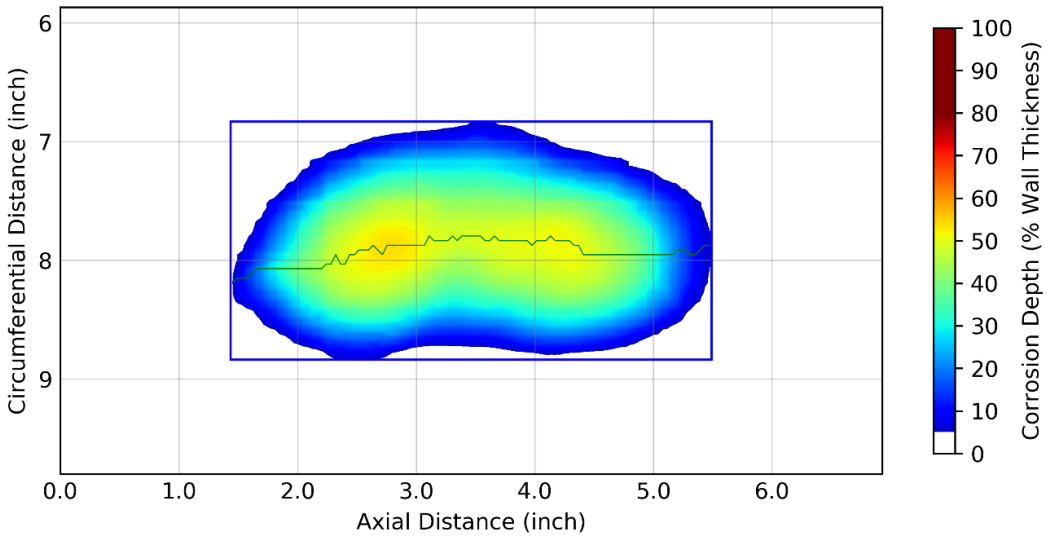

Figure E.41 – Laser Scan Plot (5.5in-JT#3-D1)

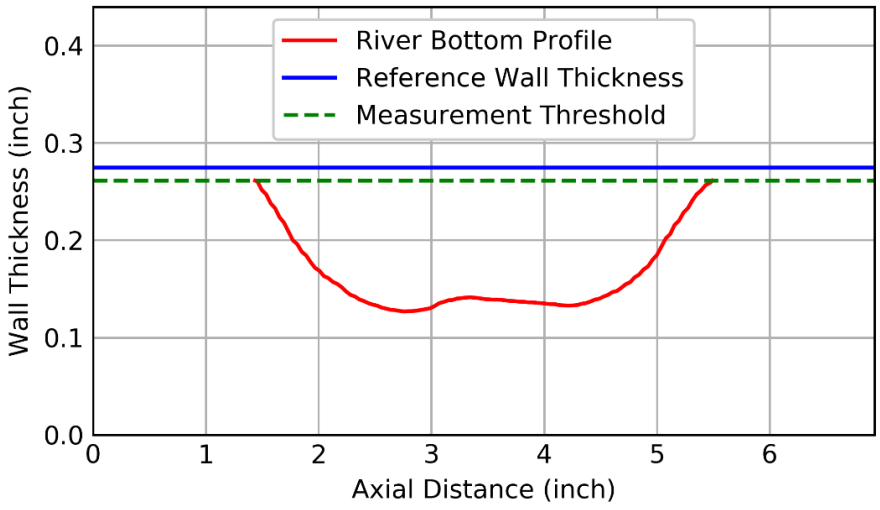

Figure E.42 – River Bottom Profile (5.5in-JT#3-D1)

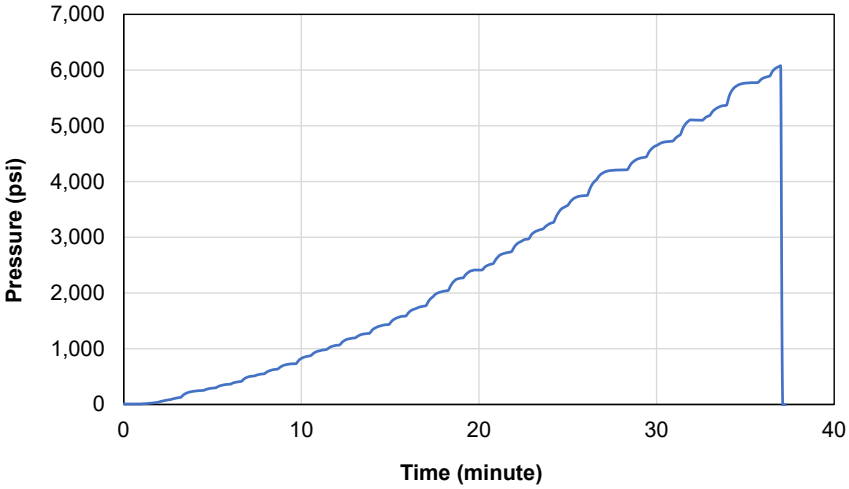

Figure E.43 – Burst Test Pressure versus Time (5.5in-JT#3-D1)

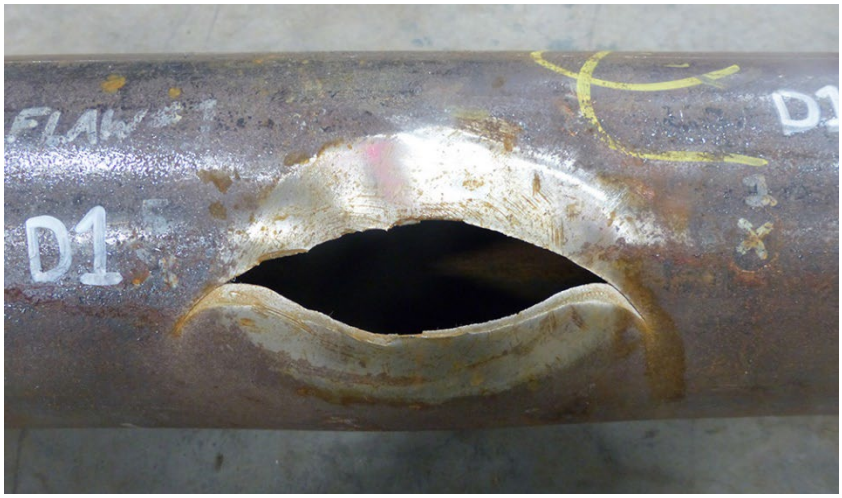

Figure E.44 – Failed Specimen (5.5in-JT#3-D1)

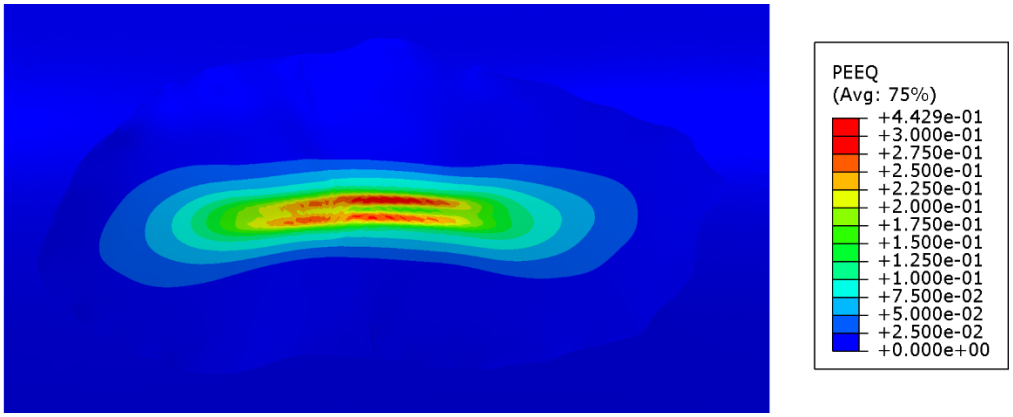

Figure E.45 – FEA Result - Plastic Strain at Peak Pressure (5.5in-JT#3-D1)

Casing Information					
Outside Diameter	5.5 inch	Nominal Wall	0.275 inch	Material Grade	J55
Metal Loss Information					
Feature ID	5.5in-JT#3-D2				
Length	4.84 inch	Width	2.56 inch	Max. Depth	63%
Burst Strength (Physical Test)					
Load Condition	Capped-End				
Burst Strength	5,736 psi				

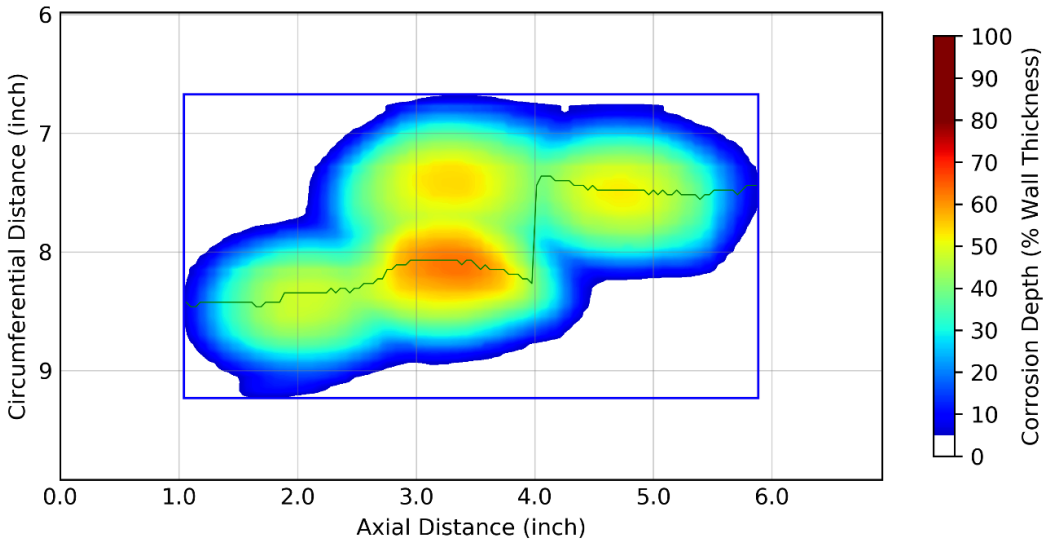

Figure E.46 – Laser Scan Plot (5.5in-JT#3-D2)

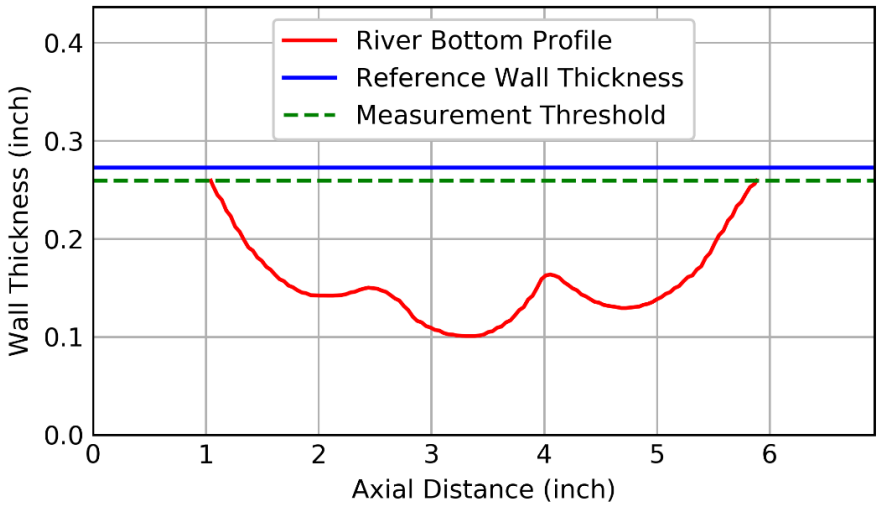

Figure E.47 – River Bottom Profile (5.5in-JT#3-D2)

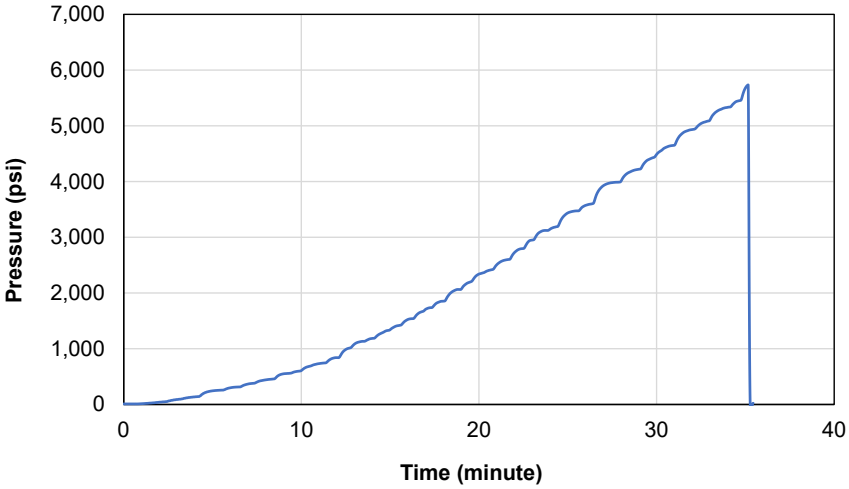

Figure E.48 – Burst Test Pressure versus Time (5.5in-JT#3-D2)

Figure E.49 – Failed Specimen (5.5in-JT#3-D2)

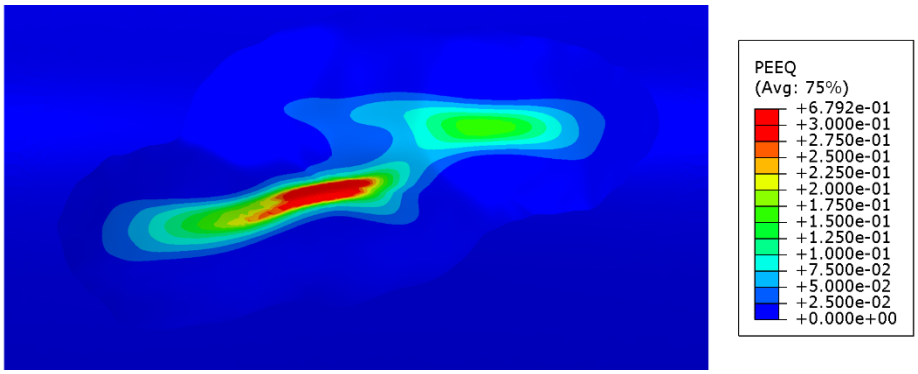

Figure E.50 – FEA Result - Plastic Strain at Peak Pressure (5.5in-JT#3-D2)

Casing Information					
Outside Diameter	5.5 inch	Nominal Wall	0.275 inch	Material Grade	J55
Metal Loss Information					
Feature ID	5.5in-JT#3-D3				
Length	3.50 inch	Width	2.44 inch	Max. Depth	59%
Burst Strength (Physical Test)					
Load Condition	Capped-End				
Burst Strength	6,948 psi				

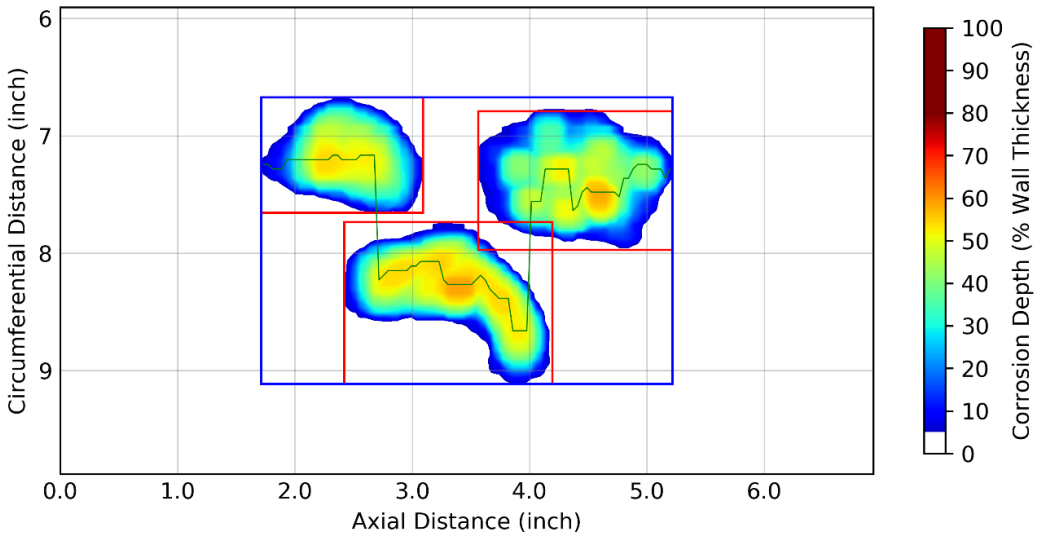

Figure E.51 – Laser Scan Plot (5.5in-JT#3-D3)

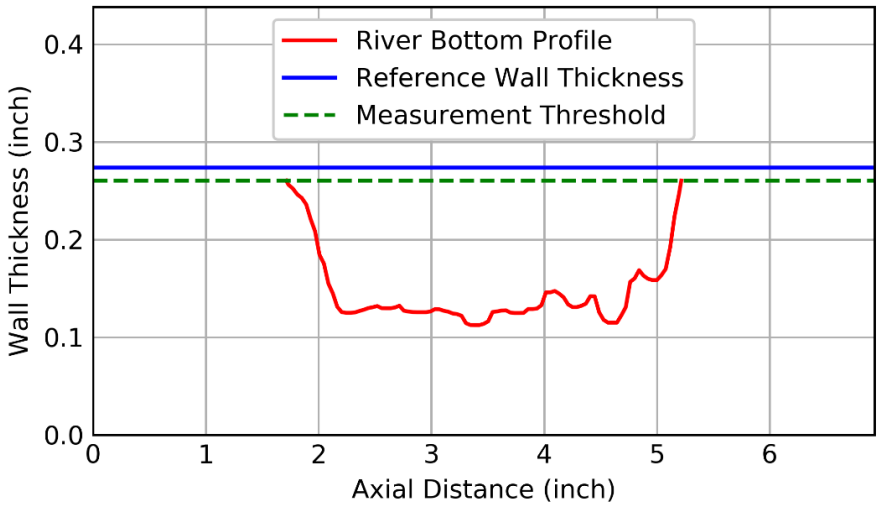

Figure E.52 – River Bottom Profile (5.5in-JT#3-D3)

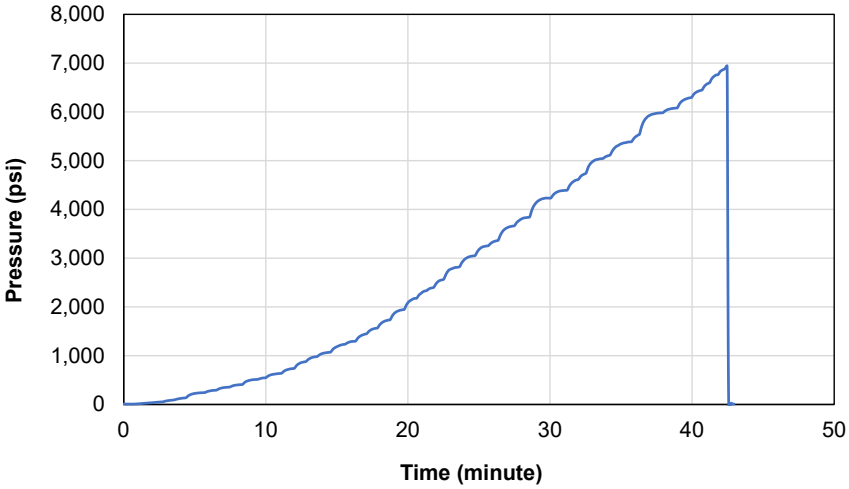

Figure E.53 – Burst Test Pressure versus Time (5.5in-JT#3-D3)

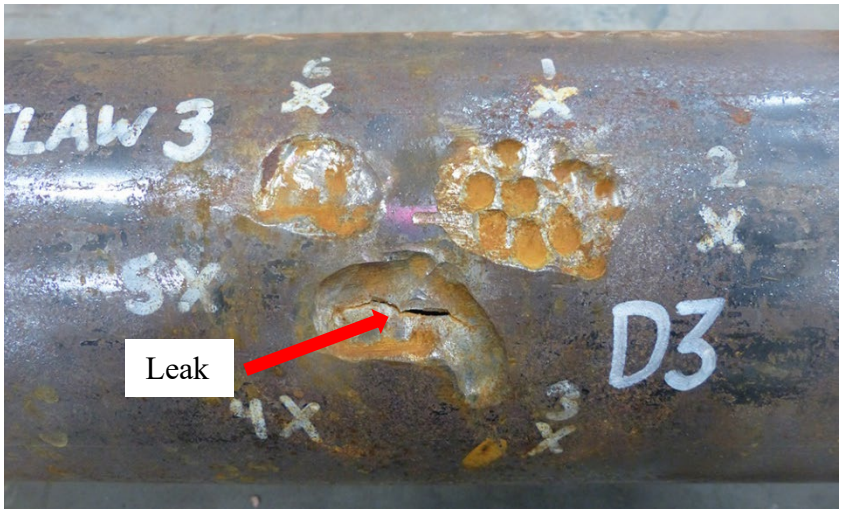

Figure E.54 – Failed Specimen (5.5in-JT#3-D3)

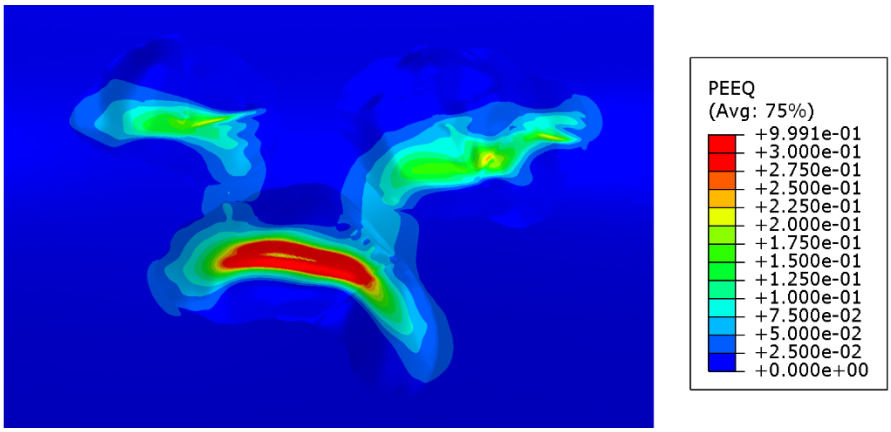

Figure E.55 – FEA Result - Plastic Strain at Peak Pressure (5.5in-JT#3-D3)

Casing Information					
Outside Diameter	5.5 inch	Nominal Wall	0.275 inch	Material Grade	J55
Metal Loss Information					
Feature ID	5.5in-JT#3-D4				
Length	3.90 inch	Width	3.62 inch	Max. Depth	58%
Burst Strength (Physical Test)					
Load Condition	Capped-End				
Burst Strength	6,584 psi				

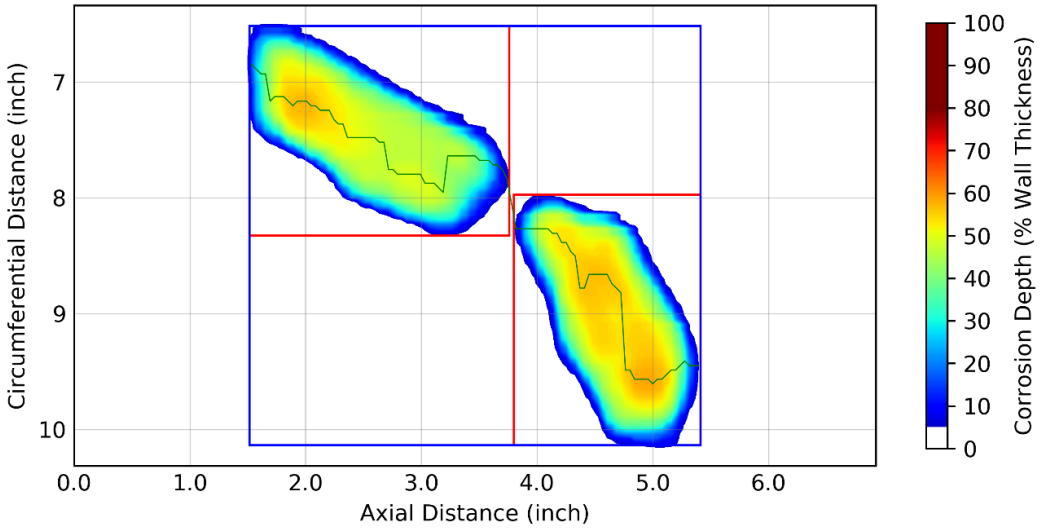

Figure E.56 – Laser Scan Plot (5.5in-JT#3-D4)

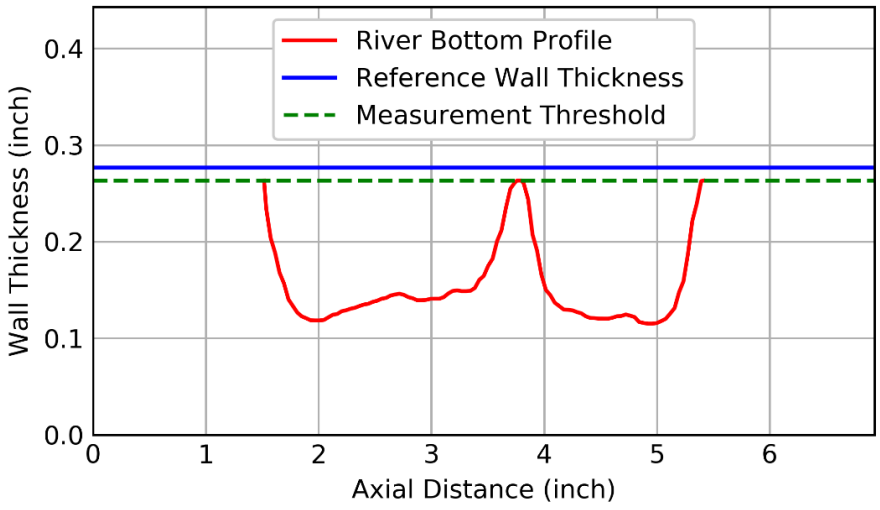

Figure E.57 – River Bottom Profile (5.5in-JT#3-D4)

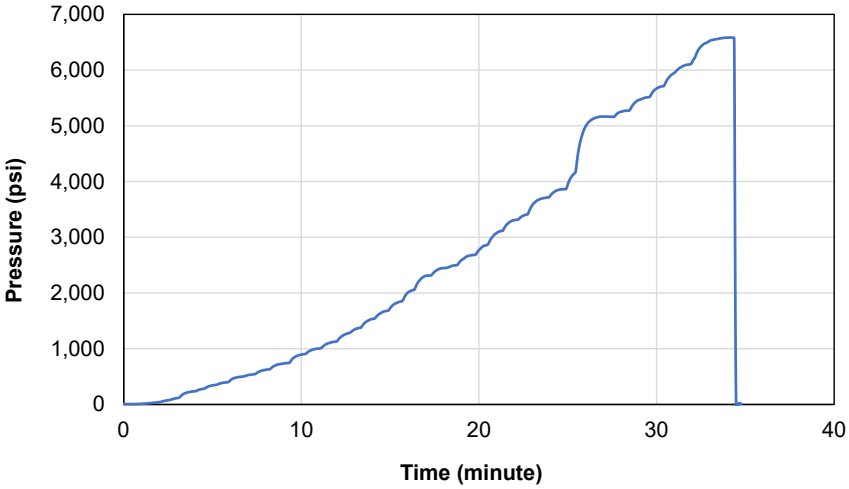

Figure E.58 – Burst Test Pressure versus Time (5.5in-JT#3-D4)

Figure E.59 – Failed Specimen (5.5in-JT#3-D4)

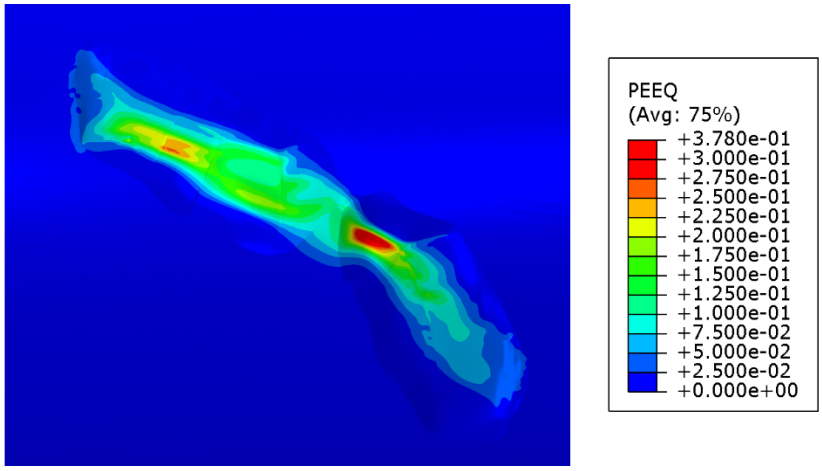

Figure E.60 – FEA Result - Plastic Strain at Peak Pressure (5.5in-JT#3-D4)

Casing Information					
Outside Diameter	5.5 inch	Nominal Wall	0.275 inch	Material Grade	J55
Metal Loss Information					
Feature ID	5.5in-JT#3-D5				
Length	1.06 inch	Width	3.94 inch	Max. Depth	57%
Burst Strength (Physical Test)					
Load Condition	Capped-End				
Burst Strength	8,085 psi				

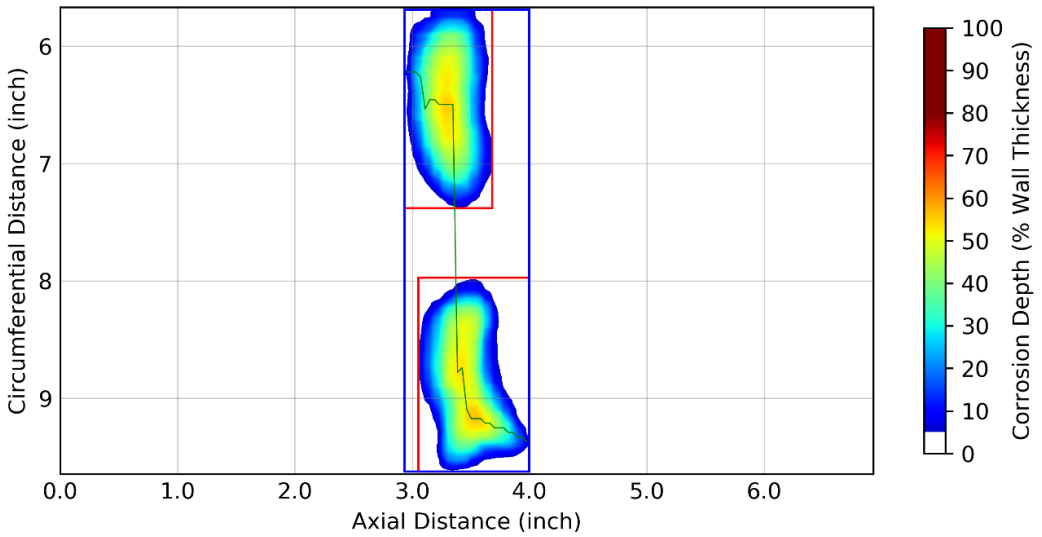

Figure E.61 – Laser Scan Plot (5.5in-JT#3-D5)

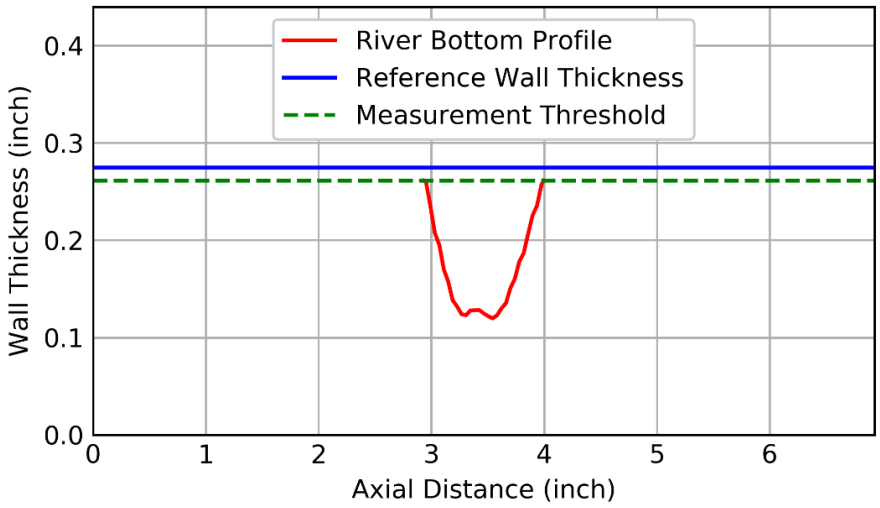

Figure E.62 – River Bottom Profile (5.5in-JT#3-D5)

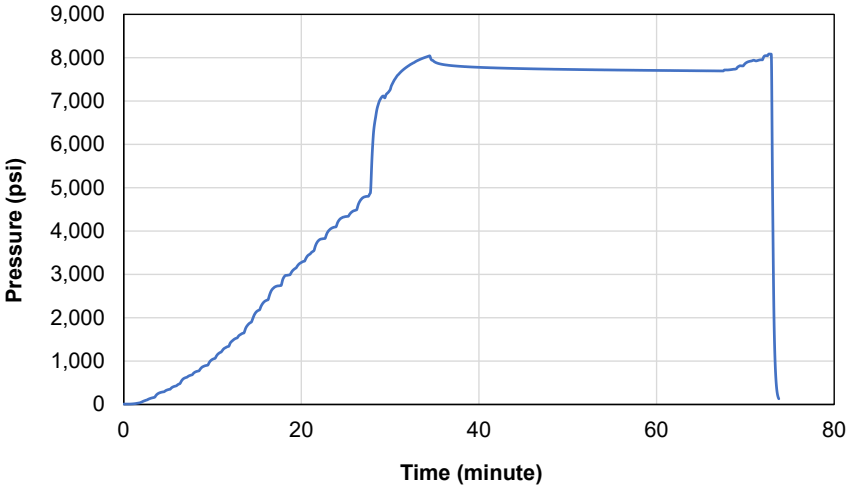

Figure E.63 – Burst Test Pressure versus Time (5.5in-JT#3-D5)

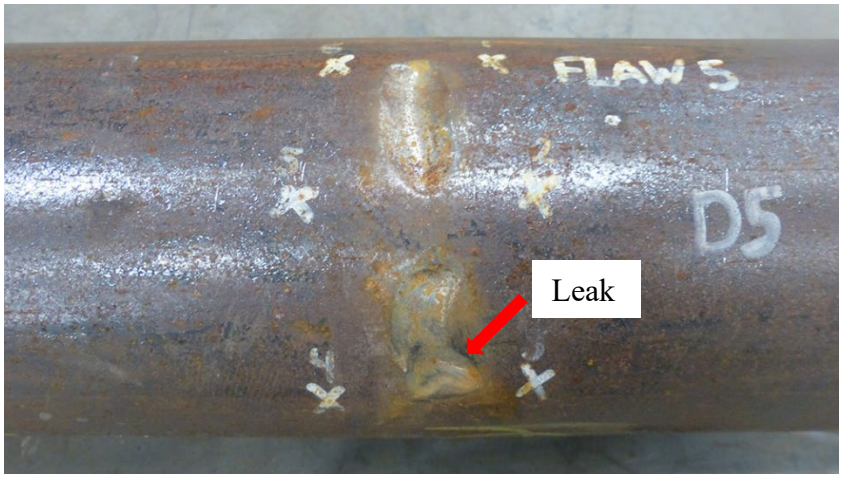

Figure E.64 – Failed Specimen (5.5in-JT#3-D5)

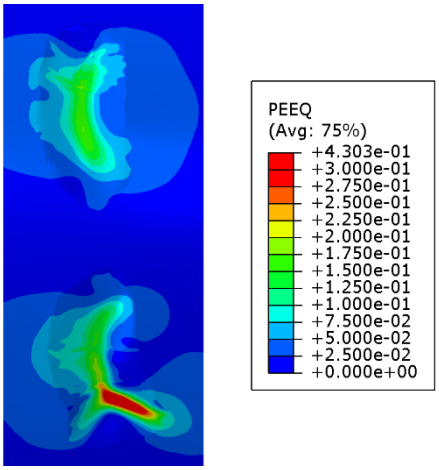

Figure E.65 – FEA Result - Plastic Strain at Peak Pressure (5.5in-JT#3-D5)

Casing Information					
Outside Diameter	5.5 inch	Nominal Wall	0.275 inch	Material Grade	J55
Metal Loss Information					
Feature ID	5.5in-JT#3-D6				
Length	3.39 inch	Width	1.18 inch	Max. Depth	61%
Burst Strength (Physical Test)					
Load Condition	Capped-End				
Burst Strength	5,944 psi				

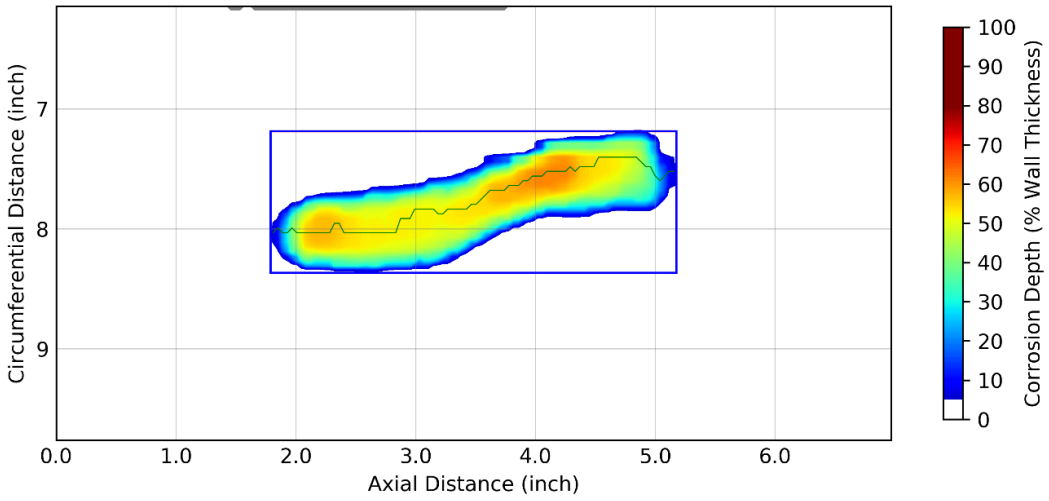

Figure E.66 – Laser Scan Plot (5.5in-JT#3-D6)

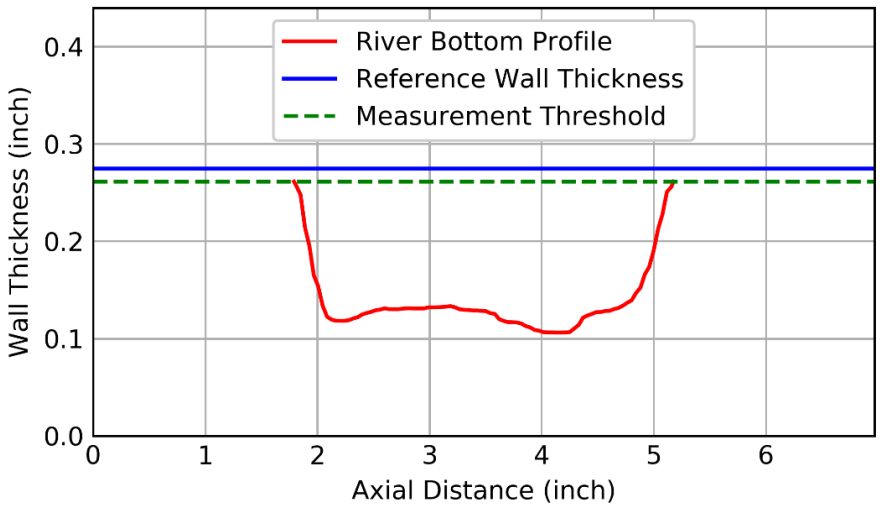

Figure E.67 – River Bottom Profile (5.5in-JT#3-D6)

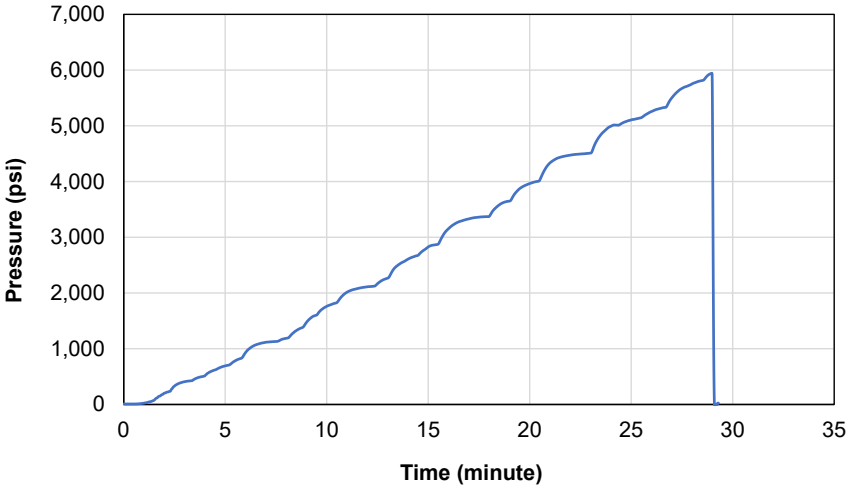

Figure E.68 – Burst Test Pressure versus Time (5.5in-JT#3-D6)

Figure E.69 – Failed Specimen (5.5in-JT#3-D6)

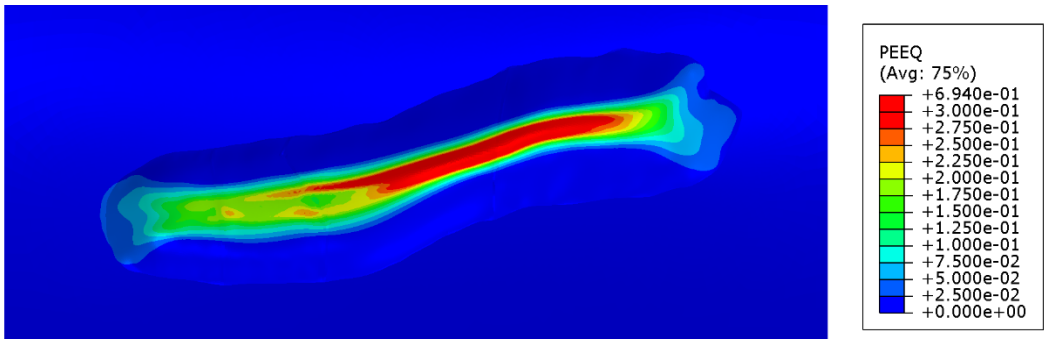

Figure E.70 – FEA Result - Plastic Strain at Peak Pressure (5.5in-JT#3-D6)

Casing Information					
Outside Diameter	7.0 inch	Nominal Wall	0.317 inch	Material Grade	J55
Metal Loss Information					
Feature ID	7.0in-JT#3-D1				
Length	4.57 inch	Width	1.85 inch	Max. Depth	47%
Burst Strength (Physical Test)					
Load Condition	Capped-End				
Burst Strength	6,135 psi				

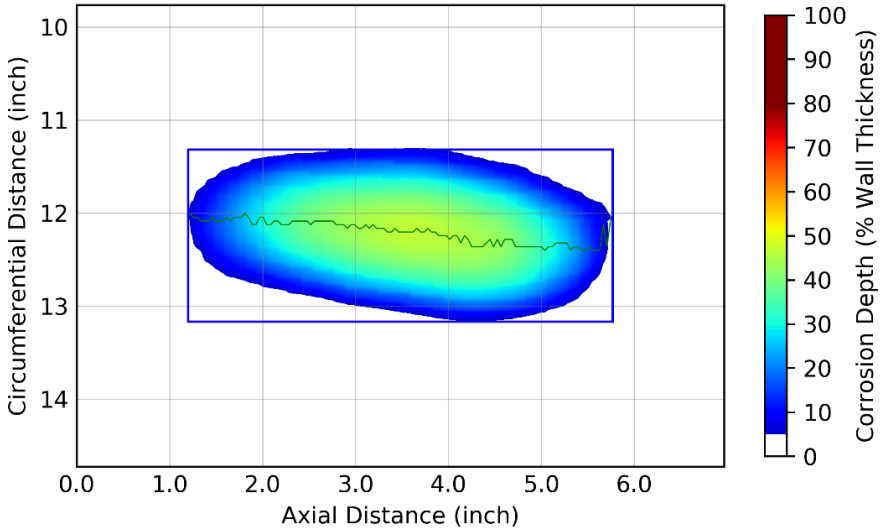

Figure E.71 – Laser Scan Plot (7.0in-JT#3-D1)

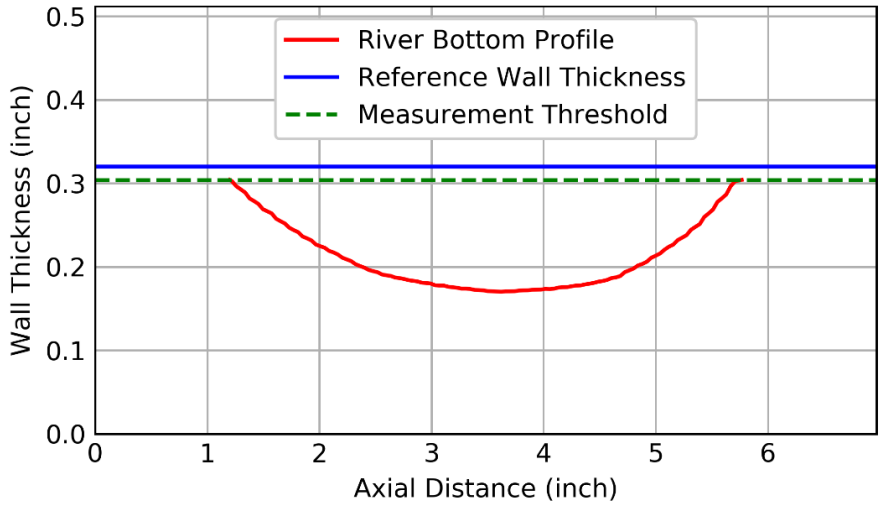

Figure E.72 – River Bottom Profile (7.0in-JT#3-D1)

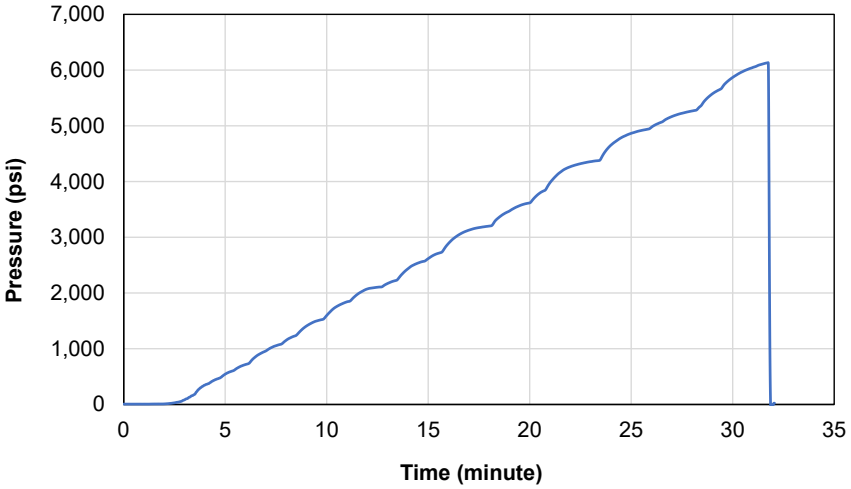

Figure E.73 – Burst Test Pressure versus Time (7.0in-JT#3-D1)

Figure E.74 – Failed Specimen (7.0in-JT#3-D1)

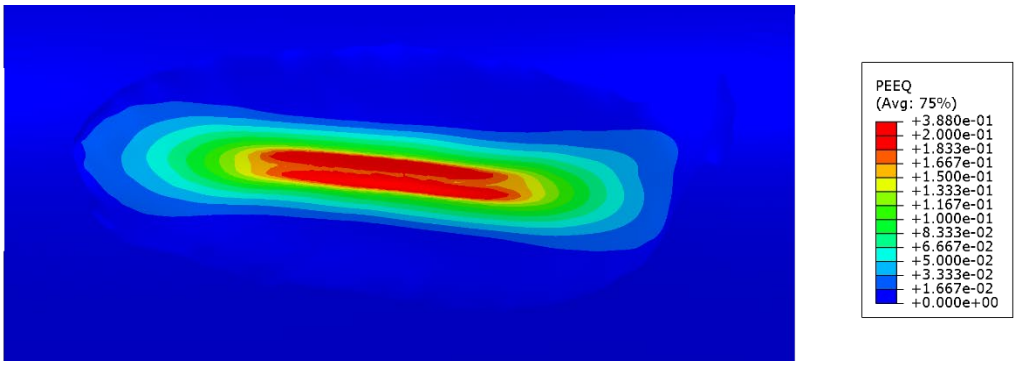

Figure E.75 – FEA Result - Plastic Strain at Peak Pressure (7.0in-JT#3-D1)

Casing Information					
Outside Diameter	7.0 inch	Nominal Wall	0.317 inch	Material Grade	J55
Metal Loss Information					
Feature ID	7.0in-JT#3-D2				
Length	6.34 inch	Width	2.72 inch	Max. Depth	47%
Burst Strength (Physical Test)					
Load Condition	Capped-End				
Burst Strength	5,823 psi				

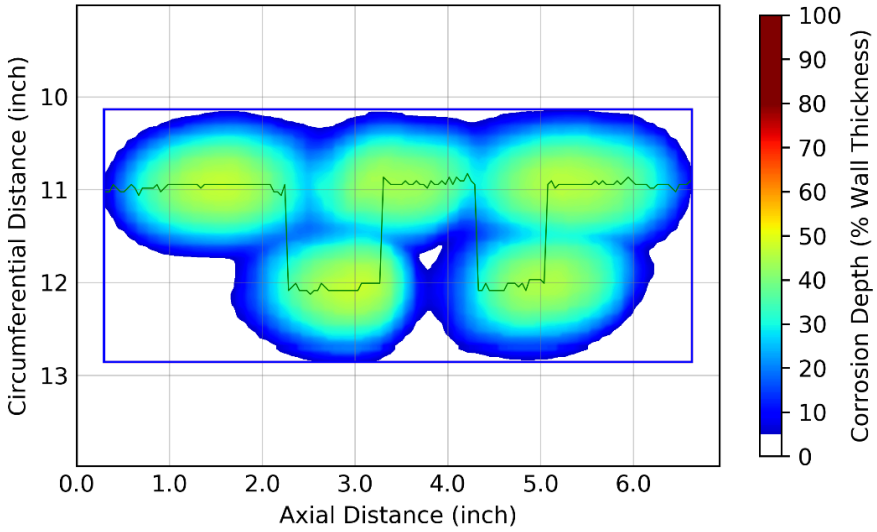

Figure E.76 – Laser Scan Plot (7.0in-JT#3-D2)

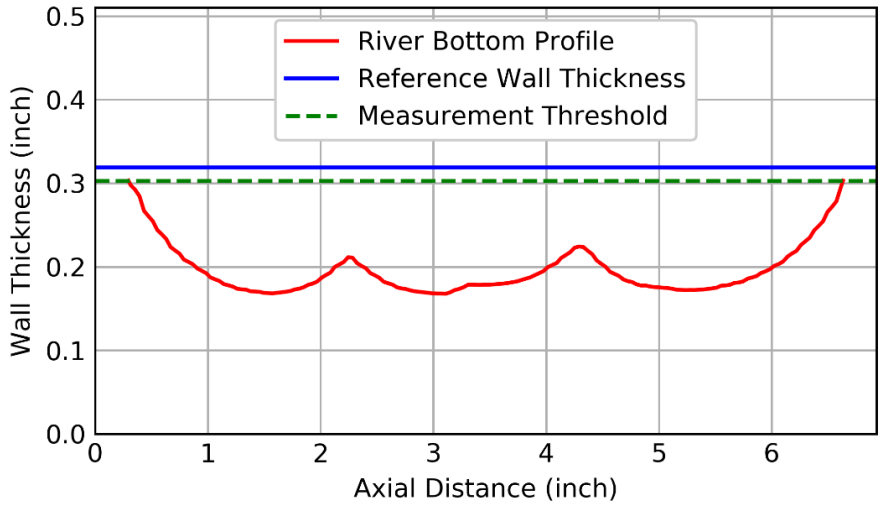

Figure E.77 – River Bottom Profile (7.0in-JT#3-D2)

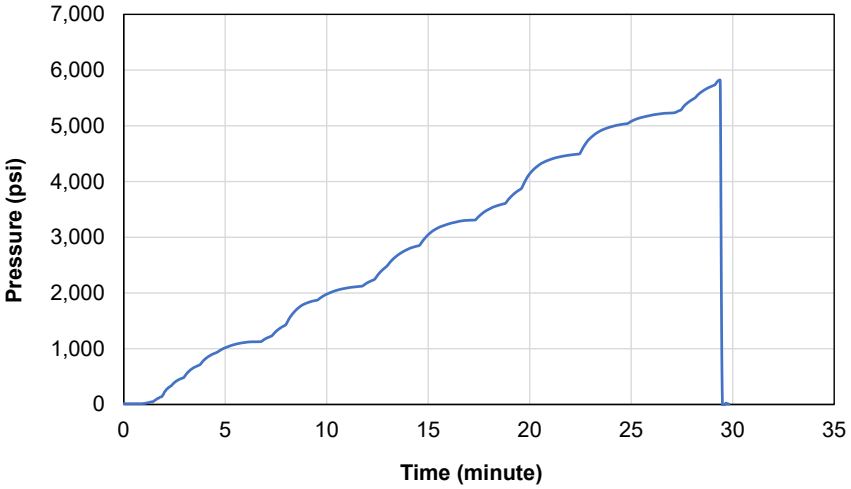

Figure E.78 – Burst Test Pressure versus Time (7.0in-JT#3-D2)

Figure E.79 – Failed Specimen (7.0in-JT#3-D2)

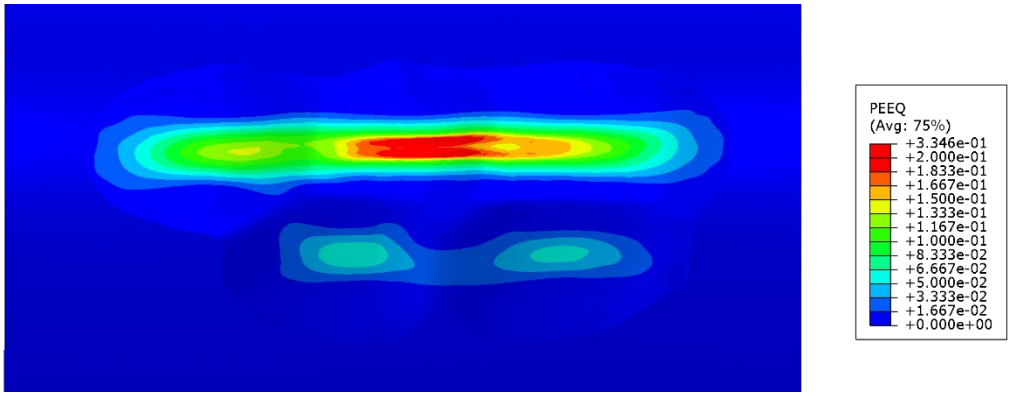

Figure E.80 – FEA Result - Plastic Strain at Peak Pressure (7.0in-JT#3-D2)

Casing Information					
Outside Diameter	7.0 inch	Nominal Wall	0.317 inch	Material Grade	J55
Metal Loss Information					
Feature ID	7.0in-JT#3-D3				
Length	3.58 inch	Width	3.62 inch	Max. Depth	50%
Burst Strength (Physical Test)					
Load Condition	Capped-End				
Burst Strength	6,900 psi				

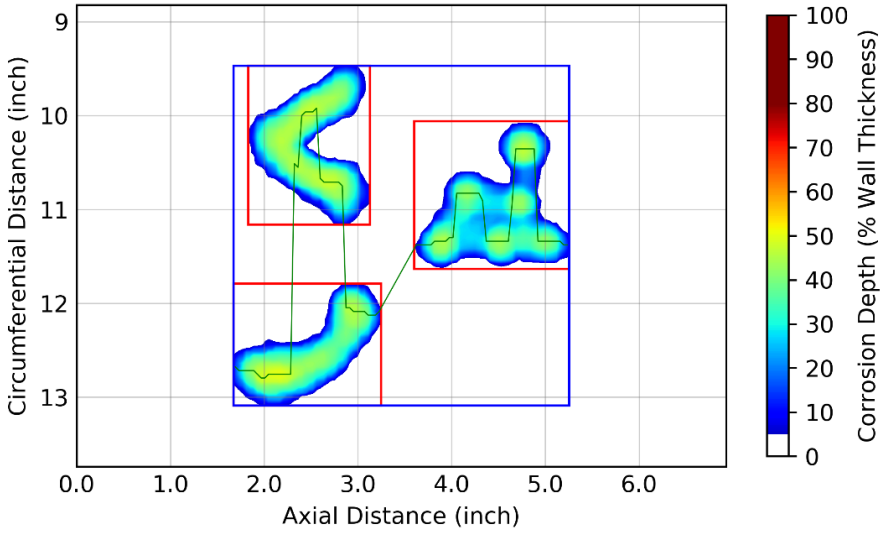

Figure E.81 – Laser Scan Plot (7.0in-JT#3-D3)

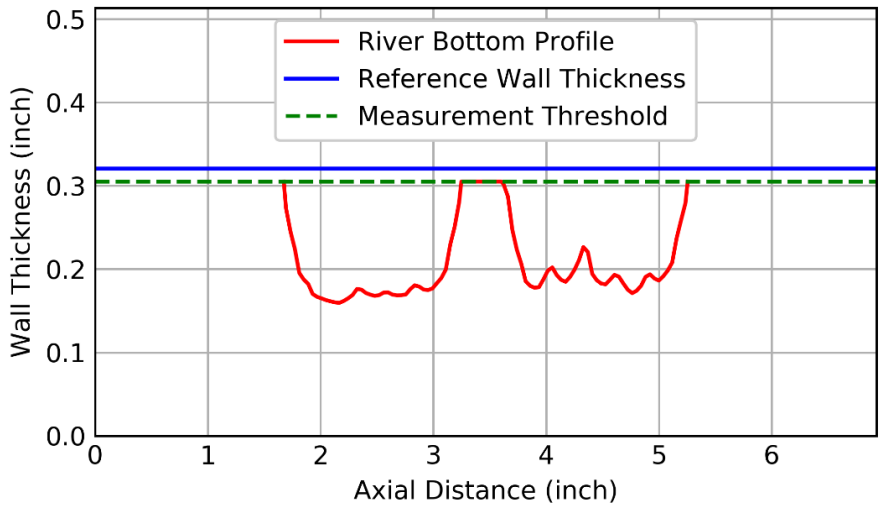

Figure E.82 – River Bottom Profile (7.0in-JT#3-D3)

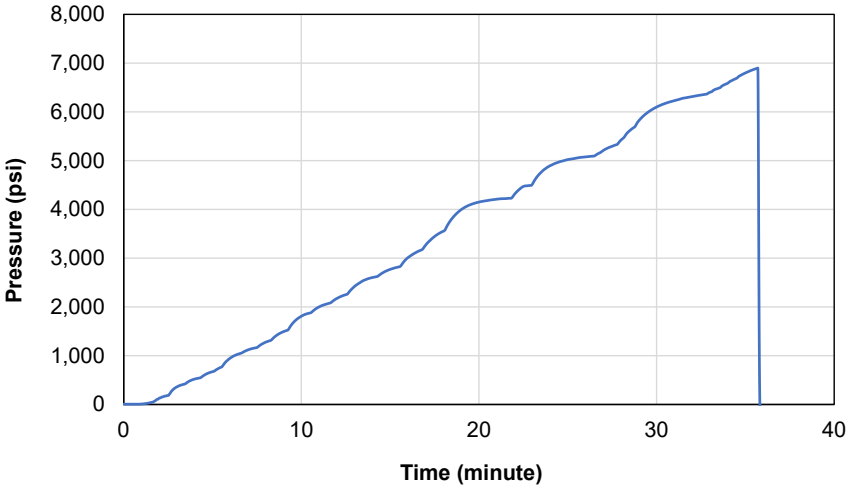

Figure E.83 – Burst Test Pressure versus Time (7.0in-JT#3-D3)

Figure E.84 – Failed Specimen (7.0in-JT#3-D3)

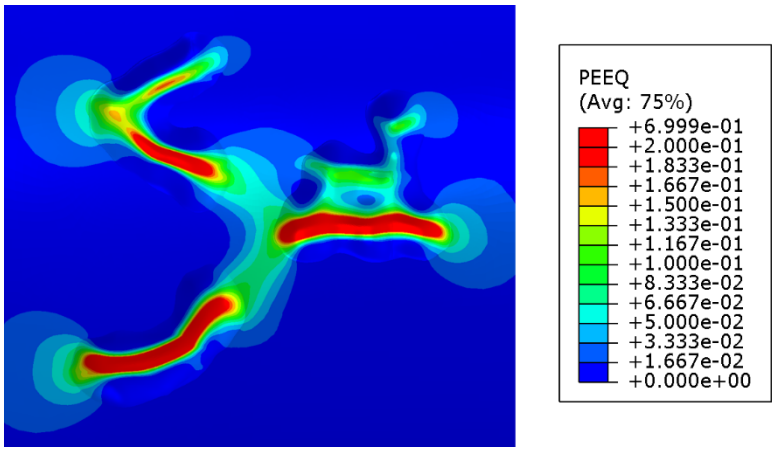

Figure E.85 – FEA Result - Plastic Strain at Peak Pressure (7.0in-JT#3-D3)

Casing Information					
Outside Diameter	7.0 inch	Nominal Wall	0.317 inch	Material Grade	J55
Metal Loss Information					
Feature ID	7.0in-JT#3-D4				
Length	5.16 inch	Width	3.54 inch	Max. Depth	54%
Burst Strength (Physical Test)					
Load Condition	Capped-End				
Burst Strength	6,287 psi				

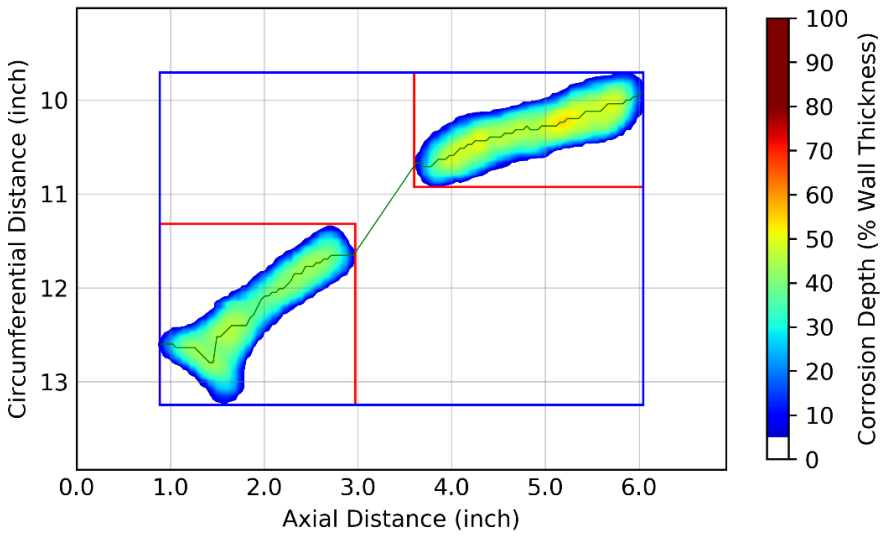

Figure E.86 – Laser Scan Plot (7.0in-JT#3-D4)

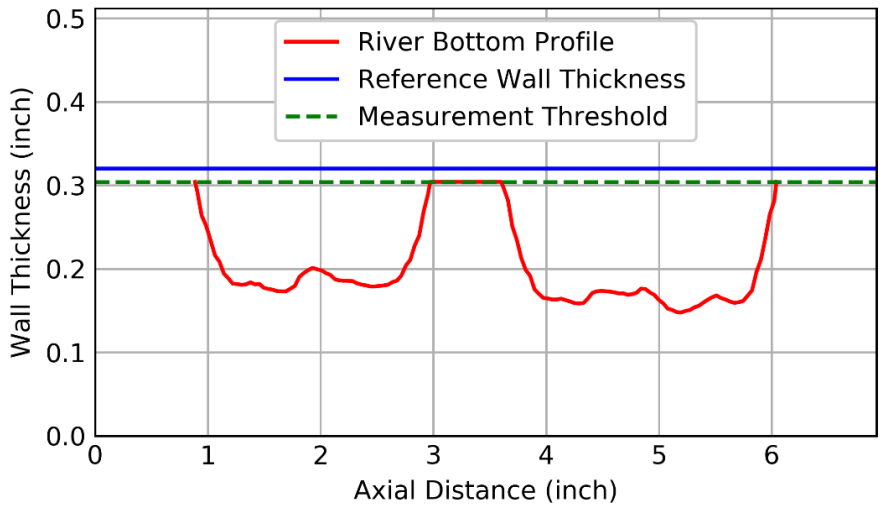

Figure E.87 – River Bottom Profile (7.0in-JT#3-D4)

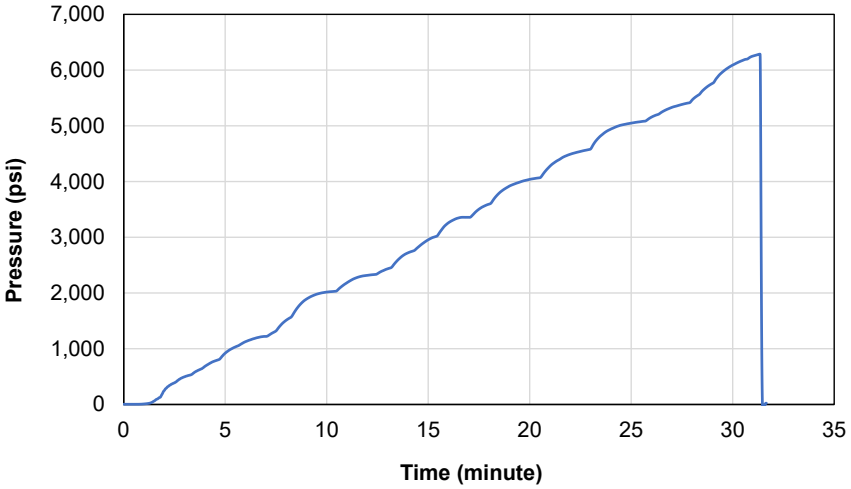

Figure E.88 – Burst Test Pressure versus Time (7.0in-JT#3-D4)

Figure E.89 – Failed Specimen (7.0in-JT#3-D4)

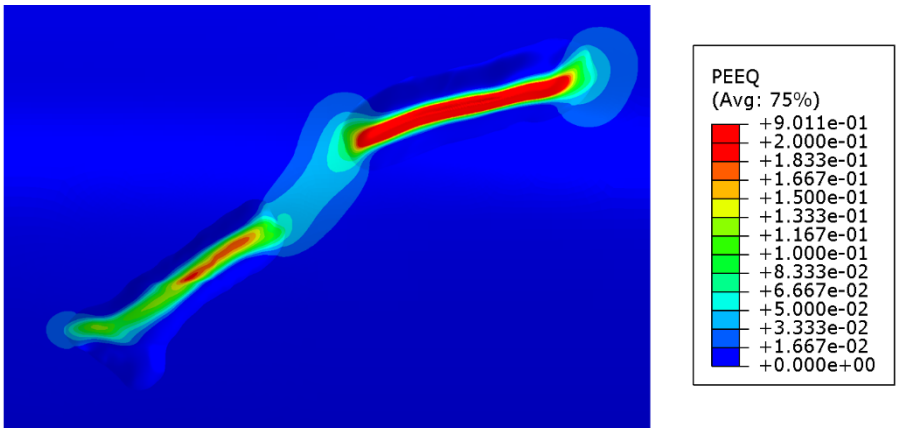

Figure E.90 – FEA Result - Plastic Strain at Peak Pressure (7.0in-JT#3-D4)

Casing Information									
Outside Diameter	7.0 inch		Nominal Wall	0.317 inch		Material Grade	J55		
Metal Loss Information									
Feature ID	7.0in-JT#3-D5								
Length	1.57 inch		Width	4.09 inch		Max. Depth	53%		
Burst Strength (Physical Test)									
Load Condition	Capped-End								
Burst Strength	7,310 psi								

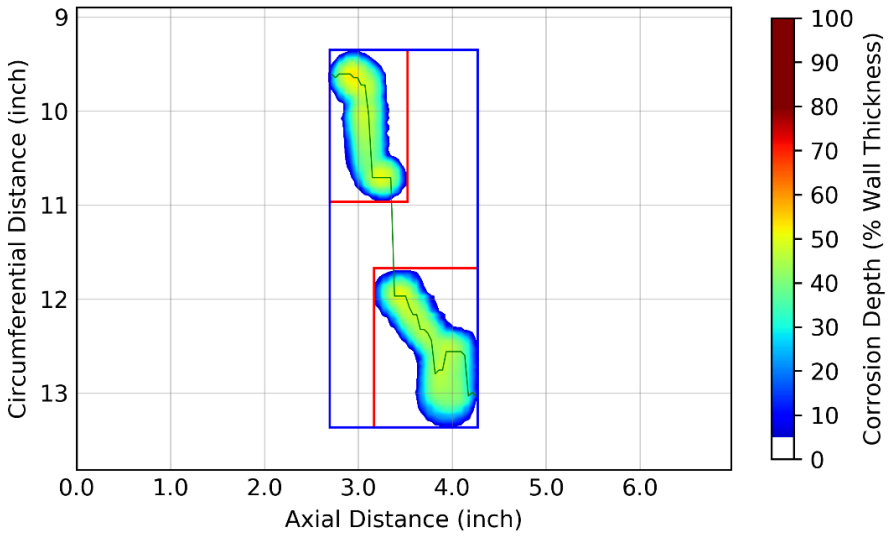

Figure E.91 – Laser Scan Plot (7.0in-JT#3-D5)

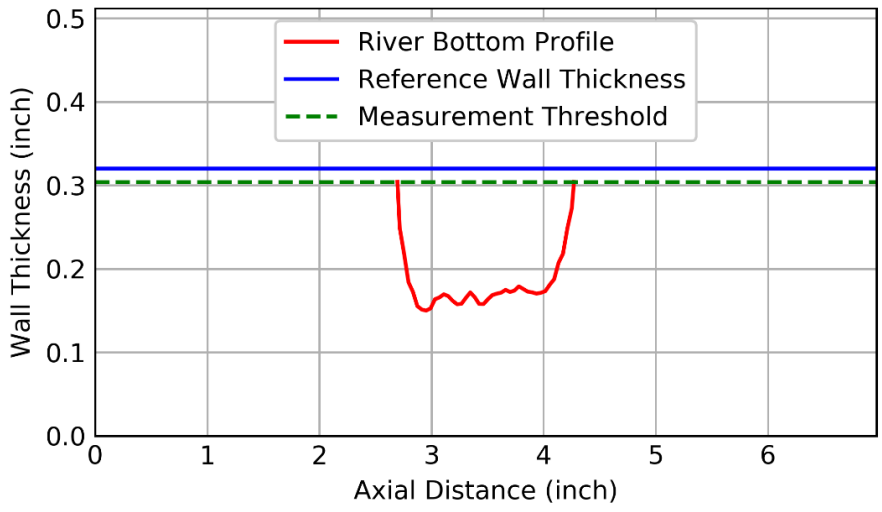

Figure E.92 – River Bottom Profile (7.0in-JT#3-D5)

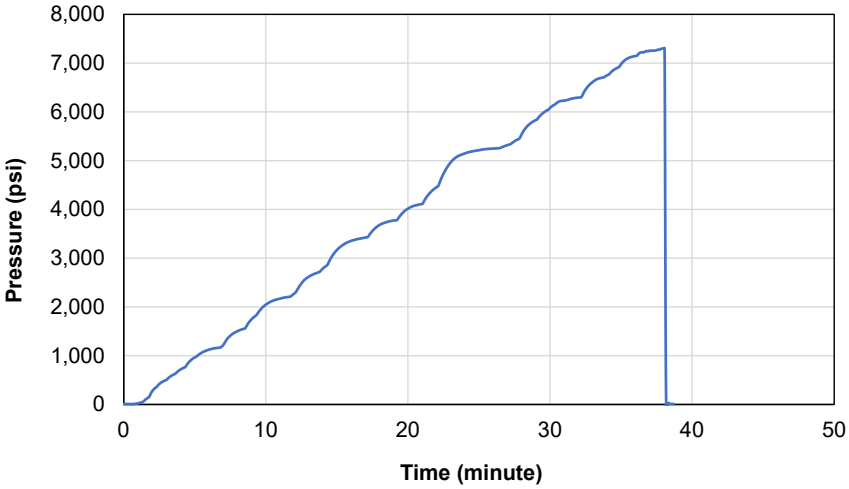

Figure E.93 – Burst Test Pressure versus Time (7.0in-JT#3-D5)

Figure E.94 – Failed Specimen (7.0in-JT#3-D5)

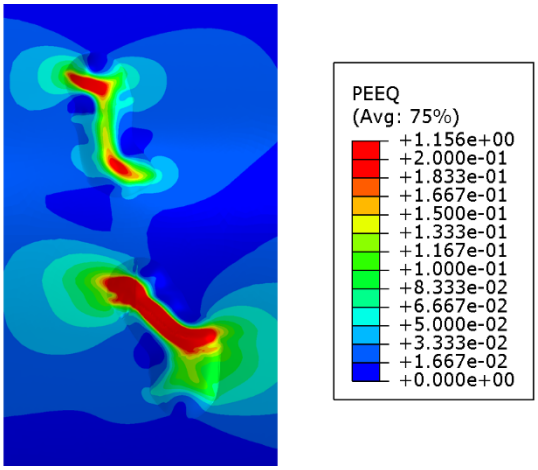

Figure E.95 – FEA Result - Plastic Strain at Peak Pressure (7.0in-JT#3-D5)

Casing Information					
Outside Diameter	7.0 inch	Nominal Wall	0.317 inch	Material Grade	J55
Metal Loss Information					
Feature ID	7.0in-JT#3-D6				
Length	3.15 inch	Width	1.26 inch	Max. Depth	64%
Burst Strength (Physical Test)					
Load Condition	Capped-End				
Burst Strength	5,802 psi				

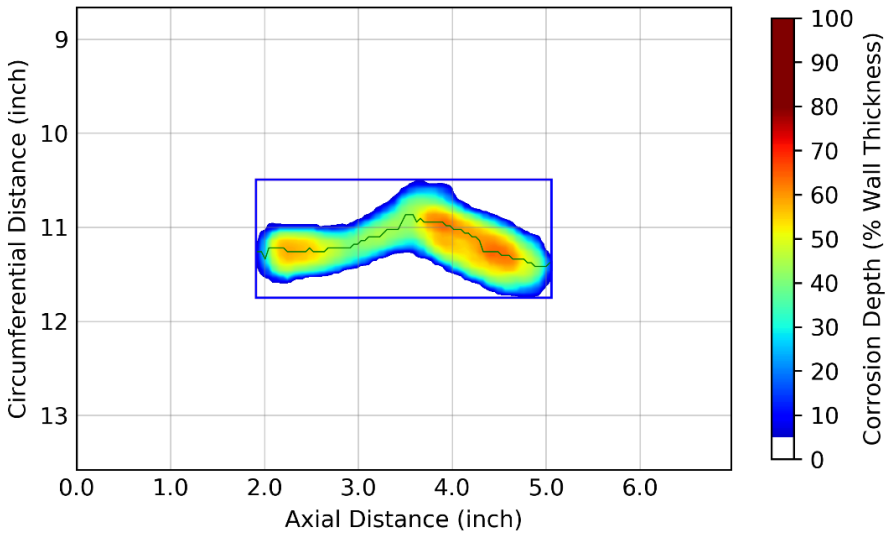

Figure E.96 – Laser Scan Plot (7.0in-JT#3-D6)

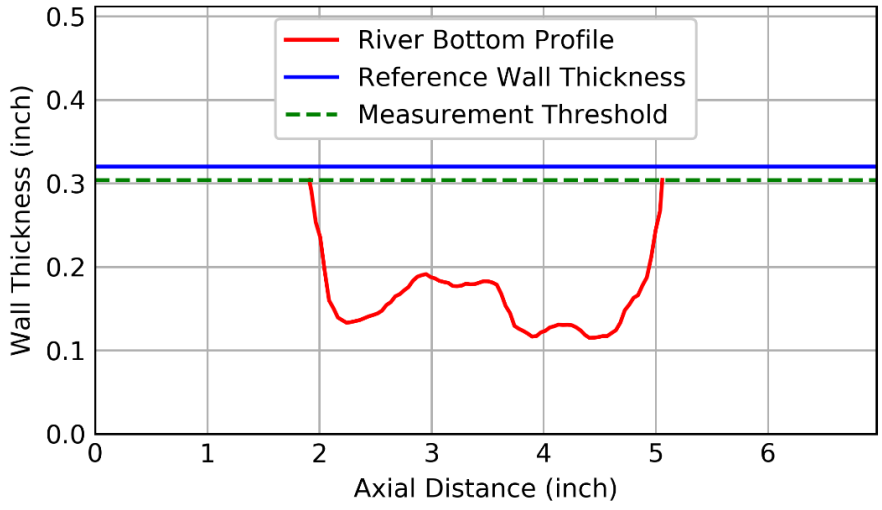

Figure E.97 – River Bottom Profile (7.0in-JT#3-D6)

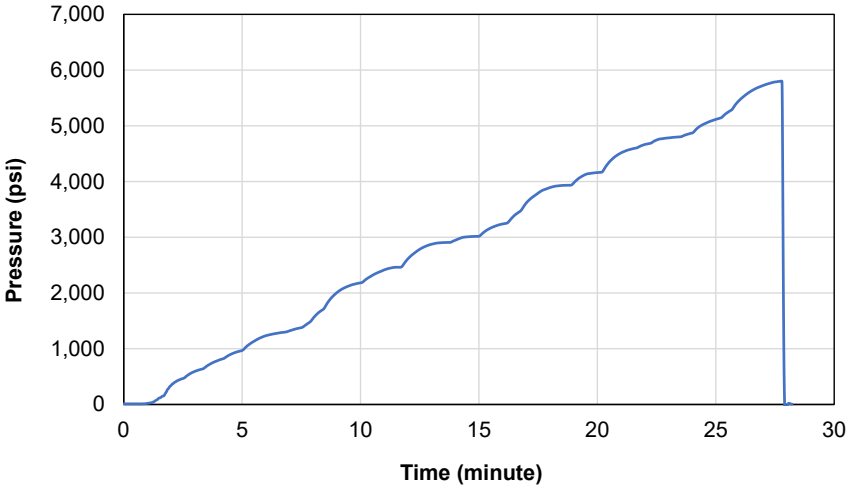

Figure E.98 – Burst Test Pressure versus Time (7.0in-JT#3-D6)

Figure E.99 – Failed Specimen (7.0in-JT#3-D6)

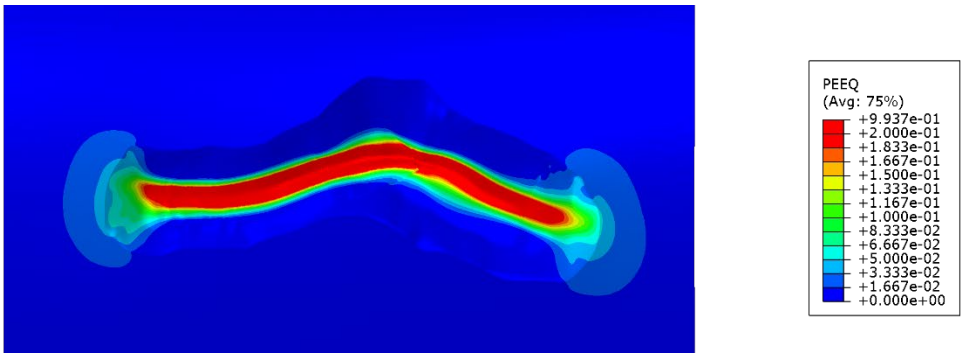

Figure E.100 – FEA Result - Plastic Strain at Peak Pressure (7.0in-JT#3-D6)